Annexure III

Reprints of published papers

Polyhedron 33 (2012) 417–424

Contents lists available at SciVerse ScienceDirect

Polyhedron

journal homepage: www.elsevier.com/locate/poly

Induction of photoluminescence and columnar mesomorphism in hemi-disc salphen type Schiff bases via nickel(II) coordination

Chira R. Bhattacharjee *, Chitraniva Datta, Gobinda Das, Rupam Chakrabarty, Paritosh Mondal

Department of Chemistry, Assam University, Silchar 788011, Assam, India

ARTICLE INFO

Article history:
Received 31 October 2011
Accepted 2 December 2011
Available online 13 December 2011

Keywords:
Nickel
Metallomesogen
Columnar mesomorphism
Density functional theory

ABSTRACT

A series of hemi-disc shaped non-mesomorphic tetradentate salicylaldimine ligands [*N*,*N*′-di-(4-hexadecyloxysalicylidene)-l,2-diamino-benzene, *N*,*N*′-di-(4-hexadecyloxysalicylidene)-4-Me-l,2-diamino-benzene, and *N*,*N*-di-(4-hexadecyloxysalicylidene)-4-NO_2-l,2-diamino-benzene, (H_2L)] were synthesized. Incorporation of nickel(II) in the tetradentate core via reaction with $Ni(OAc)_2{\cdot}4H_2O$ afforded a series of four coordinate mesogenic NiL derivatives. The ligands and complexes were characterized by elemental analyses, FT-IR, UV–Vis, FAB-mass, ^1H and ^{13}C NMR (for ligands only). The mesomorphic behavior of the complexes were probed by polarizing optical microscopy, differential scanning calorimetry and powder X-ray diffraction technique. The non-mesogenic ligands upon coordination with nickel(II) exhibited monotropic/enantiotropic phase transition showing rectangular columnar mesophases (Col_r) with *c*2*mm* symmetry. A antiparallel dimeric association forming a disc-like arrangement in the mesophase is proposed on the basis of XRD-study. Solution electrical conductivity measurements are consistent with the non-electrolytic nature of the complexes. At room temperature with 330 nm excitation, the complexes showed blue emission both in the solid state (~481 nm, $\Phi = 7\%$) and in solution (~456 nm, $\Phi = 23\%$) while the ligands are non-emissive. The DFT study carried out at BLYP/DNP level revealed a distorted square planar structure for the nickel(II) complexes.

1. Introduction

The technologies based on physical properties such as light emission or charge transport ability and related materials are currently receiving significant attention owing to their potential applications such as displays, solar cells, active components for image and data treatment storage etc. [1–5]. Of specific interest are luminescent liquid-crystalline materials that are considered very attractive for potential applications in optoelectronic devices because of their excellent charge-transport properties [1,3–10]. Combining luminescence properties in soft materials to generate new electronic devices is a fast growing field of research [3–10]. Design and synthesis of such luminescent photoresponsive liquid crystals is significant particularly in the context of their potential applications in organic light emitting diodes (OLEDs), information storage, sensors, and enhanced contrast displays [11,12]. Metallomesogens (metal containing liquid crystals) are ideal candidates for tuning smart multifunctional properties owing to the combination of optical, electronic and magnetic characteristics. Studies on light-emitting mesogens were mainly focused on organic compounds, while luminescent metallomesogens caught the fancy of researchers rather recently. Emissive metallomesogen with metals such as lanthanides, Zn, Pd, Pt, Au, and Ag have been well documented [6–10]. We recently developed a series of photoluminescent metallomesogen based on salicylaldimine Schiff-base ligands [11,13–15]. Transition metal complexes with salen-type ligands have been extensively studied mainly due to their ability to catalyze an extremely broad range of chemical transformations, including the asymmetric ring-opening of epoxides, aziridination, cyclopropanation, epoxidation of olefins and formation of cyclic and linear polycarbonates [16–19]. Moreover, nonlinear optical (NLO) properties of such materials have also been explored in recent years [20–23]. Nevertheless, application studies on metal–salen derivatives remained sparse in the literature, even though these compounds are known to be photoluminescent for a long time [20–25]. Choice of metal ion, nature and position of the substituents on side aromatic ring as well as spacers are known to greatly tune the mesogenic as well as photophysical behavior. For some compounds even a minor changes within the spacer can lead to major differences in molecular organization and in turn liquid-crystalline behavior [26–31]. Metal–salen complexes with 5-substituted alkoxy or alkyl chains exhibiting smectic mesomorphism are well documented [32–35]. Metallomesogen based on 4-substituted salen-type framework Schiff base ligands has been sparsely investigated [26–30]. Recently we have reported a series of structurally analogous 4-substituted zinc(II), oxovanadium(IV), Ni(II) as well as some copper(II) complexes, using cyclohexane/phenylene diamine spacer exhibited different type of columnar phase

* Corresponding author. Tel.: +91 03842 270848; fax: +91 03842 270342.
E-mail address: crbhattacharjee@rediffmail.com (C.R. Bhattacharjee).

0277-5387/$ - see front matter © 2011 Elsevier Ltd. All rights reserved.
doi:10.1016/j.poly.2011.12.001

[11,13,15,36–38]. Complexes with shorter alkoxy substituent, $[VO(4\text{-}C_nH_{2n+1}O)_2salen]ClO_4$ (n = 3, 8, 10) with similar spacer lacked liquid crystalline behavior [26]. When complexed with non-discoid ligands, a molecular shape with a reduced length-to-breadth ratio is formed favouring a disc-like metallomesogens [39]. Such structures tend to form columnar mesophases [39]. Compounds exhibiting columnar phases with axially linked discs are of particular interest as potential one-dimensional photoconductors, semiconductors, organic light emitting diodes (OLED) and photovoltaic cells [40–50]. A series of analogous nickel(II) complexes with cyclohexane spacer showing columnar rectangular mesophase have been reported recently by us [15]. However, there appears to be no record of nickel(II) complexes with rigid aromatic spacer. As a part of our continued and systematic investigation directed towards soft materials, in this article we describe synthesis of newer tetradentate Schiff base ligands bearing aromatic spacer with different electron withdrawing/donating substituent, and induction of luminescence and columnar mesomorphism via formation of hemi-disc shaped nickel(II) complexes. The ligands are non-mesogenic devoid of any luminescence.

2. Experimental

2.1. Physical measurements

The C, H and N analyses were carried out using PE2400 elemental analyzer. The ^{1}H NMR spectra were recorded on Bruker DPX-400 MHz spectrometer in $CDCl_3$ (chemical shift in δ) solution with TMS as internal standard. ^{13}C NMR spectra were recorded on a JEOL AL300 FT NMR spectrometer. Molar conductance of the compounds was determined in CH_2Cl_2 (ca. 10^{-3} mol L^{-1}) at room temperature using MAC-554 conductometer. UV–Vis absorption spectra of the compounds in CH_2Cl_2 were recorded on a Shimadzu UV-160PC spectrophotometer. Photoluminescence spectra were recorded on a Shimadzu RF-5301PC spectrophotometer. The fluorescence quantum yield in dichloromethane was determined by dilution method using 9,10-diphenyl anthracene as standard. Infrared spectra were recorded on a Perkin–Elmer L 120-000A spectrometer on KBr disc. Mass spectra were recorded on a Jeol SX-102 spectrometer with fast atom bombardment. The optical textures of the different phase of the compounds were studied using a polarizing microscope (Nikon optiphot-2-pol) attached with Instec hot and cold stage HCS302, with STC200 temperature controller of 0.1 °C accuracy. The thermal behavior of the compounds were studied using a Perkin–Elmer differential scanning calorimeter (DSC) Pyris-1 spectrometer with a heating or cooling rate of 5 °C/min. Variable temperature powder X-ray diffraction (PXRD) of the samples were recorded on a Bruker D8 Discover instrument using Cu Kα radiation.

2.2. Computational analysis

All the structures were completely optimized using the hybrid HF-DFT method, labeled as BLYP. The BLYP functional is comprised of a hybrid exchange functional as defined by Becke and the non-local Lee–Yang–Parr correlation functional [51]. We used DFT semicore pseudopotential with double numerical basis set plus polarization functions (DNP), which is comparable with the Gaussian 6-31G(d,p) basis set in size and quality [52]. All structures were relaxed without any symmetry constraints. Convergence in energy, force, and displacement was set as 10^{-5} Hartree (Ha), 0.001 Ha/Å, and 0.005 Å, respectively. All calculations were performed with the DMol3 program package [52–54].

Global hardness (η) of an electronic system is defined [55] as the second derivative of total energy (E) with respect to the number of electrons (N) at constant external potential, $v(\vec{r})$

$$\eta = \frac{1}{2}\left(\frac{\delta^2 E}{\delta N^2}\right)_{v(r)} = \left(\frac{\delta \mu}{\delta N}\right)_{v(\vec{r})}$$

Global softness is the inverse of global hardness with a factor of half

$$S = \frac{1}{2\eta} = \left(\frac{\delta^2 N}{\delta E^2}\right)_{v(\vec{r})} = \left(\frac{\delta N}{\delta \mu}\right)_{v(\vec{r})}$$

By applying finite difference approximation the global hardness and softness are expressed as:

$$\eta = \frac{\mathrm{IE} - \mathrm{EA}}{2}, \quad S = \frac{1}{\mathrm{IE} - \mathrm{EA}}$$

where IE and EA are the first vertical ionization energy and the electron affinity of the molecule, respectively. Using Koopmans' theorem IE and EA can be approximated as negative of E_{HOMO} and E_{LUMO}, respectively and thus chemical hardness and chemical softness can be written as [56].

$$\eta = \frac{E_{\mathrm{LUMO}} - E_{\mathrm{HOMO}}}{2} \quad \text{and} \quad S = \frac{2}{E_{\mathrm{LUMO}} - E_{\mathrm{HOMO}}}, \quad \text{respectively.}$$

2.3. Materials

The materials were procured from Tokyo Kasei and Lancaster Chemicals. All solvents were purified and dried using standard procedures. Silica (60–120 mesh) from Spectrochem was used for chromatographic separation. Silica gel G (E-Merck, India) was used for TLC.

2.4. Synthesis of hexadecyloxysalicyldehyde

Alkoxysalicyldehyde derivatives were prepared following reported method [11,13,15,36–38]. 2,4-Dihydroxybenzaldehyde (10 cm^3, 1.38 g), $KHCO_3$ (10 cm^3, 1.00 g), KI (catalytic amount) and 1-bromohexadecane (10 cm^3, 2.8 g) were mixed in 250 mL of dry acetone. The mixture was heated under reflux for 24 h, and then filtered, while hot, to remove any insoluble solids. Dilute HCl was added to neutralize the warm solution followed by extraction with chloroform (100 cm^3). The combined chloroform extract was concentrated to give a purple solid. The solid was purified by column chromatography using a mixture of chloroform and hexane (v/v, 1/1) as eluent. Evaporation of the solvents afforded a white solid product.

Synthesis of 16-opd and 16-mpd are reported in our earlier observations [11,13].

2.4.1. Synthesis of N,N′-bis(4-(4′-hexadecyloxy)-salicylidene)-4-NO_2-1,2-phenylenediamine (16-npd)

An ethanolic solution of 2-hydroxy-(4-hexadecyloxy)-salicylaldehyde (0.39 g, 1 mmol) was added to an ethanolic solution of 4-NO_2-1,2-phenylenediamine (0.07 g, 0.5 mmol). The solution mixture was refluxed with a few drops of acetic acid as catalyst for 3 h to yield the yellow Schiff base *N,N′*-bis(4-(4′-*n*-alkoxy)-salicylidene)-4-NO_2-1,2-phenylenediamine. The compound was collected by filtration and recrystallized from absolute ethanol to obtain a pure compound.

Yield: 0.33 g, 75%. FAB Mass (*m*/*e*, fragment): *m*/*z*: calc. 841.6; found: 842.6 [M+H$^+$]; *Anal.* Calc. for $C_{52}H_{79}N_3O_6$: C, 74.1; H, 9.4; N, 4.9. Found: C, 74.2; H, 9.5; N, 4.8%. ^{1}H NMR (400 MHz, $CDCl_3$): δ = 13.02 (s, 1H, H^5), 8.78 (s, 1H, H^4), 7.79 (d, J = 8.4 Hz, H^9), 7.25 (d, 2H, H^6), 7.18 (t, J = 8.2 Hz, 2H, H^1), 6.69 (d, J = 2.5 Hz, 2H, H^3), 6.97 (dd, J = 2.4 Hz, J = 8.3 Hz, 2H, H^2), 3.98(t, J = 6.6 Hz, 2H, –OCH_2), 0.96 (t, J = 6.7 Hz, 6H, CH_3), 0.98 (m, –CH_2 of methylene pro-

ton in side chain); IR (ν_{max}, cm^{-1}, KBr): 3513 (νOH), 2922 (ν_{as}(C–H), CH_3), 2873 (ν_s(C–H), CH_3), 1625 (νC=N), 1294 (ν(C–O)).

2.4.2. Synthesis of nickel(II) complexes

General procedure. The ligand 16-opd (0.79 g, 1 mmol) or 16-mpd (0.81 g, 1 mmol) or 16-npd (0.84 g, 1 mmol) was dissolved in minimum volume of absolute ethanol. To this, an equimolar amount of nickel acetate $Ni(OAc)_2{\cdot}4H_2O$ (0.02 g, 0.1 mmol) in methanol was then added slowly and stirred for 2 h at room temperature. A red solid formed immediately was filtered, washed with diethyl ether and recrystallized from chloroform–ethanol (1:1).

Ni-16opd. Yield = 0.60 g (75%). FAB Mass (*m*/*e*, fragment): *m*/*z*: calc. 852.5; found: 853.5 [M+H$^+$]; *Anal*. Calc. for $C_{52}H_{78}N_2O_4Ni$: C, 73.1; H, 9.2; N, 3.2. Found: C, 73.1; H, 9.2; N, 3.1%. ^{1}H NMR (400 MHz, $CDCl_3$): δ = 8.22 (s, 1H, H^4), 7.69 (d, *J* = 8.5 Hz, H^9), 7.17 (d, 2H, H^6), 7.10 (t, *J* = 8.4 Hz, 2H, H^1), 7.16 (dd, *J* = 2.3 Hz, *J* = 9.1, 2H, H^8), 6.61 (d, *J* = 2.4 Hz, 2H, H^3), 6.49 (dd, *J* = 2.4 Hz, *J* = 8.2 Hz, 2H, H^2), 3.95 (t, *J* = 6.8 Hz, 2H, –OCH_2), 0.91 (t, *J* = 6.8 Hz, 6H, CH_3), 0.87 (m, –CH_2 of methylene proton in side chain); IR (ν_{max}, cm^{-1}, KBr): 2922 (ν_{as}(C–H), CH_3), 2870 (ν_s(C–H), CH_3), 1611 (νC=N), 534 (ν_{Ni-N}), 459 (ν_{Ni-O}).

Ni-16mpd. Yield = 0.22 g, 76%. FAB Mass (*m*/*e*, fragment): *m*/*z*: calc. 866.5; found: 867.5 [M+H$^+$]; *Anal*. Calc. for $C_{53}H_{80}N_2O_4Ni$: C, 73.3; H, 9.2; N, 3.2. Found: C, 73.4; H, 9.3; N, 3.1%. ^{1}H NMR (400 MHz, $CDCl_3$): δ = 8.19 (s, 1H, H^4), 7.72 (d, *J* = 8.5 Hz, H^9), 7.21 (d, 2H, H^6), 7.11 (t, *J* = 8.4 Hz, 2H, H^1), 7.16 (dd, *J* = 2.33 Hz, *J* = 9.1, 2H, H^8), 6.61 (d, *J* = 2.4 Hz, 2H, H^3), 6.49 (dd, *J* = 2.44 Hz, *J* = 8.28 Hz, 2H, H^2), 3.92 (t, *J* = 6.8 Hz, 2H, –OCH_2), 0.91 (t, *J* = 6.8 Hz, 6H, CH_3), 0.87 (m, –CH_2 of methylene proton in side chain); IR (ν_{max}, cm^{-1}, KBr): 2922 (ν_{as}(C–H), CH_3), 2870 (ν_s(C–H), CH_3), 1613 (νC=N), 532 (ν_{Ni-N}), 461 (ν_{Ni-O}).

Ni-16npd. Yield = 0.64 g, 75%. FAB Mass (*m*/*e*, fragment): *m*/*z*: calc. 897.5; found: 898.5 [M+H$^+$]; *Anal*. Calc. for $C_{52}H_{77}N_3O_6Ni$: C, 69.4; H, 8.6; N, 4.6. Found: C, 69.3; H, 8.5; N, 4.5%. ^{1}H NMR (400 MHz, $CDCl_3$): δ = 8.23 (s, 1H, H^4), 7.77 (d, *J* = 8.5 Hz, H^9), 7.25 (d, 2H, H^6), 7.17 (t, *J* = 8.4 Hz, 2H, H^1), 7.18 (dd, *J* = 2.33 Hz, *J* = 9.1, 2H, H^8), 6.64 (d, *J* = 2.45 Hz, 2H, H^3), 6.42 (dd, *J* = 2.4 Hz, *J* = 8.2 Hz, 2H, H^2), 3.93 (t, *J* = 6.5 Hz, 2H, –OCH_2), 0.90 (t, *J* = 6.8 Hz, 6H, CH_3), 0.88 (m, –CH_2 of methylene proton in side chain); IR (ν_{max}, cm^{-1}, KBr): 2921 (ν_{as}(C–H), CH_3), 2870 (ν_s(C–H), CH_3), 1616 (νC=N), 531 (ν_{Ni-N}), 457 (ν_{Ni-O}).

3. Results and discussion

3.1. Synthesis and structural assessment

The compounds (16-opd/16-mpd/16-npd and Ni-16opd/Ni-16mpd/Ni-16npd) could be achieved through a facile and straightforward procedure [11,13,15,36–38]. The synthetic strategy for the ligands [(L = *N*,*N*′-bis(4-(4′-*n*-hexadecyloxy)-salicylidene)1,2-phenylenediamine/4-Me-1,2-phenylenediamine/4-NO_2-1,2-phenylenediamine), hereafter abbreviated as 16-opd/16-mpd/16-npd] and the Ni(II) complexes (Ni-16opd/Ni-16mpd/Ni-16npd) are presented in Scheme 1. The complexes (Ni-16opd/Ni-16mpd/Ni-16npd), were prepared by the reaction of appropriate ligand with nickel acetate (1:1 molar ratio) in ethanol/methanol and recrystallized from methanol/CH_2Cl_2; the complexes were isolated as red colored solids in good yields. The compounds were characterized by ^{1}H and ^{13}C NMR, FT-IR, UV–Vis spectroscopy and elemental analysis. From the IR study, it was found that the shift of ν_{CN} vibrational stretching frequency at ca.1625 cm^{-1} to lower wave number ($\Delta\nu \sim 30$ cm^{-1}) and absence of ν_{OH} mode upon chelation, clearly suggested the coordination of azomethine-N and phenolate-O to the metal. Appearance of additional bands at ~450–480 and ~527–549 cm^{-1} in the spectra of the complexes assigned to Ni–O and Ni–N stretching vibrations that are not observed in the spectra of the ligands furnished evidence for [N,O] binding mode of the ligand. The $\nu_{C=N}$ stretching frequency is rather independent of the length of alkoxy side chain in both ligands and their complexes. The FAB-mass spectra of the compounds matched well with their formula weights. Solution electrical conductivity of complexes recorded in CH_2Cl_2 (10^{-3} M) was found to be <10 Ω^{-1} cm^{-1} mol^{-1}, much lower than is expected for a 1:1 electrolyte, thus confirming the non-electrolytic nature of the complex. ^{1}H NMR spectra of the ligands showed two characteristic signals at δ = 13.4–13.8 ppm corresponding to the OH proton and at δ = 8.5 ppm due to the imine proton. Moreover upon complexation, lack of proton signal corresponding to the OH group of the free ligands and the upfield shift of the imine proton further attested the coordination of azomethine-N.

3.2. Photophysical properties

The electronic spectra of the free ligands exhibited three bands (Fig. 1) in the region of ~288–366 nm assigned to π–π^* transitions, which involves molecular orbitals essentially localized on the C=N group and the benzene ring. The absorption maxima are red shifted in 16-npd ligand owing to the presence of the NO_2 chromophore in the ligand. The complexes exhibited two intense red shifted bands (Fig. 2) at ~312–325 nm and ~383–401 nm resulting from the metal-perturbed ligand-centered transitions, which have the same origin as the two principal bands of the ligand spectrum. In addition, the complexes also displayed a broad unstructured low intensity band centered at ~447–462 nm assigned to ligand to metal charge transfer transitions (LMCT) charge transfer transition ($N \rightarrow Ni^{2+}$) which might have obscured the d–d bands.

The photoluminescence properties of the compounds were investigated in dichloromethane solution and in thin films, at room temperature. The ligands are non-emissive, but their corresponding Ni(II) complexes displayed strong blue emission both in solution and solid state (Fig. 3), usually observed in similar Schiff-based metal complexes, with the emission maximum centered at ~454–488 nm originating from π–π^* singlet ligand-centered excited state [57–60,32]. The emission maxima for typical compound Ni-18opd in solid state (~481 nm, Φ = 7%) is considerably red shifted with respect to that recorded in solution (~456 nm, Φ = 23%). In solid state after complexation, the free rotation of the flexible bonds of the ligand is reduced and hence energy dissipation through non-radiative channels decreases leading to shift of emission wavelength to lower energy. Moreover in the solid state, a larger electronic delocalization and intermolecular aromatic interaction leads to a lowering of energy of the electronic states [57–60,32]. The spectral data are summarized in Table 1.

3.3. Thermal microscopy and differential scanning calorimetry study

The thermal behavior of the compounds (Table 2) was investigated by polarizing optical microscopy (POM) and differential scanning calorimetry (DSC) study. The ligands are found to be non-mesomorphic. However, on co-ordination to nickel(II) ion mesomorphism was induced, reflecting conformational rigidification of the ligand on complexation. Monotropic mesomorphism was encountered for Ni-16npd and Ni-16mpd complexes. The Ni-16opd showed enantiotropic mesomorphic behavior. Polarized optical microscopy of a representative complex (Ni-16opd) revealed that, upon cooling the sample from isotropic phase, a spherulitic growth appeared which coalesce to a fan-like texture (Fig. 4) at ~130 °C with large homeotropic regions, suggesting a columnar mesophase (Col). The mesophase is stable down to room temperature. The DSC thermogram (Fig. 5) for the complex (Ni-16opd) exhibited two transitions in heating and two in cooling cycle.

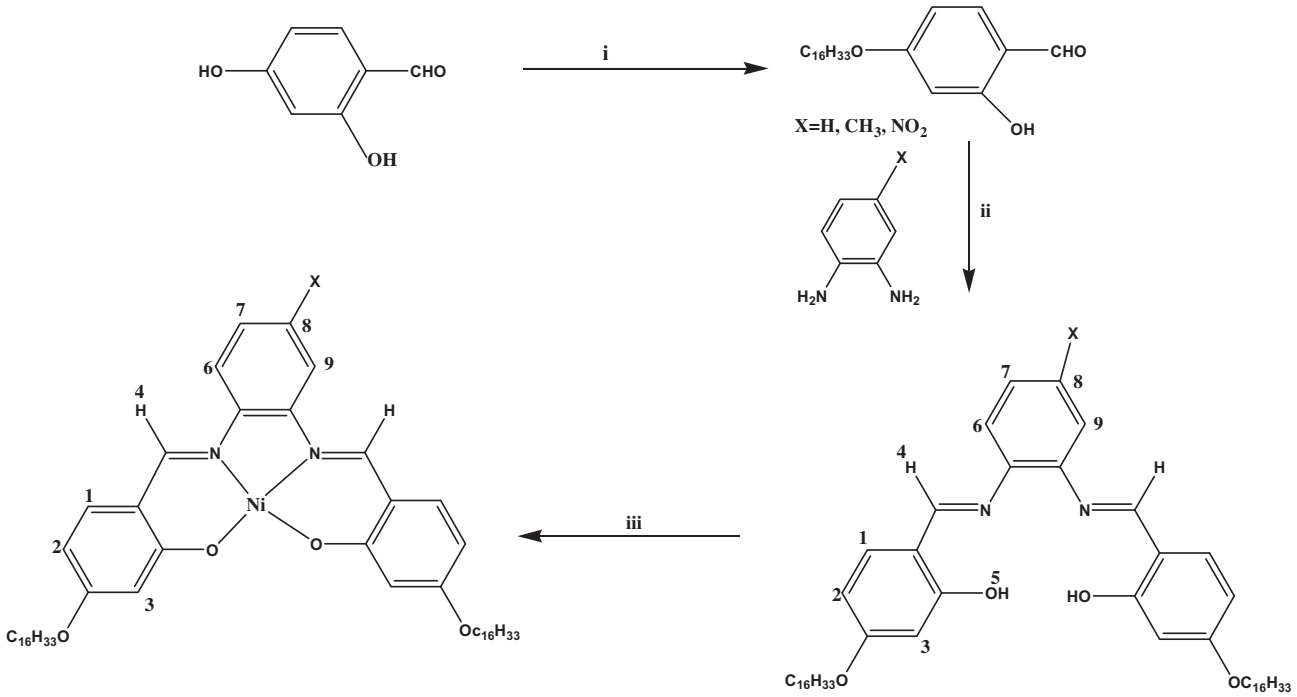

Scheme 1. (i) $C_{16}H_{33}Br$, $KHCO_3$, KI, dry acetone, Δ, 40 h, (ii) glacial AcOH, absolute EtOH, Δ, 4 h and (iii) $Ni(OAc)_2{\cdot}4H_2O$, MeOH, Stirr, 2 h.

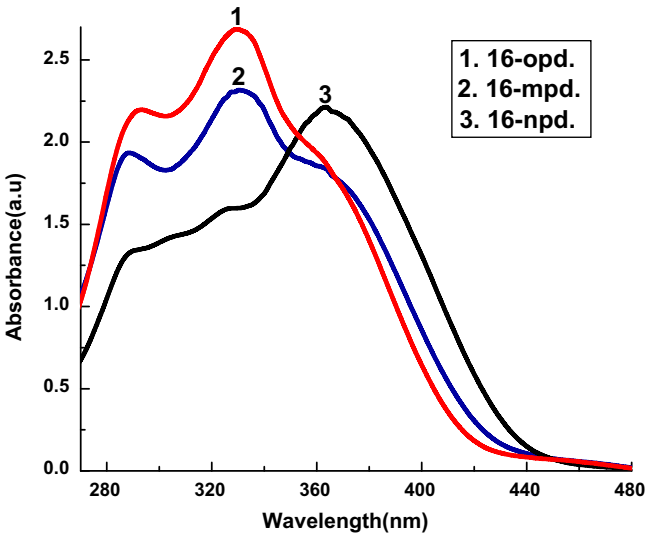

Fig. 1. Absorption spectra of the ligands.

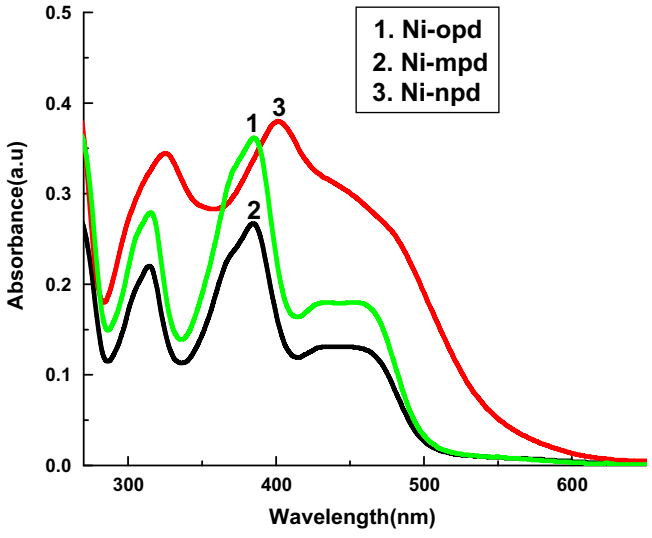

Fig. 2. Absorption spectra of the complexes.

The melting temperatures of the complexes showed a decreasing trend with X = H, CH_3, and NO_2 in that order (Table 2). The isotropisation temperatures, however, reflected a different trend with the nitro substituted complex exhibiting highest value (209.2 °C) and the methyl substituted one showing the least (125.2 °C). Another interesting aspect is the quite low enthalpy values for the phase transitions in the unsubstituted complex (Ni-16opd) compared to those observed for the substituted ones (Ni-16mpd and Ni-16npd). In general, complexes with higher molecular weights tend to exhibit larger enthalpy changes during mesophase to isotropic liquid transitions [27]. Relatively high enthalpies for mesophase transition to isotropic state in the substituted complexes, Ni-16mpd and Ni-16npd could be indicative of the formation of a higher order columnar phase in this system [61].

In our earlier reports, we have found that, the VO-16opd showed lamellar columnar mesomorphism (Col_l) [36]. However, Zn-16opd/Zn-16mpd complexes exhibited columnar rectangular (Col_r/Col_h) mesophase [11,13].

3.4. XRD-study

The mesophase structure was confirmed by temperature-dependent X-ray diffraction analysis (Table 3). The spectrum was recorded for a typical compound, Ni-16opd at 130 °C. In the low angle region two fundamental sharp reflections were observed characteristic of a rectangular columnar mesophase (Fig. 6). Further, there are two diffuse reflections in the wide angle region. One corresponds to 4.9 Å, for molten alkyl chains, the

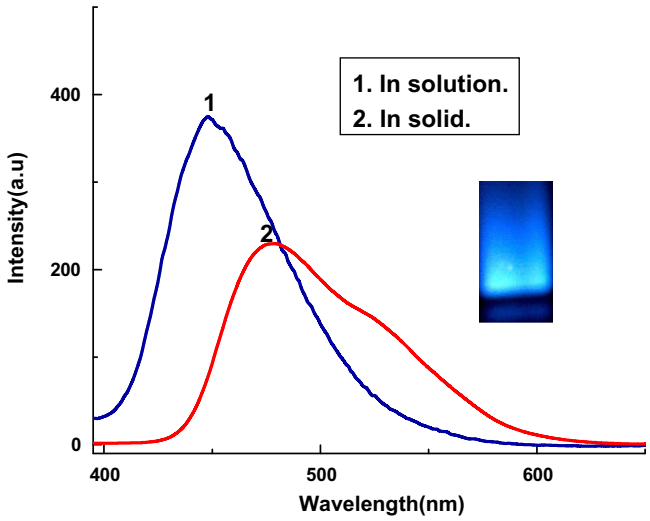

Fig. 3. Emission spectra of the Ni-16opd complex.

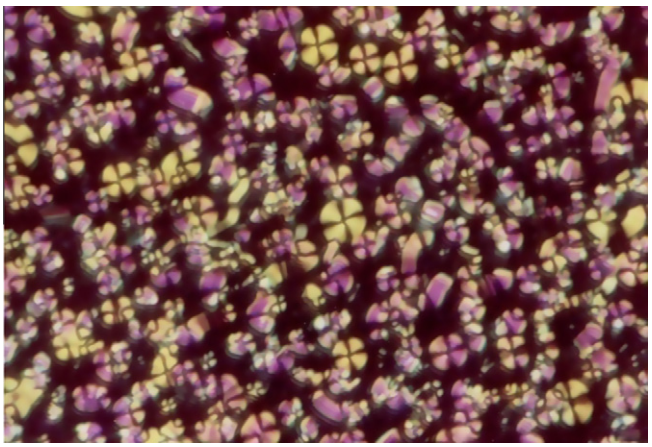

Fig. 4. POM texture of Ni-16opd complex.

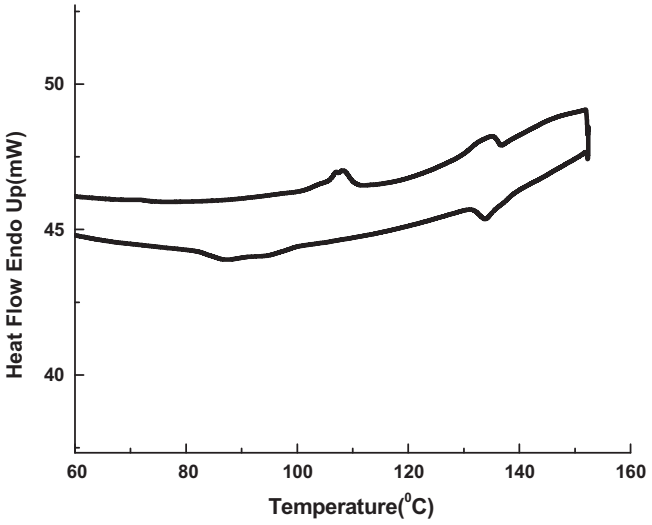

Fig. 5. DSC thermogram of Ni-16opd complex.

Table 1
UV–Vis and photoluminescence data of the compounds.

Compounds	$\pi \rightarrow \pi^*$ (ε, l mol^{-1} cm^{-1})	LMCT (ε, l mol^{-1} cm^{-1})	PL[a] (solution)	PL[a] (solid)
16opd	292 nm (22000) 329 nm (26800) 363 nm (18981)			
Ni-16opd	315 nm (2770) 385 nm (3610)	447 nm (1800)	456 nm	481 nm
16mpd	289 nm (19300) 330 nm (23100) 365 nm (18110)			
Ni-16mpd	314 nm (2200) 385 nm (2670)	448 nm (1310)	454 nm	478 nm
16npd	295 nm (13400) 335 nm (16851) 367 nm (21850)			
Ni-16npd	326 nm (3450) 402 nm (3800)	462 nm (2820)	468 nm	488 nm

[a] Photoluminescence data.

Table 2
POM and DSC data of the complexes.

Compounds	T (°C)	Transition	ΔH (kJ mol^{-1})
Ni-16opd	108.2 (heating)	Cr–Col$_r$	2.9
	135.0 (heating)	Col$_r$–I	2.6
	133.9 (cooling)	I–Col$_r$	2.5
	87.1 (cooling)	Col$_r$–Cr	0.93
Ni-16mpd	84.4 (heating)	Cr–Col$_r$	12.8
	125.2 (heating)	Col$_r$–I	12.9
Ni-16npd	78.3 (heating)	Cr–Col$_r$	14.8
	209.2 (heating)	Col$_r$–I	15.4

relatively sharper one at about 3.6 Å, well separated from the broad peak is due to the regular stacking of the molecules within the columnar mesophase. In the wide angle region the presence of another less broad peak at about 7.6 Å may indicate the formation of dimers (Fig. 7) along the axis of the column. Moreover, due to the absence of (21) peak in the XRD spectrum, the symmetry of the lattice can be further assigned to a *c2mm* plane group [39,62,63]. The lattice constants of this rectangular phase are a = 38.2 Å and b = 15.4 Å. The lattice parameter a = 38.2 Å is larger than the radius of the half-disc shaped molecule (~20.6 Å). Therefore the hemi-disc molecules in the mesophase are believed to organize themselves in an anti-parallel fashion (Fig. 7). A similar type of molecular self assembly was reported earlier [15,37,39,64].

3.5. DFT-study

The optimized structure of the complex is shown in (Fig. 8). The complexes are neutral with Ni^{2+} in d^8-system. We optimized singlet and triplet state of the complexes and found singlet square planar geometry is more stable. The 3D isosurface plots of the lowest unoccupied molecular orbital (LUMO) and the highest occupied molecular orbital (HOMO) for the nickel complex (Ni-16opd) is shown in (Figs. 9 and 10). In all the complexes, electron density of the HOMO is mainly localized in between Ni–O and Ni–N bonds, while the electron density of the LUMO is localized on nickel atoms. The Ni–O (apical) interaction in the dimer (Figs. 9 and 10) expectedly occur between molecular orbitals of sigma (O) and pi*(Ni). The HOMO, LUMO energy difference of the complexes depends on the electronic nature of the substituents [65–67]. The energy differences decrease in the order of Ni-16mpd > Ni-16opd > Ni-16npd. The HOMO–LUMO energy separation can be used as a measure of

Table 3
XRD-data of the Ni-16opd.

Compound	$D_{obs.}$ (Å)[a]	$D_{calc.}$ (Å)[b]	hk[c]	Parameters[d]
Ni-16opd	19.3	19.2	20	$Col_r - c2mm$
	14.1	14.3	11	a = 38.2 Å
	10.3	10.4	31	b = 15.4 Å
	7.6			S = 588.3 Å^2
	4.9			V_m = 1551 Å^3
	3.5			h = 2.1 Å
				S_{col} = 294.1

[a] $D_{obs.}$ is experimentally and theoretically measured diffraction spacings at 130 °C.
[b] $D_{calc.}$ is experimentally and theoretically measured diffraction spacings at 130 °C.
[c] hk are indexation of the reflections.
[d] Mesophase parameters, molecular volume V_m is calculated using the formula: $V_m = M/\lambda\rho NA$, where M is the molecular weight of the compound, N_A is the Avogadro number, ρ is the volume mass ($\approx$1 g cm^{-3}), and $\lambda(T)$ is a temperature correction coefficient at the temperature of the experiment (T). $\lambda = VCH_2(T_0)/VCH_2(T)$, T_0 = 25 °C. $VCH_2(T) = 26.5616 + 0.02023(T)$. h is the intermolecular repeating distance deduced directly from the measured molecular volume and the lattice area according to $h = V_m/S$. For the Col_r phase, the lattice parameters a and b are deduced from the mathematical expression: $a = 2d_{20}$ and $1/d_{hk} = \sqrt{h^2/a^2 + k^2/b^2}$, where a, b are the parameters of the Col_r phase, S is the lattice area, S_{col} is the columnar cross-section ($S = ab$, $S_{col} = S/2$).

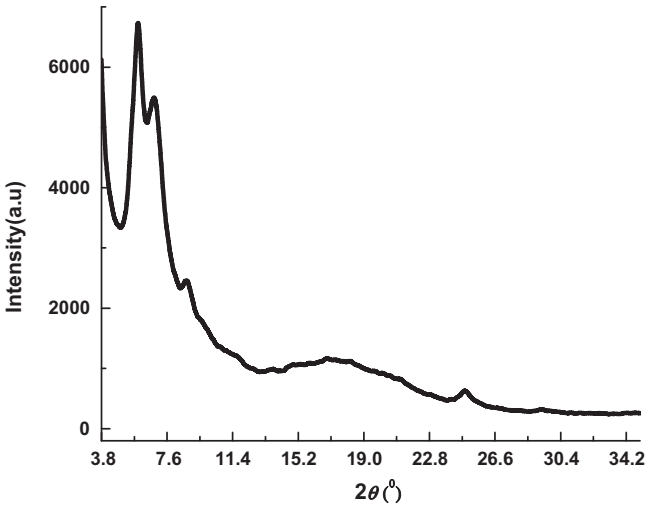

Fig. 6. XRD-pattern of Ni-16opd.

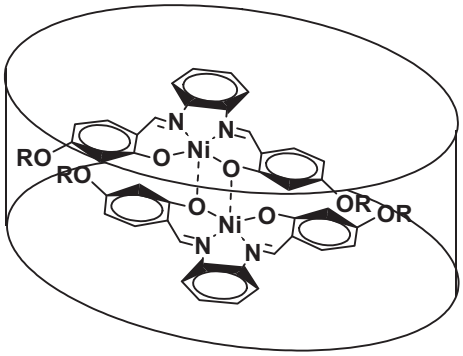

Fig. 7. Dimeric interaction of molecules.

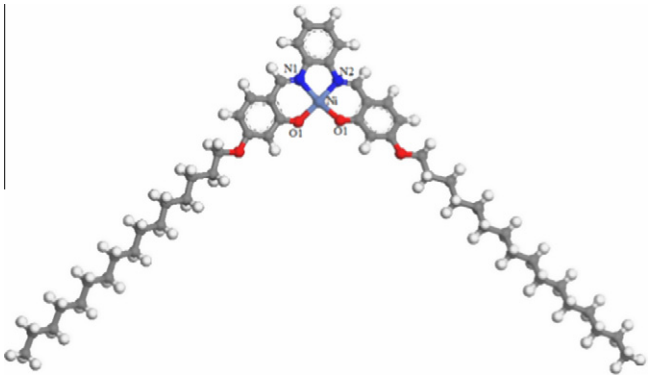

Fig. 8. Optimized structure of Ni-16opd.

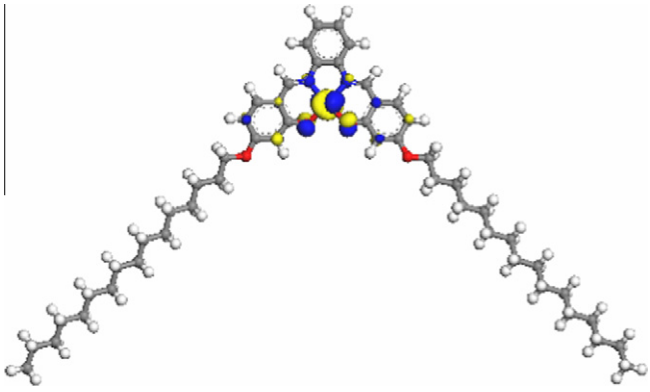

Fig. 9. LUMO energy diagram of Ni-16opd.

kinetic stability of the molecule and could indicate the reactivity pattern of the molecule. A small HOMO–LUMO gap implies a low kinetic stability and high chemical reactivity, because it is energetically favorable to add electrons to LUMO or to extract electrons from a HOMO. We further calculated the chemical softness values for both model complexes from their HOMO and LUMO energies. The chemical softness values of hydrogen, methyl and nitro-substituted complexes are 2.058, 2.051 and 3.643 eV^{-1}, respectively. The higher softness value obtained for the later complex indicated the lower stability of the complex compared to the hydrogen and methyl containing one. Some of the selective geometric parameters of optimized hydrogen, methyl and nitro-substituted nickel complex, evaluated by DFT calculation at BLYP/DNP level are reported in Table 4. From DFT data, it is noticed that the complexes have an average Ni–O and Ni–N bond lengths are in the range of 1.93–1.92 and 2.00–1.99 Å, respectively. The average bond angles are in the range of 94.70–92.8 and 83.20–83.6 for O1–Ni–O2 and N1–Ni–N2, respectively, around the nickel atom deviate substantially from the tetrahedral values indicating a distorted planar four coordinate geometry. The dihedral angles O(1)O(2)N(1)N(2) and N(1)O(1)O(2)N(2) as computed from DFT are found to lie in the range 15–20° (Table 4) reflecting the deviation from planarity. A strained conformation of the $[N_2O_2]$-donor tetradentate ligand with long pendant alkyl side chains is believed to have caused the deviation from planar symmetry. Moreover, a short rigid central spacer group in the present complexes presumably prevented the formation of a tetrahedral environment around nickel(II), leading to a distorted square planar geometry. The length of the complexes based on the fully extended structure is found to be ~40.7 Å (measured from the two terminal end of the side alkyl chain).

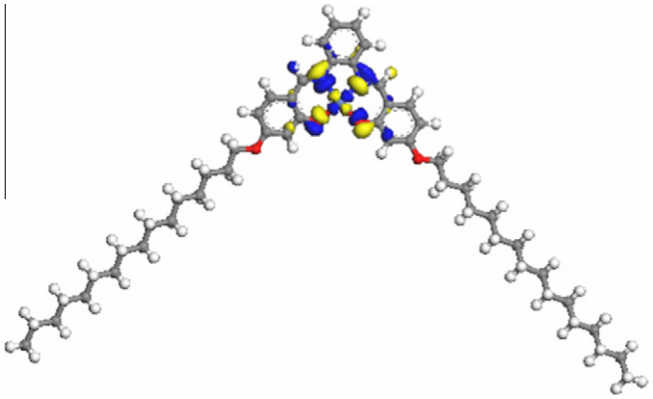

Fig. 10. HOMO energy diagram of Ni-16opd.

Table 4
DFT data of the complexes. Bond lengths are reported in Å and bond angles in degrees.

Structure parameter	Ni-opd	Ni-mpd	Ni-npd
Ni–O(1)	1.929	1.930	1.921
Ni–O(2)	1.930	1.931	1.919
Ni–N(1)	1.999	1.999	1.989
Ni–N(2)	1.999	2.001	1.983
O(1)–Ni–O(2)	94.67	94.58	92.84
N(1)–Ni–N(2)	83.16	83.20	83.56
N(1)–Ni–O(2)	165.14	165.65	167.55
O(1)–Ni–N(1)	92.76	92.71	92.72
O(1)–Ni–N(2)	165.29	165.45	167.98
N(2)–Ni–O(2)	92.63	92.58	93.09
HOMO in eV	−3.584	−3.542	−3.920
LUMO in eV	−2.612	−2.567	−3.371
ΔE in eV	0.972	0.975	0.549
Chemical softness	2.058	2.051	3.643
O(1)O(2)N(2)N(1)	19.3	18.8	16.2
N(1)O(1)O(2)N(2)	17.9	17.5	15.0

4. Conclusion

A new series of Ni(II)–salphen complexes bearing differently substituted aromatic spacer have been successfully synthesized. Lower conductivity values confirm the non electrolytic nature of the complexes. The ligands are found to be non-mesogenic and non-luminescent, however, all the complexes exhibited unprecedented columnar rectangular structure with *c2mm* symmetry and also exhibited intense blue light emission both in solid state and solution. Based on the spectral and DFT study, a distorted square planar geometry around the Ni(II) center have been conjectured. The mesomorphic behavior of the complexes as a function of the spacer substituent is collated.

Acknowledgments

The authors thank SAIF, NEHU and CDRI, Lucknow for analytical and spectral data. CD acknowledges financial support from UGC, Government of India. Dr. R.C. Deka, Tezpur University, India, is acknowledged for computational facility.

References

[1] Y. Molard, F. Dorson, V. Circu, T. Roisnel, F. Artzner, S. Cordier, Angew. Chem., Int. Ed. 49 (2010) 3351.
[2] C.S. Pecinovsky, E.S. Hatakeyama, D.L. Gin, Adv. Mater. 20 (2008) 174.
[3] X. Feng, W. Pisula, L. Zhi, M. Takase, K. Mullen, Angew. Chem., Int. Ed. 47 (2008) 1703.
[4] M.J. Baena, P. Espinet, C.L. Folcia, J. Ortega, J. Etxebarria, Inorg. Chem. 49 (2010) 8904.
[5] J. Arias, M. Bardaji, P. Espinet, C.L. Folcia, J. Ortega, J. Etxebarria, Inorg. Chem. 48 (2009) 6205.
[6] E. Terazzi, S. Torelli, G. Bernardinelli, J.-P. Rivera, J.-M. Benech, C. Bourgogne, B. Donnio, D. Guillon, D. Imbert, J.-C.G. Bunzli, A. Pinto, D. Jeannerat, C. Piguet, J. Am. Chem. Soc. 127 (2005) 888.
[7] M. Ghedini, D. Pucci, A. Crispini, A. Bellusci, M. La Deda, I. Aiello, T. Pugliese, Inorg. Chem. Commun. 10 (2007) 243.
[8] F. Camerel, R. Ziessel, B. Donnio, C. Bourgogne, D. Guillon, M. Schmutz, C. Iacovita, J.-P. Bucher, Angew. Chem., Int. Ed. 46 (2007) 2659.
[9] V.N. Kozhevnikov, B. Donnio, D.W. Bruce, Angew. Chem., Int. Ed. 47 (2008) 6286.
[10] D. Pucci, G. Barberio, A. Bellusci, A. Crispini, M. La Deda, M. Ghedini, E.I. Szerb, Eur. J. Inorg. Chem. (2005) 2457.
[11] C.R. Bhattacharjee, G. Das, P. Mondal, N.V.S. Rao, Polyhedron 29 (2010) 3089.
[12] K. Binnemans, J. Mater. Chem. 19 (2009) 448.
[13] C.R. Bhattacharjee, G. Das, P. Mondal, S.K. Prasad, D.S.S. Rao, Eur. J. Inorg. Chem. (2011) 1418.
[14] C.R. Bhattacharjee, G. Das, P. Goswami, P. Mondal, S.K. Prasad, D.S.S. Rao, Polyhedron 30 (2011) 1040.
[15] C.R. Bhattacharjee, G. Das, P. Mondal, Eur. J. Inorg. Chem. (2011) 5390.
[16] P.G. Cozzi, L.S. Dolci, A. Garelli, M. Montalti, L. Prodi, N. Zaccheroni, New J. Chem. 27 (2003) 692.
[17] P.G. Cozzi, Chem. Soc. Rev. 33 (2004) 410.
[18] C. Gennari, U. Piarulli, Chem. Rev. 103 (2003) 3071.
[19] R.I. Kureshy, I. Ahmad, N.H. Khan, S.H.R. Abdi, K. Pathak, J. Catal. 238 (2006) 134.
[20] V. Aubert, V. Guerchais, E. Ishow, K.T. Hoang, I. Ledoux, K. Nakatani, L.H. Bozec, Angew. Chem., Int. Ed. 47 (2008) 577.
[21] B.J. Coe, in: J.A. McCleverty, T.J. Meyer (Eds.), Comprehensive Coordination Chemistry II, vol. 9, Elsevier Pergamon, Oxford, 2004, pp. 621–687.
[22] J. Chiffre, F. Averseng, G.G.A. Balavoine, J.-C. Daran, G. Iftime, P.G. Lacroix, E. Manoury, K. Nakatani, Eur. J. Inorg. Chem. (2001) 2221.
[23] I. Sasaki, L. Vender, A.S. Saquet, P.G. Lacroix, Eur. J. Inorg. Chem. (2006) 3294.
[24] I. Aiello, M. Ghedini, F. Neve, D. Pucci, Chem. Mater. 9 (1997) 2107.
[25] A.K. Singh, S. Kumari, K.R. Kumar, B. Sridhar, T.R. Rao, Polyhedron 27 (2008) 181.
[26] Y. Abe, A. Iyoda, K. Seto, A. Moriguchi, T. Tanase, H. Yokoyama, Eur. J. Inorg. Chem. (2008) 2148.
[27] Y. Abe, K. Nakabayashi, N. Matsukawa, H. Takashima, M. Iida, T. Tanase, M. Sugibayashi, H. Mukai, K. Ohta, Inorg. Chim. Acta 359 (2006) 3934.
[28] Y. Abe, N. Nakazima, T. Tanase, S. Katano, H. Mukai, K. Ohta, Mol. Cryst. Liq. Cryst. 466 (2007) 129.
[29] Y. Abe, K. Nakabayashi, N. Matsukawa, M. Iida, T. Tanase, M. Sugibayashia, K. Ohta, Inorg. Chem. Commun. 7 (2004) 580.
[30] Y. Abe, H. Akao, Y. Yoshida, H. Takashima, T. Tanase, H. Mukai, K. Ohta, Inorg. Chim. Acta 359 (2006) 3147.
[31] A. Glebowska, P. Przybylski, M. Winek, P. Krzyczkowaska, A. Krowczynski, Z. Szydlowska, D. Pociecha, E. Gorecka, J. Mater. Chem. 19 (2009) 1395.
[32] E. Cavero, S. Uriel, P. Romero, J.L. Serrano, R. Giménez, J. Am. Chem. Soc. 129 (2007) 11608.
[33] Z. Rezvani, A.R. Abbasi, K. Nejati, M. Seyedahmadian, Polyhedron 24 (2005) 1461.
[34] K. Nejati, Z. Rezvani, New J. Chem. 27 (2003) 1665.
[35] Z. Rezvani, M.A. Ghanea, K. Nejati, S.A. Baghaei, Polyhedron 28 (2009) 2913.
[36] C.R. Bhattacharjee, G. Das, P. Mondal, S.K. Prasad, D.S.S. Rao, Inorg. Chem. Commun. 14 (2011) 606.
[37] C.R. Bhattacharjee, G. Das, P. Mondal, Liq. Cryst. 38 (2011) 441.
[38] C.R. Bhattacharjee, G. Das, P. Mondal, S.K. Prasad, D.S.S. Rao, Liq. Cryst. 38 (2011) 615.
[39] F. Morale, R.W. Date, D. Guillon, D.W. Bruce, R.L. Finn, C. Wilson, A.J. Blake, M. Schroder, B. Donnio, Chem. Eur. J. 9 (2003) 2484.
[40] S. Kumar, Chem. Soc. Rev. 35 (2006) 83.
[41] J.W. Goodby, V. Gortz, S.J. Cowling, G. Mackenzie, P. Martin, D. Plusquellec, T. Benvegnu, P. Boullanger, D. Lafont, Y. Queneau, S. Chambert, J. Fitremann, Chem. Soc. Rev. 36 (2007) 1971.
[42] M. O'Neill, S.M. Kelly, Adv. Mater. 15 (2003) 1135.
[43] R. Cristiano, H. Gallardo, A.J. Bortoluzzi, I.H. Bechtold, C.E.M. Campos, R.L. Longo, Chem. Commun. (2008) 5134.
[44] S. Sergeyev, W. Pisula, Y.H. Geerts, Chem. Soc. Rev. 36 (2007) 1902.
[45] Y. Shirota, H. Kageyama, Chem. Rev. 107 (2007) 953.
[46] M. Sawamura, K. Kawai, Y. Matsuo, K. Kanie, T. Kato, Nature 419 (2002) 702.
[47] I. Seguy, P. Jolinat, P. Destruel, R. Mamy, J. Appl. Phys. 89 (2001) 5442.
[48] A.M. Van de Craats, N. Stutzmann, M.M. Nielsen, M. Watson, Adv. Mater. 15 (2003) 495.
[49] S. Laschat, A. Baro, N. Steinke, F. Giesselmann, C. Hagele, G. Scalia, R. Judele, E. Kapatsina, S. Sauer, A. Schreivogel, M. Tosoni, Angew. Chem., Int. Ed. 46 (2007) 4832.
[50] D. Pucci, I. Aiello, A. Bellusci, A. Crispini, M. Ghedini, M. La Deda, Eur. J. Inorg. Chem. (2009) 4274.
[51] C. Lee, W. Yang, R.G. Parr, Phys. Rev. B 37 (1988) 785.
[52] B. Delley, J. Chem. Phys. 92 (1990) 508.
[53] B. Delley, J. Chem. Phys. 113 (2000) 7756.
[54] B. Delley, J. Phys. Chem. 100 (1996) 6107.
[55] R.G. Parr, R.G. Pearson, J. Am. Chem. Soc. 105 (1983) 7512.
[56] T.A. Koopmans, Physica 1 (1933) 104.

[57] Y.H. Xing, J. Han, G.H. Zhou, Z. Sun, X.J. Zhang, B.L. Zhang, Y.H. Zhang, H.Q. Yuan, M.F. Ge, J. Coord. Chem. 61 (2008) 715.
[58] J.-M. Lin, W.-B. Chen, X.-M. Lin, A.-H. Lin, C.-Y. Ma, W. Dong, C.-E. Tian, Chem. Commun. 47 (2011) 2402.
[59] T. Chattopadhyay, M. Mukherjee, K.S. Banu, A. Banerjee, E. Suresh, E. Zangrando, D. Das, J. Coord. Chem. 62 (2009) 967.
[60] H.-J. Son, W.-S. Han, J.-Y. Chun, B.-K. Kang, S.-N. Kwon, J. Ko, S.J. Han, C. Lee, S.J. Klm, S.O. Kang, Inorg. Chem. 47 (2008) 5666.
[61] D. Pucci, A. Crispini, M. Ghedini, E.I. Sezerb, M. La Deda, Dalton Trans. 40 (2011) 4614.
[62] A.G. Serrette, C.K. Lai, T.M. Swager, Chem. Mater. 6 (1994) 2252.
[63] H. Zheng, C.K. Lai, T.M. Swager, Chem. Mater. 7 (1995) 2067.
[64] S.T. Trzaska, T.M. Swager, Chem. Mater. 10 (1998) 438.
[65] Z. Zhou, R.G. Parr, J. Am. Chem. Soc. 112 (1990) 5720.
[66] J.-I. Aihara, J. Phys. Chem. A 103 (1999) 7487.
[67] Z. Zhou, R.G. Parr, J. Am. Chem. Soc. 111 (1989) 7371.

Materials Science and Engineering C 32 (2012) 735–741

Contents lists available at SciVerse ScienceDirect

Materials Science and Engineering C

journal homepage: www.elsevier.com/locate/msec

Novel photoluminescent mesogenic Schiff-base ligands bearing $[N_4O_4]$ donors and their bimetallic Zn(II) complexes

Chira R. Bhattacharjee *, Chitraniva Datta, Gobinda Das, Paritosh Mondal

Department of Chemistry, Assam University, Silchar 788011, Assam, India

ARTICLE INFO

Article history:
Received 16 August 2011
Received in revised form 19 December 2011
Accepted 18 January 2012
Available online 26 January 2012

Keywords:
Zinc
Schiff-base
Photoluminescent
DFT

ABSTRACT

Novel photoluminescent salicylaldimine ligands condensed from 3′, 3′, 4′, 4′-tetraminobiphenyl and 4-substituted long alkoxy salicylaldehyde possessing two sets of tetradentate $[N_2O_2]$ donor site and their binuclear zinc(II) complexes have been synthesized. The mesogenic and photophysical properties were investigated. The compounds were characterized by FT-IR, ^1H and ^{13}C NMR, UV–vis, elemental analyses, solution electrical conductivity measurements and FAB mass spectrometry. The mesomorphic behavior of these compounds was probed by differential scanning calorimetry and polarized optical microscopy. The ligand with six carbon chain length showed monotropic nematic mesomorphism at 128°C. However, the ligand with alkoxy tail of carbon length 12 showed enantiotropic SmC phase. The complexes are devoid of any mesomorphism. The low molar conductance values in CH_2Cl_2 indicate that the complexes are non-electrolytes. At 330 nm excitation, the ligand emits green light at ~516 nm ($\Phi = 30\%$) and ~549 nm ($\Phi = 16\%$) in solution and solid state, respectively. At similar excitation wavelength, the complexes exhibit blue light in solution at ~452 nm ($\Phi = 20\%$) and green light in solid state ~555 nm ($\Phi = 11\%$). The DFT calculations were performed using DMol3 program at BLYP/DNP level to ascertain the stable electronic structure of the complex.

1. Introduction

Metal Schiff-base complexes have been investigated for their diverse properties [1,2]. Transition metal complexes with salen-type ligands have been extensively studied mainly due to their ability to catalyze variety of chemical transformations, including the asymmetric ring-opening of epoxides, aziridination, cyclopropanation, epoxidation of olefins and formation of cyclic and linear polycarbonates [3–6]. Nonlinear optical (NLO) properties of such materials have been explored in recent years [7–10]. Materials exhibiting light emission or charge transport ability are currently drawing lot of attention due to their potential applications in display devices, solar cells, active components for image and data treatment and storage etc. [11]. Liquid crystalline materials owing to their orientational order could be attractive candidates for enhancing such charge mobility. Additionally, if these materials emit light, a polarized emission could be obtained from a uniformly aligned film. Thus, emitting liquid crystals are very promising materials for display applications [12–14]. Since the discovery of organic light emitting (OLED) devices, zinc complexes have received much attention because of their many advantageous electroluminescent properties, such as electron transporting ability, light emitting efficiency, high thermal stability and great diversity of tunable electronic properties [15–23]. Soft materials that combine both luminescence and liquid crystallinity are thus one of the rapidly growing fields for applications in light emitting devices, information storage systems, sensors, and enhanced contrast displays [24–30]. Very recently we reported a series of green emissive Zn(II) Schiff-base complexes exhibiting columnar mesomorphism [31,32]. Serrano et al. reported a series of mono-, di-, or tridecyloxy-4-benzoyloxysalicylidene-3,3′-diaminobenzidine and their bimetallic Cu(II) and VO(II) complexes [33]. The ligands and their complexes have been shown to exhibit columnar hexagonal mesomorphism when they possess 8 or 12 terminal chains and smectic C mesomorphism with 4 terminal chains. In the course of our sustained effort in this domain of research we were interested in designing a compartmental binucleating Schiff base ligand with four terminal chains and explore its ligational aspects with different metal ions. The effect of a short alkoxy chain (C_6) vis-à-vis that of a relatively longer one (C_{12}) on the mesomorphism is also considered a point worth investigation.

Accordingly, herein, we describe synthesis and photophysical properties of two new binucleating mesogenic Schiff-bases derived from 4-n-alkoxy salicylaldehyde and 3′, 3′, 4′, 4′-tetraminobiphenyl and their bimetallic zinc(II) complexes.

2. Experimental section

2.1. Physical measurements

The C, H and N analyses were carried out using PE2400 elemental analyzer. Molar conductance of the compounds were determined in CH_2Cl_2 (*ca* 10^{-3} mol L^{-1}) at room temperature using MAC-554

* Corresponding author. Tel.: +91 03842 270848; fax: +91 03842 270342.
E-mail address: crbhattacharjee@rediffmail.com (C.R. Bhattacharjee).

0928-4931/$ – see front matter © 2012 Elsevier B.V. All rights reserved.
doi:10.1016/j.msec.2012.01.016

conductometer. The ^{1}H-NMR spectra were recorded on a Bruker DPX-400 MHz spectrometer in $CDCl_3$ (chemical shift in δ) solution with TMS as internal standard. Ultraviolet–visible absorption spectra of the compounds in CH_2Cl_2 were recorded on a Shimadzu UV-160PC spectrophotometer. Photoluminescence spectra were recorded on a Shimadzu RF-5301PC spectrophotometer. The fluorescence quantum yield in dichloromethane was determined by dilution method using 9, 10-diphenyl anthracene as standard. Infrared spectra were recorded on a Perkin-Elmer L 120-000A spectrometer on KBr disc. The optical textures of the different phase of the compounds were studied using a polarizing microscope (Nikon optiphot-2-pol) attached with Instec hot and cold stage HCS302, with STC200 temperature controller of 0.1°C accuracy. The thermal behavior of the compounds was studied using a Perkin-Elmer differential scanning calorimeter (DSC) Pyris-1 spectrometer with a heating or cooling rate of 5°C/min. Quantum chemical calculation on was carried out using density functional theory (DFT) as implemented in DMol3 package.

2.2. Materials

The materials were procured from Tokyo Kasei, Japan and Lancaster Chemicals. All solvents were purified and dried using standard procedures. Silica (60–120 mesh) from Spectrochem was used for chromatographic separation. Silica gel G (E-Merck, India) was used for TLC.

2.3. Synthesis and analysis

The general preparative route for salicylaldimine based Schiff bases is presented in Scheme 1.

2.3.1. Synthesis of n-alkoxysalicyldehydes (n = 6, 12)

Alkoxysalicyldehyde derivatives were prepared following a reported method [31,32]. 2, 4-Dihydroxybenzaldehyde (10 mmol, 1.38 g), $KHCO_3$ (10 mmol, 1 g), KI (catalytic amount) and 1-bromohexane (10 mmol, 1.6 g) or 1-bromododacane (10 mmol, 2.4 g) were mixed in 250 mL of dry acetone. The mixture was heated under reflux for 24 h, and then filtered, while hot, to remove any insoluble solids. Dilute HCl was added to neutralize the warm solution, which was then extracted with chloroform (100 mL). The combined chloroform extract was concentrated to give a purple solid. The solid was purified by column chromatography using a mixture of chloroform and hexane (v/v, 1/1) as eluent. Evaporation of the solvents afforded a white solid product.

2.3.2. Synthesis of Schiff base ligand (6 bps)

An ethanolic solution of 2-hydroxy-(4-hexyloxy)-salicyldehyde (0.88 g, 4 mmol) or 2-hydroxy-(4-dodecyloxy)-salicyldehyde (1.22 g, 4 mmol) was added to an ethanolic solution of 3′,3′,4′,4′-tetraminobiphenyl (0.21 g, 1 mmol). The solution mixture was refluxed with a few drops of acetic acid as catalyst for 3 h to yield the yellow Schiff base. The compound was collected by filtration and recrystallized from absolute ethanol to obtain a pure compound. Yield: 0.81 g (75%). m.p., 133°C. Anal. Calc. for $C_{64}H_{78}N_4O_8$: C, 74.5; H, 7.6; N, 5.4. Found: C, 74.7; H, 7.8; N, 5.3%; FAB Mass (m/e, fragment): m/z: calc. 1030.5; found: 1031[M + H$^+$]; ^{1}H NMR (400 MHz, $CDCl_3$): δ = 13.07 (s, 1H, H^4), 8.51 (s, 1H, H^5), 7.14 (t, J = 8.43 Hz, 2H, H^2), 6.54 (d, J = 2.44 Hz, 2H, H^3), 6.49 (dd, J = 2.44 Hz, J = 8.29 Hz, 2H, H^2), 3.97 (t, J = 6.8 Hz, 2H, -OCH_2), 0.89 (t, J = 6.8 Hz, 6H, CH_3). ^{13}C NMR(75.45 MHz; $CDCl_3$; Me_4Si at 25°C, ppm), δ = 107.5(−C1), 130.7(−C2), 160.9(−C16), 160.6(−C5), 122.4(−C8), 161.6(−C11), 144.4(−C15), 121.8(−C9), 135.7(−C12). IR ($\nu^{-1}_{max,\ cm}$, KBr): 3500 (ν_{OH}), 2925 ($\nu_{as(C-H),}CH_3$), 2921 ($\nu_{as(C-H),}$ CH_2), 2873 ($\nu_{s(C-H),}CH_3$), 2850 ($\nu_{as(C-H),}$ CH_2), 1629 ($\nu_{C=N}$), 1298 (ν_{C-O}).

2.3.3. Synthesis of Schiff base ligand (12 bps)

Yield: 1.08 g (76%). m.p., 117°C. Anal. Calc. for $C_{88}H_{126}N_4O_8$: C, 77.2; H, 9.2; N, 4.1. Found: C, 77.1; H, 9.1; N, 4.2%; FAB Mass (m/e, fragment): m/z: calc. 1366.9; found: 1367[M + H$^+$]; ^{1}H NMR (400 MHz, $CDCl_3$): δ = 13.06 (s, 1H, H^4), 8.55 (s, 1H, H^5), 7.13 (t, J = 8.42 Hz, 2H, H^2), 6.53 (d, J = 2.43 Hz, 2H, H^3), 6.48 (dd, J = 2.44 Hz, J = 8.27 Hz, 2H, H^2), 3.99 (t, J = 6.8 Hz, 2H, –OCH_2), 0.88 (t, J = 6.8 Hz, 6H, CH_3). ^{13}C NMR(75.45 MHz; $CDCl_3$; Me_4Si at 25°C, ppm), δ = 106.5(−C1), 130.8(−C2), 161.9(−C16), 162.6(−C5), 122.4(−C8), 161.6(−C11), 143.4(−C15), 121.7(−C9), 135.6(−C12). IR ($\nu^{-1}_{max,\ cm}$, KBr): 3500 (ν_{OH}), 2924 ($\nu_{as(C-H),}CH_3$), 2922 ($\nu_{as(C-H),}$ CH_2), 2874($\nu_{s(C-H),}CH_3$), 2851 ($\nu_{as(C-H),}$ CH_2), 1628 ($\nu_{C=N}$), 1297 (ν_{C-O}).

2.3.4. Synthesis of dinuclear zinc(II) complex (Zn_2–6 bps)

2.3.4.1. General procedure. The ligand 6 bps (0.051 g, 0.05 mmol) or 12 bps (0.068 g, 0.05 mmol) was dissolved in minimum volume of absolute ethanol. To this, an equimolar amount of zinc acetate $Zn(OAc)_2$•$2H_2O$ (0.02 g, 0.1 mmol) in methanol was then added slowly and stirred for 2 h at room temperature. A brown solid formed was filtered, washed with diethyl ether and finally with chloroform–ethanol (1:1).

Yield: 0.05 g (75%). m.p., 318°C. Anal. Calc. for $C_{64}H_{74}Zn_2N_4O_8$: C, 66.3; H, 6.4; N, 4.8. Found: C, 66.5; H, 6.3; N, 4.8%; FAB Mass (m/e, fragment): m/z: calc. 1156.4; found: 1157[M + H$^+$];^{1}H NMR (400 MHz, $CDCl_3$): 8.54 (s, 1H, H^5), 7.11 (t, J = 8.38 Hz, 2H, H^2), 6.51 (d, J = 2.39 Hz, 2H, H^3), 6.47 (dd, J = 2.44 Hz, J = 8.29 Hz, 2H, H^2), 3.91 (t, J = 6.8 Hz, 2H, –OCH_2), 0.87 (t, J = 6.8 Hz, 6H, CH_3). IR ($\nu^{-1}_{max,\ cm}$, KBr): 2924 ($\nu_{as(C-H),}$ CH_3), 2922 ($\nu_{as(C-H),}$ CH_2), 2871 ($\nu_{s(C-H),}CH_3$), 2849 ($\nu_{as(C-H),}$ CH_2), 1614 ($\nu_{C=N}$), 1296 (ν_{C-O}).

2.3.4.1.1. Zn_2–12 bps. Yield: 0.06 g (78%). m.p., 312°C. Anal. Calc. for $C_{88}H_{122}Zn_2N_4O_8$: C, 70.7; H, 8.2; N, 3.7. Found: C, 70.5; H, 8.3; N, 3.8%; FAB Mass (m/e, fragment): m/z: calc. 1493.7; found: 1494[M + H$^+$]; ^{1}H NMR (400 MHz, $CDCl_3$): 8.57 (s, 1H, H^5), 7.12 (t, J = 8.37 Hz, 2H, H^2), 6.54 (d, J = 2.38 Hz, 2H, H^3), 6.48 (dd, J = 2.45 Hz, J = 8.28 Hz, 2H, H^2), 3.92 (t, J = 6.7 Hz, 2H, –OCH_2), 0.88 (t, J = 6.7 Hz, 6H, CH_3). IR ($\nu^{-1}_{max,\ cm}$, KBr): 2923 ($\nu_{as(C-H),}CH_3$), 2922 ($\nu_{as(C-H),}$ CH_2), 2871 ($\nu_{s(C-H),}CH_3$), 2848 ($\nu_{as(C-H),}$ CH_2), 1611 ($\nu_{C=N}$), 1295 (ν_{C-O}).

3. Result and discussion

3.1. Spectral investigation

The synthetic procedure for ligands and metal complexes are depicted in Scheme 1. The Schiff base ligands were synthesized by literature procedures [31,32] and were identified by ^{1}H NMR and elemental analysis. The compounds were obtained as yellow microcrystalline solids in good yields. The bimetallic zinc(II) complexes, prepared by reacting the appropriate tetraimine with zinc(II) acetate dihydrate in methanol, were isolated as a deep-brown solid in good yield. The complexes were soluble in chloroform and dichloromethane and insoluble in ethanol. The CHN microanalyses of the Schiff base ligands (6 bps, 12 ps) and the complexes (Zn_2–6 bps) are consistent with the proposed formulas, confirming the bimetallic composition of the complex. The FAB-mass spectra of the compounds matched well with their formula weights. The IR spectrum of the Schiff base ligand showed a broad band in the region 3480–3466 cm^{-1} attesting the presence of OH group. The band disappears upon complexation. The azomethine nitrogen $\nu_{C=N}$ stretching frequency of the free ligand appears at ~1629 cm^{-1}, that shifted to lower wave numbers in the spectrum (Supplementary information, Fig. S1) of the complexes (~1614 cm^{-1}), indicating the involvement of azomethine nitrogen in coordination. The ligand with four terminal chains around, serves as a chelating agent with two sets of tetradentate [N_2O_2] core each set comprising of two phenolate-oxygen and two azomethine nitrogen atoms (Scheme 1). Appearance of medium intensity bands at 480–45° Cm^{-1} attributable to

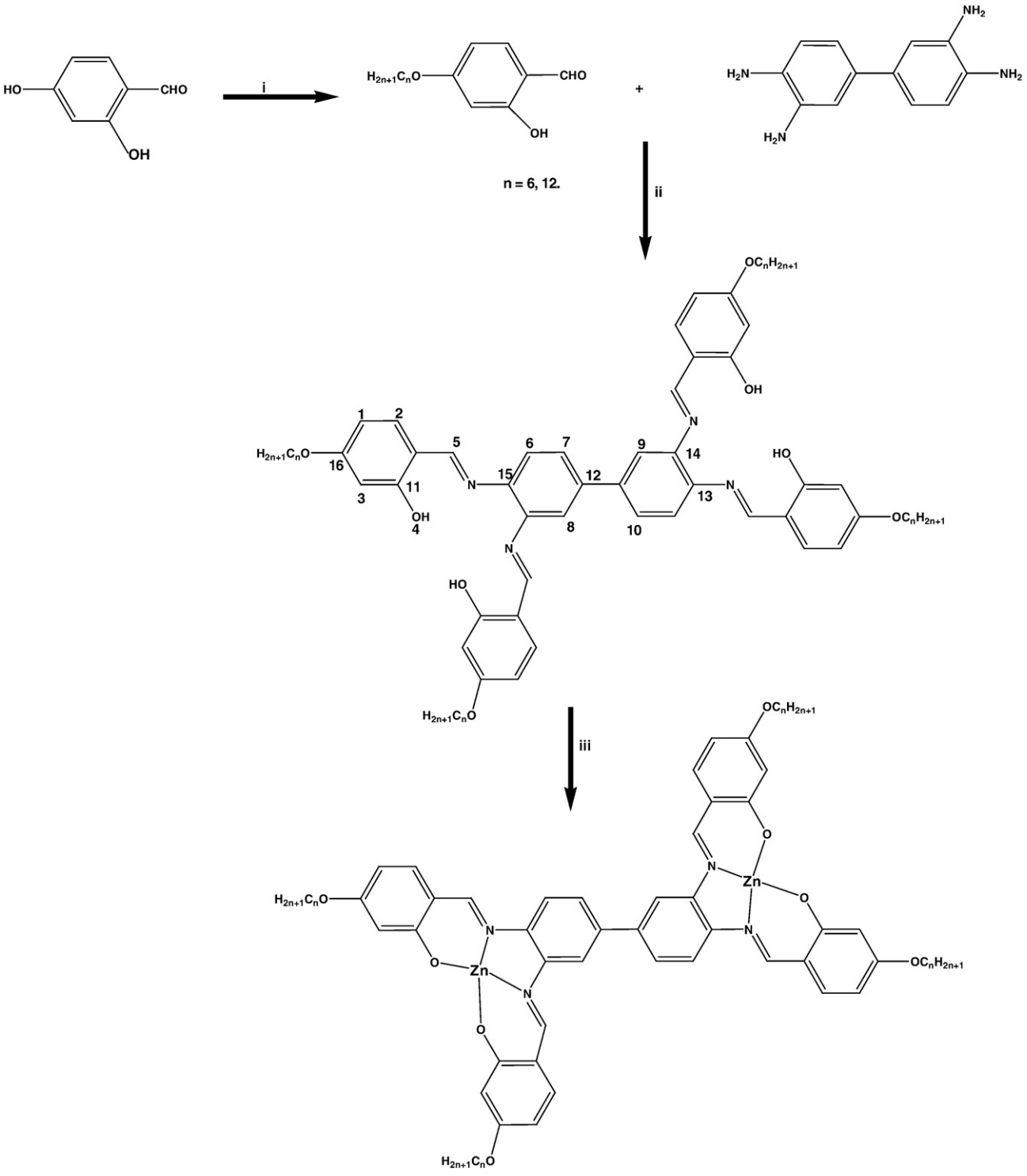

Scheme 1. i.$C_nH_{2n+1}Br$, $KHCO_3$, KI, dry acetone, Δ, 40 h, and ii. glacial AcOH, absolute EtOH Δ, 4 h **iii**. $Zn(OAc)_2.2H_2O$, MeOH, TEA. Δ, 1 h.

ν_{M-N} and ν_{M-O}, respectively. ^1H NMR spectra of ligands show signal at δ 13.4–13.8 ppm, corresponding to the proton of the OH group. The proton NMR signal of the imine group appears at δ 8.5 ppm for ligand. Absence of the phenolic –OH proton and a downfield shift in the peak positions of the –N = CH proton in the ^1H NMR spectrum of the metal complex, (Supplementary information, Fig. S2), (further suggest binding through the phenolate oxygen and the azomethine nitrogen atoms of the ligand to the metal ion [19,31,32]. Solution electrical conductivity of complexes recorded in CH_2Cl_2 (10^{-3} M) were found to be $<10\ \Omega^{-1}\,cm^{-1}\,mol^{-1}$, much lower than is expected for a 1:1 electrolyte, thus confirming the non-electrolytic nature of the complex [34,35].

3.2. Photophysical properties

The UV–vis absorption spectrum (Fig. 1) of free ligand consists of an intense band centered at ~399 nm attributed to π–π* transitions of the azomethine group. Another intense band (~333 nm) in the higher energy region was related to π–π* transitions of benzene rings. These

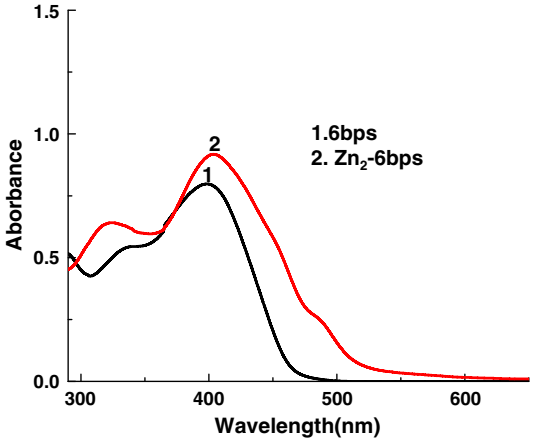

Fig. 1. UV-visible spectra of 6-bs and Zn-6 bps.

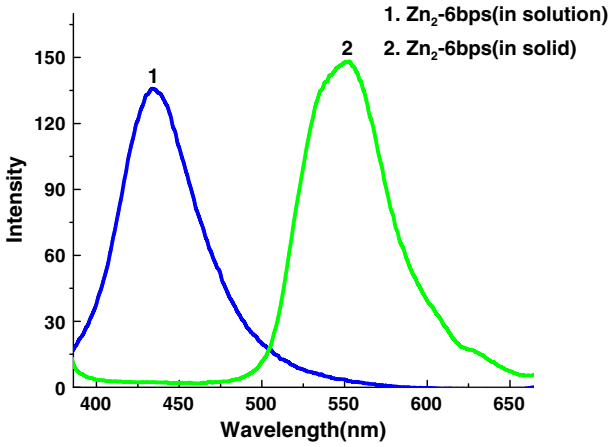

Fig. 3. Emission spectrum of Zn_2-6 bps in solution and in solid state.

transitions shifted to lower wave in the complexes. A shoulder at ~488 nm has been assigned to MLCT transition.

Photoluminescence study of the ligands and zinc(II) complexes was carried out at room temperature in dichloromethane solution and also in the solid state (Figs. 2–3). The ligands emit green light both in solution as well as in the solid state at 512 nm ($\Phi = 30\%$) and 549 nm ($\Phi = 16\%$), respectively, when excited at 330 nm. The solid state emission spectrum of the complexes was recorded by placing a uniform powder sheet between two quartz plates. Generally Schiff base systems exhibit florescence due to intraligand π–π* transitions [36]. Quite surprisingly, upon complexation, the emission maxima are shifted to higher energy ($\lambda_{max} = 452$ nm, $\Phi = 20\%$) resulting in blue light emission. This is not usual, as one would expect the emission band of the free ligand to be at higher energy related to that of the complex because of its relatively high-energy excitation band. This anomaly can be explained by the fact that excited states originating from complexes of Zn^{2+} are typically ligand-centered (LC) in nature owing to the inability of the d^{10} metal center to participate in low-energy charge transfer for metal-centered transitions [37–39]. However, in solid state the complexes emit green light at ~555 nm ($\Phi = 11\%$). In solid state after complexation, the free rotation of the flexible bonds of the ligand is reduced and hence energy dissipation through non-radiative channels decreases leading to shift of emission

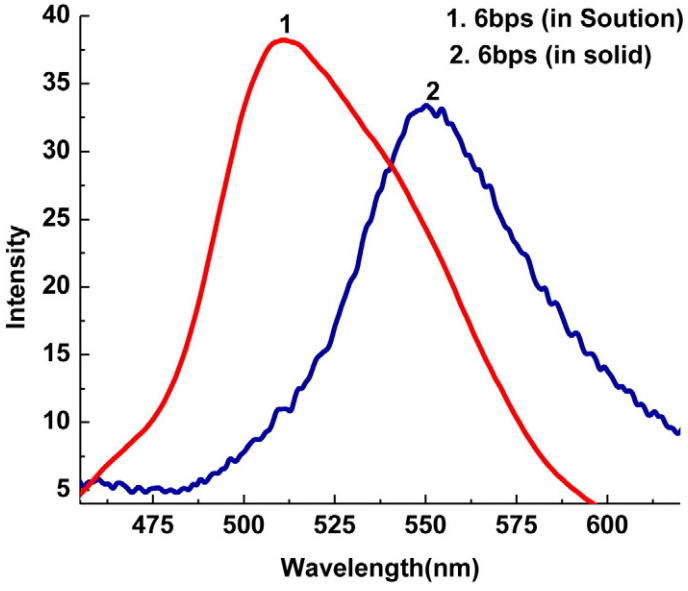

Fig. 2. Emission spectrum of 6-bps in solution and in solid state.

wave length to lower energy. The intense emission observed at room temperature in the complex stems from the intraligand (π–π*) fluorescence, and the role of the Zn^{2+} ion is to provide stability to the ligand [40]. The spectral data of all the compounds are shown in Table 1.

3.3. Mesomorphic behavior: polarizing optical microscopy (POM) and differential scanning (DSC) studies

Hot-stage polarizing optical microscopy has been used to study the interference patterns of the birefringent liquid crystalline materials. Characteristic textures associated with different mesophases were identified by comparison with those reported in the literature. The ligand, 6 bps exhibited monotropic liquid-crystalline behavior. On slow cooling from the isotropic liquid, the compound showed a birefringent schlieren texture (Fig. 4) typical of a nematic mesophase at ~128°C. DSC study (Table 2) showed two transitions in heating run and one in the cooling run (Fig. 5). The transition at 133.7°C ($\Delta H = 13.2$ kJmol^{-1}) is due to the N–I transition. Isotropic to nematic transition could not be detected in DSC, probably due to slow crystallization or vitrification of the mesophases. Owing to the high viscous nature of the 6 bps compound, transition peaks observed in DSC were rather broad. Quite interestingly the long chain compound 12-bps showed enantiotropic SmC phase with four brush defects (Fig. 6). The DSC thermogram exhibited two sharp transitions in heating and two in cooling cycle (Fig. 7). The marked difference in the mesomorphic behavior of 6 bps and12bps due to the presence of short (C_6) and long (C_{12}) alkoxy chain is noteworthy. We are, however, unable to provide any suitable explanation at this moment. Increased alkoxy chain length might have affected the overall orientation of the molecule including the torsional twist of the biphenyl rings which in turn modified the intermolecular association. Pertinent here is to mention that somewhat similar biphenyl based compartmental Schiff base ligands with ester linkages showed smectic mesomorphism [33]. Though host of other related compartmental Schiff base ligands are documented with no reported mesogenicity [41]. Owing to the high

Table 1
UV–visible and photoluminescence data of ligands (n–bps) and Zn_2–nbps complexes.

Compounds	$\pi \rightarrow \pi^*$ (ε, l mol^{-1} cm^{-1})	$\pi \rightarrow \pi^*$ (ε, l mol^{-1} cm^{-1})	MLCT (ε, l mol^{-1} cm^{-1})	PL[a] (Solution)	PL[a] (Solid)
6 bps	335 (5300)	399 (9800)	–	512	549
Zn_2–6 bps	323 (11,200)	398 (9100)	488 (2200)	452	555
12 bps	330 (5200)	399 (9700)	–	516	554
Zn_2–12 bps	316 (5400)	396 (8200)	488 (2300)	451	558

[a] Photoluminescence data of compounds.

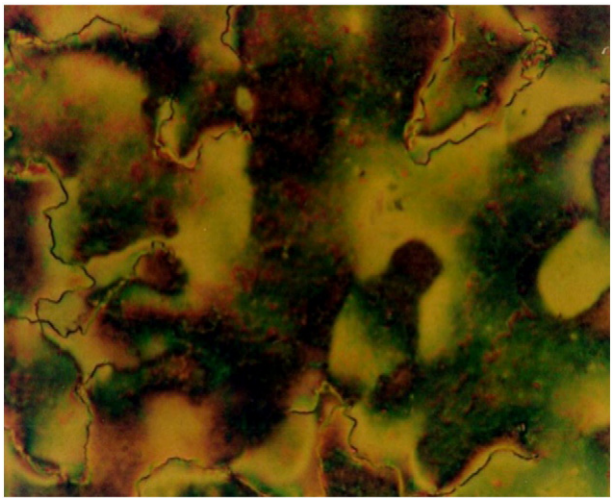

Fig. 4. Schlieren texture of nematic phase (6 bps) at 128° C.

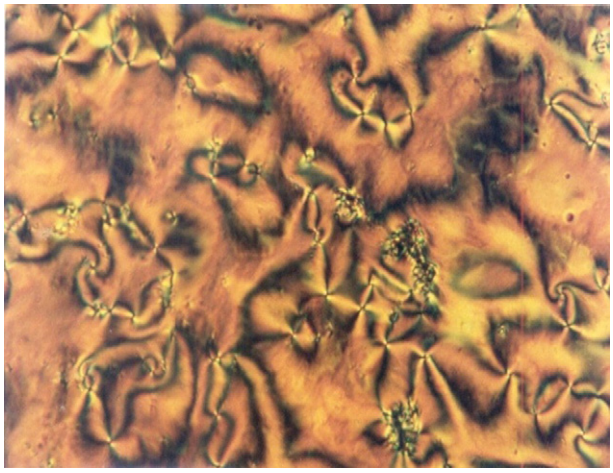

Fig. 6. Schlieren texture of SmC (12 bps) at 117° C.

Table 2
DSC data of the complexes.

Compounds	T [°C][a]	Transition[b]	ΔH [kJmol^{-1}]
6 bps	70.3	Cr–N	1.3
	133.7	N–I	13.2
	47.2	I–Cr	0.79
12 bps	96.5	Cr–SmC	74.4
	117.8	SmC–I	14.6
	116.1	I–SmC	13.8
	91.7	SmC–Cr	74.1

[a] Transition temperature obtained from onset peak.
[b] Cr: crystal; N: Nematic phase; SmC: Smectic phase; I: Isotropic phase.

viscous nature of the compound (6 bps) transition peaks observed in DSC were rather broad. Upon coordination to zinc(II) the mesogenic property of the Schiff base ligands were completely lost. Desired molecular shape to enhance anisotropy in intermolecular forces is often not possible to achieve for chemical feasibility reasons. Thus unfavorable structural orientation of the resulting binuclear complex molecules is believed to have upset the mesogenicity in the present case. Similar loss of mesomorphism was earlier reported for related binuclear Schiff base metal complexes of copper (II) and nickel (II) [42].

3.4. DFT study

As a representative case, the ground state geometries in the gas phase of the ligand molecule (6 bps) and its zinc complex, Zn_2–6 bps (Fig. 8) were fully optimized using the restricted BLYP/DNP methods without imposing any symmetry constrain. The BLYP functional used throughout this study, comprises of a hybrid exchange functional as defined by Becke and the non-local Lee–Yang–Parr correlation functional [43]. The basis set chosen in this study is DNP, the double-numerical atomic orbitals augmented by polarization functions. All calculations were performed with the DMol3 program package [44–46]. In our calculations, self consistent field procedures are performed with a convergence criterion of 2×10^{-5} a.u. on the total energy and 10^{-6} a.u. on electron density. The 3D isosurface plots of the lowest unoccupied molecular orbital (LUMO) and the highest occupied molecular orbital (HOMO) of the complex are shown in (Figs. 9 and 10). The HOMO and LUMO energies of the ligand are calculated to be −4.70 eV and −2.49 eV, respectively, ΔE = 2.21 eV. The corresponding energies of the Zn-complex found to be −4.74 eV, −2.76 eV and ΔE = 1.98 eV, respectively, matched well with those reported for similar Schiff base complexes of zinc [32,33]. The HOMO–LUMO energy difference decreases substantially on incorporation of two zinc ions into the ligand framework. The HOMO–LUMO energy separation can be related to kinetic stability and in turn reactivity pattern of the molecule. A small HOMO–LUMO gap implies a low kinetic stability and high chemical reactivity, because it is energetically favorable to add electrons to LUMO or to extract

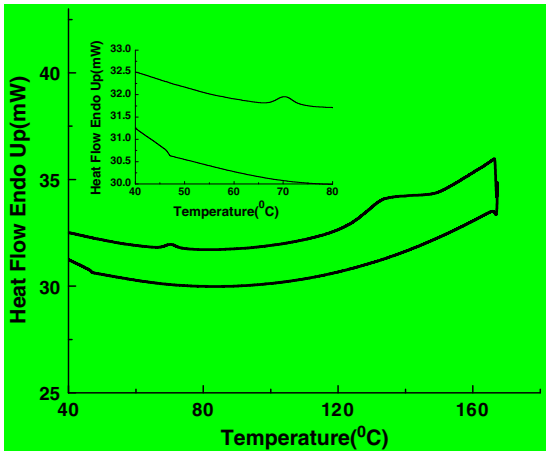

Fig. 5. DSC thermogram of 6 bps.

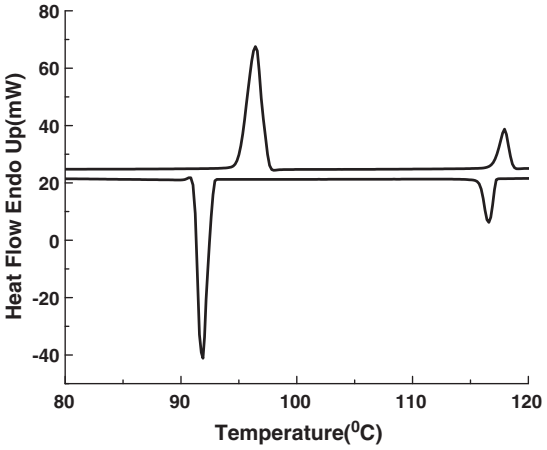

Fig. 7. DSC thermogram of (12 bps).

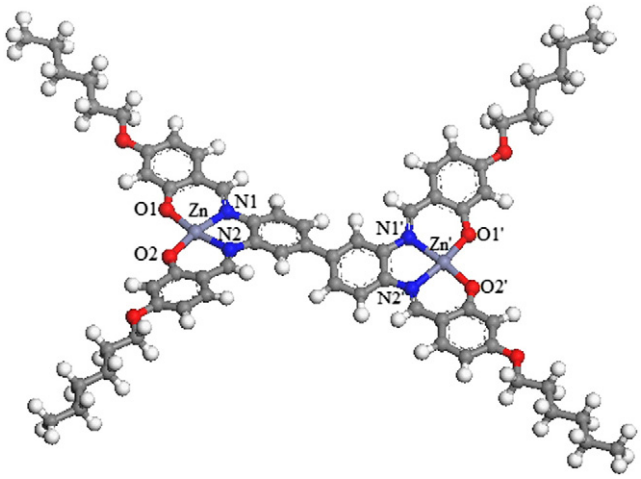

Fig. 8. Optimized structure of Zn_2-6bsps.

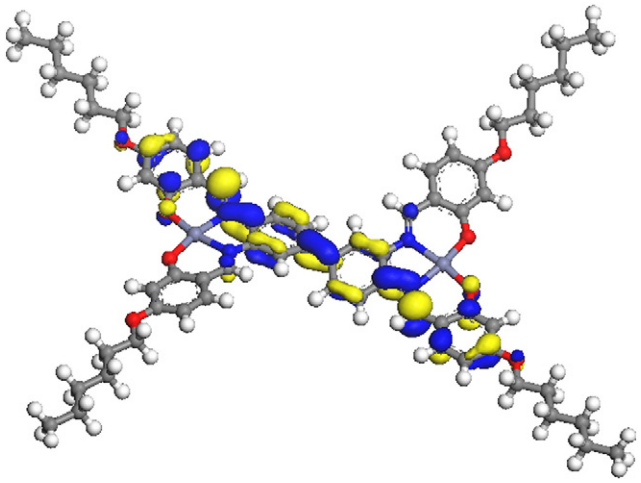

Fig. 10. LUMO diagram of Zn_2-6 bps.

electrons from a HOMO. Selective geometric parameters of the optimized zinc complex were evaluated by DFT at BLYP/DNP level (Table 3). The complex has an average Zn–O and Zn–N bond lengths 1.97 and 2.10 Å, respectively. The average bond angles 97.6° and 79.3° for O1–Zn–O2 and N1–Zn–N2, respectively, around the zinc atom which deviate substantially from the tetrahedral values indicated a distorted planar four coordinate geometry. These geometrical parameters match well with structurally characterized analogous zinc complexes [36,45]. Biphenyl, a short rigid central bridge presumably prevented the formation of a tetrahedral environment around zinc (II), leading to a distorted square planar geometry.

Table 3
Selected bond length and bond angles of Zn_2–6 bps, from DFT.

Zn		Zn′	
Structure parameter	Bond lengths (Å) and bond angles in (°)	Structure parameter	Bond lengths (Å) and bond angles in (°)
Zn–O1	1.968	Zn′–O1	1.972
Zn–O2	1.970	Zn′–O2	1.970
Zn–N1	2.105	Zn′–N1	2.095
Zn–N2	2.098	Zn′–N2	2.102
O1–Zn–O2	97.6	O1–Zn′–O2	97.5
N1–Zn–N2	79.2	N1–Zn′–N2	79.4
O1–Zn–N1	91.5	O1–Zn′–N1	92.1
O2–Zn–N2	91.9	O2–Zn′–N2	91.8
O1–Zn–N2	169.9	O1–Zn′–N2	169.5
O2–Zn–N1	169.7	O2–Zn′–N1	169.8

4. Conclusion

In this work synthesis of two new compartmental salen type Schiff base compounds with four terminal chains (short and long) and its binuclear Zn(II) complexes is described. The ligands besides being fluorescent exhibit monotropic nematic/SmC mesophase transition, however, the complexes lack any mesomorphism but exhibited intense fluorescence. Interestingly different chain lengths of alkoxy group promoted quite different mesomorphic behavior. Based on spectral and DFT study, four coordinate distorted square planar geometry around Zn(II) center has been conjectured. The strategy adopted herein can be effectively employed to access a variety of newer bimetallic systems with tunable molecular construction motifs leading to smart multifunctional materials. An attractive option would be to access paramagnetic photoluminescent bimetallomesogens.

Supplementary materials related to this article can be found online at doi:10.1016/j.msec.2012.01.016.

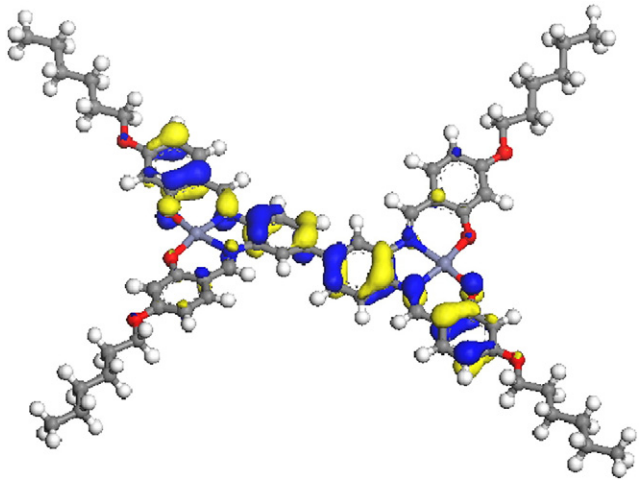

Fig. 9. HOMO energy diagram of Zn_2-6 bps.

Acknowledgments

The authors thank SAIF, NEHU and CDRI, and Lucknow for analytical and spectral data. CD acknowledges financial support from UGC, Government of India. Dr. R.C. Deka, Tezpur University, India, is acknowledged for computational facility.

References

[1] A.A. Khandar, K. Nejati, Polyhedron. 19 (2000) 607–613.
[2] S.C. Bhatia, J.M. Bindlish, A.R. Saini, P.C. Jain, J. Chem. Soc. Dalton Trans. (1981) 1773.
[3] P.G. Cozzi, L.S. Dolci, A. Garelli, M. Montalti, L. Prodi, N. Zaccheroni, New J. Chem. 27 (2003) 692–697.
[4] P.G. Cozzi, Chem. Soc. Rev. 33 (2004) 410–421.
[5] C. Gennari, U. Piarulli, Chem. Rev. 103 (2003) 3071–3100.
[6] R.I. Kureshy, I. Ahmad, N.H. Khan, S.H.R. Abdi, K. Pathak, J. Catal. 238 (2006) 134–141.
[7] V. Aubert, V. Guerchais, E. Ishow, K.T.- Hoang, I. Ledoux, K. Nakatani, L.H. Bozec, Angew. Chem. Int. Ed. 47 (2008) 577–580.
[8] B.J. Coe, in: J.A. McCleverty, T.J. Meyer (Eds.), Comprehensive Coordination Chemistry II, vol. 9, Elsevier Pergamon, Oxford, 2004, pp. 621–687.
[9] J. Chiffre, F. Averseng, G.G.A. Balavoine, J.-C. Daran, G. Iftime, P.G. Lacroix, E. Manoury, K. Nakatani, Eur. J. Inorg. Chem. (2001) 2221–2226.
[10] I. Sasaki, L. Vender, A.S. Saquet, P.G. Lacroix, Eur. J. Inorg. Chem. (2006) 3294–3302.
[11] S.R. Forrest, Nature 428 (2004) 911–918.
[12] M. Ghedini, D. Pucci, A. Crispini, A. Bellusci, M. La Deda, I. Aiello, T. Pugliese, Inorg. Chem. Commun. 10 (2007) 243–247.
[13] C. Pettinari, N. Masciocchi, L. Pandolfo, D. Pucci, Chem. Eur. J. 16 (2010) 1106–1123.
[14] E.I. Sezerb, A.M. Talarico, I. Aiello, A. Crispini, N. Godbert, D. Pucci, T. Pugliese, M. Ghedini, Eur. J. Inorg. Chem. (2010) 3270–3277.

[15] F. Morale, R.L. Finn, S.R. Collinson, A.J. Blake, C. Wilson, D.W. Bruce, D. Guillon, B. Donnio, M. Schroder, New. J. Chem. 32 (2008) 297–305.
[16] G. Barberio, A. Bellusci, A. Crispini, M. Ghedini, A. Golemme, P. Prus, D. Pucci, Eur. J. Inorg. Chem. (2005) 181–188.
[17] F. Morale, R.W. Date, D. Guillon, D.W. Bruce, R.L. Finn, C. Wilson, A.J. Blake, M. Schroder, B. Donnio, Chem. Eur. J. 9 (2003) 2484–2501.
[18] E. Cavero, S. Uriel, P. Romero, J.L. Serrano, R. Giménez, J. Am. Chem. Soc. 129 (2007) 11608–11618.
[19] D. Pucci, I. Aiello, A. Bellusci, A. Crispini, M. Ghedini, M. La Deda, Eur. J. Inorg. Chem. (2009) 4274–4281.
[20] E. Terrazzi, J.-M. Bénech, J.-P. Rivera, G. Bernardinelli, B. Donnio, D. Guillon, C. Piguet, Dalton Trans. (2003) 769–772.
[21] R. Giménez, A.B. Manrique, S. Uriel, J. Barberá, J.L. Serrano, Chem. Commun. (2004) 2064–2065.
[22] P. Ovejero, M.J. Mayoral, M. Cano, J.A. Campo, J.V. Heras, P. Fernández-Tobar, M. Valién, E. Pinilla, M.R. Torres, Mol. Cryst. Liq. Cryst. 481 (2008) 34–55.
[23] K.A. Ames, S.R. Collinson, A.J. Blake, C. Wilson, J.B. Love, D.W. Bruce, B. Donnio, D. Guillon, M. Schröder, Eur. J. Inorg. Chem. (2008) 5056–5066.
[24] D. Pucci, I. Aiello, A. Bellusci, A. Crispini, I. De Franco, M. Ghedini, M. La Deda, Chem. Commun. (2008) 2254–2256.
[25] D. Pucci, G. Barberio, A. Bellusci, A. Crispini, M. La Deda, M. Ghedini, E.I. Sezerb, Eur. J. Inorg. Chem. (2005) 2457–2463.
[26] D. Pucci, G. Barberio, A. Crispini, O. Francescangeli, M. Ghedini, M. La Deda, Eur. J. Inorg. Chem. (2003) 3649–3661.
[27] V.N. Kozhevnikov, B. Donnio, D.W. Bruce, Angew. Chem. Int. Ed. 47 (2008) 6286–6289.
[28] R. Gimenez, M. Pinol, J.L. Serrano, Chem. Mater. 16 (2004) 1377–1383.
[29] Y. Sagara, S. Yamane, T. Mutai, K. Araki, T. Kato, Adv. Funct. Mater. 19 (2009) 1869–1875.
[30] K. Binnemans, J. Mater. Chem. 19 (2009) 448–453.
[31] C.R. Bhattacharjee, G. Das, P. Mondal, N.V.S. Rao, Polyhedron. 29 (2010) 3089–3096.
[32] C.R. Bhattacharjee, G. Das, P. Mondal, S.K. Prasad, D.S.S. Rao, Eur. J. Inorg. Chem. (2011) 1418–1424.
[33] J. Barbera, R. Gimenez, M. Marcos, J.L. Serrano, P.J. Alonso, J.I. Martinez, Chem. Mater. (2003) 958–964.
[34] M. Bagherzadeh, M. Amini, J. Coord. Chem. 10 (2010) 3849–3858.
[35] W.J. Geary, Coord. Chem. Rev. 7 (1971) 81–122.
[36] T. Chattopadhyay, M. Mukherjee, K.S. Banu, A. Banerjee, E. Suresh, E. Zangrando, D. Das, J. Coord. Chem. 62 (2009) 967–979.
[37] P. Roy, K. Dhara, M. Manassero, J. Ratha, P. Banerjee, Inorg. Chem. 46 (2009) 6405–6412.
[38] C.L. Dollberg, C. Turro, Inorg. Chem. 40 (2001) 2484–2485.
[39] D.M. Roundhill, in: J.P. Fackler (Ed.), Modern Inorganic Chemistry Series, Plenum Press, New York, 1994, pp. 56–57.
[40] S.-F. Hung, X.-H. Ling, H.-C. Fang, X.-L. Zhan, Z.-Y. Zhou, L. Chen, X.-P. Cai, Transition Met. Chem. 34 (2009) 115–120.
[41] G. Venkatachalam, N. Raja, D. Pandiarajan, R. Ramesh, Spectrochim. Acta Part A 71 (2008) 884–891.
[42] D.B. Patel, P.K. Bhattacharya, Mol. Cryst. Liq. Cryst. 432 (2005) 47–57.
[43] C. Lee, W. Yang, R.G. Parr, Phys. Rev. B 37 (1988) 785–789.
[44] B.J. Delley, Chem. Phys. 92 (1990) 508–518.
[45] M.S. Gordon, Chem. Phys. Lett. 76 (1980) 163–168.
[46] H.-C. Lin, C.-C. Huang, C.-H. Shi, Y.-H. Liao, C.-C. Chen, Y.-C. Lin, Y.-H. Liu, Dalton Trans. (2007) 781–791.

Liquid Crystals
Publication details, including instructions for authors and subscription information:
http://www.tandfonline.com/loi/tlct20

Liquid crystalline dinuclear copper(II) complexes accessed from photoluminescent tridentate [ONO]-donor Schiff base ligands

Chira R. Bhattacharjee [a] , Chitraniva Datta [a] , Gobinda Das [a] & Paritosh Mondal [a]
[a] Department of Chemistry, Assam University, Silchar, 788011, Assam, India

Available online: 20 Mar 2012

To cite this article: Chira R. Bhattacharjee, Chitraniva Datta, Gobinda Das & Paritosh Mondal (2012): Liquid crystalline dinuclear copper(II) complexes accessed from photoluminescent tridentate [ONO]-donor Schiff base ligands, Liquid Crystals, 39:5, 639-646

To link to this article: http://dx.doi.org/10.1080/02678292.2012.669855

Liquid Crystals,
Vol. 39, No. 5, May 2012, 639–646

Taylor & Francis
Taylor & Francis Group

Liquid crystalline dinuclear copper(II) complexes accessed from photoluminescent tridentate [ONO]-donor Schiff base ligands

Chira R. Bhattacharjee*, Chitraniva Datta, Gobinda Das and Paritosh Mondal

Department of Chemistry, Assam University, Silchar 788011, Assam, India

(*Received 2 December 2011; final version received 22 February 2012*)

Two new liquid crystalline dinuclear copper(II) complexes of the type $[Cu_2L_2^n]$, H_2L^n = (E)-5-(hexadecyloxy)-2-((2-hydroxyethylimino) methyl) phenol(L) and (E)-5-(hexadecyloxy)-2-((2-hydroxypropylimino) methyl) phenol (L′), have been synthesised. The compounds were characterised by Fourier transform infrared spectroscopy, ^1H and ^{13}C nuclear magnetic resonance, ultraviolet-visible spectroscopy, elemental analyses, solution electrical conductivity measurements and fast atom bombardment mass spectrometry. The phase behaviours of the compounds were examined by differential scanning calorimetry and polarised optical microscopy. Interestingly the ligand L showed a monotropic smectic A (SmA) mesophase at ∼75°C while the ligand L′ incorporating a methyl group in the spacer lacks any mesomorphism. The complexes were all found to exhibit a thermally stable enantiotropic SmA phase in the range ∼114–118°C. The ligands are blue light emitters with broad emission maxima at ∼469 nm. The density functional theory calculations revealed a distorted square planar structure around each copper(II) centre in the dinuclear framework.

Keywords: copper; dinuclear complex; Schiff base; photoluminescence; DFT

1. Introduction

Research on metallomesogens has received tremendous impetus during the last few decades owing to versatile physico-chemical properties (colour, magnetism, polarisability, redox behaviour etc) of such metal-organic frameworks [1–12]. Metallomesogens combine the unique properties of anisotropic fluids with the electronic and optical properties of metal complexes. While numerous examples of mononuclear metallomesogens exhibiting novel mesomorphic properties have been widely reported, examples of bi-metallomesogens are still quite rare [13–21]. The design of binuclear metallomesogens thus constitutes a key step for the development of magnetic and conductive materials [19, 21, 22]. Among the documented bimetallic mesogens, majority is diamagnetic [23–25] and only a very few are paramagnetic [13–22]. Paramagnetism induced by a metal centre can lead to interesting chemical and physical properties [26–29]. Most bimetallomesogens reported in the literature exhibit columnar discotic phases [13, 17–19, 22, 24, 30–32]. Bimetallomesogens are still limited to copper carboxylates and dithiocarboxylates, ortho- or cyclopalladated compounds, and dicopper β-diketonate and β-enaminoketonate complexes [22–25, 32]. Owing to unusual geometries, polarisability, paramagnetism and large birefringence, leading to unique functional behaviours, metallomesogens incorporating multiple metal ions are a recurring theme of current research [13–21]. Despite inherent challenges in synthesising bimetallomesogens, quite a good number of such complexes are on record [13–26, 30–32]. Mesogenic behaviour can be modulated by the choice of metal ions, and the nature and position of the substituents of the alkoxy tail and/or spacer group [27]. Metal complexes of salicylaldimines are among the earliest and most extensively studied class of metallomesogens [3–5, 33]. The salicylaldimine fragment is well recognised as a good promesogenic unit as the azomethine linkage is stabilised by intramolecular hydrogen bonding in addition to being a good donor site for coordination with metals [3, 33]. Light emitting liquid crystalline materials are considered promising candidates for display applications [6–8]. Simpler one-ring nonmesogenic Schiff bases have been complexed to metal ions to produce ordered mesophases [33–35]. Incidentally there appears to be no record of Schiff base mesogens containing one ring until a recent report on a series of luminescent mesogenic one-ring-based salicylaldimine Schiff bases and their lanthanide complexes from our group [36]. Lai and Leu [13] reported a series of oxygen-bridged bimetallomesogens containing copper(II), palladium(II), oxovanadium(IV) and iron(II) ions based on salicylaldimines ligands, namely, N-(3-hydroxypropyl)-4-alkoxysalicylaldimines and N-(3-hydroxypropyl)-4-(4-alkoxybenzoyl)salicylaldimines. The copper and palladium complexes exhibited smectic A (SmA) phases; however, vanadyl and iron complexes did not show any mesogenicity. In this

*Corresponding author. Email: crbhattacharjee@rediffmail.com

ISSN 0267-8292 print/ISSN 1366-5855 online

http://dx.doi.org/10.1080/02678292.2012.669855
http://www.tandfonline.com

context, we were particularly interested to assess the effect of the substituent on amine moiety and its influence on the mesogenicity of the binuclear complexes. Accordingly in this article we describe the synthesis of two new tridentate [NOO]-donor photoluminescent Schiff base ligands viz. (E)-5-(hexadecyloxy)-2-((2-hydroxyethylimino) methyl) phenol(L) and (E)-5-(hexadecyloxy)-2-((2-hydroxypropylimino) methyl) phenol (L′), the former (L) being mesomorphic also. The binuclear copper(II) complexes of both of these ligands are mesogenic although devoid of luminescent properties.

2. Results and discussion

The Schiff base ligands were synthesised by condensation of 4-alkoxysubstituted aldehyde with a 2-amino-1-ethanol and 2-aminopropan-1-ol with slight modification of the literature procedures [7–11, 36]. The synthetic strategy for the ligands [LH = (E)-5-(hexadecyloxy)-2-((2-hydroxyethylimino) methyl) phenol and (E)-5-(hexadecyloxy)-2-((1-hydroxypropan-2-ylimino) methyl) phenol], and their bimetallic copper complexes, $[Cu_2(L/L')_2]$ are presented in Scheme-1. Complexes formed from a reaction of the appropriate ligand with copper acetate in an ethanol–methanol solution in Cu: L/L′ in a 2:2 ratio at ambient temperature are isolated as a greenish blue coloured solid in good yields. The compounds were characterised by Fourier transform infrared (FT-IR) spectroscopy, ^{1}H and ^{13}C nuclear magnetic resonance (NMR), ultraviolet-visible (UV-vis), elemental analyses, solution electrical conductivity measurements and fast atom bombardment (FAB) mass spectrometry. The CHN analyses of the ligands and their complexes are consistent with the proposed formulae, confirming the bimetallic composition of the complexes. FAB mass spectra of the compounds are concordant with their formula weights. The IR spectra of the Schiff base ligands showed a broad band in the region 3380–3366 cm^{-1} attesting the presence of OH functionality. Upon complexation, this band disappears. The azomethine nitrogen $\nu_{C=N}$ stretching frequency of the free ligand appears at ~1626 cm^{-1}, which becomes shifted to lower wave number (~1613 cm^{-1}) in the complexes indicating the involvement of azomethine nitrogen in the coordination. Appearances of medium intensity bands at ~450–480 cm^{-1} are attributable to ν_{Cu-N} and ν_{Cu-O}. ^{1}H NMR spectra of the ligands showed a broad signal at δ_H 13.4–13.8 ppm, corresponding to the phenolic proton. Appearance of a sharp peak at ca. δ_H 8.10 ppm characteristic of

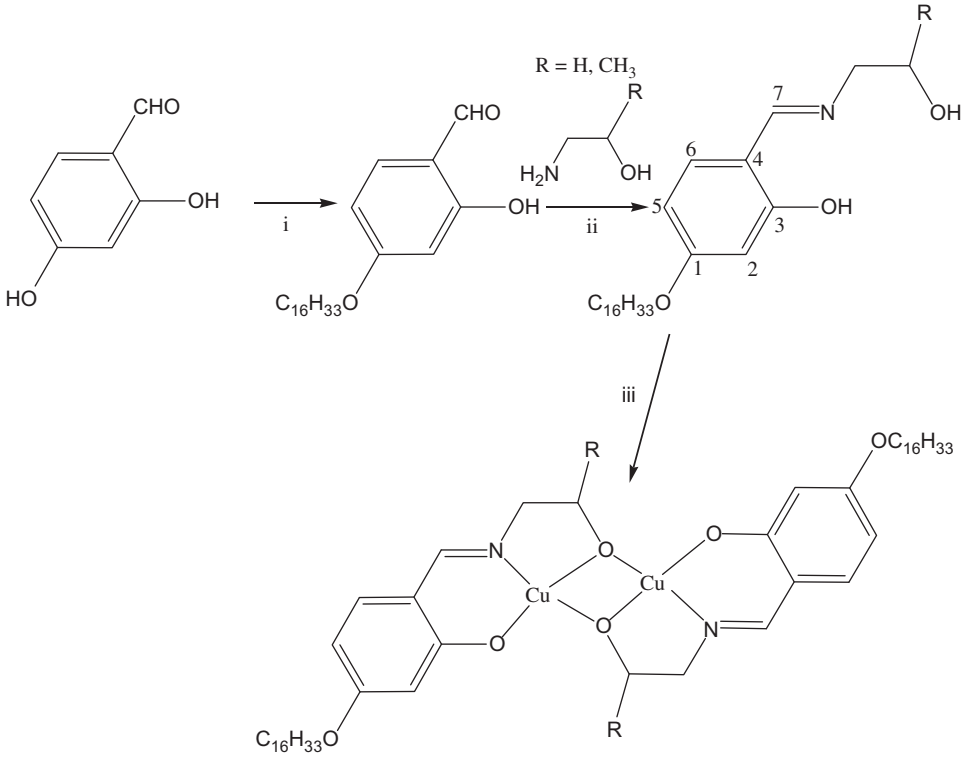

Scheme 1. (i) $C_nH_{2n+1}Br$, $KHCO_3$, KI, dry acetone, Δ, 40 h; (ii) glacial AcOH, absolute EtOH Δ, 4 h; (iii) $Cu(OAc)_2$. H_2O, MeOH, 1 h.

the imine proton (H-C=N) confirmed the formation of the Schiff base. The alcoholic proton appeared, expectedly, as a triplet at δ 3.74 ppm in the ligands. Owing to the paramagnetic nature of the complexes, ^{1}H NMR spectra revealed only broad unresolved signals [13]. Solution electrical conductivities of the complexes recorded in CH_2Cl_2 (10^{-3}M) were found to be $<10\ \Omega^{-1}\ cm^{-1}\ mol^{-1}$ confirming the non-electrolytic nature of the complex.

The absorption spectra of the ligands exhibited three bands (Figure 1) owing to the π–π^* transition of the aromatic rings in the region 255–291 nm. The band at 348 nm is due to the π–π^* transition of the C=N fragment. Upon complexation, these bands are red shifted to 279 nm, 310 nm and 391 nm.

Photoluminescence studies of the ligands (L/L′) were carried out at room temperature in dichloromethane solution and also in the solid state (Figure 2) The ligands exhibited an emission maximum at 447 nm (Φ = 30%) in solution when excited at 350 nm. In the solid state the emission maximum is red shifted to 469 nm (Φ = 9%). This shift is due to the intermolecular aromatic interaction which is weaker in solution than that in the solid state [6–8, 37, 38]. Moreover, in the solid state, a larger electronic delocalisation leads to a lowering of the energy of the electronic states. Generally Schiff base systems exhibit fluorescence due to intraligand π–π^* transitions [39]. The complexes did not exhibit any fluorescence presumably because paramagnetic ions quench the fluorescence of organic ligands by enhancing the rate of non-radiative processes that compete with the fluorescence [40]. It may be noted that quenching of the fluorescence of a ligand by paramagnetic metal ions on complexation is a rather common phenomenon which is explained by processes such as magnetic perturbation, redox activity, electronic energy transfer, etc [41].

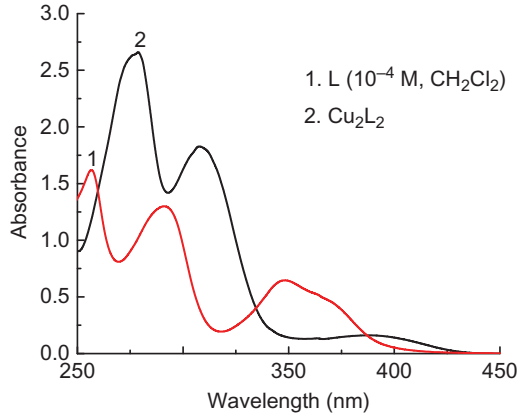

Fig. 1. UV-vis spectra of L and Cu_2 L_2.

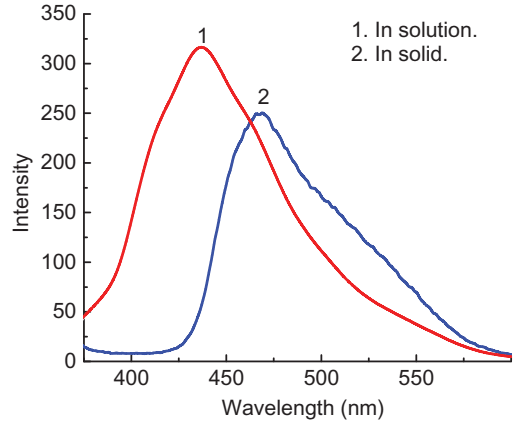

Fig. 2. Emission spectra of ligands in solution and in the solid state.

The mesomorphic behaviour of the compounds was probed by polarised optical microscopy and differential scanning calorimetry (DSC). The ligand L showed monotropic mesomorphism. On heating, the sample transformed directly to the isotropic liquid while during cooling from an isotropic liquid it first showed a batonnets texture which coalesces to a high birefringent fanlike texture (Figure 3) at 75°C. On further cooling it solidified at 60°C. The mesophase was identified as a SmA phase on the basis of these diagnostic features. The DSC trace for the compound L also showed one transition in the heating cycle and two in the cooling run (Figure 4). The transition at 75.1°C (ΔH = 1.9 kJ mol^{-1}) is due to the change from the isotropic to the smectic A phase. The presence of the alcoholic -OH group tends to induce attractive intermolecular interactions via the H-bond (HO. . . HO. . .) resulting in liquid crystalline behaviour. Analogous Schiff base compounds with no reported mesogenicity have been documented [13]. Detail investigations of the mesomorphic properties of such a one-ring system were first reported by our

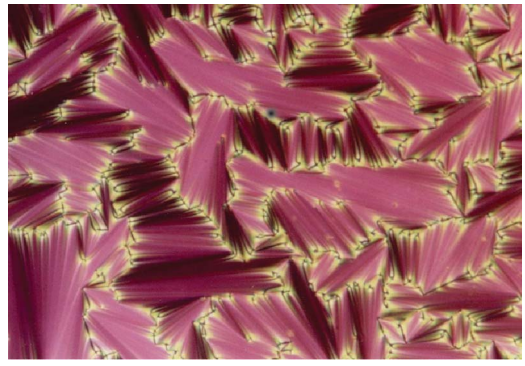

Fig. 3. Fanlike texture of the SmA phase at 75°C.

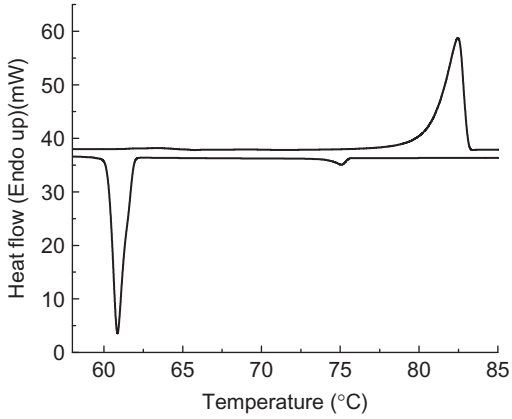

Fig. 4. DSC thermogram of L.

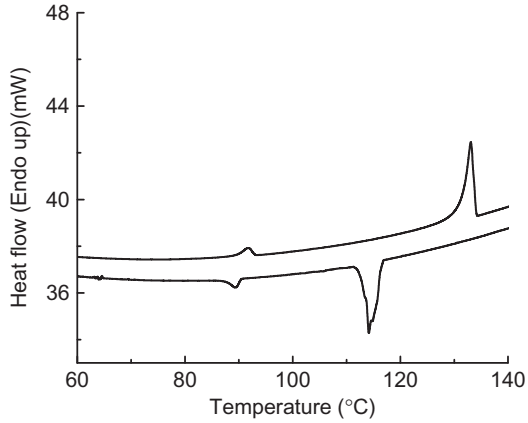

Fig. 6. DSC thermogram of Cu_2L_2.

group [36]. Quite surprisingly, incorporation of a methyl group in the amine moiety of this ligand (L′) upsets the mesomorphism. This is ascribed to the steric hindrance caused by the tetrahedral methyl group, which resulted in loss of mesomorphism [13]. The complexes, however, all exhibited enantiotropic smectic mesomorphism. A typical broken focal conic-shaped texture (Figure 5) with homeotropic domain was observed at 114°C upon slow cooling from their isotropic liquid. The mesophase was identified as a SmA phase based on the optical texture. The DSC thermogram (Figure 6) showed two endothermic peaks in the heating cycle and two exothermic peaks in the cooling cycle. The peak at ∼114–118°C is due to the isotropic–smectic A phase transition. Owing to the highly viscous nature of the complexes and the severe restriction in the molecular mobility, a pronounced hysteresis in transition temperature has been noted. The reversible thermal behaviour of the complexes was confirmed by DSC on subsequent heating–cooling runs (Table 1). It is pertinent here to mention that the structurally similar bimetallomesogens, [bis[N-(3-hydroxypropyl)-4-octanoylsalicylaldiminato] copper(II) complex reported earlier showed a monotropic SmA mesophase [13]. Bimetallic copper (II) complexes bearing azo-linkage at the side aromatic ring showing a SmA phase are also on record [14]. The mesophase textures observed in these cases closely resemble the fanlike textural pattern seen in the present compounds.

Table 1. Mesophase transition temperatures (T, °C) and associated enthalpies (ΔH, kJ mol^{-1}) of the compounds.

Compounds	Heating	Cooling
L	Cr 82.4 (65) I	I 75.1 (1.9) SmA 60.8 (60.7) Cr
L′	Cr 84.7 (61.3) I	I 65.4 (59.8) Cr
Cu_2L_2	Cr 91.7 (3.0) SmA 133.0 (27.5) I	I 114.1 (27.9) SmA 89.3 (2.6) Cr
$Cu_2L'_2$	Cr 63.5 (2.1) SmA 136.2 (47.4) I	I 118.9 (47.3) SmA 63.5 (2.3) Cr

Cr: crystalline; I: isotropic; SmA: smectic A.

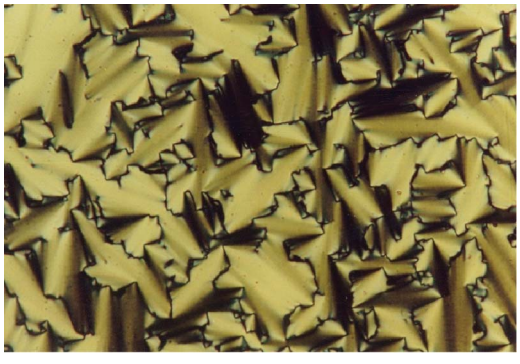

Fig. 5. Broken focal conic-shaped texture of the SmA phase at 114°C.

As efforts to obtain single crystals of the complexes failed, density functional theory (DFT) calculations were performed to investigate the electronic structure of the copper(II) complexes (Figures 7 and 8). Full geometry optimisation of the complexes without symmetry constraints has been carried out by DMol3 program package [42] using Kohn–Sham theory. The generalised gradient approximation (GGA) was used in the calculations. At the GGA level, we have chosen the BLYP (Becke-Lee-Yang-Parr) functional [42–45] which incorporates Becke's exchange and the Lee–Yang–Parr correlation [43]. The DNP (Double Numerical Polarisation) basis functions, chosen in the present study, are the double-numerical atomic orbitals augmented by polarisation functions, i.e. functions with angular momentum one higher than that of the highest occupied orbital in the free atom [45]. The DNP basis set is believed to be more

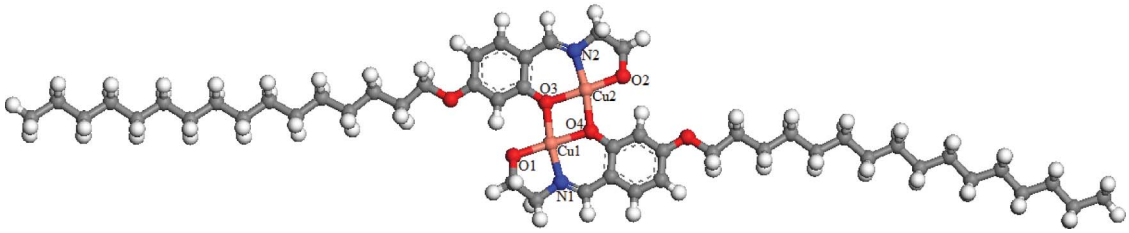

Fig. 7. DFT structure of Cu_2 L_2.

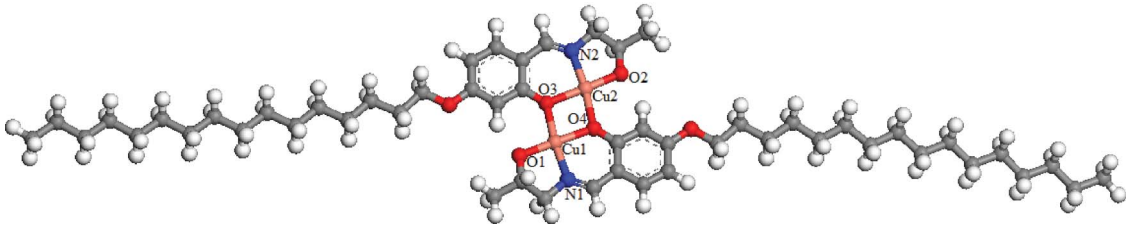

Fig. 8. DFT structure of $Cu_2L'_2$.

accurate than a Gaussian basis set 6-31G** of similar size. In our calculations, self-consistent field procedures are performed with a convergence criterion of 2×10^{-5} a.u. on the total energy and 10^{-6} a.u. on the electron density. Some of the significant geometric parameters of the optimised copper complexes evaluated at the BLYP/DNP level are shown in Table 2. The molecular structures of the complexes are nearly flat with two copper atoms lying ~3.15 Å apart. The geometry around each metal centre is slightly distorted square planar. The HOMO (Highest Occupied Molecular Orbital) and LUMO (Lowest Unoccupied Molecular Orbital) energies of the complex Cu_2L_2 are calculated to be -3.502 eV and -3.035 eV, respectively, where $\Delta E = 0.467$ eV and those of Cu_2 L'_2 are found to be -3.515 and -3.052, where $\Delta E = 0.463$ eV.

3. Conclusion

Two new tridentate [ONO]-donor one-ring Schiff base ligands with substituted long alkoxy group and their dinuclear copper(II) complexes have been synthesised and their mesomorphic and photophysical properties investigated. The ligands are found to be intense blue light emitters, showing emission maxima in the range ~447–469 nm both in solution and in the solid state. Interestingly, the steric constraints imposed by the methyl group in the spacer of the Schiff base ligand are speculated to have upset the mesogenicity; however, in the absence of the methyl group, liquid crystallinity could be observed. Lower conductivity values confirm the non-electrolytic nature of the complexes. Thermally very stable, the complexes exhibited a fanlike textural pattern characteristic

Table 2. Selected bond length and bond angles of Cu_2 L_2/ $Cu_2L'_2$, from DFT.

	Cu_2 L_2	$Cu_2L'_2$
Structure parameter	Bond lengths (Å) and bond angles (deg)	Bond lengths (Å) and bond angles (deg)
Cu1—O1	1.921	1.919
Cu1—N1	1.954	1.961
Cu2—O2	1.920	1.919
Cu2—N2	1.958	1.922
Cu2—O3	2.045	2.041
Cu2—O4	2.060	2.058
Cu1—O3	2.047	2.046
Cu1—O4	2.054	2.044
O1—Cu1—O3	103.1	103.4
O4—Cu—N1	92.0	92.0
O—Cu—O	79.5	79.6
N2—Cu2—O2	85.7	86.1
Cu1—Cu2	3.151	3.144

of the enantiotropic SmA mesophase. Based on the spectral and density functional theory (DMol3) study, a distorted square planar geometry around each metal centre in the dinuclear framework has been conjectured. The synthetic strategy employed may be profitably utilised to access dinuclear complexes of different metals.

4. Experimental section

4.1 Physical measurements

The C, H and N analyses were carried out using a PE2400 elemental analyser (Perkin Elmer, USA). Molar conductances of the compounds were determined in CH_2Cl_2 (ca. 10^{-3} mol L^{-1}) at room temperature using a MAC-554 conductometer (Macroscientific Works, India). The ^{1}H -NMR spectra were recorded on a Bruker DPX-400MHz spectrometer (Bruker AXS, India) in $CDCl_3$ (chemical shift in δ) solution with TMS (Tetramethylsilane) as internal standard. UV-vis absorption spectra of the compounds in CH_2Cl_2 were recorded on a Shimadzu UV-1601PC spectrophotometer (Shimadzu, Asia Pacific, Pte. Ltd., Singapore). The mass spectra were recorded on JEOL SX102 FAB mass spectrometer (JEOL, Japan) Photoluminescence spectra were recorded on a Shimadzu RF-5301PC spectrophotometer (Shimadzu, Asia Pacific, Pte. Ltd., Singapore). The fluorescence quantum yields in dichloromethane were determined by a dilution method using 9,10-diphenyl anthracene as standard. IR spectra were recorded on a Perkin-Elmer L 120-000A spectrometer (Perkin Elmer, USA) on a KBr disc. The optical textures of the different phases of the compounds were studied using a polarising microscope (Nikon optiphot-2-pol, Nikon Corporation, Tokyo, Japan) with an Instec hot and cold stage HCS302 attached, with a STC200 temperature controller of 0.1°C accuracy. The thermal behaviours of the compounds were studied using a Perkin-Elmer differential scanning calorimeter (Perkin Elmer International, Switzerland) Pyris-1 spectrometer with a heating or cooling rate of 5°C/min. Quantum chemical calculations were performed using DFT as implemented in the DMol3 package.

4.2 Materials

The materials were procured from Tokyo Kasei, Japan and Lancaster Chemicals, USA. All solvents were purified and dried using standard procedures. Silica (60–120 mesh) from Spectrochem was used for chromatographic separation. Silica gel G (E-Merck, India) was used for TLC (Thin Layer Chromatography).

4.3 Synthesis and analysis: Synthesis of hexadecyloxysalicyldehyde

Alkoxysalicyldehyde derivatives were prepared following the general method reported in the literature [7–11, 36]. 2, 4-Dihydroxybenzaldehyde (10 mmol, 1.38 g), $KHCO_3$ (10 mmol, 1.5 g), KI (catalytic amount) and 1-bromohexadecane (10cm^3, 3g) were mixed in 250 cm^3 of dry acetone. The mixture was heated under reflux for 24 h, and then filtered, while hot, to remove any insoluble solids. Dilute HCl was added to neutralise the solution, which was then extracted with chloroform (100 cm^3). The combined chloroform extract was concentrated to give a purple solid. The solid was purified by column chromatography using a mixture of chloroform and hexane (v/v, 1/1) as eluent. Evaporation of the solvents afforded a white solid product.

4.3.1. (E)-5-(hexadecyloxy)-2-((2-hydroxyethyl imino) methyl) phenol (L)

An ethanolic solution of 2-hydroxy-(4-hexadecyloxy)-salicylaldehyde (0.36 g, 1 mmol) was added to an ethanol solution of 2-amino-1-ethanol (0.06 g, 1 mmol) The solution mixture was refluxed with a few drops of acetic acid as catalyst for 3 h to yield the yellow Schiff base. The compound was collected by filtration and recrystallised from absolute ethanol to obtain a pure compound.

Yield: 0.308 g (78%) yellow coloured solid; melting point (m.p.) 87°C. Anal.: calc. for $C_{25}H_{43}NO_3$ (405.6): C, 74.06; H, 10.69; N 3.45; found: C, 74.07; H, 10.67; N, 3.46%. ^{1}H NMR (400 MHz, $CDCl_3$): δ 0.87 (t, J=6.4 Hz, -CH_3, 3H), 1.27–1.83 (m, -CH_2 of methylene proton in side chain), 3.60 (t, J=4.1Hz, -CH_2N=C, 2H), 3.73 (t, J=4.0Hz, -CH_2OH, 2H), 3.91 (t, J=8.1Hz, -OCH_2, 2H), 7.09 (d, J= 8.6Hz, -C_6H_4, 1H), 8.53 (s, -N=CH, ^{1}H), 13.8 (s,1H, OH); ^{13}C NMR (75.45 MHz; $CDCl_3$; Me_4Si at 25°C, ppm) δ= 161.3 (-C1), 101.3 (-C2), 161.9 (-C3), 116.6 (-C4), 107.3 (-C5), 132.7 (-C6), 162.1(-C7), 69.6 (-NCH_2), 68.4 (-OCH_2); FAB (m/e, fragment): m/z: calc. 405.6; found: 406.6[M+H$^+$]; IR (ν_{max}, cm^{-1}, KBr):3433(νOH), 2918(ν_{as}(C-H), CH_3), 2919(ν_{as}(C-H), CH_2), 2849(ν_s(C-H), CH_3), 2850(ν_{as}(C-H), CH_2), 1626(νC=N), 1287(νC-O).

4.3.2. (E)-5-(hexadecyloxy)-2-((2-hydroxypropy limino) methyl) phenol (L′)

Yield: 0.322 g (75%) yellow coloured solid; m.p. 88°C. Anal.: calc. for $C_{26}H_{45}NO_3$ (419.3): C, 74.42; H, 10.81; N 3.34; found: C, 74.41; H, 10.83; N, 3.33%. ^{1}H NMR (400 MHz, $CDCl_3$): δ 0.89 (t, J=6.4Hz, -CH_3, 3H), 1.28 (s, -CH_3) 1.27–1.83 (m, -CH_2 of methylene proton

in side chain), 3.62 (t, *J*=4.1Hz, -CH_2N=C, 2H), 3.74 (t, *J*=4.0Hz, -CH_2OH, 2H), 3.93 (t, *J*=8.1Hz, -OCH_2, 2H), 7.08 (d, *J*= 8.6Hz, -C_6H_4, 1H), 8.51 (s, -N=CH, ^{1}H), 13.7 (s,1H, OH); FAB (m/e, fragment): m/z: calc. 419.3; found: 420.3[M+H^+]; IR (ν_{max}, cm^{-1}, KBr):3432(νOH), 2917(ν_{as}(C-H), CH_3), 2916(ν_{as} (C-H), CH_2), 2845(ν_s(C-H), CH_3), 2851(ν_{as}(C-H), CH_2), 1622(νC=N), 1283(νC-O).

4.3.3. Syntheses of the copper complexes

The ligand L (0.40 g, 1 mmol) or L′ (0.41 g, 1 mmol) was dissolved in a minimum volume of absolute ethanol. An equimolar amount of copper acetate $Cu(OAc)_2$. H_2O (0.19 g, 1 mmol) in methanol was then added slowly and stirred for 2 h at room temperature. A greenish blue solid formed immediately and this was filtered, washed with diethyl ether and recrystallised from chloroform-ethanol (1:1).

4.3.4. Bis [N-(2-hydrooxyethyl)-4-hexadecyloxy salicyldiminato] copper (II): Cu_2L_2

Yield=0.442 g, 75%. Anal.: calc. for $C_{50}H_{82}Cu_2N_2O_6$: C, 64.28; H, 8.85; N, 3.00; found: C, 64.27; H, 8.86; N, 3.01%. IR ($\nu_{max,\,cm}{}^{-1}$, KBr): 2921($\nu_{as(C-H),}$ CH_3), 2851($\nu_{as(C-H),}$ CH_2), 1612($\nu_{C=N}$), 1252(ν_{C-O}, ether), 1148 (ν_{C-O}, phenolic); FAB (m/e, fragment): m/z: calc. 932.4; found: 933.5[M+H^+].

4.3.5. Bis [N-(2- hydroxypropan-2-ylimino)-4-hexa decyloxysalicyldiminato] copper (II): $Cu_2L'_2$

Yield=0.446 g, 78%. Anal.: calc. for $C_{52}H_{86}Cu_2N_2O_6$: C, 64.90; H, 9.01; N, 2.91; found: C, 64.91; H, 9.02; N, 2.92%. IR ($\nu_{max,\,cm}{}^{-1}$, KBr): 2922($\nu_{as(C-H),}$ CH_3), 2849($\nu_{as(C-H),}$ CH_2), 1613($\nu_{C=N}$), 1251(ν_{C-O}, ether), 1147 (ν_{C-O}, phenolic). FAB (m/e, fragment): m/z: calc. 962.5; found: 963.5[M+H^+].

Acknowledgments

The authors thank SAIF, NEHU and CDRI, Lucknow for analytical and spectral data. CD acknowledges financial support from UGC, Government of India. Dr R.C. Deka, Tezpur University, India, is acknowledged for the computational facilities.

References

[1] Donnio, B.; Guillon, D.; Deschenaux, R.; Bruce, D.W. *Comprehensive Coordination Chemistry II*; Elsevier: Oxford, 2003; Vol. 7, pp 357–627.
[2] Coe, B.J. *Comprehensive Coordination Chemistry II*; Elsevier Pergamon: Oxford, 2004; Vol. 9, pp 621–687.
[3] Hoshino, N. *Coord. Chem. Rev.* **1998**, *174*, 77–108.
[4] Giroud-Godquin, A.M.; Maitlis, P.M. *Angew. Chem. Int. Ed.* **1991**, *30*, 375–402.
[5] Espinet, P.M.; Esteruelas, A.; Oro, L.A.; Serrano, J.L.; Sola, E. *Coord. Chem. Rev.* **1992**, *117*, 215–274.
[6] Pucci, D.; Aiello, I.; Bellusci, A.; Crispini, A.; Ghedini, M.; La Deda, M.; *Eur. J. Inorg. Chem.* **2009**, 4274–4281.
[7] Bhattacharjee, C.R.; Das, G.; Mondal, P.; Rao, N.V.S. *Polyhedron*, **2010**, *29*, 3089–3096.
[8] Bhattacharjee, C.R.; Das, G.; Mondal, P.; Prasad, S. K.; Rao, D.S.S. *Eur. J. Inorg. Chem.* **2011**, 1418–1424.
[9] Bhattacharjee, C.R.; Das, G.; Mondal, P.; Prasad, S.K.; Rao, D.S S. *Inorg.Chem.Commun.* **2011**, *14*, 606–612.
[10] Bhattacharjee, C.R.; Das, G.; Mondal, P. *Liq. Cryst.* **2011**, *38*, 441–449.
[11] Bhattacharjee, C.R.; Das, G.; Mondal. P.; Prasad, S.K.; Rao, D.S S. *Liq. Cryst.* **2011**, *38*, 615–623.
[12] Barberio, G.; Bellusci, A.; Crispini, A.; Ghedini, M.; Golemme, A.; Prus, P.; Pucci, D. *Eur. J. Inorg. Chem.* **2005**, 181–188.
[13] Lai, C.K.; Leu, Y.-F. *Liq. Cryst.* **1998**, *25*, 689–698.
[14] Rezvani, Z.; Ghanea, M.A.; Nejati, K.; Baghaei, S.A. *Polyhedron* **2009**, *28*, 2913–2918.
[15] Espinet, P.; Hernandez, C.; M.-Alvarez, J.M.; Miguel, J.A. *Inorg. Chem.* **2004**, *43*, 843–845.
[16] Lai, C.K.; Lin, R.; Lu, M.-Y.; Kao, K.-C. *J. Chem. Soc., Dalton. Trans.* **1998**, 1857–1862.
[17] Ku, S.-M.; Wu, C.-Yi.; Lai, C.K. *J. Chem. Soc., Dalton. Trans.* **2000**, 3491–3492.
[18] Li, S.-Y.; Chen, C.-J.; Lo, P.-Y.; Sheu, H.-S.; Lee, G.-H.; Lai, C.K. *Tetrahedron* **2010**, *66*, 6101–6112.
[19] Barbera, J.; Gimenez, R.; Marcos, M.; Serrano, J.L.; Alonso, P.J.; Martinez, J.I. *Chem. Mater.* **2003**, *15*, 958–964.
[20] Chae, H.W.; Kadkin, O.N.; Choi, M.-G. *Liq. Cryst.* **2009**, *36*, 53–60.
[21] Marcos, M.; Omenat, A.; Barbera, J.; Duran, F.; Serrano, J.L. *J. Mater. Chem.* **2004**, *14*, 3321–3327.
[22] Lai, C.K.; Serrette, A.G.; Swager, T.M. *J. Am. Chem. Soc.* **1992**, *114*, 7948–7949.
[23] Espinet, P.; Lalinde, E.; Marcos, M. Perez, J.; Serrano, J.L. *Organometallics* **1990**, *9*, 555–560.
[24] Eguchia, S.; Nozaki, T.; Miyasaka, H.; Matsumoto, N.; Okawa, H. Kohata, S.; H-Miyajima, N. *J. Chem. Soc., Dalton Trans.* **1996**, 1761–1762.
[25] Ghedini, M.; Pucci, D.; Munno, G.D.; Viterbo, D.; Neve, F.; Armentano, S. *Chem. Mater.* **1991**, *3*, 65–72.
[26] Lai, C.K.; Chang, C.-H.; Tsai, C.-H. *J. Mater. Chem.* **2007**, *17*, 2319–2328.
[27] Glebowska, A.; Przybylski, P.; Winek, M.; Krzyczkowaska, P.; Krowczynski, A.; Szydlowska, Z.; Pociecha, D.; Gorecka, E. *J. Mater. Chem.* **2009**, *19*, 1395–1398.
[28] Barbera, J.; Levelut, A.M.; Marcos, M.; Romero, P.; Serrano, J.L. *Liq.Cryst.* **1991**, *10*, 119–126.
[29] Barbera, J.; Gimenez, R.; Gimeno, N.; Marcos, M.; Pina, M.D.C.; Serrano, J.L. *Liq. Cryst.* **2003**, *30*, 651–661.
[30] Lai, C.K.; Chen, F.-G.; Ku, Y.-J.; Tsai, C.-H.; Lin, R. *J. Chem. Soc., Dalton. Trans.* **1997**, 4683–4687.
[31] Lai, C.K.; Lu, M.-Y.; Lin, F.-J. *Liq. Cryst.* **1997**, *23*, 313– 315.
[32] Serrette, A.G.; Lai, C.K.; Swager, T.M. *Chem. Mater.* **1994**, *6*, 2252–2268.
[33] Binnemans, K.; G.-Walrand, C. *Chem. Rev.* **2002**, *102*, 2303–2345.
[34] Galyametdinov, Yu.G.; Ivanova, G.I.; A. Prosvirin, V.; Kadkin, O. *Russ. Chem. Bull.* **1994**, *43*, 938–940.
[35] Galyametdinov, Yu.; Athanassopoulou, G.M.A.; Griesar, K.; Kharitonova, O.; Soto, E.A.; Bustamante,

W.; Tinchurina, L.; Ovchinnikov, I.; Haase, W. *Chem. Mater.* **1996**, *8*, 922–926.
[36] Bhattacharjee, C.R.; Das, G.; Goswami, P.; Mondal, P.; Prasad, S.K. Rao, D.S.S. *Polyhedron* **2011**, *30*, 1040–1047.
[37] Son, H.-J.; Han, W.-S.; Chun, J.-Y.; Kang, B.-K.; Kwon, S.-N.; Ko, J.; Han, S. J.; Lee, C.; Klm, S.J.; Kang, S.O. *Inorg. Chem.* **2008**, *47*, 5666–5676.
[38] Cavero, E.; Uriel, S.; Romero, P.; Serrano, J.L.; Giménez, R. *J. Am. Chem. Soc.* **2007**, *129* 11608–11618.
[39] Chattopadhyay, T.; Mukherjee, M.; Banu, K.S.; Banerjee, A.; Suresh, E.; Zangrando, E.; Das, D. *J. Coord. Chem.* **2009**, *62*, 967–979.
[40] Chen, X.; Yamaguchi, A.; Namekawa, M.; Kamijo, T.; Teramae, N.; Tong, A. *Ana. Chim. Acata.* **2011**, *24*, 94–100.
[41] Lu, Y.; Liu, J.W. *J. Am. Chem. Soc.* **2007**, *129*, 9838–9839.
[42] Delley, B. *J. Chem. Phys.* **1990**, *92*, 508–518.
[43] Lee, C.; Yang, W.; Parr, R. G. *Phys. Rev. B: Condens. Matter Mater. Phys.* **1988**, *37*, 785–789.
[44] Koelling, D.D.; Harmon, B.N. *J. Phys. C: Solid State Phys.* **1977**, *10*, 31707–3114.
[45] Douglas, M.; Kroll, N.M. *Ann. Phys.* **1974**, *82*, 89–155.

Liquid Crystals
Publication details, including instructions for authors and subscription information:
http://www.tandfonline.com/loi/tlct20

Green emissive salicylaldimine-based polar Schiff bases with short alkoxy tails and their copper(II)/oxovanadium(IV) complexes: synthesis and mesomorphism

Chira R. Bhattacharjee [a] , Chitraniva Datta [a] , Gobinda Das [a] & Paritosh Mondal [a]
[a] Department of Chemistry, Assam University, Assam, India
Version of record first published: 30 Jan 2012.

To cite this article: Chira R. Bhattacharjee , Chitraniva Datta , Gobinda Das & Paritosh Mondal (2012): Green emissive salicylaldimine-based polar Schiff bases with short alkoxy tails and their copper(II)/oxovanadium(IV) complexes: synthesis and mesomorphism, Liquid Crystals, 39:3, 373-385

To link to this article: http://dx.doi.org/10.1080/02678292.2011.652199

Liquid Crystals,
Vol. 39, No. 3, March 2012, 373–385

Taylor & Francis
Taylor & Francis Group

Green emissive salicylaldimine-based polar Schiff bases with short alkoxy tails and their copper(II)/oxovanadium(IV) complexes: synthesis and mesomorphism

Chira R. Bhattacharjee*, Chitraniva Datta, Gobinda Das and Paritosh Mondal

Department of Chemistry, Assam University, Assam, India

(*Received 11 November 2011; final version received 19 December 2011*)

A series of salicylaldimine-based copper(II) and oxovanadium(IV) complexes of the type $[ML_2]$ (M = Cu and VO, L = N,N′-bis-(4-X-amino phenyl (4′-n-alkoxy)-salicylaldiminato), $n = 4$, 6; X = Cl, NO_2) have been synthesised. The mesomorphic behaviour of the ligands and their complexes was probed by polarising optical microscopy and differential scanning calorimetry. The formation of mesophases was dependent not only on the electronic or the steric factors of the substituents but also on metal centre. The ligands all showed a smectic or nematic mesophase. However, nitro-substituted compounds with ($n = 4$) lacked any mesomorphism. Complexes (X = Cl, NO_2, $n = 4$, 6 and M = Cu) exhibited smectic A phases. The vanadyl complexes did not show any mesogenicity. Variable temperature magnetic susceptibility measurements were carried out for the copper and vanadyl complexes. The complexes obey the Curie–Weiss law. Cyclic voltammetry showed a single electron quasireversible response for the complexes. Density functional theory analysis study revealed a distorted square planar and square pyramidal geometry for the copper(II) and vanadyl complexes, respectively. At 330 nm excitation, the ligands showed green emission in the solid state (∼ 516–559 nm, Φ = 12–9%) at room temperature.

Keywords: metallomesogen; copper; vanadium; photoluminescence; DFT

1. Introduction

The design and synthesis of paramagnetic complexes associated with multifunctional properties such as magnetic, electronic, mesogenic or photoluminescent properties desirable for technological applications is quite a challenging task for synthetic chemists [1–5]. The research domain of metallomesogens has expanded rapidly and received an enormous boost over the last few decades [6–14]. Metal complexes derived from Schiff base ligands feature amongst the earliest and most widely studied classes of metallomesogens [12–14]. The advantages of incorporating the imine functionality lie in the diverse range of potential structures and their ease of preparation. The salicylaldimine fragment is well recognised as a good liquid crystalline material because the azomethine linkage is stabilised by intramolecular hydrogen bonding, and it has the ability to coordinate metals [14, 15]. Moreover, if such materials emit light, they could be used in electro-optical devices and organic light-emitting diodes [16]. Compounds that combine both luminescence and liquid crystallinity are fast emerging as among the most promising candidates for varied applications in materials science [16–22]. In an earlier report, we described the first example of blue emissive one-ring salicylaldimine ligands exhibiting smectic mesomorphism [18]. In the last few years, a wide variety of metallomesogens have been synthesised based on salicylaldimine ligands [15, 23]. Among the first row transition metals, metallomesogens with copper(II)/VO(IV)/Ni(II) and Zn(II) ions exhibiting various smectic, nematic and columnar liquid crystalline phases have been prepared and studied by our group recently [17, 19, 24–29]. Coordination compounds of redox active metals that exhibit paramagnetism can produce novel conductors, magneto-optic data storage, and display devices [5, 30]. Unlike other transition metals, the presence of dative bonding between oxovanadium(IV) cores leads to a polymeric V=O. . .V=O. . . chain formation. Oxovanadium complexes are thus quite significant in the context of novel ferroelectric/piezoelectric and non-linear optical materials [30].

The liquid crystalline behaviour of an organic compound is essentially dependent on its molecular architecture, in which a slight change in its molecular geometry brings about considerable variation in its mesomorphic properties [31, 32]. The majority of the metallomesogens based on salicylaldimine fragments that have been reported so far possess an alkyl or alkoxy tail on either side of the aromatic rings [15, 27–29, 33–42]. However, metallomesogens of salicylaldimine-type ligands with polar substituents have not been adequately addressed [28, 43, 44]. The effect of polar substituents in a variety of mesogenic systems has been sporadically investigated during

*Corresponding author. Email: crbhattacharjee@rediffmail.com

ISSN 0267-8292 print/ISSN 1366-5855 online

http://dx.doi.org/10.1080/02678292.2011.652199
http://www.tandfonline.com

recent years. Introducing a lateral polar substituent at the aromatic core plays key role in phase behaviour [45–47]. Recently a systematic investigation on a variety of salicylaldimine-based oxovanadium(IV) complexes, bearing both alkyl, alkoxy or polar substituent, was reported by us [27–29]. All the compounds exhibited different type of mesophases.

As a part of our systematic investigation, the present article mainly focuses on the influence of the aromatic substituents on the mesomorphic and photophysical properties of the compounds. Accordingly we wish to report here a series of newer low molecular weight oxovanadium(IV) and copper(II) complexes with lateral polar groups. It is pertinent to mention here that the Schiff base reported herein exhibited green emission, hitherto unreported for such 4-substituted salicylaldimine compounds.

2. Results and discussion

Synthesis of the compounds was carried out following a procedure (Scheme 1) similar to that reported earlier for related systems by us [27–30]. The ligands [N,N′-bis-(4-X-amino phenyl (4′-n-alkoxy)-salicylaldiminato)] are hereafter abbreviated as *n*-X, where *n* indicates the number of carbon atoms in alkoxy chains, $n = 4, 6$; X=Cl, NO_2 and their Cu(II), VO(IV) complexes (Cu-n-X/ VO-n-X).

Infrared (IR) spectra of the complexes showed a shift of ν_{CN} vibrational stretching frequency at ca. 1625 cm^{-1} to a lower wave number ($\Delta\nu \sim 30$ cm^{-1}) and absence of ν_{OH} mode and phenolate oxygen upon chelation, clearly suggesting the coordination of azomethine-N and phenolate-O to the metal. The $\nu_{C=N}$ stretching frequency is rather independent of the length of alkoxy side chain in both ligands and their complexes. The vanadyl(V=O) stretching at ca.

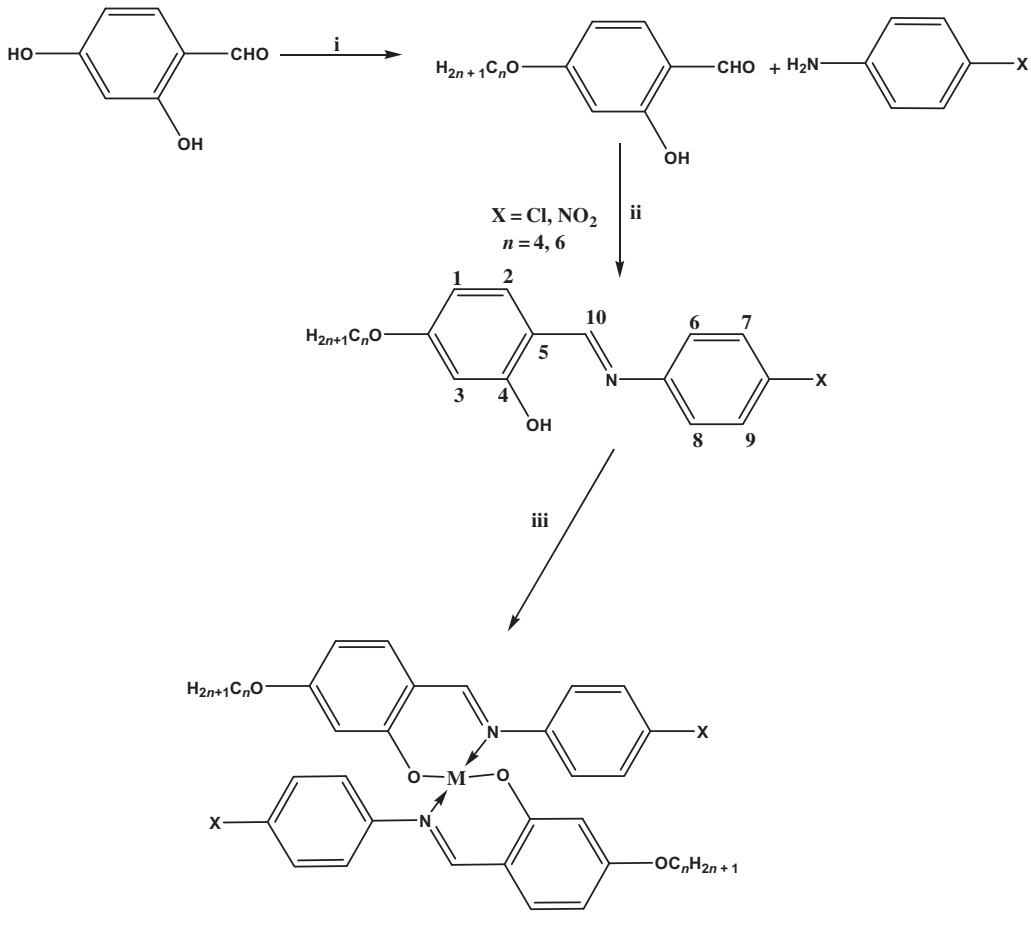

Scheme 1. (i) $C_nH_{2n+1}Br$, $KHCO_3$, KI, dry acetone, Δ, 40 h, and (ii) glacial AcOH, absolute EtOH Δ, 4 h (iii) $Cu(OAc)_2$. H_2O/ $VOSO_4.5H_2O$, MeOH, TEA. Δ, 1 h.

980 cm^{-1} is suggestive of the absence of any intermolecular (. . .V=O. . .V=O. . .) interaction, indicating the monomeric nature of the complexes. The presence of linear chain interactions usually cause $\nu_{V=O}$ to shift to a lower wave number (ca. 870 cm^{-1}). The IR data also showed the V=O stretching frequency to be insensitive to the length of the alkoxy side chain. Moreover, two weak bands in the low-energy region (400–600 cm^{-1}) assignable to $\nu_{(M\text{-}N)}$ and $\nu_{(M\text{-}O)}$ provide compelling evidence for the coordinated metal ion in the ligand framework. The redox behaviour for Cu-6-NO_2/VO-6-NO_2 complexes was probed by cyclic voltammetry in dichloromethane solution in the potential range −4.0–1.4 V versus SCE electrode at a scan rate of 0.05 V s^{-1}. The voltammogram (Figure 1) displayed a quasireversible (peak separation >100 mV) one-electron response. The peak separation ($E_{1/2} = +0.453 E_p^{\,c} = -0.485$ V, $E_p^{\,a} = -0.385$ V, $\Delta E_p = 0.100$ V) is assigned to the Cu (II)/Cu (I) couple. The electrochemical behaviour of the vanadium complex (VO-6-NO_2) also displayed a quasireversible (peak-to-peak separation >100 mV) cyclic voltammetric response due to the VO^{3+}/VO^{2+} couple at ($E_{1/2} = +0.605$ V, $E_p^{\,c} = 0.391$ V, $E_p^{\,a} = 0.822$ V, $\Delta E_p = 0.431$ V).

The effective magnetic moments of the complex VO-6-NO_2 and Cu-6-NO_2 were found to be 1.72B.M (d^1) and 1.81B.M (d^9), respectively. The inverse magnetic susceptibility for a representative complex, VO-6-NO_2, is plotted against temperature (Figure 2), satisfying the Curie–Weiss equation. The effective magnetic moment did not vary appreciably in the range of experimental temperature.

The ultraviolet–visible (UV-vis) absorption spectra (Figure 3) of the ligands consists of an intense band centred at ∼344–372 nm attributed to π–π^* transitions of the azomethine group. Another weak band (at 288–291 nm) in the higher energy region was due to π–π^* transitions of benzene rings. Upon complexation these bands are red shifted (Figures 4 and 5). The UV-vis data are summarised in Table 1. Photoluminescence studies of the compounds were carried out at room temperature in the solid state (Figure 6). The ligands emit green light at 538 nm ($\Phi = 12\%$) for chloro-substituted compounds and at 559 nm ($\Phi = 9\%$) for the nitro-substituted ones when excited at 330 nm. The solid state emission spectrum of the complex was recorded by placing a uniform powder sheet between two quartz plates. The λ_{max} values of all the nitro-substituted compounds are red shifted owing to the electron-withdrawing nature of the –NO_2 group. The Schiff bases exhibit fluorescence due to intraligand (π–π^*) transitions [48]. Complexes did not

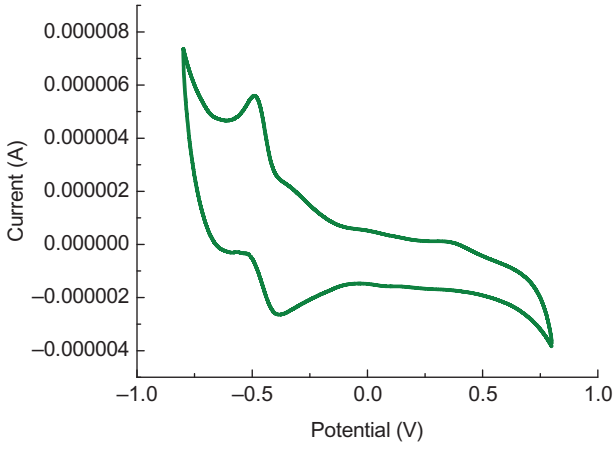

Figure 1. Cyclic voltammogram of Cu-6-NO_2.

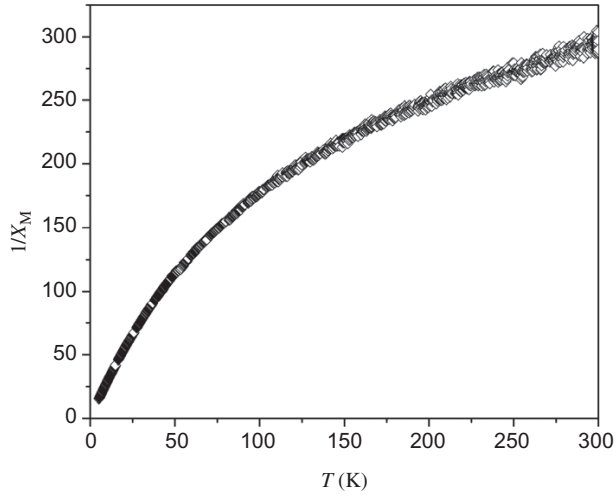

Figure 2. Variation of inverse magnetic susceptibility of VO-6-NO_2 with temperature.

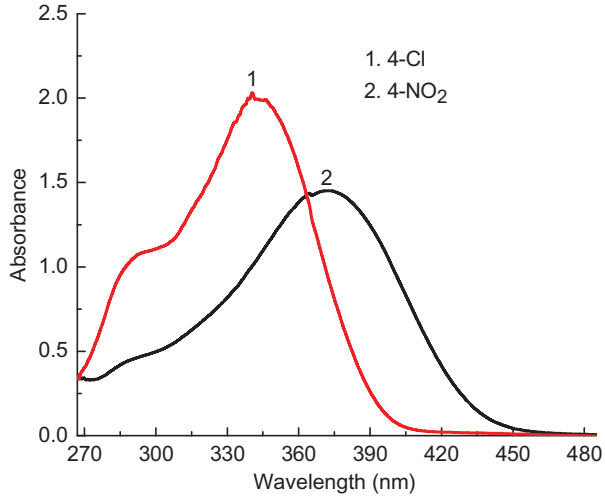

Figure 3. UV-visible spectra of 4-Cl and 4-NO_2.

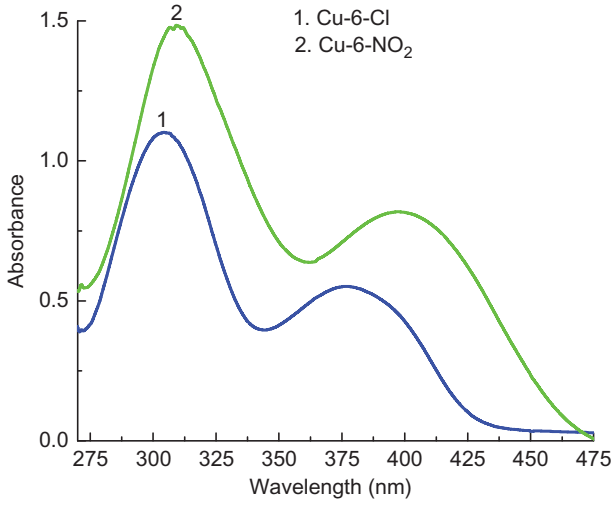

Figure 4. UV-visible spectra of Cu-6-Cl and Cu-6-NO_2.

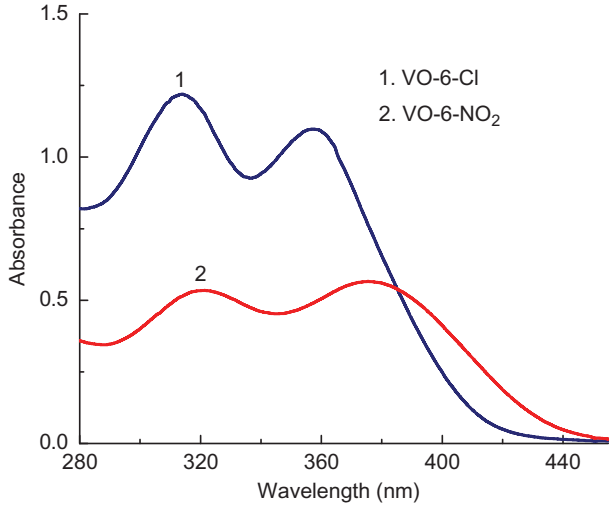

Figure 5. UV-visible spectra of VO-6-Cl and VO-6-NO_2.

exhibit any emission, presumably because paramagnetic ions quench the fluorescence of organic ligands by enhancing the rate of non-radiative processes (intersystem crossing, etc.) that compete with fluorescence [49, 50]. It may be noted that quenching of fluorescence of a ligand by paramagnetic metal ions on complexation is a rather usual phenomenon which is explained by processes such as magnetic perturbation, redox-activity, electronic energy transfer, etc.

The mesomorphic properties of the compounds were investigated using polarised optical microscopy (POM) and differential scanning calorimetry (DSC). The phase transitions and thermodynamic data are summarised in Table 2. The formation of mesophases is strongly dependent on the electronic and/or the steric factors of the substituents. Compound 4-NO_2 was found to be non-mesogenic. However, the 4-Cl

Table 1. UV-visible and photoluminescence data of ligands and complexes.

Compounds	$\pi \rightarrow \pi^*$ (ε, l mol^{-1} cm^{-1})	PL[a] (Solid)
4-Cl	290(11300)	538
	342(14200)	
VO-4-Cl	314(11200)	–
	358(14100)	
Cu-4-Cl	305(12200)	–
	378(13200)	
6-Cl	292(11400)	541
	343(14300)	
VO-6-Cl	313(12200)	–
	354(14100)	
Cu-6-Cl	304(12400)	–
	377(13400)	
4-NO_2	294(4700)	554
	374(14500)	
VO-4-NO_2	323(5200)	–
	379(5400)	
Cu-4-NO_2	312(14300)	–
	401(8100)	
6-NO_2	295(4600)	559
	377(14400)	
VO-6-NO_2	326(5300)	–
	381(5200)	
Cu-6-NO_2	314(14200)	–
	406(8200)	

[a] Photoluminescence data.

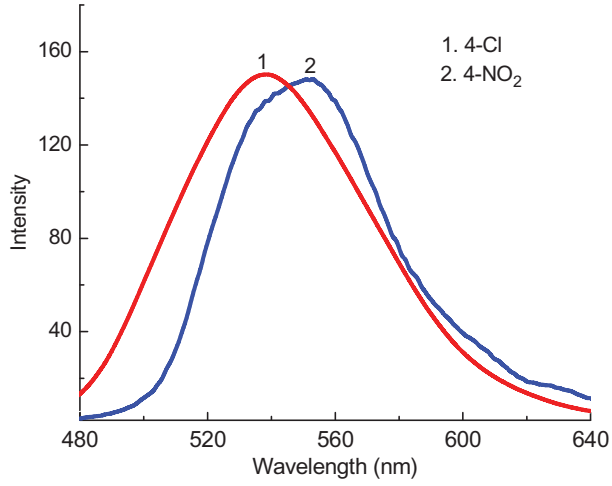

Figure 6. Photoluminescence spectra of 4-Cl and 4-NO_2.

compound showed an enantiotropic SmA mesophase. The compound melts to an isotropic liquid at 118°C. Upon cooling the sample a highly birefringent fanlike texture is formed, which is characteristic of the SmA phase (Figure 7). The DSC trace (Figure 8) showed three transitions in the heating cycle and two in the cooling cycle. The compound is thermally quite stable. Although a crystal-to-crystal phase transition was encountered in DSC, in the POM study this could

Table 2. Phase transitions temperatures (T, °C), associated enthalpies (ΔH, kJ mol^{-1}) of *n*-X and their complexes.

Compounds	Heating	Cooling
4-Cl	Cr 93.2(7.5)Cr 96(12.8)SmA 118.7(3.8)I	I 116.7(3.4)SmA71.8(6.0)Cr
4-NO_2	Cr 116.7 (7.9) I	I 56.8(8.5)Cr
6-Cl	Cr 78.1 (15.6) SmA 122.6 (4.1) I	I 121.4 (3.9) SmA 47.4 (14.5)
6-NO_2	Cr 42.3(0.7)N92.6(0.7)I	I 91.5(0.8)N41.7(0.5)Cr
Cu-4-Cl	Cr 236.6(26.4) I	I 198.2(5.3)SmA193.7(1.6)Cr
Cu-4-NO_2	Cr 234.7(21.6) I	Cr 45.8(9.6) I
Cu-6-Cl	Cr 216.1(20.0) I	I 208.6(1.7) SmA 176.0(20.8)
Cu-6-NO_2	Cr 217.2(17.3)SmA227.0(71.2)I	I 211.3(71.1)SmA201.4(4.7)Cr
VO-6-Cl	Cr 182.2(21.4)I	I68.1(14.2)Cr
VO-6-NO_2	Cr 178.2(12.4)I	I58.1(13.2)Cr

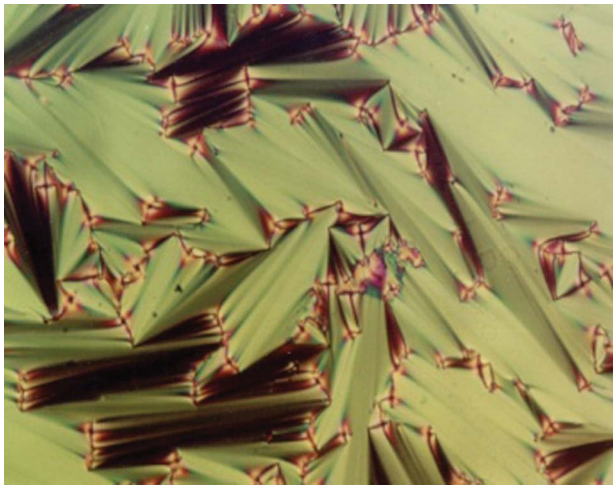

Figure 7. Fan-like texture of SmA phase(4-Cl).

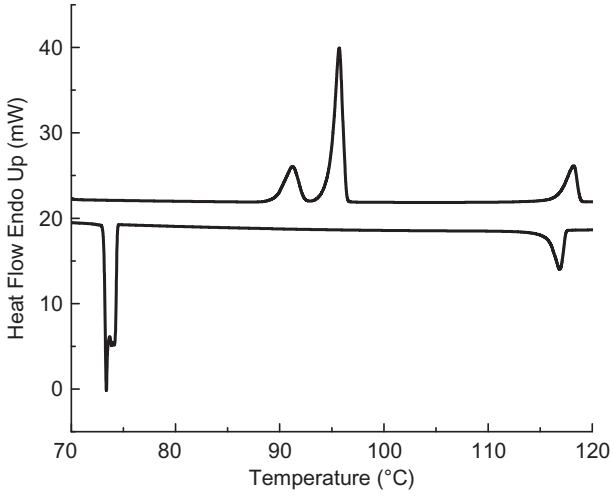

Figure 8. DSC thermogram of (4-Cl).

not be detected. A quite different trend, however, was observed for the 6-Cl and 6-NO_2 compounds. The 6-Cl compound exhibited a SmA phase over a wide temperature range. Surprisingly, unlike the other compounds being reported here, the compound 6-NO_2 showed a nematic phase (N) (Figure 9) with a very low enthalpy value ($\Delta H = 0.81$ Kj mol^{-1}). The DSC traces (Figure 10) showed two transitions both in heating and cooling cycles. We have no suitable explanation for

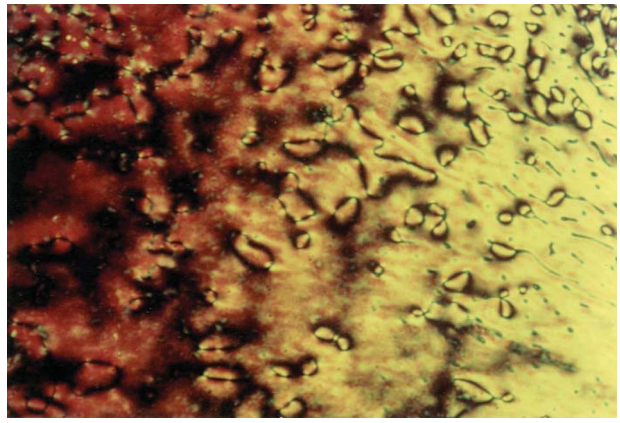

Figure 9. Schlieren texture of N phase (6-NO_2).

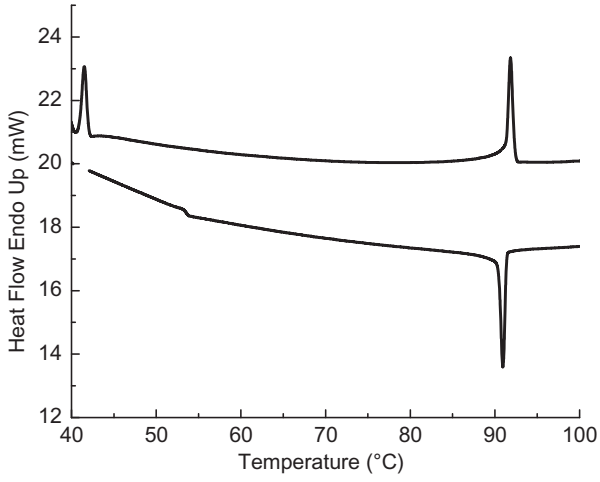

Figure 10. DSC thermogram of 6-NO_2.

this behaviour at this stage. For the ligands, both the melting point and clearing point of chloro-substituted compounds is about 30°C higher than in the nitro-substituted compound. In our previous report we also noted similar behaviour; in addition, the nitro compound with carbon chain length $n = 10$ and 18 displayed a SmA phase [28]. The melting temperatures of the complexes were always substantially higher than those of the ligands. When nitro substituted, the mesomorphism was upset in complexes with a carbon chain length $n = 4$. Copper complexes were all found to be mesogenic and revealed a SmA phase (Figure 11) at ~200–225°C. Owing to the highly viscous nature of the compound and the severe restriction in the molecular mobility, a pronounced hysteresis in the transition temperature was noted. Among the whole series of complexes, only Cu-6-NO_2 exhibited enantiotropic mesomorphism with high thermal stability. The compounds Cu-4-Cl and Cu-6-Cl showed monotropic mesomorphism. The DSC thermogram for the typical compound Cu-6-NO_2 is shown in Figure 12. None of the vanadyl complexes showed any mesogenicity.

The first task for the density functional theory (DFT) calculation is to determine the lowest energy electronic structure of the representative compounds. Geometry optimisations and energy calculations of Cu-6-Cl (Figure 13), Cu-6-NO_2 (Figure 14), VO-6-Cl (Figure 15) and VO-6-NO_2 (Figure 16) complexes were performed using the unrestricted BLYP/DNP methods without imposing any symmetry constraints. The BLYP functional used comprises a hybrid exchange functional as defined by Becke, and the non-local Lee–Yang–Parr correlation functional [51]. The basis set chosen in this study is DNP, the double-numerical atomic orbitals augmented by polarisation functions. All calculations were performed with the

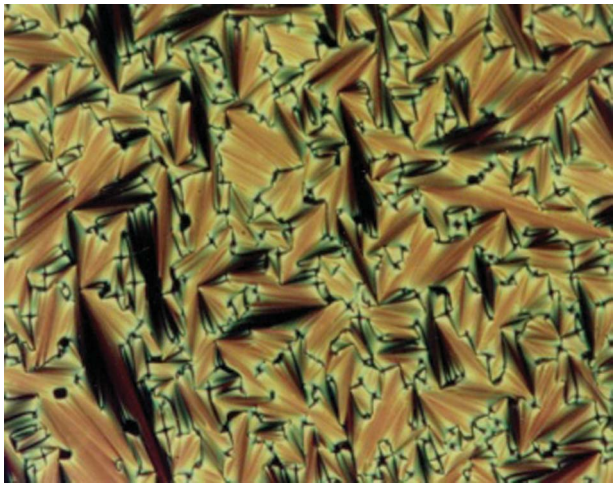

Figure 11. Focal conic texture of SmA phase. (Cu-6-NO_2).

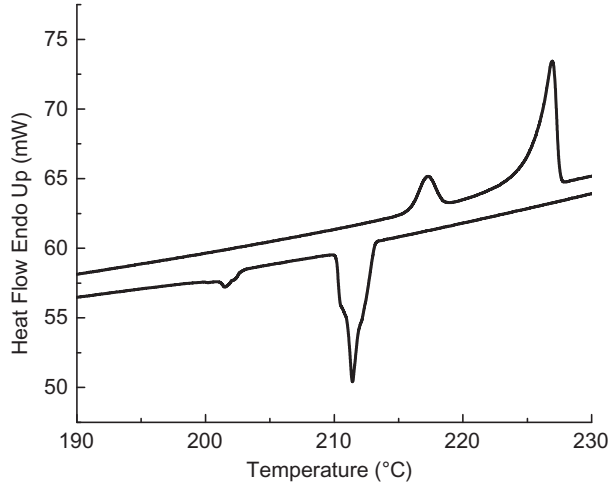

Figure 12. DSC trace of Cu-6-NO_2.

DMol3 program package [52]. The 3D iso-surface plots of the lowest unoccupied molecular orbital (LUMO) and highest occupied molecular orbital (HOMO) of copper and vanadium complexes are shown in Figures 17–24. The analysis of the wave function indicates that the electron absorption corresponds to the transition from the ground to the first excited state, and is mainly described by one-electron excitation from the HOMO to the LUMO. In both the copper complexes, the electron density of the HOMO is localised mainly on the aromatic rings bearing the alkoxy substituent, while the LUMO is localised on and around the copper atom. The noticeable differences in the distribution of electron densities on the HOMO as well as LUMO of Cu-6-Cl and Cu-6-NO_2 complexes may be ascribed to the nature of the different substituent on the aromatic rings. The molecular orbital energies of HOMO and LUMO of Cu-6-Cl are calculated as −5.149 eV and −4.044 eV, respectively, $\Delta E = 1.105$ eV. Corresponding energies for Cu-6-NO_2 complex have been found to be −5.563 eV and −4.471 eV, respectively, $\Delta E = 1.092$ eV. It is also noted, from Figures 21–24, in both vanadium complexes the electron density of HOMO is localised on the vanadium atom. The LUMO of VO-6-Cl is localised on the V–N bond along with the C=N double bond, while the LUMO of VO-6-NO_2 is concentrated mainly on the –NO_2 substituent containing the aromatic ring. The orbital energies of HOMO and LUMO of the V-Cl complex were evaluated to be −5.134 eV and −3.244 eV, respectively, $\Delta E = 1.890$ eV. The corresponding energies for the VO-6-NO_2 complex have been calculated as −5.536 eV and −3.769 eV, respectively, $\Delta E = 1.767$ eV. A relatively lower HOMO and LUMO energy gap for copper and vanadium complexes explains the eventual charge transfer interactions taking place within the molecule.

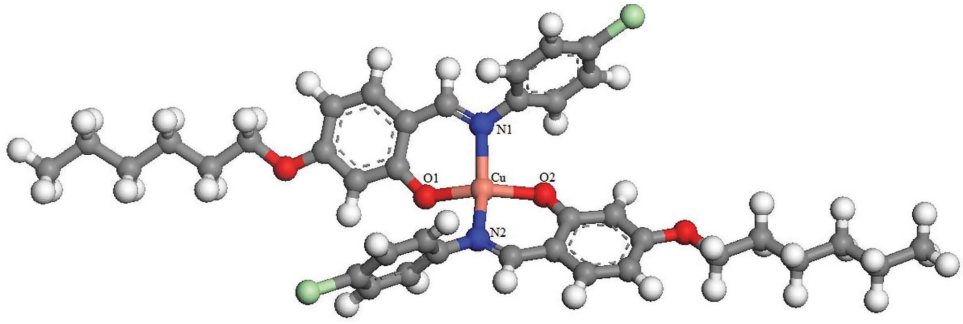

Figure 13. Optimised structure of Cu-6-Cl.

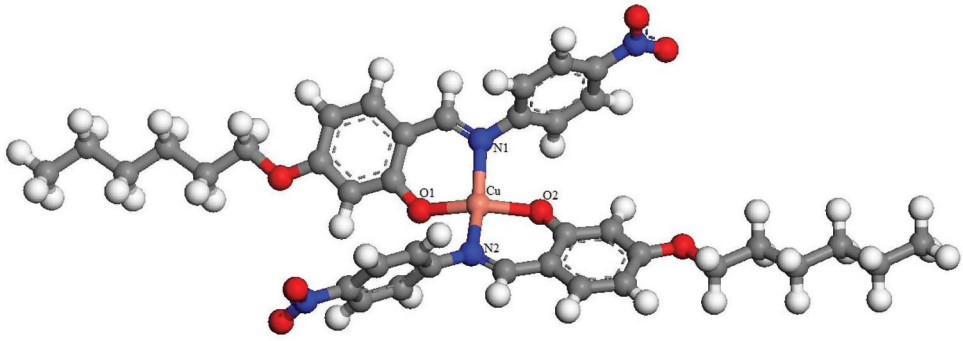

Figure 14. Optimised structure of Cu-6-NO_2.

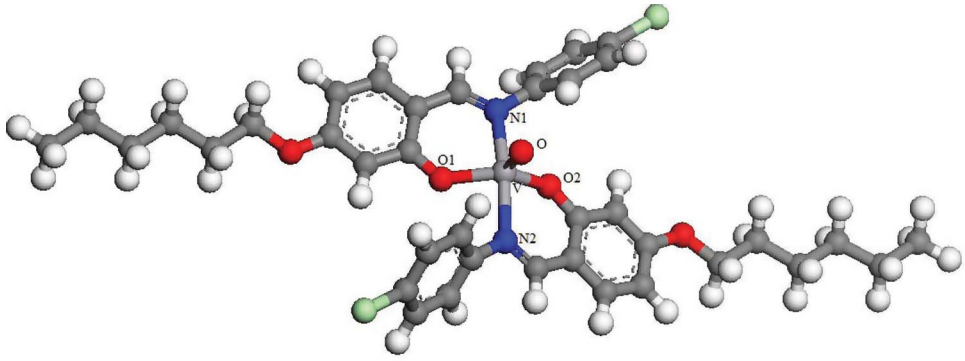

Figure 15. Optimised structure of VO-6-Cl.

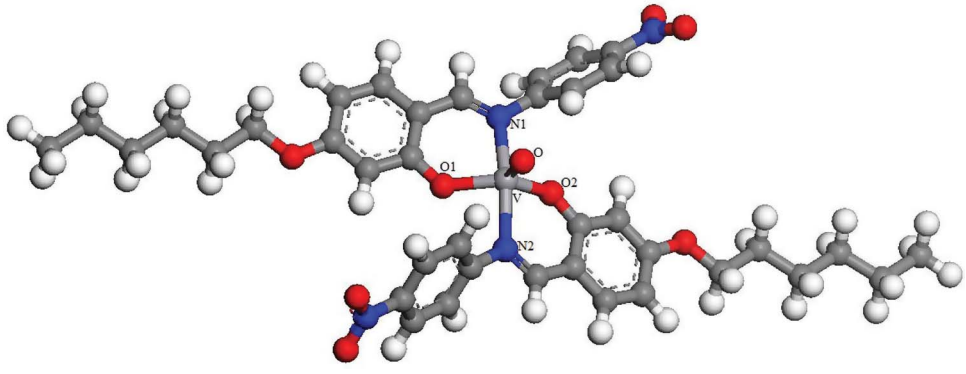

Figure 16. Optimised structure of VO-6-NO_2.

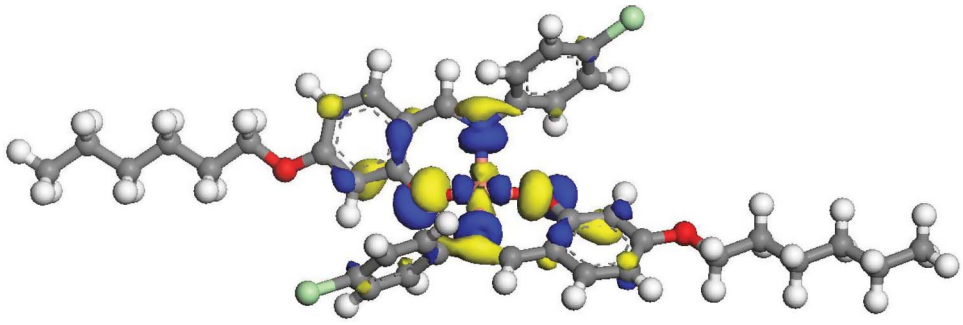

Figure 17. HOMO of Cu-6-Cl.

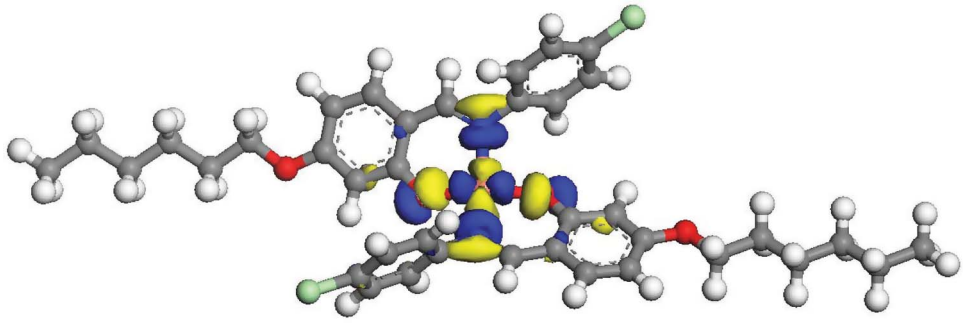

Figure 18. LUMO of Cu-6-Cl.

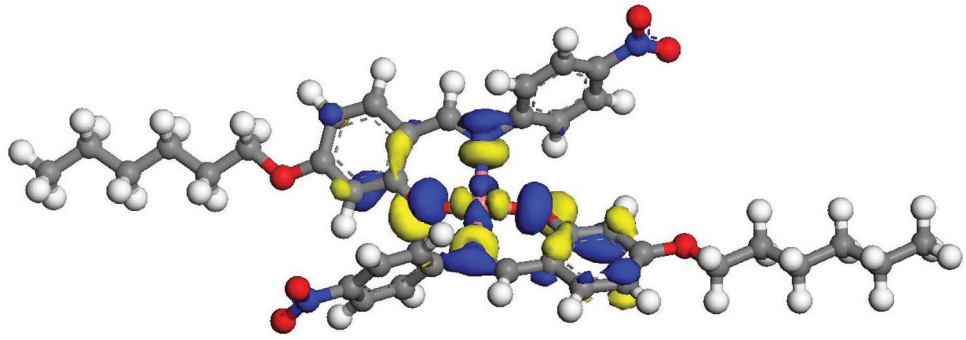

Figure 19. HOMO of Cu-6-NO_2.

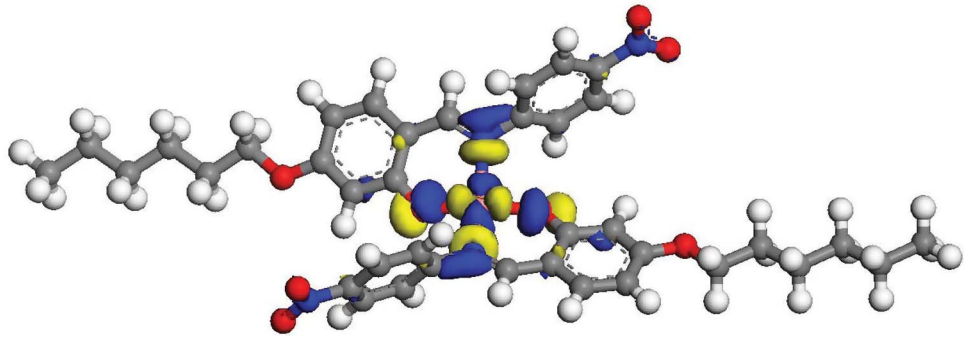

Figure 20. LUMO of Cu-6-NO_2.

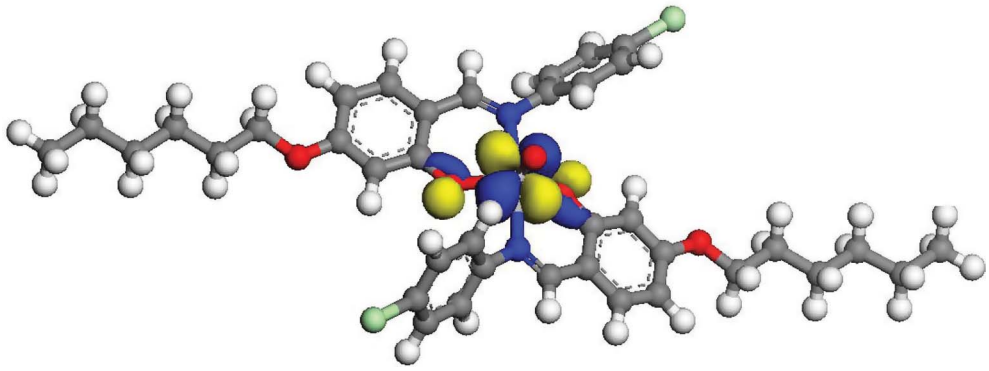

Figure 21. HOMO of VO-6-Cl complex.

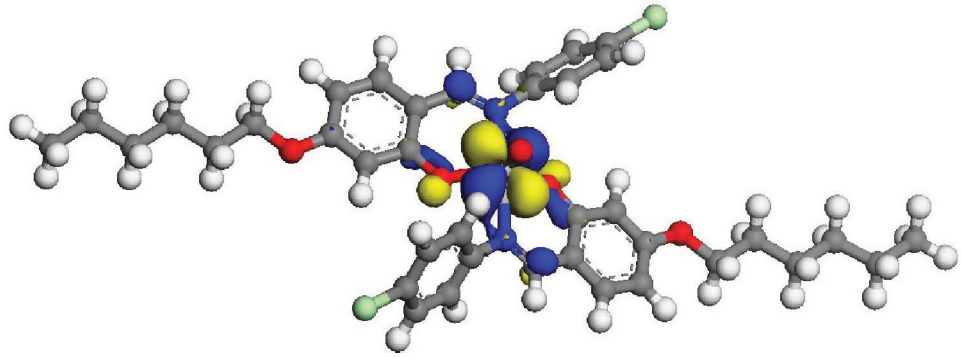

Figure 22. LUMO of VO-6-Cl complex.

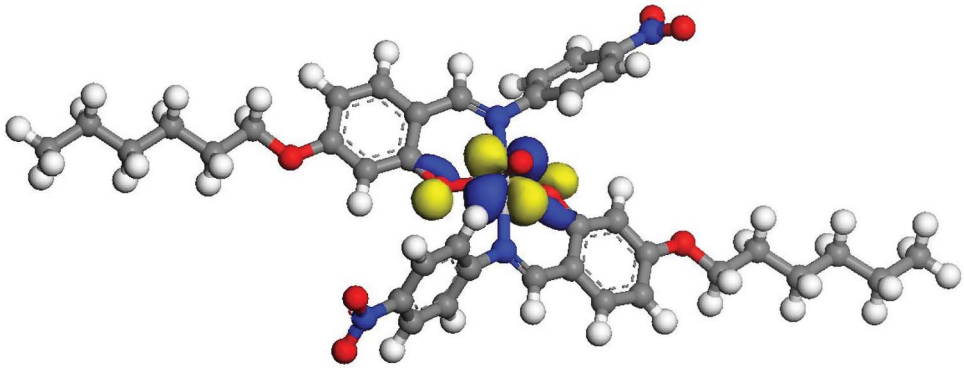

Figure 23. HOMO of VO-6-NO_2 complex.

The lower energy differences also reflect the chemical activity of these copper and vanadium complexes. Hence, copper complexes are predictably more reactive than vanadium complexes. The chemical hardness values of Cu-6-Cl, Cu-6-NO_2, V-6-Cl and V-6-NO_2 complexes were evaluated as 0.553, 0.546, 0.945 and 0.884 eV, respectively, at BLYP/DNP level. The maximum hardness principle [53] states that the higher the hardness, the higher is the stability, i.e. the lower is the reactivity. It was also noted that the introduction of the -NO_2 substituent increases the reactivity of the copper and vanadium complexes. Some of the significant geometric parameters of optimised copper and vanadium complexes, evaluated by DFT calculation at BLYP/DNP level, are shown in the Table 3 and Table 4, respectively. The Cu–O1, Cu–O2, Cu–N1 and Cu–N2 bond lengths of the Cu-6-Cl complex are 1.947, 1.946, 2.041 and 2.043 Å, respectively, implying the presence of regular σ and dative bonding. The bond angles O1–Cu–O2, N1–Cu–N2, O1–Cu–N1 and

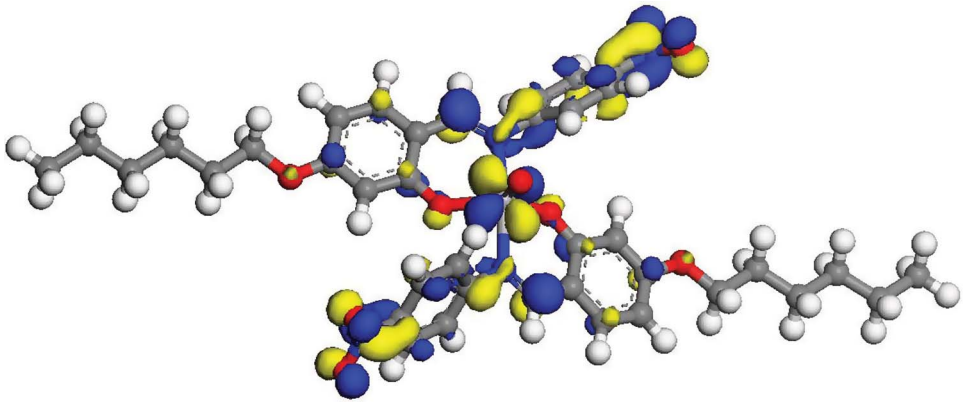

Figure 24. LUMO of VO-6-NO_2 complex.

Table 3. Selected bond lengths (Å) and bond angles (°) of Cu-6-Cl and Cu-6-NO_2 complexes optimised at the BLYP/DNP level.

Structure parameter	Cu-6-Cl	Cu-6-NO_2
Cu—O1	1.947	1.941
Cu—O2	1.946	1.939
Cu—N1	2.041	2.047
Cu—N2	2.043	2.052
O1—Cu—O2	151.4	154.5
N1—Cu—N2	147.7	150.7
O1—Cu—N1	93.0	92.7
O2—Cu—N2	93.0	92.7

Table 4. Selected bond lengths (Å) and bond angles (°) of VO-6-Cl and VO-6-NO_2 complexes optimised at the BLYP/DNP level.

Structure parameter	VO-6-Cl	VO-6-NO_2
V—O1	1.950	1.944
V—O2	1.950	1.944
V—O	1.623	1.622
V—N1	2.175	2.178
V—N2	1.177	2.178
O1—V—O2	127.6	127.7
N1—V—N2	163.4	162.6
O1—V—N1	86.5	86.4
O2—V—N2	86.4	86.4

O2–Cu–N2 around the Cu atom are calculated to be 151.40°, 147.70°, 93.00° and 93.00°, respectively, suggested a slightly distorted square planar geometry. These geometrical parameters match well with related structurally characterised square planar copper complexes [54]. The bond angles of 127.60° and 163.40° for O1–V–O2 and N1–V–N2, respectively, in complex VO-6-Cl, and 127.70° and 162.60° for O1–V–O2 and N1–V–N2, respectively, in the VO-6-NO_2 complex confirm a distorted square pyramidal geometry around the vanadyl(IV) centre.

3. Conclusion

Two series of oxovanadium(IV) and copper(II) salicylaldimine complexes bearing polar substituent on aromatic rings have been successfully synthesised. A lower conductivity value confirms the non-electrolytic nature of the complexes. The mesomorphic properties of the compounds are strongly dependent on substituent as well as on carbon chain length. The ligands are found to exhibit smectic/nematic mesomorphism. However, the nitro-substituent compound with a C_4 tail lacks any mesomorphism. None of the oxovanadium complexes are found to be monogenic. Interestingly, the copper complexes except the nitro-substituted one (C_4 tail) are mesogenic and showed smectic A phase at >200°C. A cyclic voltammetry study revealed a quasireversible one-electron response for all the complexes. Variable temperature magnetic susceptibility studies suggested occurrence of isolated spin centres with hardly any exchange interaction. The $\nu_{V=O}$ band at ~980 cm^{-1} also suggested the lack of any discernible . . .V=O. . . V=O. . . interaction. Based on spectral and DFT studies, a tentative five-coordinate square pyramidal structure for vanadium, and a square planar structure for copper complexes have been proposed.

4. Experimental details

4.1 Physical measurements

The C, H and N analyses were carried out using a PE2400 elemental analyser. The ^{1}H-NMR spectra were recorded on a Bruker DPX-400MHz spectrometer in $CDCl_3$ (chemical shift in δ) solution

with TMS as internal standard. UV-vis absorption spectra of the compounds in CH_2Cl_2 were recorded on a Shimadzu UV-160PC spectrophotometer. Photoluminescence spectra were recorded on a Shimadzu RF-5301PC spectrophotometer. The fluorescence quantum yield in dichloromethane was determined by using 9, 10-diphenyl anthracene as standard. IR spectra were recorded on a Perkin-Elmer L 120-000A spectrometer on a KBr disc. Mass spectra were recorded on a Jeol SX-102 spectrometer with fast atom bombardment. The optical textures of the different phase of the compounds were studied using a polarising microscope (Nikon optiphot-2-pol) attached with Instec hot and cold stage HCS302, with STC200 temperature controller of 0.1°C accuracy. The thermal behaviour of the compounds was studied using a Perkin-Elmer differential scanning calorimeter Pyris-1 spectrometer with a heating or cooling rate of 5°C min^{-1}. Quantum chemical calculations on complexes were carried out using DFT as implemented in the DMol3 package.

4.2 Materials

The materials were procured from Tokyo Kasei and Lancaster Chemicals. All solvents were purified and dried using standard procedures. Silica (60–120 mesh) from Spectrochem was used for chromatographic separation. Silica gel G (E-Merck, India) was used for thin-layer chromatography.

4.3 Synthesis of 4-n-octadecyloxysalicylaldehyde

2,4-dihydroxybenzaldehyde (2.7 g, 20 mmol), potassium bicarbonate (2 g, 20 mmol), potassium iodide (catalytic amount) and 1-bromobutane (2.7 g, 20 mmol) or 1-bromohexane (3.2 g, 20 mmol) were mixed in 400 cm^3 dry acetone. The mixture was refluxed for 40 h and filtered when hot to remove insoluble solids. Dilute hydrochloric acid was added to neutralise the warm solution, which was then extracted twice with $CHCl_3$. The combined $CHCl_3$ extracts were concentrated to give a purple solid. The solid was purified by column chromatography with silica gel (100–200) mesh with a mixture of hexane: $CHCl_3$ (1:1). The solvent was evaporated to give a white solid product.

4.4 Synthesis of the ligands

4.4.1 N-(4-n-butyloxysalicylidene)-4′-4-chlroaniline (4-Cl)

An ethanolic solution of (4-n-hexcyloxy)-salicyldehyde (0.19 g, 1 mmol) was added to an ethanolic solution of 4-chloroaniline (0.12 g, 1 mmol). The solution mixture was refluxed for 3 h with few drops of acetic acid as catalyst to yield the Schiff base N-(4-n-octadecyloxysalicylidene)-4′-n-chloroaniline. The solid was collected by filtration and recrystallised several times from absolute ethanol to give a pure compound.

Yield: 0.23 g (75%); m.p., 118°C. FAB Mass (m/e, fragment): m/z: calc. 303.1; found: 304.1[M+H^+]; Anal. Calc. for $C_{17}H_{18}ClNO_2$ (303.1): C, 67.21; H, 5.97; N 4.61. Found: C, 67.22; H, 5.95; N, 4.62%. ^{1}H NMR (400 MHz, $CDCl_3$): δ 0.88 (t, $J = 6.8$ Hz, 3H, CH_3), 0.93–1.8 (m, 4H, (-CH_2)2), 3.95 (t, $J = 6.7$ Hz, 2H, -OCH_2), 6.49 (s, 1H, H^1), 6.3 (d, $J = 6.3$, 1H, H^2), 7.3 (d, $J = 7.2$, 1H, H^3), 8.21 (s, 1H, CH=N), 13.7 (s, 1H, OH). IR (ν_{max}, cm^{-1}, KBr): 3435 (ν_{OH}), 2917 (ν_{as}(C-H), CH_3), 2879 (ν_s(C-H), CH_3), 1631 ($\nu_{C=N}$), 1277 (νC-O).

4.4.2 N-(4-n-hexyloxysalicylidene)-4′-6-chlroaniline (6-Cl)

Yield: 0.24 g (70%); m.p., 122°C. FAB Mass (m/e, fragment): m/z: calc. 331.1; found: 332.1 [M+H^+]; Anal. Calc. for $C_{19}H_{22}ClNO_2$ (331.1): C, 68.77; H, 6.68; N 4.22. Found: C, 68.72; H, 6.65; N, 4.23%. ^{1}H NMR (400 MHz, $CDCl_3$): δ 0.88 (t, $J = 6.8$ Hz, 3H, CH_3), 0.94–1.7 (m, 4H, (-CH_2)4), 3.94 (t, $J = 6.6$ Hz, 2H, -OCH_2), 6.48 (s, 1H, H^1), 6.4 (d, $J = 6.2$, 1H, H^2), 7.4 (d, $J = 7.1$, 1H, H^3), 8.22 (s, 1H, CH=N), 13.8 (s, 1H, OH). IR (ν_{max}, cm^{-1}, KBr): 3434 (ν_{OH}), 2918 (ν_{as}(C-H), CH_3), 2874 (ν_s(C-H), CH_3), 1632 ($\nu_{C=N}$), 1276 (νC-O).

4.4.3 N-(4-n-butyloxysalicylidene)-4′-4-nitroaniline (4-NO_2)

Yield: 0.25 g (75%); m.p., 116°C. FAB Mass (m/e, fragment): m/z: calc. 314.1; found: 315.1 [M+H^+]; Anal. Calc. for $C_{17}H_{18}N_2O_4$ (314.1): C, 64.96; H, 5.77; N 8.91. Found: C, 64.95; H, 5.75; N, 8.92%. ^{1}H NMR (400 MHz, $CDCl_3$): δ 0.96 (t, $J = 6.8$ Hz, 3H, CH_3), 0.94–1.7 (m, 4H, (-CH_2)2), 3.94 (t, $J = 6.6$ Hz, 2H, -OCH_2), 6.46 (s, 1H, H^1), 6.4 (d, $J = 6.2$, 1H, H^2), 7.4(d, $J = 7.1$, 1H, H^3), 8.22 (s, 1H, CH = N), 13.8 (s, 1H, OH). IR (ν_{max}, cm^{-1}, KBr): 3434 (ν_{OH}), 2918 (ν_{as}(C-H), CH_3), 2874 (ν_s(C-H), CH_3), 1632 ($\nu_{C=N}$), 1276 (νC-O), 1516 (ν_{as}(NO)), 1350 ((ν_s(NO)).

4.4.4 N-(4-n-hexyloxysalicylidene)-4′-6-nitroaniline (6-NO_2)

Yield: 0.25 g (75%); m.p., 122°C. FAB Mass (m/e, fragment): m/z: calc. 342.1; found: 343.1 [M+H^+]; Anal. Calc. for $C_{19}H_{22}N_2O_4$(342.1): C, 64.96; H, 5.77; N

8.91. Found: C, 66.65; H, 6.48; N, 8.18%. ^{1}H NMR (400 MHz, $CDCl_3$): δ 0.94 (t, $J = 6.7$ Hz, 3H, CH_3), 0.92–1.8 (m, 4H, (-CH_2)4), 3.93 (t, $J = 6.5$ Hz, 2H, -OCH_2), 6.44 (s, 1H, H^1), 6.42 (d, $J = 6.3$, 1H, H^2), 7.53 (d, $J = 7.1$, 1H, H^3), 8.21 (s, 1H, CH=N), 13.8 (s, 1H, OH). IR (ν_{max}, cm^{-1}, KBr): 3434 (ν_{OH}), 2918 (ν_{as}(C-H), CH_3), 2876 (ν_s(C-H), CH_3), 1632 ($\nu_{C=N}$), 1276 (νC-O), 1517 (ν_{as}(NO)), 1352 ((ν_s(NO)).

4.5 Synthesis of Cu(II) complexes (Cu-n-X, n = 4, 6 and X = Cl, NO_2)

The ligand 4-Cl (0.30 g, 1 mmol) or 6-Cl (0.33 g, 1 mmol) or 4-NO_2 (0.31 g, 1 mmol) or 6-NO_2 (0.34 g, 1 mmol) was dissolved in a minimum volume of absolute ethanol and copper acetate $Cu(OAc)_2$. H_2O (0.09 g, 0.5 mmol) in methanol was then added slowly and stirred for 2 h at room temperature. A pink solid, formed immediately, was filtered, washed with diethyl ether and recrystallised from chloroform-ethanol (1:1).

4.5.1 Cu-4-Cl

Yield: 0.29 g (75%); m.p., 237°C. FAB Mass (m/e, fragment): m/z: calc. 669.1; found: 670.1 [M+H^+]; Anal. Calc. For $C_{34}Cl_2H_{34}CuN_2O_4$ (669.1): C, 61.03; H, 5.12; N 4.19. Found: C, 61.02; H, 5.13; N, 4.18%. IR (ν_{max}, cm^{-1}, KBr): 2914 (ν_{as}(C-H), CH_3), 2874 (ν_s(C-H), CH_3), 1611 ($\nu_{C=N}$), 1274 (νC-O).

4.5.2 Cu-6-Cl

Yield: 0.31 g (76%); m.p., 227°C. FAB Mass (m/e, fragment): m/z: calc. 725.1; found: 726.1 [M+H^+]; Anal. Calc. for $C_{38}H_{42}Cl_2CuN_2O_4$ (725.1): C, 62.94; H, 5.84; N 3.86. Found: C, 61.92; H, 5.83; N, 3.85%. IR (ν_{max}, cm^{-1}, KBr): 2914 (ν_{as}(C-H), CH_3), 2874 (ν_s(C-H), CH_3), 1612 ($\nu_{C=N}$), 1274 (νC-O).

4.6 Synthesis of oxovanadium (IV) complexes (VO-n-X, n = 4, 6 and X = Cl, NO_2)

The ligand 4-Cl (0.30 g, 1 mmol) or 6-Cl (0.33 g, 1 mmol) or 4-NO_2 (0.31 g, 1 mmol) or 6-NO_2 (0.34 g, 1 mmol) was dissolved in minimum volume of absolute ethanol, and vanadyl sulphate, $VOSO_4.5H_2O$ (0.12 g, 0.5 mmol) dissolved in methanol was added to it followed by addition of triethylamine and reflux for 2 h. A greenish solid, formed immediately, was filtered, washed with diethyl ether and recrystallised from chloroform-ethanol.

4.6.1 VO-4-Cl

Yield: 0.31 g, 75%. Anal. Calc. for $C_{34}H_{34}$ $Cl_2N_2O_5V$ (671.1): C, 60.72; H, 5.10; N, 4.17. Found: C, 60.71; H, 5.11; N, 4.16%; FAB Mass (m/e, fragment): m/z: calc. 671.1; found: 672.1[M+H^+]. IR (ν_{max}, cm^{-1}, KBr): 2912 (ν_{as}(C-H), CH_3), 2873 (ν_s(C-H), CH_3), 1612 (νC=N), 981 ($\nu_{V=O}$).

VO-6-Cl

Yield: 0.31 g, 70%. Anal. Calc. for $C_{38}H_{42}$ $Cl_2N_2O_5V$ (727.1): C, 62.64; H, 5.81; N, 3.84. Found: C, 62.63; H, 5.82; N, 3.85%; FAB Mass (m/e, fragment): m/z: calc. 727.1; found: 728.1[M+H^+]. IR (ν_{max}, cm^{-1}, KBr): 2916 (ν_{as}(C-H), CH_3), 2877 (ν_s(C-H), CH_3), 1615 (νC=N), 982 ($\nu_{V=O}$).

4.6.2 VO-4-NO_2

Yield: 0.32 g, 76%. Anal. Calc. for $C_{34}H_{34}$ N_4O_9V (693.1): C, 58.88; H, 4.94; N, 8.08. Found: C, 58.86; H, 4.93; N, 8.07%; FAB Mass (m/e, fragment): m/z: calc. 693.1; found: 694.1[M+H^+]. IR (ν_{max}, cm^{-1}, KBr): 2917 (ν_{as}(C-H), CH_3), 2876 (ν_s(C-H), CH_3), 1613 (νC=N), 981 ($\nu_{V=O}$).

4.6.3 VO-6-NO_2

Yield: 0.34 g, 75%. Anal. Calc. for $C_{38}H_{42}$ N_4O_9V (749.2): C, 60.88; H, 5.65; N, 7.47. Found: C, 60.87; H, 5.64; N, 7.46%; FAB Mass (m/e, fragment): m/z: calc. 749.2; found: 750.2[M+H^+]. IR (ν_{max}, cm^{-1}, KBr): 2918 (ν_{as}(C-H), CH_3), 2876 (ν_s(C-H), CH_3), 1610 (νC=N), 983 ($\nu_{V=O}$).

Acknowledgements

The authors thank the Department of Science and Technology and University Grants Commission, New Delhi, for financial support and Prof. R.C. Deka (Tezpur University, India) for assistance with the theoretical calculations. Sophisticated Analytical Instrumentation Facility, North East Hill University, Shillong is acknowledged for spectral results.

References

[1] Lai, C.K.; Chang, C.-H.; Tsai, C.-H. *J. Mater. Chem*. **2007**, *17*, 2319–2328.
[2] Barbera, J.; Levelut, A.M.; Marcos, M.; Romero, P.; Serrano, J.L. *Liq. Cryst*. **1991**, *10*, 119–126.
[3] Barbera, J.; Gimenez, R.; Gimeno, N.; Marcos, M.; Pina, M.D.C.; Serrano, J.L. *Liq. Cryst*. **2003**, *30*, 651–661.

[4] Chou, S.-Y.; Chen, C.-J.; Tsai, S.-L.; Sheu, H.-S.; Lee, G.-H.; Lai, C.K. *Tetrahedron* **2009**, *65*, 1130–1139.
[5] Abe, Y.; Iyoda, A. Seto, K. Moriguchi, A.; Tanase, T.; Yokoyama, H. *Eur. J. Inorg. Chem*. **2008**, 2148–2157.
[6] Aiello, I.; Ghedini, M.; Neve, F.; Pucci, D. *Chem. Mater*. **1997**, *9*, 2107–2112.
[7] Singh, A.K.; Kumari, S.; Kumar, K.R.; Sridhar, B.; Rao, T.R. *Polyhedron* **2008**, *27*, 181–186.
[8] La Deda, M.; Grisolia, A.; Aiello, I.; Crispini, A.; Ghedini, M.; Belviso, S.; Amati, M. Lelj, F. *Dalton Trans*. **2004**, 2424–2431.
[9] Jung, B.M.; Huang, Y.D.; Chang, J.Y. *Liq. Cryst*. **2010**, *37*, 85–92.
[10] Donnio, B.; Guillon, D.; Deschenaux, R.; Bruce, D.W. *Comprehensive Coordination Chemistry II*; Elsevier: Oxford, **2003**, vol. 7; pp 357–627.
[11] Date, R.W.; Bruce, D.W. *Liq. Cryst*. **2004**, *31*, 1435–1444.
[12] Espinet, P.; Esteruelas, M.A.; Oro, L.A.; Serrano, J.L.; Sola, E. *Coord. Chem. Rev*. **1992**, *117*, 215–274.
[13] Giroud-Godquin, A.M.; Maitlis, P.M. *Angew. Chem. Int. Ed*. **1991**, *30*, 375–402.
[14] Hoshino, N. *Coord. Chem. Rev*. **1998**, *174*, 77–108.
[15] Prajapati, A.K.; Bonde, N. *Liq. Cryst*. **2006**, *33*, 1189–1197.
[16] Pucci, D.; Aiello, I.; Bellusci, A.; Crispini, A.; Ghedini, M.; La Deda, M. *Eur. J. Inorg. Chem*. **2009**, 4274–4281.
[17] Bhattacharjee, C.R.; Das, G.; Mondal, P.; Rao, N.V.S. *Polyhedron* **2010**, *29*, 3089–3096.
[18] Bhattacharjee, C.R.; Das, G.; Goswami, P.; Mondal, P.; Prasad, S.K.; Rao, D.S.S. *Polyhedron* **2011**, *30*, 1040–1047.
[19] Bhattacharjee, C.R.; Das, G.; Goswami, P.; Mondal, P.; Prasad, S.K.; Rao, D.S.S. *Eur. J. Inorg. Chem*. **2011**, 1418–1424.
[20] Kozhevnikov, V.N.; Donnio, B.; Bruce, D.W. *Angew. Chem. Int. Ed*. **2008**, *47*, 6286–6289.
[21] Forrest, S.R. *Nature (London, UK)* **2004**, *428*, 911.
[22] Ghedini, M.; Pucci, D.; Crispini, A.; Bellusci, A.; La Deda, M.; Aiello, I.; Pugliese, T. *Inorg. Chem. Commun*. **2007**, *10*, 243–247.
[23] Shanker, G.; Yelamaggad, C.V. *J. Mater. Chem*. **2011**, DOI: 101039/C1jm11947h.
[24] Bhattacharjee, C.R.; Das, G.; Mondal, P.; Prasad, S.K.; Rao, D.S.S. *Inorg. Chem. Commun*. **2011**, *14*, 606–612.
[25] Bhattacharjee, C.R.; Das, G.; Mondal, P. *Liq. Cryst*. **2011**, *38*, 441–449.
[26] Bhattacharjee, C.R.; Das, G.; Mondal, P.; Prasad, S.K.; Rao, D.S.S. *Liq. Cryst*. **2011**, *38*, 615–623.
[27] Bhattacharjee, C.R.; Das, G.; Purkayastha, D.D.; Mondal. P. *Liq. Cryst*. **2011**, *38*, 717–727.
[28] Bhattacharjee, C.R.; Das, G.; Purkayastha, D.D.; Mondal, P.; Kanoo. P. *J. Coord. Chem*. **2011**, *64*, 2746–2760.
[29] Bhattacharjee, C.R.; Das, G.; Mondal, P. *J. Coord. Chem*. **2011**, *64*, 3273–3289.
[30] Ghedini, M.; Morrone, S.; Bartolino, R.; Formoso, V.; Francescangeli, O.; Yang, B. *Chem. Mater*. **1993**, *5*, 876–882.
[31] Glebowska, A.; Przybylski, P.; Winek, Krzyczkowaska, M.P.; Krowczynski, A.; Szydlowska, Z.; Pociecha, D.; Gorecka, E. *J. Mater. Chem*. **2009**, *19*, 1395–1398.
[32] Szydlowska, J.; Krowczynski, A.; Gorecka, E.; Pociecha, D. *Inorg. Chem*. **2000**, *39*, 4879–4885.
[33] Caruso, U.; Diana, R.; Panunzi, B.; Roviello, A.; Tingoli, M.; Tuzi, A. *Inorg. Chem. Commun*. **2009**, *12*, 1135–1138.
[34] Kumari, S.; Singh, A.K.; Rao, T.R. *Mater. Sci. Eng. C* **2009**, *29*, 2454–2458.
[35] Singh, A.K.; Kumari, S.; Rao, T.R.; *Mater. Sci. Eng. C* **2011**, *31*, 1144–1147.
[36] Li, S.-Y.; Chen, C.-J.; Lo, P.-Y.; Sheu, H.-S.; Lee, G.-H.; Lai, C.K.; *Tetrahedron* **2010**, *66*, 6101–6112.
[37] Zheng, H.; Lai, C.K.; Swager, T.M. *Chem. Mater*. **1994**, *6*, 2252–2268.
[38] Zheng, H.; Lai, C.K.; Swager, T.M. *Chem. Mater*. **1995**, *7*, 2067–2077.
[39] Abe, Y.; Nakabayashi, K.; Matsukawa, N.; Takashima, H.; Iida, M.; Tanase, T.; Sugibayashi, M.; Mukai, H.; Ohta, K. *Inorg. Chim. Acta*. **2006**, *359*, 3934–3946.
[40] Sleven, J.; Cardinaels, T.; Binnemans, K.; Guillon, D.; Donnio, B. *Liq. Cryst*. **2002**, *29*, 1425–1433.
[41] Poelsma, S.N.; Servante, A.H.; Fanizzi, F.P.; Matlis, P.M. *Liq. Cryst*. **1994**, *16*, 675–685.
[42] Barbera, J.; Gimenez, R.; Serrano, J.L.; Alonso, P.J.; Martinez, J.I. *Chem. Mater*. **2003**, *15*, 958–964.
[43] Wang, C.-S.; Wang, I-W.; Cheng, K.-L.; Lai, C.K. *Tetrahedron* **2006**, *62*, 9383–9392.
[44] Eran, B.B.; Yorur, C.; Tschierske, C.; Prehm, M.; Baumeister, U. *J. Mater. Chem*. **2007**, *17*, 2319–2328.
[45] Duan, M.; Tasaka, T.; Okamoto, H.; Petrov, V.F.; Takenaka, S. *Liq. Cryst*. **2000**, *27*, 1195–1205.
[46] Fillppov, S.K.; Kolomiets, I.P.; Sokolova, O.S.; Antonov, E.A.; Zorin, I.M.; Bilibin, A.Y. *Liq. Cryst*. **1998**, *24*, 787–791.
[47] Yeap, G.-Y.; Ha, S.-T.; Lim, P.-L.; Boey, P.-L.; Ito, M.M.; Sanehisa, S.; Youhei, Y. *Liq. Cryst*. **2006**, *33*, 205–211.
[48] Chattopadhyay, T.; Mukherjee, M.; Banu, K.S.; Banerjee, A.; Suresh, E.; Zangrando, E.; Das, D. *J. Coord. Chem*. **2009**, *62*, 967–979.
[49] Chen, X.; Yamaguchi, A.; Namekawa, M.; Kamijo, T.; Teramae, N.; Tong, A. *Anal. Chim. Acta*. **2011**, *24*, 94–100.
[50] Lu, Y.; Liu, J.W. *J. Am. Chem. Soc*. **2007**, *129*, 9838–9839.
[51] Lee C.; Yang, W.; Parr, R.G. *Phys. Rev. B: Condens. Matter Mater. Phys*. **1988**, *37*, 785–789.
[52] Delley, B. *J. Chem. Phys*. **1990**, *92*, 508–518.
[53] Pearson, R.G. *J. Chem. Educ*. **1987**, *64*, 561–567.
[54] Khandar, A.A.; Nejati, K. *Polyhedron* **2000**, *19*, 607–613.

Liquid Crystals
Publication details, including instructions for authors and subscription information:
http://www.tandfonline.com/loi/tlct20

Induced columnar mesomorphism in non-discoid VO^{2+} salphen complexes: Transition between two rectangular columnar phases

Chira R. Bhattacharjee [a], Chitraniva Datta [a], Gobinda Das [a] & Paritosh Mondal [a]
[a] Department of Chemistry, Assam University, Silchar, 788011, Assam, India
Version of record first published: 08 May 2012.

To cite this article: Chira R. Bhattacharjee , Chitraniva Datta , Gobinda Das & Paritosh Mondal (2012): Induced columnar mesomorphism in non-discoid VO^{2+} salphen complexes: Transition between two rectangular columnar phases, Liquid Crystals, 39:7, 819-826

To link to this article: http://dx.doi.org/10.1080/02678292.2012.684074

Liquid Crystals,
Vol. 39, No. 7, July 2012, 819–826

Taylor & Francis
Taylor & Francis Group

Induced columnar mesomorphism in non-discoid VO^{2+} salphen complexes: Transition between two rectangular columnar phases

Chira R. Bhattacharjee*, Chitraniva Datta, Gobinda Das and Paritosh Mondal

Department of Chemistry, Assam University, Silchar 788011, Assam, India

(*Received 29 February 2012; final version received 4 April 2012*)

A new series of oxovanadium(IV) complexes of the type [VOL], L = N, N′-di-(4-*n*-alkoxysalicylidene)-4-Me-l,2-diamino-benzene (n = 14,16, 18) have been synthesised and their mesomorphic properties investigated. The compounds were characterised by Fourier transform infrared spectroscopy, ^{1}H and ^{13}C nuclear magnetic resonance spectroscopy, ultraviolet–visible spectroscopy, elemental analyses, solution electrical conductivity measurements and fast atom bombardment mass spectrometry. The phase behaviour of the compounds was examined by differential scanning calorimetry and polarised optical microscopy. The ligands are non-mesogenic, but upon coordination with vanadium(IV), exhibited enantiotropic rectangular columnar mesomorphism. The mesophase symmetry and the molecular organisation in the mesophases were confirmed by variable temperature powder X-ray diffraction study. An interesting phase behaviour exhibiting two types of rectangular columnar phases ($Colr_1$ to $Colr_2$) was observed for the vanadyl complexes, the former ($Colr_1$) being stable down to room temperature. Solution electrical conductivity measurements showed non-electrolytic nature of the complexes. Cyclic voltammetry revealed a single electron quasi-reversible response (VO^{2+}/VO^{3+}) for the complexes. Density functional theory study carried out using the DMol3 program indicated a distorted square pyramidal geometry for the complexes.

Keywords: vanadium; metallomesogen; columnar mesophase; density functional theory

1. Introduction

Oxovanadium(IV) salen type complexes have received significant attention due to their interesting physicochemical properties, bioactivities and catalytic functions in organic and inorganic transformations [1–8]. However, the design and synthesis of such materials desirable for technological applications is fraught with many challenges. In contrast to other transition metals, occurrence of weak intermolecular . . . V=O . . . .V=O . . . non-polar interaction involving oxovanadium(IV) cores leads to a polymeric chain formation which often frustrates the exhibition of mesogenic properties [1]. Oxovanadium complexes are thus quite significant in the context of novel ferroelectric/piezoelectric and non-linear optical (NLO) materials [7].

Metal containing liquid crystals are the most promising candidates for achieving such tuneable multifunctional properties because of the combination of optical, electronic and magnetic characteristics with those of anisotropic fluidity [9–11]. Due to unusual geometries and paramagnetism, metallomesogens incorporating VO(IV) metal ions continue to be a recurring theme of current research [12–19]. A rather large number of liquid crystalline vanadyl(IV) complexes have been reported [1, 20–26] and metal-salen complexes with 5-substituted alkoxy or alkyl chains exhibiting smectic mesomorphism are well documented [3, 4, 6, 8]. The 4-substituted salen type metallomesogens are, however, scanty. A series of mesogenic salen- and salphen- vanadyl complexes containing 4-substituted alkoxy tails on side aromatic ring are on record [1, 2, 5].

Recently our group has developed a series of structurally analogous 4-substituted zinc(II), oxovanadium(IV), nickel(II) as well as some copper(II) complexes using a cyclohexane/phenylene diamine spacer that exhibited different type of columnar phases [7, 20–25]. For non-discoid ligands, a molecular shape with a reduced aspect ratio often leads to the formation of discotic metallomesogens. Compounds that form columnar discotic liquid-crystalline mesophases with axially linked discs are of particular interest as potential one-dimensional photoconductors, semiconductors, organic light emitting diodes (OLEDs) and photovoltaic cells [27–36].

As a part of our continued efforts [7, 20–25] towards discotic metallomesogen, in this article we describe the synthesis and mesomorphic properties of a series of hemi-disc shaped oxovanadium(IV)–salphen complexes bearing a methyl-substituted aromatic spacer. Though the ligands are non-mesogenic, incorporation of vanadyl(IV) induced a very interesting mesomorphic behaviour. Pertinent here is to

*Corresponding author. Email: crbhattacharjee@rediffmail.com

ISSN 0267-8292 print/ISSN 1366-5855 online

http://dx.doi.org/10.1080/02678292.2012.684074
http://www.tandfonline.com

mention that analogous oxovanadium(IV) complexes dealt with in our earlier reports containing differently substituent aromatic spacer showed different phase transition behaviour [20–25].

2. Results and discussion

Synthesis of the compounds was achieved through a facile and straightforward procedure [7]. The synthetic strategy for the ligands [(L=N, N′-bis(4-(4′-n-alkoxy) salicylidene)1, 2-phenylenediamine), hereafter abbreviated as nmpd, where n indicates the number of carbon atoms in alkyl chains, n = 14, 16, 18 and mpd = 4-Me-1, 2-phenylenediamine] and the oxovanadium(IV) complexes (VO-nmpd) are presented in Scheme 1.

The mononuclear oxovanadium(IV) complexes, VO-nmpd (n = 14,16,18), were prepared by the reaction of the appropriate ligand with vanadyl sulphate (1:1 molar ratio) and recrystallised from methanol/dichloromethane; the complexes were isolated as greenish yellow solids in good yields. The compounds were characterised by elemental analyses, Fourier transform infra-red (FT-IR) spectroscopy, ultraviolet–visible (UV-vis) spectroscopy, ^{1}H and ^{13}C nuclear magnetic resonance (NMR) and mass spectrometry.

The analytical and spectral data of the compounds are in good agreement with the proposed formulae. A weak broad band in the region 3250–3350 cm^{-1} due to a hydrogen bonded -OH group in the free Schiff base ligand was not observed in the IR spectra of the complexes, indicating that the phenolic oxygen is deprotonated and coordinated in the complexes. A strong $\nu_{(C=N)}$ band appearing in the range 1612–1610 cm^{-1} for the complexes is considerably red shifted compared to that of the free Schiff base ligands (~1,629 cm^{-1}), indicating coordination of the azomethine nitrogen to the metal. Observance of the vanadyl(V=O) stretching mode at a relatively higher wave number (~980 cm^{-1}) is suggestive of the absence of any intermolecular (. . . V=O . . . V=O . . .) interaction, indicating the monomeric nature of the complexes [37–39]. Such linear chain interactions usually cause $\nu_{V=O}$ to shift to lower wave number (~870 cm^{-1}). ^{1}H NMR spectra of the ligands showed signals at δ = 13.4–13.8 ppm and 8.5 ppm, corresponding to the OH-proton and imine proton, respectively. The fast atom bombardment (FAB) mass spectra of the vanadyl(IV) complexes are concordant with their formula weights. The solution electrical conductivity of the complexes recorded in dichloromethane (10^{-3}M) was found to be < 10 Ω^{-1}cm^{-1}mol^{-1}, much lower than expected for a 1:1 electrolyte, thus confirming the non-electrolytic nature of the complex.

The electronic absorption spectrum (see Figure S1 in the supplementary material which is available via the multimedia link on the online article webpage) of ligand 16-mpd showed two bands at ~290 nm and

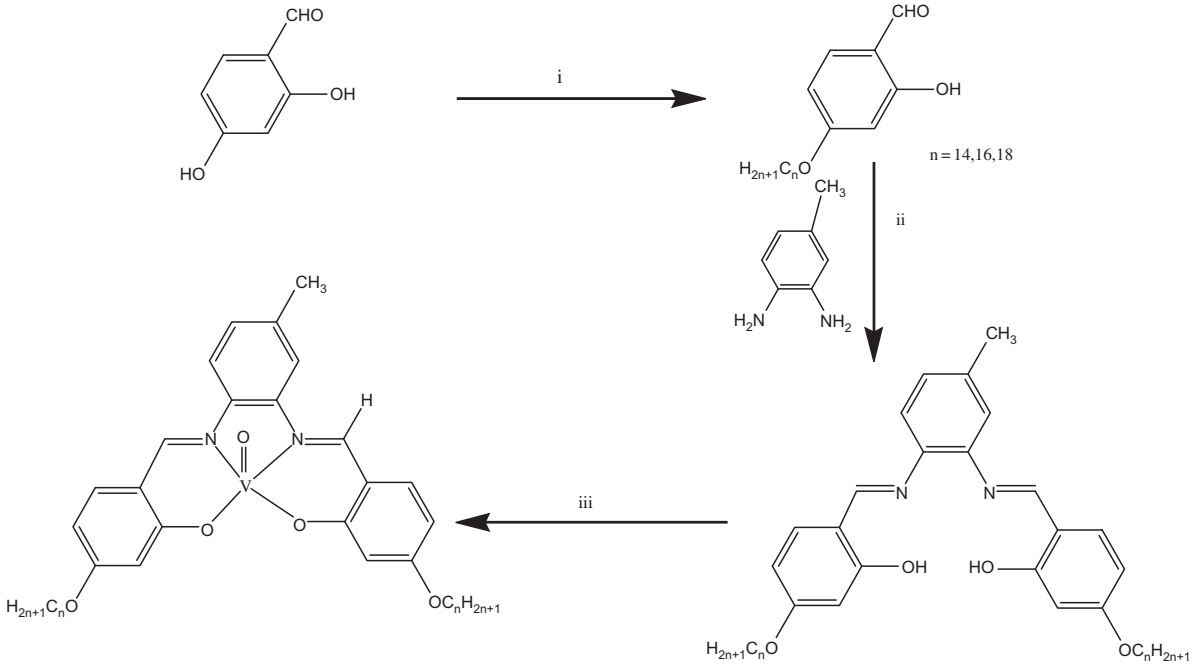

Scheme 1. (i) $C_nH_{2n+1}Br$, $KHCO_3$, KI, dry acetone, Δ, 40 h. (ii) Glacial AcOH, absolute EtOH, Δ, 4 h. (iii) $VOSO_4.5H_2O$, MeOH, TEA. Δ, 1 h.

~326 nm attributed, respectively, to a π–π^* transition localised on the aromatic rings and a third intense peak at ~364 for n–π^* transition of the imine chromophore. Upon complexation with VO(IV), these bands are red shifted to a longer wavelength (Table 1). The complexes exhibited a strong band at ~401 nm, due to a ligand-to-metal charge-transfer (LMCT) transition. A similar observation was noted for all other compounds (Table 1).

The redox behaviour for a typical complex (VO-16mpd) was probed by cyclic voltammetry in dichloromethane solution in the potential range –1.0 to 1.4 V versus saturated calomel electrode (SCE) at a scan rate of 0.05 Vs^{-1}. The voltammogram (Figure 1) displayed a quasi-reversible (peak separation ~82 mV) one-electron response at (Ep^c = 0.64 V, Ep^a = 0.86 V, ΔEp = 0.22 V) assigned to a VO(V)/VO(IV) couple.

The mesomorphic behaviour of the complexes was investigated by polarising optical microscopy (POM) and differential scanning calorimetry (DSC). The ligands did not show liquid crystallinity, but the complexes exhibited enantiotropic columnar mesophases. Table 2 summarises the phase behaviour of these compounds. In the POM study, the sample transformed to the isotropic liquid at ~192°C.

Upon cooling, a typical broken mosaic texture is observed at ~185°C (Figure 2). This is a very characteristic feature of rectangular columnar mesophase. On further cooling, the texture of this phase transformed to another pattern with focal conic texture at ~40°C. Interestingly, this optical texture remained unaltered till room temperature (Figure 2). The DSC traces obtained at a rate of 5°C min^{-1} (Figure 2) showed two transitions in the heating cycle and two in the cooling cycle. All the compounds possessed excellent thermal stability. The reversibility of the thermal behaviour was confirmed by DSC on subsequent heating–cooling runs. The formation of mesophases was dependent on the carbon length of terminal chains. The clearing temperatures slightly increased with a reduction in the carbon chain length of terminal alkoxy groups. The Col-I/I-Col phase transition enthalpy is found to be (~ΔH = 14.3–14.9 $kJmol^{-1}$).

Table 1. UV-visible spectal data of ligands (n-mpd) and complexes (VO-nmpd).

	λ_{max}(nm)	
Compound	$\pi \rightarrow \pi^*$ (ε, l mol^{-1} cm^{-1})	LMCT (ε, l mol^{-1} cm^{-1})
18-mpd	288 (13000)	–
	326 (15900)	
	364 (22400)	
VO-18mpd	325 (26300)	401 (29100)
16-mpd	290 (12900)	–
	326 (15900)	
	362 (22200)	
VO-16mpd	326 (26400)	400 (29100)
14-mpd	290 (12900)	–
	334 (16000)	
	364 (22400)	
VO-14mpd	325 (26300)	402 (29100)

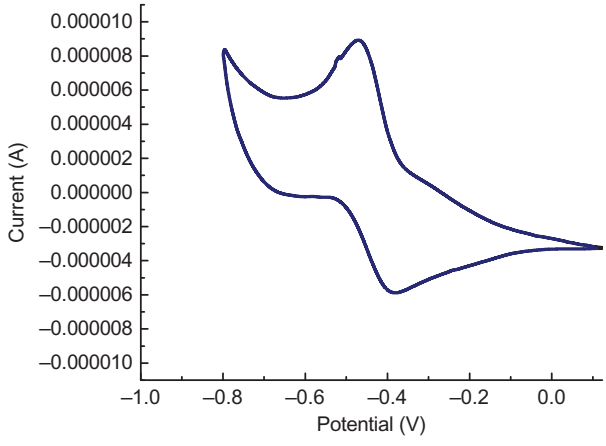

Figure 1. Cyclic voltamogram of VO-16mpd.

Table 2. DSC data of the complexes.

Compounds	Heating (ΔH, $kJmol^{-1}$)	Cooling (ΔH, $kJmol^{-1}$)
VO-18mpd	Col_{r1} 50.3(14.3) Col_{r2} 193.0(14.9) I	I179.6(14.7)Col_{r2}46.7(14.1) Col_{r1}
VO-16mpd	Col_{r1} 54.5(13.9) Col_{r2} 194.3(14.7) I	I184.7(14.1)Col_{r2}49.3(13.8) Col_{r1}
VO-14mpd	Col_{r1} 56.7(14.4) Col_{r2} 196.0(14.6) I	I189.6(14.3)Col_{r2}52.1(14.4) Col_{r1}

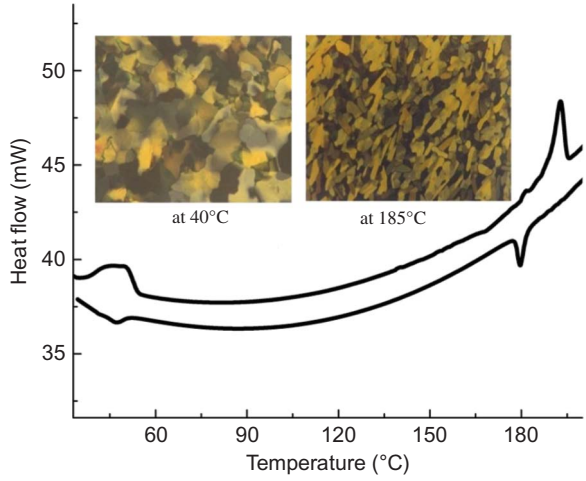

Figure 2. Combined DSC curve and POM texture of VO-16mpd.

The relatively high enthalpy value is ascribed to the increased mesophase order caused by rather large van der Waal's interactions between the core groups of the neighbouring molecules in the two-dimensional (2D) rectangular mesophase relative to that of the one-dimensional (1D) mesophase.

The columnar phase transformation from one rectangular type (Col_{r1}) to another (Col_{r2}), as observed in the POM and DSC study, was confirmed by the X-ray diffraction (XRD) study. It is argued that this behaviour originated from an increase in the intercolumnar distance concomitant with closer packing of the discs within the same column. The Col_{r1} mesophase formed showed marked stability and did not crystallise even at room temperature, as evidenced by DSC and POM study.

Such columnar phase transformation behaviour between two rectangular columnar mesophase is uncommon but not unprecedented [40]. The mesomorphic properties of such 'salphen' type complexes appear to be strongly dependent on the aromatic spacer and metal ions. In earlier reports, we found that the analogous oxovanadium complexes without any substituent in the aromatic spacer group showed lamellar columnar mesomorphism [7]. Interestingly, complexes of other metal ions such as Zn(II) and Ni(II) of 'salphen' type ligands with similar spacer group showed Col_h and Col_r mesophases, respectively [20, 25]. The mesophase structures were also confirmed by variable temperature powder XRD experiments, performed on a representative compound VO-16mpd (Table 3). At 40°C, in the small-angle region, several sharp Bragg reflections were observed (Figure 3) which could be indexed to rectangular 2D lattices of the Col_r phase [41–44]. In the wide angle region, diffuse reflections corresponding to a spacing of ~4.5 Å can be attributed to the average distance between the liquid-like (molten) aliphatic side chains. A less intense peak at ca.7.1 Å indicates dimeric interaction of the hemi-disc shaped molecules along the columnar axis (Figure 5).

Quite a different diffractogram (Figure 4) is obtained for VO-16mpd at 190°C. In this case, two fundamental sharp reflections were observed in the low angle region, which can be indexed as the (20) and (11) reflections of a rectangular lattice. Scattering centred around 4.5 Å in the wide angle region relates to the liquid-like order of the peripheral tails. Notably in both cases, in the absence of any hk pairs with $h + k = 2n + 1$, the symmetry of the lattice can be further assigned to a *c2mm* plane group [41–44]. Moreover the XRD pattern did not show any reflections around 3.0–3.5Å, clearly suggesting lack of any kind of long-range order between molecules due to π–π intermolecular interactions within the columns.

Table 3. Powder XRD data of VO-16mpd.

Compound	d_{obs} (Å)[a]	d_{calc} (Å)[b]	hk[c]	Parameters[d]
VO-16mpd at 40°C	18.78	18.76	20	a = 37.56 Å
	14.12	14.14	11	b = 15.24 Å
	13.05	13.07	31	S = 572.41 Å^2
	9.71	9.73	40	S_{col} = 286.20
	7.13	7.15		V_m = 1663.49 A^3
	4.51	4.53		–
VO-16mpd at 190°C	17.50	17.52	20	a = 35Å, b = 13.86 Å
	12.83	12.82	11	S = 485.1 Å^2
	6.52	6.54		S_{col} = 242.55
	4.96	4.97		V_m = 1483.05 Å^3

[a]d_{obs} and [b]d_{calc} are experimentally and theoretically measured diffraction spacings at 190°C. [hk][c] are indexation of the reflections. Mesophase parameters d, molecular volume V_m is calculated using the formula: $V_m = M/\lambda\rho N_A$ where M is the molecular weight of the compound, N_A is the Avogadro number, ρ is the volume mass (≈1 g cm^{-3}), and $\lambda(T)$ is a temperature correction coefficient at the temperature of the experiment (T), $\lambda = VCH_2\ (T_0)/VCH_2\ (T)$, T_0 = 25°C.$VCH_2\ (T) = 26.5616 + 0.02023.T$, h is the intermolecular repeating distance deduced directly from the measured molecular volume and the lattice area according to $h = V_m/S$. For the Col_r phase, the lattice parameters a and b are deduced from the mathematical expression: $a = 2d_{20}$ and $1/d_{hk} = \sqrt{h^2/a^2 + k^2/b^2}$, where a, b are the parameters of the Col_r phase, S is the lattice area and S_{col} is the columnar cross-section ($S = ab$, $S_{col} = S/2$).

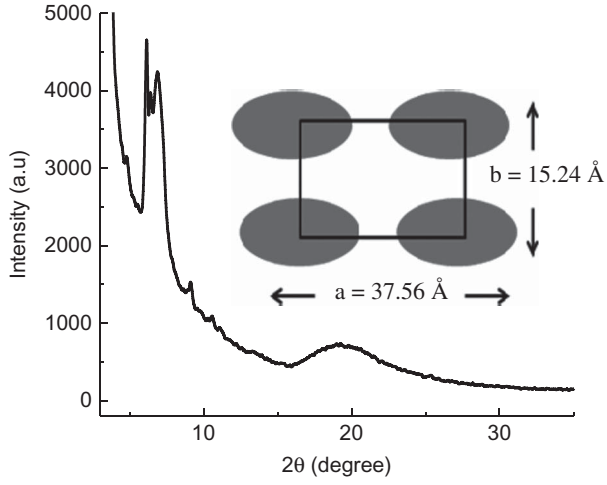

Figure 3. Powder XRD pattern of VO-16mpd at 40°C.

The lattice constant 'a' in both cases is larger than the radius of the half disc so the two half disc molecules organise themselves in head-to-head fashion, to form a discoid shell (Figure 5). This observation, coupled with the findings of the POM and DSC study, clearly confirmed the existence of two rectangular columnar phases.

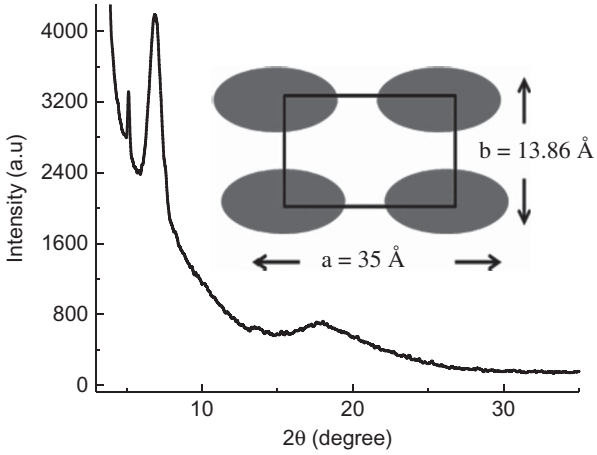

Figure 4. Powder XRD pattern of VO-16mpd at 190°C.

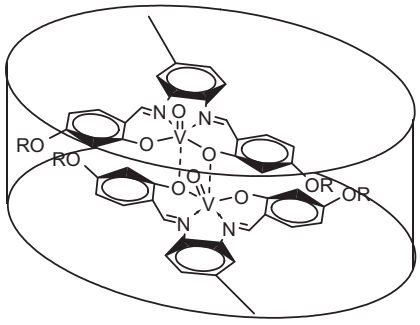

Figure 5. Dimeric interactions of half disc shaped molecules in the column.

Despite several efforts, an X-ray quality single crystal could not been grown, so density functional theory (DFT) studies were undertaken to ascertain the optimised geometry of the VO-16mpd complex molecule (Figure 6). The ground state geometries in the gas phase of the complex were fully optimised using the unrestricted BLYP/DNP methods without imposing any symmetry constrain. The BLYP functional, used throughout this study, comprises of a hybrid exchange functional as defined by Becke and the non-local Lee–Yang–Parr correlation functional [45–48]. The basis set chosen is DNP, the double-numerical atomic orbitals augmented by polarisation functions. Relativistic effects were taken into account with an all-electron scalar relativistic method based on the Douglas–Kroll–Hess (DKH) transformation. All calculations were performed with the DMol3 program package. It has been found that the average V–O and V–N bond lengths are 2.0 and 2.1Å, respectively, which matched quite well with the other related vanadium salphen complexes [7]. The bond angles 86.79° and 86.85° for O–V–O and N–V–N, respectively, revealed a distorted square pyramidal geometry around the vanadyl centre. Highest occupied molecular orbital (HOMO) and lowest unoccupied molecular orbital (LUMO) diagrams of the complex are shown in Figures S2 and Figure S3 in the supplementary material which is available via the multimedia link on the online article webpage. The HOMO and LUMO energies of the complex are calculated to be −4.9eV and −3.1 eV, respectively, $\Delta E = 1.8$ eV. The electron density of the LUMO is scattered over the C–N bonds and the phenyl rings of the ligand, while the HOMO is localised primarily on the vanadyl centre. Some of the selective geometric parameters of the optimised complex, VO-16mpd are shown in Table 4.

3. Conclusions

A series of new VO^{2+}(IV)-salphen complexes bearing methyl substituted aromatic spacer have been successfully synthesised. A rare columnar phase transformation behaviour between two rectangular

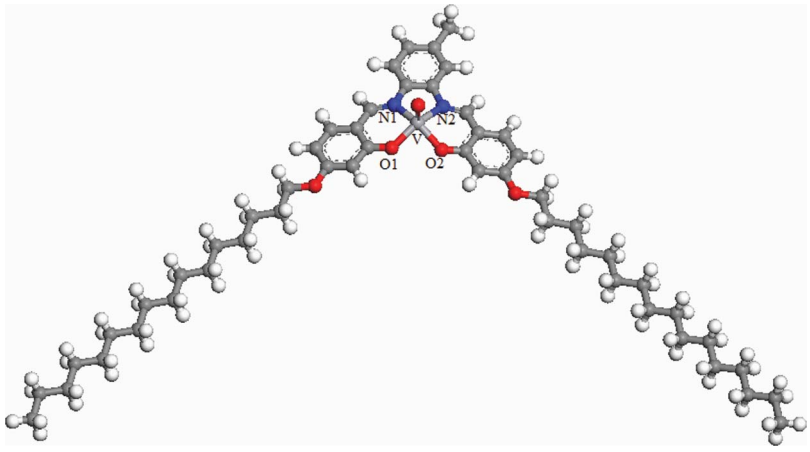

Figure 6. Optimised structure of VO-16mpd.

Table 4. Selected bond length and bond angles of VO-16mpd, from DFT study.

Structure parameter	Distance (Å)/Bond angles (°)
V-N	2.1
V-O	1.9
V=O	1.6
N-V-O	86.8
O-V-O	86.7
N-V-N	76.7

phase both belonging to *c2mm* symmetry is observed upon coordination of the $[N_2O_2]$-donor Schiff base ligand with the metal ion. Two half disc shaped molecules with long alkoxy tail organise themselves in the mesophase via VO$\cdots\cdots$VO$\cdots$ dimeric interaction forming a disc-like shape. An alkoxy chain length dependant marginal variation in the mesomorphic transition and isotropisation temperature was noted. Analogous oxovanadium complexes without any substituent in the aromatic spacer group have been previously shown to exhibit lamellar columnar mesomorphism [7]. It would be quite interesting to assess vanadyl complexes with a differently substituted 'salphen' type framework and to explore their mesomorphic behaviour. Cyclic voltammetry displayed a quasi-reversible one-electron response for the VO^{2+}/VO^{3+} redox couple. Based on the spectral and density functional calculations study, a square pyramidal five-coordinate geometry around the VO^{2+}(IV) centre is conjectured. The work demonstrates that coordination to a vanadyl centre not only induces liquid crystallinity in a non-mesomorphic 'salphen' type ligand bearing long alkoxy tail, but that slight modification in the 'salphen' core can also lead to a quite different mesomorphism furnishing a synthetic handle to tune such properties.

4. Experimental section

4.1. Physical measurements

The C, H and N analyses were carried out using PE2400 elemental analyser (Perkin Elmer, USA). The ^{1}H-NMR spectra were recorded on Bruker DPX-400MHz spectrometer (Bruker AXS, India) in $CDCl_3$ (chemical shift in δ) solution with tetramethylsilane (TMS) as internal standard. Molar conductance of the compounds was determined in dichloromethane ($\sim 10^{-3}$ mol L^{-1}) at room temperature using MAC-554 conductometer (Macroscientific Works, India). Ultraviolet–visible absorption spectra of the compounds in dichloromethane were recorded on a Shimadzu UV-160PC spectrophotometer (Shimadzu, Asia Pacific, Pte. Ltd, Singapore). Electrochemical measurements were performed using computer-controlled CHI −660C electrochemical workstation (CH-Instrument Inc., USA) with Pt-disk electrodes. All measurements were carried out under nitrogen environment at 298K with reference to SCE in acetonitrile using $[n\text{Bu}_4\text{N}][\text{ClO}_4]$ as supporting electrolyte. Infrared spectra were recorded on a Perkin-Elmer L 120-000A spectrometer (Perkin Elmer, USA) on a KBr disc. Mass spectra were recorded on a JEOL SX-102 spectrometer (JEOL, Japan) with fast atom bombardment. The optical textures of the different phase of the compounds were studied using a polarising microscope (Nikon optiphot-2-pol, Nikon Corporation, Tokyo, Japan) attached to a Instec hot and cold stage HCS302, with STC200 temperature controller of 0.1°C accuracy. The thermal behaviour of the compounds were studied using a Perkin-Elmer differential scanning calorimeter (DSC) Pyris-1 spectrometer (Perkin Elmer International, Switzerland) with a heating or cooling rate of 5°C/min. Variable temperature powder X-ray diffraction (PXRD) of the samples were recorded on a Bruker D8 Discover instrument (Germany) using Cu-Kα radiation. Quantum chemical calculation on VO-16mpd was carried out using density functional theory (DFT) as implemented in the DMol3 package.

4.2. Materials

The materials were procured from Tokyo Kasei, Japan, and Lancaster Chemicals, USA. All solvents were purified and dried using standard procedures. Silica (60–120 mesh) from Spectrochem was used for chromatographic separation. Silica gel G (E-Merck, India) was used for thin layer chromatography (TLC).

4.3. Synthesis and analysis

The synthesis of the ligands are described in our earlier report [20].

4.3.1. Synthesis of oxovanadium(IV) complexes (VO-nmpd)

The ligand 18-mpd (0.086g, 0.1mmol) or 16-mpd (0.081g, 0.1mmol) or 14-mpd (0.075g, 0.1mmol) was dissolved in a minimum volume of absolute ethanol. An equimolar amount of vanadyl sulphate, $VOSO_4.5H_2O$ (0.02g, 0.1mmol) in methanol was then added slowly followed by the addition of triethylamine and refluxed for 2 h. A greenish yellow solid formed immediately. This was filtered, washed with diethyl ether and recrystallised from methanol/dichloromethane (1:1).

4.3.2. VO-18mpd

Yield: 0.139 g, 75%. FAB mass (m/e, fragment): m/z: calc. 931.61; found: 932.61[M+H$^+$]; Analysis calculated for $C_{57}H_{88}N_2O_5V$ (932.61): C, 73.44; H, 9.51; N 3.0. Found: C, 73.41; H, 9.52; N, 3.11%. IR (ν_{max}, cm^{-1}, KBr): 2920 (ν_{as}(C-H), CH_3), 2850 (ν_s(C-H), CH_3), 1612 (νC=N), 981 (νV=O).

4.3.3. VO-16mpd

Yield: 0.126 g, 70%. FAB mass (m/e, fragment): m/z: calc. 875.55; found: 876.55[M+H$^+$]; Analysis calculated for $C_{53}H_{80}N_2O_5V$ (876.55): C, 72.65; H, 9.20; N 3.20. Found: C, 72.64; H, 9.22; N, 3.21%. IR (ν_{max}, cm^{-1}, KBr): 2924 (ν_{as}(C-H), CH_3), 2852 (ν_s(C-H), CH_3), 1611 (νC=N), 982 (νV=O).

4.3.4. VO-14mpd

Yield: 0.131 g, 75%. FAB mass (m/e, fragment): m/z: calculated 819.49; found: 820.49 [M+H$^+$]; Analysis calculated for $C_{49}H_{72}N_2O_5V$ (820.49): C, 71.77; H, 8.85; N 3.42. Found: C, 71.75; H, 8.82; N, 3.41%. IR (ν_{max}, cm^{-1}, KBr): 2923 (ν_{as}(C-H), CH_3), 2851 (ν_s(C-H), CH_3), 1609 (νC=N), 984 (νV=O).

Acknowledgements

The authors thank the University Grants Commission, New Delhi, for financial support and Professor R.C. Deka (Tezpur University, India) for assistance with the theoretical calculations. The Sophisticated Analytical Instrumentation Facility, North Eastern Hill University, Shillong, is acknowledged for some spectral results.

References

[1] Abe, Y.; Iyoda, A.; Seto, K.; Moriguchi, A.; Yokoyama, H. *Eur. J. Inorg. Chem.* **2008**, 2148–2157.
[2] Abe, Y.; Nakabayashi, K.; Matsukawa, N.; Iida, M.; Tanase, T.; Sugibayashia, M.; Ohta, K. *Inorg. Chem. Commun.* **2004**, *7*, 580–583.
[3] Aiello, I.; Ghedini, M.; Neve, F.; Pucci, D. *Chem. Mater.* **1997**, *9*, 2107–2112.
[4] Nejati, K.; Rezvani, Z. *New J. Chem.* **2003**, *27*, 1665–1669.
[5] Abe, Y.; Nakabayashi, K.; Matsukawa, N.; Takashima, H.; Iida, M.; Tanase, T.; Sugibayashi, M.; Mukai, H.; Ohta, K. *Inorg. Chim. Acta.* **2006**, *359*, 3934–3946.
[6] Blake, A.B.; Chipperfield, J.R.; Hussain, W.; Paschke, R.; Sinn, E. *Inorg. Chem.* **1995**, *34*, 1125–1129.
[7] Bhattacharjee, C.R.; Das, G.; Mondal, P.; Prasad, S.K.; Rao, D.S.S. *Inorg. Chem. Commun.* **2011**, *14*, 606–612.
[8] Ohta, A.; Yamamoto, Y.; Kamihata, H.; Lee, Y.H.; Ichikawa, F.; Ohta, K.; Abe, Y.; Hoshino, N.; Kojima, M.; Hayami, S. *Inorg. Chem. Commun.* **2012**, *16*, 89–91.
[9] Giroud-Godquin, A.-M.; Maitlis, P.M. *Angew. Chem., Int. Ed. Engl.* **1991**, *30*, 375–402.
[10] Espinet, P.; Esteruelas, M.A.; Oro, L.A.; Serrano, J.L.; Sola, E. *Coord. Chem. Rev.* **1992**, *117*, 215–274.
[11] Hoshino, N. *Coord. Chem. Rev.* **1998**, *174*, 77–108.
[12] Zheng, H.; Lai, C.K.; Swager, T.M. *Chem. Mater.* **1994**, *6*, 2252–2268.
[13] Zheng, H. Lai, C.K.; Swager, T.M. *Chem. Mater.* **1995**, *7*, 2067–2077.
[14] Ghedini, M.; Morrone, S.; Bartolino, R.; Formoso, V.; Francescangeli, O.; Yang, B. *Chem. Mater.* **1993**, *5*, 876–882.
[15] Sleven, J.; Cardinaels, T.; Binnemans, K.; Guillon, D.; Donnio, B. *Liq. Cryst.* **2002**, *29*, 1425–1433.
[16] Poelsma, S.N.; Servante, A.H.; Fanizzi, F.P.; Matlis, P.M. *Liq. Cryst.* **1994**, *16*, 675–685.
[17] Barbera, J.; Gimenez, R.; Serrano, J.L.; Alonso, P.J.; Martinez, J.I. *Chem. Mater.* **2003**, *15*, 958–964.
[18] Serrette, A.; Carroll, P.J.; Swager, T.M. *J. Am. Chem. Soc.* **1992**, *114*, 1887–1889.
[19] Meyer, E.; Zucco, C.; Gallardo, H. *J. Mater. Chem.* **1998**, *8*, 1351–1354.
[20] Bhattacharjee, C.R.; Das, G.; Mondal, P.; Rao, N.V.S. *Polyhedron*, **2010**, *29*, 3089–3096.
[21] Bhattacharjee, C.R.; Das, G.; Mondal, P.; Prasad, S.K.; Rao, D.S.S. *Eur. J. Inorg. Chem.* **2011**, 1418–1424.
[22] Bhattacharjee, C.R.; Das, G.; Mondal, P. *Eur. J. Inorg. Chem.* **2011**, 5390–5399.
[23] Bhattacharjee, C.R.; Das, G.; Mondal, P. *Liq. Cryst.* **2011**, *38*, 441–449.
[24] Bhattacharjee, C.R.; Das, G.; Mondal, P.; Prasad, S.K.; Rao, D.S.S. *Liq. Cryst.* **2011**, *38*, 615–623.
[25] Bhattacharjee, C.R.; Datta, C.; Das, G.; Chakrabarty, R.; Mondal, P. *Polyhedron.* **2012**, *33*, 417–424.
[26] Bhattacharjee, C.R.; Das, G.; Dhar Purkayastha, D; Mondal, P. *Liq. Cryst.* **2011**, *38*, 717–727.
[27] Kumar, S. *Chem. Soc. Rev.* **2006**, *35*, 83–109.
[28] Goodby, J.W.; Gortz, V.; Cowling, S. J.; Mackenzie, G.; Martin, P.; Plusquellec, D.; Benvegnu, T.; Boullanger, P.; Lafont, D.; Queneau, Y.; Chambert, S.; Fitremann, J. *Chem. Soc. Rev.* **2007**, *36*, 1971–2032.
[29] O'Neill, M.; Kelly, S.M. *Adv. Mater.* **2003**, *15*, 1135–1146.
[30] Cristiano, R.; Gallardo, H.; Bortoluzzi, A.J.; Bechtold, I.H.; Campos, C.E.M.; Longo, R.L. *Chem. Commun.* **2008**, 5134–5136.
[31] Sergeyev, S.; Pisula, W.; Geerts, Y.H. *Chem. Soc. Rev.* **2007**, *36*, 1902–1929.
[32] Shirota, Y.; Kageyama, H. *Chem. Rev.* **2007**, *107*, 953–1010.
[33] Sawamura, M.; Kawai, K.; Matusuo, Y.; Kanie, K.; Kato, T.; *Nature* **2002**, *419*, 702–705.
[34] Seguy, I.; Jolinat, P.; Destruel, P.; Mamy, R. *J. Appl. Phys.* **2001**, *89*, 5442–5448.
[35] Van de Craats, A.M.; Stutzmann, N.; Nielsen, M.M.; Watson, M. *Adv. Mater.* **2003**, *15*, 495–499.
[36] Laschat, S.; Baro, A.; Steinke, N.; Giesselmann, F.; Hagele, C.; Scalia, G.; Judele, R.; Kapatsina, E.; Sauer, S.; Schreivogel, A.; Tosoni, M. *Angew. Chem., Int. Ed.* **2007**, *46*, 4832–4887.
[37] Bagherzadeh, M.; Amini, M. *J. Coord. Chem.* **2010**, *63*, 3849–3858.
[38] Yuan, C.; Lu, L.; Gao, X.; Wu, Y.; Guo, M.; Li, Y.; Fu, X.; Zhu, M. *J. Biol. Inorg. Chem.* **2009**, *14*, 841–851.
[39] Chohan, Z.H.; Sumrra, S.H.; Youssoufi, M.H.; Hadda, T.B. *J. Coord. Chem.* **2010**, *63*, 3981–3998.
[40] Yelamaggad, C.V.; Achalkumar, A.S.; Rao, D.S.S.; Prasad, S.K. *J. Mater. Chem.* **2007**, *17*, 4521–4529.

[41] Ghedini, M.; Pucci, D.; Crispini, A.; Bellusci, A.; Deda, M. La; Aiello, I.; Pugliese, T. *Inorg. Chem. Commun.* **2007**, *10*, 243–246.
[42] Morale, F.; Finn, R.L.; Collinson, S.R.; Blake, A.J.; Wilson, C.; Bruce, D.W.; Guillon, D.; Donnio, B.; Schroder, M. *New. J. Chem.* **2008**, *32*, 297–305.
[43] Morale, F.; Date, R.W.; Guillon, D.; Bruce, D.W.; Finn, R.L.; Wilson, C.; Blake, A.J.; Schroder, M.; Donnio, B. *Chem. Eur. J.* **2003**, *9*, 2484–2501.
[44] Mocanu, A.S.; Amela-Cortes, M.; Molard, Y.; Circu, V.; Cordiera, S. *Chem. Commun.* **2011**, *47*, 2056–2658.
[45] Lee, C.; Yang, W.; Parr, R.G. *Phys. Rev. B*, **1988**, *37*, 785–789.
[46] Delley, B. *J. Chem. Phys.* **1990**, *92*, 508–518.
[47] Suzuki, K.; Nada, T.; Sastre, G.; Katada, N.; Niwa, M. *J. Phys. Chem. C* **2009**, *113*, 5672–5680.
[48] Aihara. J. *J. Phys. Chem. A* **1999**, *103*, 7487–7495.

Phase Transitions: A Multinational Journal
Publication details, including instructions for authors and subscription information:
http://www.tandfonline.com/loi/gpht20

Oxovanadium (IV) complexes of bidentate [N,O] donor Schiff-base ligands: synthesis and mesomorphism

Chira R. Bhattacharjee [a], Chitraniva Datta [a], Gobinda Das [a] & Paritosh Mondal [a]

[a] Department of Chemistry, Assam University, Silchar-788011, Assam, India

Version of record first published: 26 Mar 2012.

To cite this article: Chira R. Bhattacharjee, Chitraniva Datta, Gobinda Das & Paritosh Mondal (2012): Oxovanadium (IV) complexes of bidentate [N,O] donor Schiff-base ligands: synthesis and mesomorphism, Phase Transitions: A Multinational Journal, 85:11, 956-972

To link to this article: http://dx.doi.org/10.1080/01411594.2012.666667

Phase Transitions
Vol. 85, No. 11, November 2012, 956–972

Oxovanadium (IV) complexes of bidentate [N,O] donor Schiff-base ligands: synthesis and mesomorphism

Chira R. Bhattacharjee*, Chitraniva Datta, Gobinda Das and Paritosh Mondal

Department of Chemistry, Assam University, Silchar-788011, Assam, India

(*Received 5 December 2011; final version received 11 February 2012*)

A series of new oxovanadium(IV) Schiff-base complexes of the type $[VO(L)_2]$, [L = N-(4-*n*-alkoxysalicylaldimine)-4′-dodecyloxyaniline, $n = 6$, 8, 16, and 18] have been synthesized. The compounds were characterized by FT-IR, ^{1}H-NMR, ^{13}C-NMR, UV-Vis, FAB-mass, and magnetic susceptibility measurements. The mesomorphic behavior of the compounds was studied by polarized optical microscopy and differential scanning calorimetry. The compounds are all highly thermally stable exhibiting smectic mesomorphism. Non-electrolytic nature of the complexes was ascertained by solution electrical conductance measurements. Cyclic voltammetry revealed a quasireversible single-electron response for VO(V)/VO(IV) couple. A $\nu_{V=O}$ stretching mode at $\sim$970 cm^{-1} indicates absence of any intermolecular V=O $\cdots$ V=O interactions. Density functional theory study was carried out using DMol3 at BLYP/DNP level to determine energy optimized structure revealed a distorted square pyramidal geometry for the vanadyl complexes.

Keywords: metallomesogen; vanadium; smectic mesomorphism; density functional theory

1. Introduction

Schiff bases have continued to play a key role as chelating ligands in main group and transition metal coordination chemistry, due to their ease of synthesis, stability under a variety of oxidative and reductive conditions, and their structural versatility associated with their diverse applications [1–6]. Among the first row transition metal complexes, oxovanadium(IV) Schiff-base complexes have received significant attention owing to their promising physico-chemical properties, bioactivities and catalytic properties in organic and inorganic transformations [7–12]. Vanadyl(IV) complexes also serve as interesting models for the clarification of several biochemical processes such as haloperoxidation [13,14], nitrogen fixation [15], phosphorylation [16], glycogen metabolism [17–19], and insulin mimicking [20,21]. Recognition of great potential of metallomesogens as advanced molecular materials led to a steady increase in interest toward liquid crystals incorporating transition metal elements [22–35]. A large number of salicylaldiminato complexes, have been synthesized using different metal ions such as copper(II), nickel(II), palladium(II),

*Corresponding author. Email: crbhattacharjee@rediffmail.com

ISSN 0141–1594 print/ISSN 1029–0338 online

http://dx.doi.org/10.1080/01411594.2012.666667
http://www.tandfonline.com

vanadium(IV), and iron [36–44]. Owing to unusual geometries and paramagnetism leading to unique functional behaviors, metallomesogens incorporating VO(IV) metal ions is a focal theme of current research [45–51]. Mesophase formation depends mainly on the intermolecular interactions between ligand groups and their arrangements around metal ions [52]. Oxovanadium(IV) complexes owing to the presence of axial coordinative interaction have provided an additional control on the liquid crystalline behavior over and above the variation in the flexibility of ligand tails [44,47,50]. Liquid crystals with transition metal core groups such as VO(IV) are a fascinating branch of material science, because the self-assemblies of coordinated metal complexes with new functionalities widen the range of potential applications [51]. Very recently, we have reported a series of oxovanadium(IV) salicylaldimine complexes bearing alkoxy and polar substituent exhibiting smectic mesomorphism [52,53].

As a part of our systematic investigation [44,52–54] on mesomorphic, and thermal properties of oxovanadium(IV) complexes with 'salen' type Schiff bases, we report herein synthesis and liquid crystalline behavior of a series of new oxovanadium(IV) Schiff base complexes containing both shorter as well as longer alkoxy substituent on either side of the ligand.

2. Experimental

2.1. *Materials*

All solvents were purified and dried using standard procedures. The materials were procured from Tokyo Kasei, Japan and Lancaster Chemicals, USA. Silica (60–120 mesh) from Spectrochem was used for chromatographic separation. Silica gel G (E-Merck, India) was used for thin layer chromatography.

2.2. *Techniques*

The C, H, and N analyses were carried out using PE2400 elemental analyzer. Molar conductance of the compounds was determined in CH_2Cl_2 (*ca* 10^{-3} mol L^{-1}) at room temperature using MAC-554 conductometer. The ^{1}H-NMR spectra were recorded on a Bruker DPX-300 spectrometer in $CDCl_3$ solution with TMS as internal standard. UV-Vis absorption spectra of the compounds in CH_2Cl_2 were recorded on a Shimadzu UV-160PC spectrophotometer. Infrared spectra were recorded on a Perkin Elmer L 120-000A spectrometer on KBr disks. The mesomorphic texture of the compounds was studied using a polarizing microscope (Nikon optiphot-2-pol) attached with Instec hot and cold stage HCS302, STC200 temperature controller configured for HCS302. The accuracies in temperatures are 0.10°C. The thermal behavior of the compounds was studied using a Perkin Elmer differential scanning calorimeter (DSC) Pyris-1 spectrometer with a heating or cooling rate of 50°C min^{-1}. The DC magnetic susceptibility data were collected on a Vibrating Sample Magnetometer, Physical Property Measurement System (Quantum Design, USA) in the temperature range 2.5–300 K with applied field of 100 Oe. Electrochemical measurements were performed using computer-controlled CHI 66°C electrochemical workstation with Pt-disk electrodes. All measurements were carried out under nitrogen environment at 298 K with reference to saturated calomel electrode (SCE) in acetonitrile using [nBu$_4$N][ClO$_4$] as supporting electrolyte.

2.3. *Synthesis and analyses*

The general preparative route for alkoxy salicylaldehydes is presented in Scheme 1. The Schiff base ligands were synthesized by condensation of the appropriate aldehyde with the C_{12}-alkoxyaniline following literature procedures [28,29]. The vanadyl (IV) complexes, VOL_2 (L = salicylaldimines) were synthesized by the interaction of hot ethanolic solution of the ligands and vanadyl sulfate in the presence of triethylamine under reflux (Scheme 2). The bidentate [N,O] donor Schiff base ligands, are abbreviated as 4-*n*-$OC_{12}H_{25}$ and their complexes as VO-*n*-$OC_{12}H_{25}$ ($n = 6$, 8, 16, and 18).

2.3.1. *Synthesis of n-alkoxysalicyldehyde (n = 6, 8, 16, and 18)*

Alkoxysalicyldehyde derivatives were prepared following the general method described in literature [47,48]. 2,4-Dihydroxybenzaldehyde (10 mmol, 1.38 g), $KHCO_3$ (10 mmol, 1 g), KI (catalytic amount) and 1-bromohexane (10 mmol, 1.6 g), 1-bromoctane (10 mmol, 1.9 g), 1-bromohexadecane (10 mmol, 3.0 g) or 1-bromo-octadecane (10 mmol, 3.3 g) were mixed in 250 mL of dry acetone. The mixture was heated under reflux for 24 h, and then filtered, while hot, to remove any insoluble solids. Dilute HCl was added to neutralize the warm solution, which was then extracted with chloroform (100 mL). The combined chloroform extract was concentrated to give a purple solid. The solid was purified by column chromatography using a mixture of chloroform and hexane (v/v, 1/1) as eluent. Evaporation of the solvents afforded a white solid product.

2.3.2. *Synthesis of hexadecyloxyaniline*

p-Hydroxy acetanilide (5 g, 0.03 mol) is refluxed with equimolar amount of hexadecyl bromide (10.9 g, 0.03 mol for 36 h in dry acetone using K_2CO_3 4.6 g) as the base and KI as the catalyst acetone was then dried off and the product was dissolved in CH_2Cl_2 and the solution was washed with saturated NaCl solution. The solution was then treated with Na_2SO_4 to absorb the moisture present in the solution. CH_2Cl_2 was then distilled off to obtain the crude 4-dodecyloxy acetanilide. 4-Dodecyloxy acetanilide was then hydrolysed for 4 h with 35% HCl in ethanol. The solution was then treated with 2 mol dm^{-3} of NaOH solution and a large amount of water upto pH = 12. The product was then filtered, recystallised with alcohol using animal charcoal to remove any colored impurity present. The synthetic route is shown in Scheme 2.

2.3.3. *4-n-Octaadecyloxysalicylaldehyde*

Yield: 5 g, 88%. Anal. for $C_{25}H_{42}O_3$: FAB mass (*m*/*e*, fragment): *m*/*z*: calcd 390.3; found: 391[M + H^+]. ^{1}H-NMR (400 MHz, $CDCl_3$): 0.99(t, $J = 5.7$, 6H, CH_3), 1.22–1.71 (m, 30H, $(CH_2)_{15}$), 3.95(t, $J = 5.9$, 2H, OCH_2), 7.41–7.42(m, 7-Ar H), 5.88(s, 1H, OH),

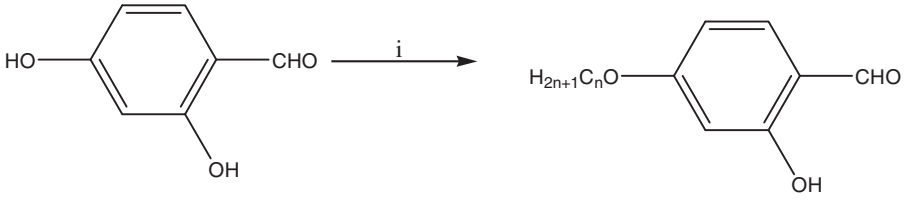

Scheme 1. i. $C_nH_{2n+1}Br$, $KHCO_3$, KI, dry acetone, Δ, 40 h.

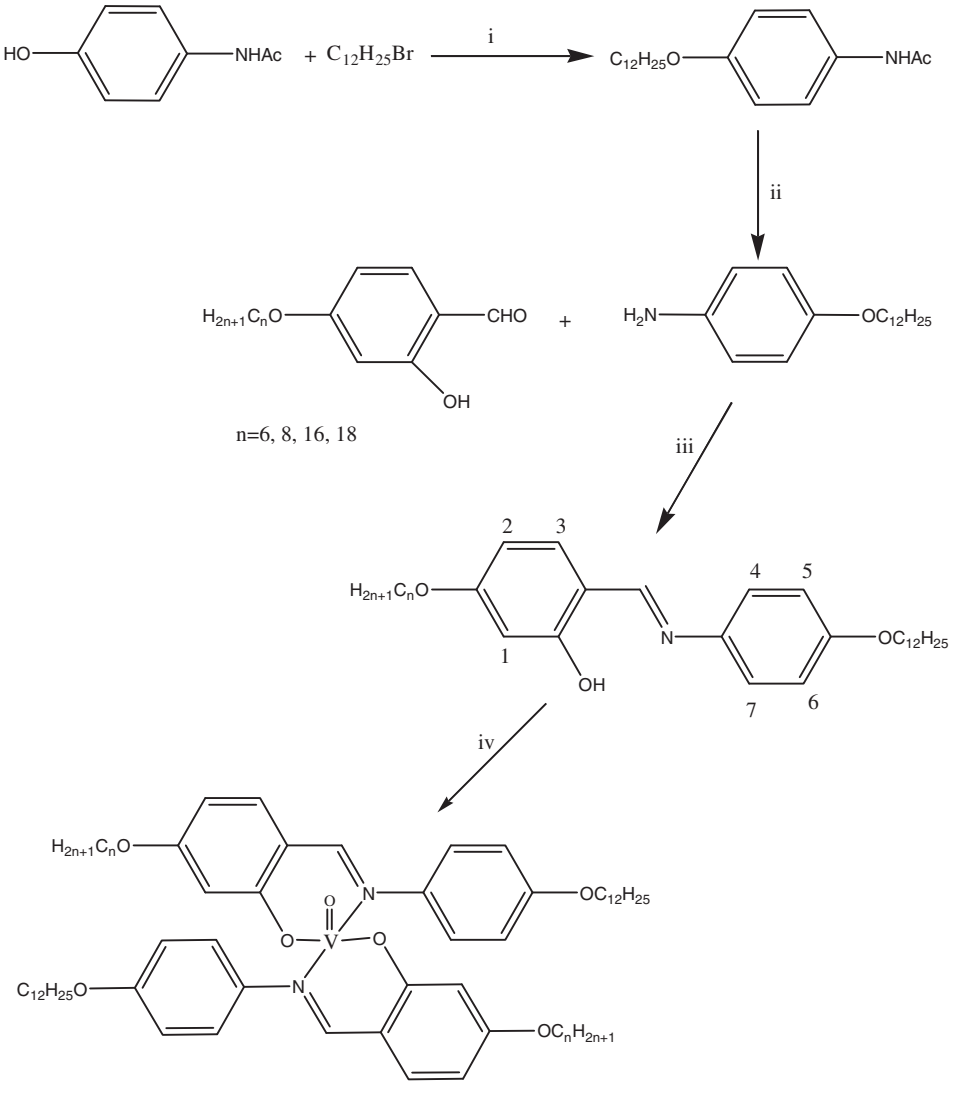

Scheme 2. 1. i. Dry K_2CO_3, Dry acetone, KI(Cat), ii. H^+/H_2O, EtOH, iii. Glacial acetic acid(cat), EtOH, reflux, 2 h, and iv. $VOSO_4.2H_2O$, TEA, Methanol reflux 1 h.

and 11.2(s, 1H, −CHO); ^{13}C-NMR (75.45 MHz; $CDCl_3$; Me4Si at 25°C, ppm) $\delta = 105.3$ (−C1), 132.1 (−C2), 103.9 (−C3), 164.6 (−C4), and 188.8(−C10). IR (ν_{max}, cm^{-1}, KBr): 3423(ν_{OH}), 2914(ν_{as}(C–H), CH_2), 2865(ν_s(C–H), CH_2), 1622($\nu_{CH=0}$), and 1278(ν_{C-O}).

2.3.4. *4-n-Hexaadecyloxysalicylaldehyde*

Yield: 5 g, 88%. Anal. for $C_{23}H_{38}O_3$: FAB mass (*m*/*e*, fragment): *m*/*z*: calcd 362.5; found: 363[M + H$^+$]. ^{1}H-NMR (400 MHz, $CDCl_3$): 0.97(t, $J = 5.7$, 6H, CH_3), 1.23–1.71 (m, 26H, $(CH_2)_{13}$), 3.94(t, $J = 5.9$, 2H, OCH_2), 7.42–7.44(m, 7-ArH), 5.82(s, 1H, OH), and 11.4(s, 1H, −CHO); ^{13}C-NMR (75.45 MHz; $CDCl_3$; Me_4Si at 25°C, ppm) $\delta = 106.3$

(−C1), 131.1 (−C2), 102.9 (−C3), 165.6 (−C4), and 187.8(−C10). IR (ν_{max}, cm^{-1}, KBr): 3423(ν_{OH}), 2914(ν_{as}(C–H), CH_2), 2866(ν_s(C–H), CH_2), 1623($\nu_{CH=0}$), and 1278(ν_{C-O}).

2.3.5. *4-n-Octyloxysalicylaldehyde*

Yield: 5 g, 80%. Anal. for $C_{15}H_{22}O_3$: FAB mass (*m*/*e*, fragment): *m*/*z*: calcd 250.1; found: 251[M + H^+]. ^{1}H-NMR (400 MHz, $CDCl_3$): 0.96(t, $J = 5.7$, 6H, CH_3), 1.21–1.74 (m, 30H, $(CH_2)_7$), 3.97(t, $J = 5.9$, 2H, OCH_2), 7.41–7.42(m, 7-ArH), 5.9(s, 1H, OH), 10.6(s, 1H, −CHO); ^{13}C-NMR (75.45 MHz; $CDCl_3$; Me4Si at 250°C, ppm) $\delta = 107.4$ (−C1), 131.1 (−C2), 103.7 (−C3), and 165.6 (−C4), 188.8(−C10). IR (ν_{max}, cm^{-1}, KBr): 3424(ν_{OH}), 2913(ν_{as}(C–H), CH_2), 2866(ν_s(C–H), CH_2), 1624($\nu_{CH=0}$), and 1277(ν_{C-O}).

2.3.6. *4-n-Hexyloxysalicylaldehyde*

Yield: 5 g, 86%. Anal. for $C_{13}H_{18}O_3$: FAB mass (*m*/*e*, fragment): *m*/*z*: calcd 222.1; found: 223[M + H^+]. ^{1}H-NMR (400 MHz, $CDCl_3$): 0.94(t, $J = 5.6$, 6H, CH_3), 1.23–1.73 (m, 8H, $(CH_2)_4$), 3.97(t, $J = 5.9$, 2H, OCH_2), 7.41–7.42(m, 7-ArH), 5.9(s, 1H, OH), 10.6(s, 1H, −CHO); ^{13}C-NMR (75.45 MHz; $CDCl_3$; Me_4Si at 25°C, ppm) $\delta = 107.3$ (−C1), 131.3 (−C2), 103.7 (−C3), 165.5 (−C4), and 188.7(−C10). IR (ν_{max}, cm^{-1}, KBr): 3423(ν_{OH}), 2912(ν_{as}(C–H), CH_3), 2913(ν_{as}(C–H), CH_2), 2846(ν_s(C–H), CH_2), 1624($\nu_{CH=0}$), and 1279(ν_{C-O}).

2.3.7. *N-(4-n-octadecyloxysalicylidene)-4′-n-dodecyloxy aniline (4-18-$OC_{12}H_{25}$)*

An ethanolic solution of (4-*n*-octadecyloxy)-salicyaldehyde (0.3 g, 1 mmol) was added to an ethanolic solution of 4-dodecyloxy aniline (0.2 g, 1 mmol). The solution mixture was refluxed with few drops of acetic acid as catalyst for 3 h to yield the Schiff base N-(4-*n*-octadecyloxysalicylidene)-4′-*n*-dodecyloxy aniline. The solid was collected by filtration and recrystallised several times from absolute ethanol to give a pure compound.

Yield: 0.37 g, 75%. Anal. Calcd for $C_{43}H_{71}NO_3$: C, 79.4; H, 11.0; and N, 2.1. Found: C, 79.5%; H, 11.1%; and N, 2.2%; FAB mass (*m*/*e*, fragment): *m*/*z*: calcd 649.5; found: 650[M + H^+]; ^{1}H-NMR (400 MH_Z, $CDCl_3$): 0.87(t, $J = 6.3$ Hz, 6H, $-CH_3$), 1.2–1.5 (m, 52H, $(CH_2)26$), 3.9(q, $J = 6.3$, 4H, OCH_2), 6.4(s,1H), 6.4(d, 8.4 Hz,2H), 6.9(d, 8.7 Hz, 5, 6H), 7.2(d, 8.7 Hz, 3H), 7.2(d, 8.7 Hz, 4, 7H), 8.5(s, 1H, CH=N), and 13.9(s, 1H, OH); ^{13}C-NMR (75.45 MHz; $CDCl_3$; Me_4Si at 25°C, ppm) $\delta = 102.4$ (−C1), 107.2 (−C2), 132.4 (−C3), 122.5 (−C4), 115.8 (−C5), 115.8 (−C6), 122.5(−C7); IR (ν_{max}, cm^{-1}, KBr):3435(ν_{OH}), 2917(ν_{as}(C–H), CH_3), 2919(ν_{as}(C–H), CH_2), 2869(ν_s(C–H), CH_3), 2845(ν_{as}(C–H), CH_2), 1630($\nu_{C=N}$), and 1278(ν_{C-O}).

2.3.8. *N-(4-n-hexadecyloxysalicylidene)-4′-n-dodecyloxy aniline (4-16-$OC_{12}H_{25}$)*

Yield: 0.38 g, 76%. Anal. Calcd for $C_{41}H_{67}NO_3$: C, 79.1; H, 10.8; and N, 2.2. Found: C, 79.2%; H, 10.7%; and N, 2.1%; FAB mass (*m*/*e*, fragment): *m*/*z*: calcd 621.5; found: 622[M + H^+]; ^{1}H-NMR (400 MH_Z, $CDCl_3$): 0.89(t, $J = 6.3$ Hz, 6H, $-CH_3$), 1.2–1.5 (m, 48H, $(CH_2)_{24}$), 3.8(q, $J = 6.3$, 4H, OCH_2), 6.5(s,1H), 6.4(d, 8.4 Hz, 2H), 6.9(d, 8.7 Hz, 5,6H), 7.2(d, 8.7 Hz, 3H), 7.6(d, 8.7 Hz, 4, 7H), 8.5(s, 1H, CH=N), and 13.9(s, 1H, OH); ^{13}C-NMR (75.45 MHz; $CDCl_3$; Me_4Si at 25°C, ppm) $\delta = 102.4$ (−C1), 107.2 (−C2), 133.4 (−C3), 121.5 (−C4), 115.8 (−C5), 115.8 (−C6), 122.5(−C7); IR (ν_{max}, cm^{-1}, KBr):3435(ν_{OH}), 2917(ν_{as}(C–H), CH_3), 2919(ν_{as}(C–H), CH_2), 2868(ν_s(C–H), CH_3), 2842(ν_{as}(C–H), CH_2), 1631($\nu_{C=N}$), and 1278(ν_{C-O}).

2.3.9. *N-(4-n-octayloxysalicylidene)-4′-n-dodecyloxy aniline (4-8-$OC_{12}H_{25}$)*

Yield: 0.33 g, 75%. Anal. Calcd for $C_{33}H_{51}NO_3$: C, 77.7; H, 10.0; and N, 2.7. Found: C, 77.6%; H, 10.1%; and N, 2.6%; FAB mass (*m*/*e*, fragment): *m*/*z*: calcd 509.3; found: 510[M + H^+]; ^{1}H-NMR (400 MH_Z, $CDCl_3$): 0.89(t, $J = 6.3$ Hz, 6H, $-CH_3$), 1.2–1.4 (m, 32H, $(CH_2)_{16}$), 3.8(q, $J = 6.3$, 4H, OCH_2), 6.5(s,1H), 6.4(d, 8.4 Hz,2H), 6.9(d, 8.7 Hz, 5,6H), 7.2(d, 8.7 Hz, 3H), 7.5(d, 8.7 Hz, 4, 7H), 8.4(s, 1H, CH=N), 13.9(s, 1H, OH); ^{13}C-NMR (75.45 MHz; $CDCl_3$; Me_4Si at 25°C, ppm) $\delta = 102.4$ (−C1), 107.2 (−C2), 133.4 (−C3), 121.5 (−C4), 115.8 (−C5), 115.8 (−C6), 122.5(−C7); IR (ν_{max}, cm^{-1}, KBr):3435(ν_{OH}), 2917(ν_{as}(C–H), CH_3), 2919(ν_{as}(C–H), CH_2), 2868(ν_s(C–H), CH_3), 2842(ν_{as}(C–H), CH_2), 1631($\nu_{C=N}$), and 1277(ν_{C-O}).

2.3.10. *N-(4-n-hexyloxysalicylidene)-4′-n-dodecyloxy aniline (4-6-$OC_{12}H_{25}$)*

Yield: 0.33 g, 75%. Anal. Calcd for $C_{31}H_{47}NO_3$: C, 77.2; H, 9.8; and N, 2.9. Found: C, 77.3%; H, 9.7%; and N, 2.8%; FAB mass (*m*/*e*, fragment): *m*/*z*: calcd 481.3; found: 482[M + H^+]; ^{1}H-NMR (400 MH_Z, $CDCl_3$): 0.91(t, $J = 6.3$ Hz, 6H, $-CH_3$), 1.2–1.4 (m, 28H, $(CH_2)_{14}$), 3.7(q, $J = 6.3$, 4H, OCH_2), 6.5(s,1H), 6.5(d, 8.4 Hz,2H), 6.9(d, 8.7 Hz, 5,6H), 7.3(d, 8.7 Hz, 3H), 7.5(d, 8.7 Hz, 4, 7H), 8.4(s, 1H, CH=N), and 13.9(s, 1H, OH); ^{13}C-NMR (75.45 MHz; $CDCl_3$; Me_4Si at 25°C, ppm) $\delta = 102.4$ (−C1), 107.2 (−C2), 133.4 (−C3), 121.5 (−C4), 115.8 (−C5), 115.8 (−C6), and 122.5(−C7); IR (ν_{max}, cm^{-1}, KBr):3435(ν_{OH}), 2917(ν_{as}(C–H), CH_3), 2918(ν_{as}(C–H), CH_2), 2867(ν_s(C–H), CH_3), 2842(ν_{as}(C–H), CH_2), 1632($\nu_{C=N}$), and 1277(ν_{C-O}).

2.4. *Synthesis of oxovanadium (IV) complexes*

To the ligand 4-18-$OC_{12}H_{25}$ (0.64 g, 1 mmol) or 4-16-$OC_{12}H_{25}$ (0.62 g, 1 mmol) or 4-8-$OC_{12}H_{25}$ (0.50 g, 1 mmol) and 4-6-$OC_{12}H_{25}$ (0.48 g, 1 mmol) dissolved in minimum volume of absolute ethanol vanadyl sulfate $VOSO_4 \cdot 5H_2O \cdot 2H_2O$ (0.11 g, 0.5 mmol) in methanol was added followed by addition of triethylamine and refluxed for 2 h. A greenish solid formed immediately was filtered, washed with diethyl ether and recrystallised from chloroform–ethanol.

2.4.1. *Oxovanadium(IV) complex, (VO-18-$OC_{12}H_{25}$)*

Yield: 0.56 g (75%) Anal. Calcd for $C_{86}H_{140}N_2O_7V$: C, 75.6; H, 10.3; and N, 2.0. Found: C, 75.5%; H, 10.4%; and N, 2.1%; FAB mass (*m*/*e*, fragment): *m*/*z*: calcd 1364.0; found: 1365[M + H^+]; IR (KBr, cm^{-1}): 1616($\nu_{C=N}$), 1132 (ν_{C-O}, phenolic), and 970($\nu_{V=O}$).

2.4.2. *Oxovanadium(IV) complex, (VO-16-$OC_{12}H_{25}$)*

Yield: 0.56 g (78%) Anal. Calcd for $C_{82}H_{132}N_2O_7V$: C, 75.2; H, 10.1; and N, 2.1. Found: C, 75.1%; H, 10.2%; and N, 2.0%; FAB mass (*m*/*e*, fragment): *m*/*z*: calcd 1307.0; found: 1308[M + H^+]; IR (KBr, cm^{-1}): 1612($\nu_{C=N}$), 1135 (ν_{C-O}, phenolic), and 969($\nu_{V=O}$).

2.4.3. *Oxovanadium(IV) complex, (VO-8-$OC_{12}H_{25}$)*

Yield: 0.45 g (76%) Anal. Calcd for $C_{66}H_{100}N_2O_7V$: C, 73.1; H, 9.2; and N, 2.5. Found: C, 73.2%; H, 9.3%; and N, 2.4%; FAB mass (*m*/*e*, fragment): *m*/*z*: calcd 1083.7; found: 1084[M + H^+]; IR (KBr, cm^{-1}): 1611($\nu_{C=N}$), 1134 (ν_{C-O}, phenolic), and 970($\nu_{V=O}$).

2.4.4. *Oxovanadium(IV) complex, (VO-6-OC$_{12}$H$_{25}$)*

Yield: 0.44 g (75%) Anal. Calcd for $C_{62}H_{92}N_2O_7V$: C, 72.4; H, 9.0; and N, 2.7. Found: C, 72.3%; H, 9.1%; and N, 2.6%; FAB mass (*m*/*e*, fragment): *m*/*z*: calcd 1027.6; found: 1028[M + H$^+$]; IR (KBr, cm^{-1}): 1614($\nu_{C=N}$), 1133(ν_{C-O}, phenolic), and 971($\nu_{V=O}$).

3. Result and discussion

3.1. *Spectral investigation*

The characterization of the compounds was made by elemental analyses, FT-IR, UV-vis, ^{1}H-NMR, and mass spectrometry. The analytical data are in good agreement with the proposed formulae. A strong band observed at ~1622–1624 cm^{-1}, in the IR spectrum is assigned to $\nu_{(C=O)}$. The IR spectra of the free ligands exhibit the characteristic bands of imine(C=N), which appear at ~1630 cm^{-1}. In metal complexes, the $\nu_{(CN)}$ band is generally shifted to lower wave numbers relative to the free ligand, indicating a decrease in the C=N bond order due to the coordination of the imine nitrogen to the metal and back bonding from the VO(IV) center to the π^* orbital of the azomethine group [41]. Moreover, the absence of ν_{OH} mode at ~3155 cm^{-1}, indicated its coordination to VO(IV) center. The $\nu_{C=N}$ stretching is rather independent of the length of alkoxy side chain. Occurrence of vanadyl (V=O) stretching mode at *ca* 970 cm^{-1} evidenced the absence of any intermolecular (···V=O···V=O···) interaction attesting the monomeric nature of the complexes [25,26]. Appearance of additional bands at ~450–480 and ~527–549 cm^{-1} in the spectra of the complexes assigned to the V–O and V–N stretching vibrations that are not observed in the spectra of the ligands furnished evidence for [N,O] binding mode of the ligand. The ^{1}H-NMR spectra of liganads showed signal at 13.4–13.8 ppm, corresponding to the proton of the OH group. The imine group appears at 8.5 ppm. The FAB-mass spectra of the vanadyl(IV) complexes are concordant with their formula weights. The electronic spectra (Figure 1) of the ligands and their complexes were recorded in dichloromethane (Table 1). The ligand exhibited two absorption bands centered at ~285 and ~350 nm, attributed to π–π^* transition localized on the aromatic rings.

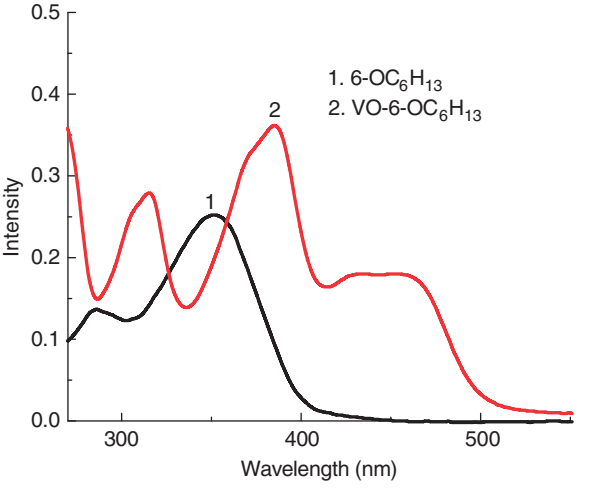

Figure 1. UV-Vis spectra of 4-6-OC$_{12}$H$_{25}$ and VO-6-OC$_{12}$H$_{25}$.

Table 1. Spectral data of the compounds.

Compounds	UV-Vis, λ_{max} (nm) (ϵ, mol L^{-1} cm^{-1}) (transition)	IR (cm^{-1})	FAB mass
$C_{43}H_{71}NO_3$ (4-18-$OC_{12}H_{25}$)	286(1360) ($\pi \rightarrow \pi^*$) 349(2530) ($\pi \rightarrow \pi^*$)	1630($\nu_{C=N}$) 3431(ν_{OH})	650
$C_{86}H_{140}N_2O_7V$ (VO-18-$OC_{12}H_{25}$)	315(2750) ($\pi \rightarrow \pi^*$) 385(3590) ($\pi \rightarrow \pi^*$) 446(1800) (LMCT)	1616($\nu_{C=N}$) 970($\nu_{V=O}$) 532(ν_{M-N}) 461(ν_{M-O})	622
$C_{41}H_{67}NO_3$ (4-16-$OC_{12}H_{25}$)	284(1350) ($\pi \rightarrow \pi^*$) 350(2530) ($\pi \rightarrow \pi^*$)	1631($\nu_{C=N}$) 3433(ν_{OH})	510
$C_{82}H_{132}N_2O_7V$ (VO-16-$OC_{12}H_{25}$)	315(2745) 381(2750) ($\pi \rightarrow \pi^*$) 441(1950) (LMCT)	1612($\nu_{C=N}$) 970($\nu_{V=O}$) 531(ν_{M-N}) 457(ν_{M-O})	482
$C_{33}H_{51}NO_3$ (4-8-$OC_{12}H_{25}$)	282(1350) ($\pi \rightarrow \pi^*$) 352(2730) ($\pi \rightarrow \pi^*$)	1632($\nu_{C=N}$) 3432(ν_{OH})	1365
$C_{66}H_{100}N_2O_7V$ (VO-8-$OC_{12}H_{25}$)	317(2550) ($\pi \rightarrow \pi^*$) 379(1750) ($\pi \rightarrow \pi^*$) 438(1640) (LMCT)	1611($\nu_{C=N}$) 969($\nu_{V=O}$) 532(ν_{M-N}) 458(ν_{M-O})	1308
$C_{31}H_{47}NO_3$ (4-6-$OC_{12}H_{25}$)	285(1350) ($\pi \rightarrow \pi^*$) 350(2630) ($\pi \rightarrow \pi^*$)	1632($\nu_{C=N}$) 3431(ν_{OH})	1084
$C_{62}H_{92}N_2O_7V$ (VO-6-$OC_{12}H_{25}$)	315(2450) ($\pi \rightarrow \pi^*$) 385(1450) ($\pi \rightarrow \pi^*$) 446(1560) (LMCT)	1614($\nu_{C=N}$) 971($\nu_{V=O}$) 531(ν_{M-N}) 453(ν_{M-O})	1228

Upon complexation, these bands are red shifted to ~315, and ~385 nm. In addition, complexes displayed a band at ~466 nm, owing to the LMCT transition [43].

3.2. *Variable temperature magnetic susceptibility study*

The temperature dependence of the magnetic susceptibilities is carried out for VO-18-$OC_{12}H_{25}$ in the temperature range 2.5–300 K under a 1 kOe applied field. The effective magnetic moment for a typical complex VO-18-$OC_{12}H_{25}$ is found to be 1.73 B.M. The χ_M^{-1} *versus T*-plot is almost linear down to 30 K and then decreases with increase of temperature. The inverse of the susceptibility plotted against temperature (Figure 2), satisfies the Curie–Weiss equation. The strength of efficient superexchange path is presumably hindered by coordinating ability of the metal ion. The vanadium complexes can thus be considered as magnetically isolated spin (d^1) centers. Absence of any maximum in χ_M *versus T* indicated nonexistence of strong exchange interactions between the spin centers.

3.3. *Electrochemical behavior*

The redox behavior of a representative VO-16-$OC_{12}H_{25}$ complex was probed by cyclic voltammetry in dichloromethane solution in the potential range –4.0 to 1.4 V *versus* SCE

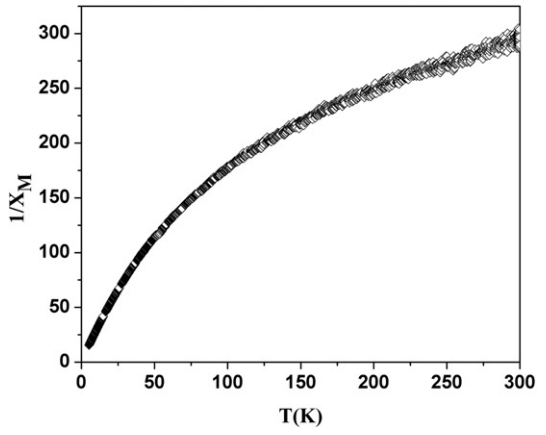

Figure 2. Variation of magnetic susceptibility of VO-18-$OC_{12}H_{25}$ with temperature.

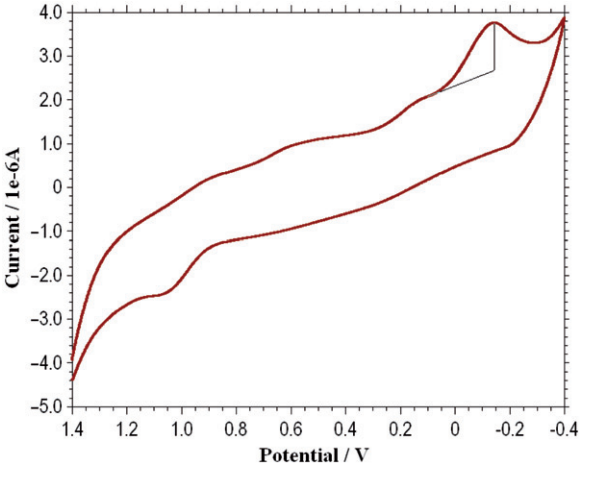

Figure 3. Cyclic voltammogram of VO-16-$OC_{12}H_{25}$.

at a scan rate of $0.05\,Vs^{-1}$. The voltammogram (Figure 3) displayed a quasireversible (peak separation $>100\,mV$) one-electron response. The peak separation ($E_{1/2} = +0.57$, $E_{pc} = -0.14\,V$, $E_p{}^a = 1.0\,V$, $\Delta E_p = 0.86\,V$) is assigned to VO^{3+}/VO^{2+} couple. On scanning to negative potential, no response is observed implying redox innocent characteristics of the ligand, supported also by the free ligand cyclic voltammetry.

3.4. *Mesomorphic behavior: polarising optical microscopy and DSC studies*

The liquid crystalline behavior of all the compounds was monitored by DSC studies and polarizing optical microscopy (POM). The phase transitions and thermodynamic data are summarized in Table 2. The compounds are all found to be mesomorphic. All the ligands exhibited enantiotropic phase transitions. Upon cooling the sample from isotropic liquid,

Table 2. Phase transitions temperatures (T, °C), associated enthalpies (ΔH, kJ mol^{-1}) of the compounds.

Compounds	Heating	Cooling
4-6-$OC_{12}H_{25}$	Cr 77.0(40.2)SmC126.1(6.7)I	I 123.8(6.0)SmC42.6(15.6)Cr
4-8-$OC_{12}H_{25}$	Cr 76.5(49.0) SmC 125.6(7.9)I	I122.9(7.5)SmC44.5(23.8)Cr
4-16-$OC_{12}H_{25}$	Cr 58.2(2.1) Cr1 89.7(71.2) SmC118.1(6.6)I	I112.5(4.8) SmC70.0(47.7)Cr
4-18-$OC_{12}H_{25}$	Cr59.3(1.9) Cr1 91.0(74.6) SmC 114.2(6.3)I	I110.4(4.3) SmC 66.8(71.4)Cr
VO-6-$OC_{12}H_{25}$	Cr68.1(2.9)SmX127(4.3) SmA167.9(5.9)I	I167.5(3.9)SmA97.7(4.9)Cr
VO-8-$OC_{12}H_{25}$	Cr72.6(2.2)SmX134.2(5.3) SmA168.7(5.4)I	I164.5(4.6)SmA96.5(4.2)Cr
VO-16-$OC_{12}H_{25}$	Cr87.3(16.7)SmX127.9(15.5) SmA146.5(11.6)I	I143.6(9.5)SmA93.9(20.9) SmX69.0(6.6)Cr
VO-18-$OC_{12}H_{25}$	Cr86.6(61.8)SmA129.5(11.8)I	I129.2(14.0)SmA54.9(31.2)Cr

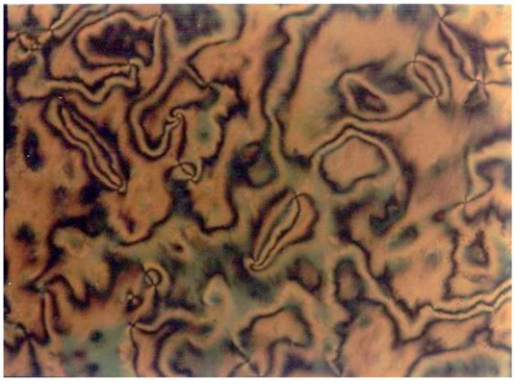

Figure 4. Schlieren texture of SmC phase.

a schlieren texture of SmC phase (Figure 4) with four brush defect at 110–125°C was observed. The DSC trace for the lower homologues (6-$OC_{12}H_{25}$ and 8-$OC_{12}H_{25}$) showed two transitions in heating and two in cooling cycle. However, in case of higher homologues (16-$OC_{12}H_{25}$ and 18-$OC_{12}H_{25}$), in addition to smectic mesophase, a crystal to crystal transition is observed in heating cycles (Figure 5) which could not be detected in POM study. The mesophase to isotropic transition temperature decreases with increase in chain length. The variation of carbon chain length with transition temperature is shown in Figure 6. The oxovanadium (IV) complexes showed SmA/SmX phases. In polarizing optical microscopic study, cooling the samples from isotropic liquid, typical batonnets are formed which coalesce to give rise to a highly birefringent fanlike texture, characteristic of the smectic A phase (Figure 7). On further cooling, the sample an arced like texture observed for all the complexes were diagnostic of unidentified SmX phase (Figure 8). The DSC trace (Figure 9) for a representative compound VO-18-$OC_{12}H_{25}$ exhibited two transitions both in heating and cooling cycles. Moreover at 73°C, a glass transition could be observed for the complex in heating run. The high-ordered SmX phase transition could

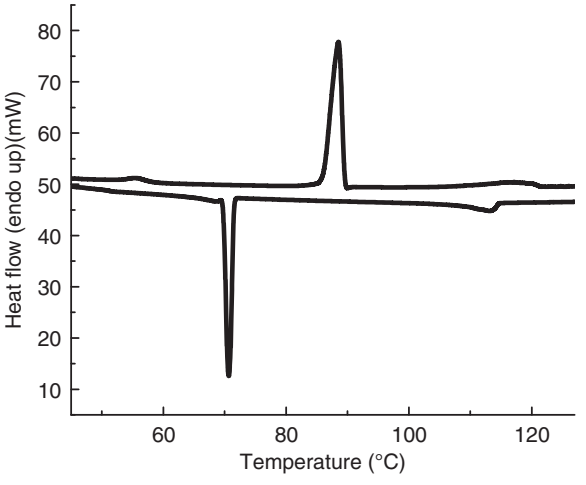

Figure 5. DSC thermogram of 4-16-$OC_{12}H_{25}$.

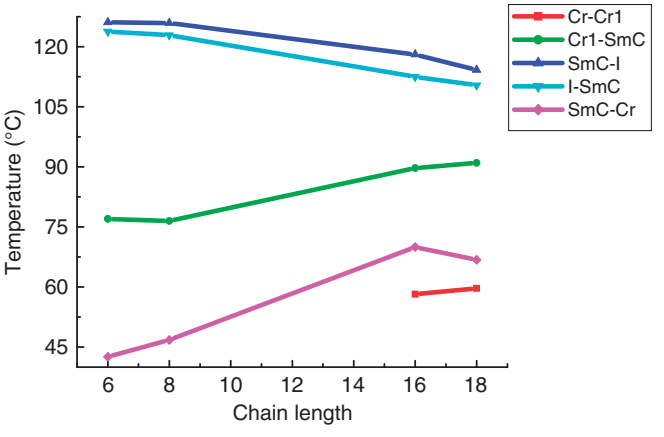

Figure 6. Variation of carbon chain length with transition temperature in ligand.

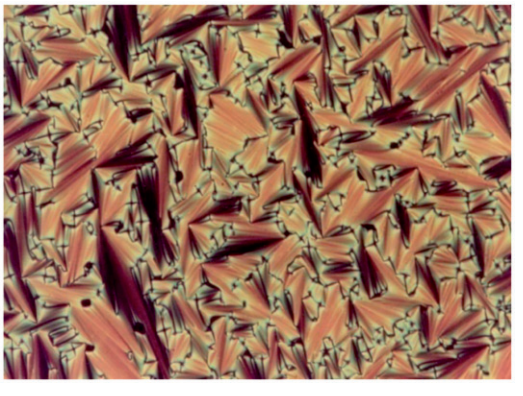

Figure 7. Fanlike texture of SmA phase.

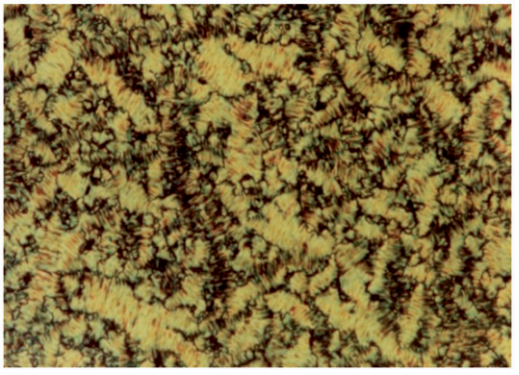

Figure 8. Unidentified SmX phase.

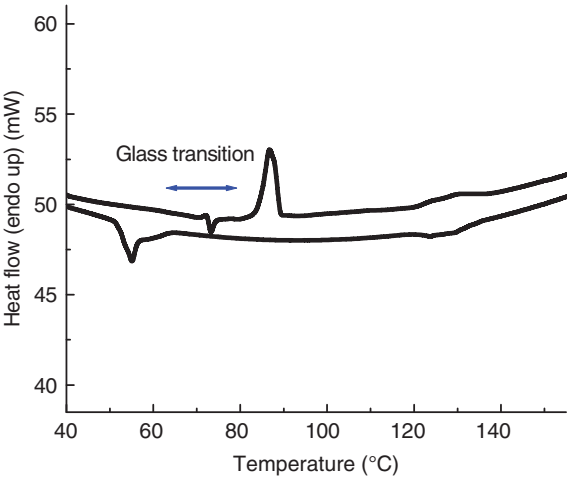

Figure 9. DSC thermogram of VO-18-$OC_{12}H_{25}$.

not be detected in DSC for VO-18-$OC_{12}H_{25}$. The variations in transition temperatures as a function of carbon chain length are depicted in Figure 10. No definitive trend was found to emerge as a function of carbon chain length variation. The isotropisation temperatures were, however, mostly decreased with increasing carbon chain length.

3.5. *Density functional theory study*

As X-ray quality crystals could not be grown, density functional theory (DFT) studies were carried out to ascertain the energy optimized structures. Geometry optimization of a representative complex, VO-6-$OC_{12}H_{25}$ (Figure 11) has been performed without applying any symmetry constrain within the generalized gradient approximation level using the Becke–Lee–Yang–Parr (BLYP) [55] exchange and correlation functional implemented in the DMol3 [56]. The DNP basis set chosen in this study is a double-numerical atomic orbital augmented by polarization functions [57]. The DNP basis set is comparable to

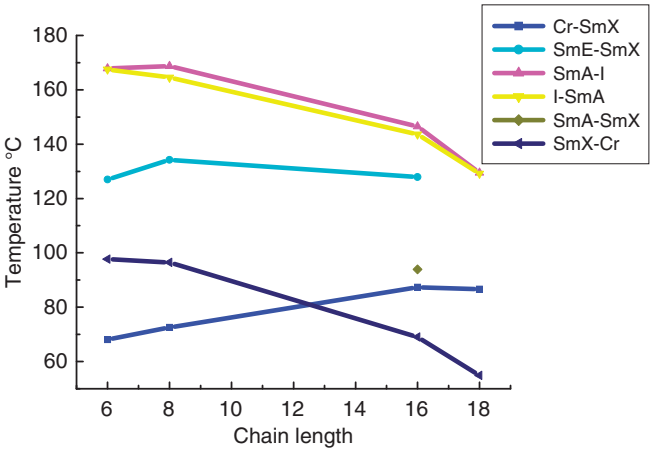

Figure 10. Variation of carbon chain length with transition temperature in complexes.

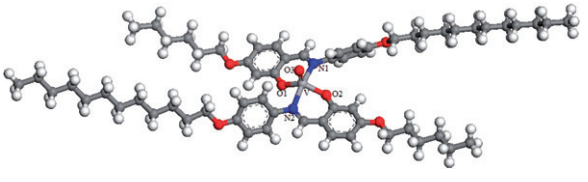

Figure 11. Optimized structure of VO-6-$OC_{12}H_{25}$.

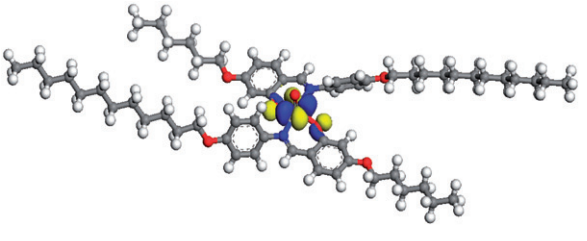

Figure 12. HOMO energy diagram of VO-6-$OC_{12}H_{25}$.

6-31G** Gaussian basis sets with a better accuracy for a similar basis set size due to core electron inclusion. The global cut off radius is set to be 5.0 Å. The convergence criteria for energy, force, and displacement were 1×10^{-5} hartree, 2×10^{-3} hartree/Å, and 5×10^{-3} Å, respectively. The 3-D isosurface plots of the lowest unoccupied molecular orbital (LUMO) and the highest occupied molecular orbital (HOMO) of the complex are shown in Figures 12 and 13. The energies of the HOMO and LUMO of the VO(IV) complex derived from DFT are found to be −3.887 and −2.310 eV, respectively ($\Delta E = 1.577$ eV). The electron density of the LUMO is localized mainly on the C–N bonds while the HOMO is a predominantly C–O bond orbitals. Geometric parameters of the optimized VO(IV) complex are furnished in Table 3. The average V–O and V–N bond lengths are 1.95 and 2.18 Å, respectively. The bond length between oxido ligand and vanadium is evaluated to

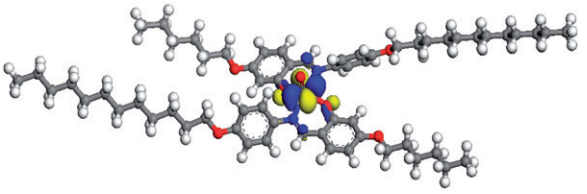

Figure 13. LUMO energy diagram of VO-6-$OC_{12}H_{25}$.

Table 3. Selected bond lengths (Å) and bond angles (°) of VO-6-$OC_{12}H_{25}$ complex optimized at the BLYP/DNP level of theory.

Structure parameter	VO-6-$OC_{12}H_{25}$
V–O(1)	1.952
V–O(2)	1.956
V–O(3)	1.622
V–N(1)	2.182
V–N(2)	2.181
O(1)–V–O(2)	130.4
N(1)–V–N(2)	161.7
N(1)–V–O(2)	86.2
O(1)–V–N(1)	84.1
O(1)–V–N(2)	86.1
N(2)–V–O(2)	86.4

be 1.623 Å. The bond angles varied from 86.2° to 161.7°, respectively, suggesting a distorted square pyramidal geometry around the vanadyl(IV) center.

4. Conclusions

Successful synthesis of a series of new oxovanadium(IV) complexes bearing long as well as short alkoxy tail on both side of aromatic ring has been demonstrated. All the compounds are found to exhibit smectic mesomorphism. No definitive trends were noted as a function of carbon chain lengths of alkoxy tails both for the ligands and complexes. Cyclic voltammetry study revealed a quasireversible one-electron response for the VO(V)/VO(IV) redox couple. The compounds are all found to be thermally quite stable. Based on DFT, spectral and magnetic studies, a distorted square pyramidal five-coordinate structure have been proposed. The synthetic strategy adopted herein can be effectively employed to access newer mesogenic vanadyl complexes.

Acknowledgments

The authors thank SAIF, NEHU, and CDRI, Lucknow for analytical and spectral data. Chitraniva Datta acknowledges financial support from UGC, Government of India. Dr R.C. Deka, Tezpur University, India, is acknowledged for computational facility.

References

[1] R. Ziessel, *Schiff-based bipyridine ligands. Unusual coordination features and mesomorphic behaviour*, Coord. Chem. Rev. 216–217 (2001), pp. 195–223.

[2] P.G. Cozzi, *Metal–Salen Schiff base complexes in catalysis: practical aspects*, Chem. Soc. Rev. 33 (2004), pp. 410–421.

[3] J.P. Costes, S. Shova, and W. Wernsdorfer, *Tetranuclear [Cu–Ln]$_2$ single molecule magnets: synthesis, structural and magnetic studies*, Dalton Trans. (2008), pp. 1843–1849.

[4] X.G. Ran, L.Y. Wang, Y.C. Lin, J. Hao, and D.R. Cao, *Syntheses, characterization and biological studies of zinc(II), copper(II) and cobalt(II) complexes with Schiff base ligand derived from 2-hydroxy-1-naphthaldehyde and selenomethionine*, Appl. Organomet. Chem. 24 (2010), pp. 741–747.

[5] K.C. Gupta and A.K. Sutar, *Catalytic activities of Schiff base transition metal complexes*, Coord. Chem. Rev. 252 (2008), pp. 1420–1450.

[6] M. Orio, O. Jarjayes, H. Kanso, C. Philouze, F. Neese, and F. Thomas, *X-ray structures of copper(II) and nickel(II) radical salen complexes: The preference of galactose oxidase for copper(II)*, Angew. Chem. Int. Ed. 49 (2010), pp. 4989–4992.

[7] Z.H. Chohan, S.H. Sumrra, M.H. Youssoufi, and T.B. Hadda, *Design and synthesis of triazole Schiff bases and their oxovanadium(IV) complexes as antimicrobial agents*, J. Coord. Chem. 63 (2010), pp. 3981–3998.

[8] Y. Abe, A. Iyoda, K. Seto, A. Moriguchi, and H. Yokoyama, *Synthesis, structures and ion-association properties of a series of schiff base oxidovanadium(V) complexes with 4-substituted long alkoxy chains*, Eur. J. Inorg. Chem. (2008), pp. 2148–2157.

[9] M. Bagherzadeh and M. Amini, *A new vanadium Schiff base complex as catalyst for oxidation of alcohols*, J. Coord. Chem. 63 (2010), pp. 3849–3858.

[10] S. Sarkar, K. Dey, S. Biswas, and B.B. Bhaumik, *Synthesis and characterization of oxovanadium(IV), vanadium(IV) and oxovanadium(V) complexes of tetradentate Schiff bases. Attempted preparation of vanadium-carbon bonded compounds through desilylation*, J. Coord. Chem. 60 (2007), pp. 1143–1156.

[11] S. Mohebbi and B. Bakhshi, *Electrochemical and spectral behavior of mononuclear oxo-vanadium(IV)salicyldiimine complexes*, J. Coord. Chem. 61 (2008), pp. 2615–2628.

[12] K.S. Patel and J.C. Bailar Jr, *The mass spectra and the steriochemistry of N,N'-bis-(salicylidene)-1,1-(dimethyl)-ethylenediamino-oxovanadium(IV)*, J. Coord. Chem. 3 (1973), pp. 113–117.

[13] C.J. Schneider, J.E. Penner-Hahn, and V.L. Pecoraro, *Elucidating the protonation site of vanadium peroxide complexes and the implications for biomimetic catalysis*, J. Am. Chem. Soc. 130 (2008), pp. 2712–2713.

[14] C. Wikete, P. Wu, G. Zampetlla, L.D. Gioia, G. Licini, and D. Rehder, *Glycine- and sarcosine-based models of vanadate-dependent haloperoxidases in sulfoxygenation reactions*, Inorg. Chem. 46 (2007), pp. 196–207.

[15] T.S. Smith, C.A. Root, J.W. Kampf, P.G. Rasmussen, and V.L. Pecoraro, *Reevaluation of the additivity relationship for vanadyl−imidazole complexes: Correlation of the EPR hyperfine constant with ring orientation*, J. Am. Chem. Soc. 122 (2000), pp. 767–775.

[16] C.R. Cornman, E.P. Zovinka, and M.H. Meixner, *Vanadium(IV) complexes of an active-site peptide of a protein tyrosine phosphatase*, Inorg. Chem. 34 (1995), pp. 5099–5100.

[17] D.C. Crans, R.L. Bunch, and L.A. Theisen, *Interaction of trace levels of vanadium(IV) and vanadium(V) in biological systems*, J. Am. Chem. Soc. 111 (1989), pp. 7597–7607.

[18] D.C. Crans, J.J. Smee, E. Gaidamauskas, and L.Q. Yang, *The chemistry and biochemistry of vanadium and the biological activities exerted by vanadium compounds*, Chem. Rev. 104 (2004), pp. 849–902.

[19] J.H. McNeill, V.G. Yuen, and H.R. Hoveyda, *Bis(maltolato)oxovanadium(IV) is a potent insulin mimic C. Orvig*, J. Med. Chem. 35 (1992), pp. 1489–1491.

[20] K.H. Thompson, J.H. McNeill, and C. Orvig, *Vanadium compounds as insulin mimics*, Chem. Rev. 99 (1999), pp. 2561–2571.

[21] A.J. Tasiopoulos, A.N. Troganis, A. Evangelou, C.P. Raptopoulou, A. Terzis, Y. Deligiannakis, and T.A. Kabanos, *Synthetic analogues for oxovanadium(IV)–glutathione interaction: An EPR, synthetic and structural study of oxovanadium(IV) compounds with sulfhydryl-containing pseudopeptides and dipeptides*, Chem. Eur. J. 5 (1999), pp. 910–921.
[22] N. Hoshino, *Liquid crystal properties of metal–salicylaldimine complexes: Chemical modifications towards lower symmetry*, Coord. Chem. Rev. 174 (1998), pp. 77–108.
[23] J.L. Serrano, *Metallomesogens. Synthesis, Properties, and Applications*, Wiley-VCH, Weinheim, 1996.
[24] B. Donnio, D. Guillon, R. Deschenaux, and D.W. Bruce, *Metallomesogens*, in *Comprehensive Coordination Chemistry II*, Vol. 7, J.A. McCleverty and T.J. Meyer, eds., Elsevier, Oxford, 2003, pp. 357–627.
[25] A.M. Giroud-Godquin and P.M. Maitlis, *Metallomesogens: Metal complexes in organized fluid phases*, Angew. Chem., Int. Ed. Engl. 30 (1991), pp. 375–402.
[26] P. Espinet, M.A. Esteruelas, L.A. Oro, J.L. Serrano, and E. Sola, *Transition metal liquid crystals: advanced materials within the reach of the coordination chemist*, Coord. Chem. Rev. 117 (1992), pp. 215–274.
[27] S.A. Hudson and P.M. Maitlis, *Calamitic metallomesogens: metal-containing liquid crystals with rodlike shapes*, Chem. Rev. 93 (1993), pp. 861–885.
[28] A. Polishchuk and T.V. Timofeeva, *Metal-containing liquid-crystal phases*, Russ. Chem. Rev. 62 (1993), pp. 291–321.
[29] D.W. Bruce, *Metal-containing liquid crystals*, in *Inorganic Material*, D.W. Bruce and D. O'Hare, eds., Wiley, Chichester, 1996, p. 429.
[30] F. Neve, *Transition metal based ionic mesogens*, Adv. Mater. 8 (1996), pp. 277–289.
[31] S.R. Collinson and D.W. Bruce, *Metallomesogens – supramolecular organization of metal complexes in fluid Phases*, in *Supramolecular Chemistry: Transition Metals in Supramolecular Chemistry*, J.P. Sauvage, ed., Wiley, New York, 1999, pp. 285–369.
[32] V.A. Molochko and N.S. Rukk, *Mesomorphic complex compound*, Russ. J. Coord. Chem. 26 (2000), pp. 829–846.
[33] K. Binnemans and C. Gorller-Walrand, *Lanthanide-containing liquid crystals and surfactants*, Chem. Rev. 102 (2002), pp. 2303–2345.
[34] B. Donnio, D. Guillon, D.W. Bruce, and R. Deschenaux, *Metallomesogens*, in *Comprehensive Coordination Chemistry II: From Biology to Nanotechnology*, Vol. 7, ch. 7.9, J.A. McCleverty, T.J. Meyer, M. Fujita, and A. Powell, eds., Elsevier, Oxford, UK, 2003, pp. 357–627.
[35] R.W. Date, E.F. Iglesias, K.E. Rowe, J.M. Elliott, and D.W. Bruce, *Metallomesogens by ligand design*, Dalton Trans. (2003), pp. 1914–1931.
[36] A.K. Prajapati and N. Bonde, *Synthesis of two naphthyl-containing homologous series of mesogenic ligands and the related metallomesogens containing Cu(II)*, Liq. Cryst. 33 (2006), pp. 1189–1197.
[37] Z. Rezvani, K. Nejati, M. Seyedahmadian, and B. Divband, *Investigation of liquid crystalline behavior of copper(II) complexes derived from Azo-containing salicylaldimine ligands with lateral hydroxyl group*, Mol. Cryst. Liq. Cryst. 493 (2008), p. 71.
[38] A.S. Mocanu, M. Ilis, F. Dumitrascu, M. Ilie, and V. Circu, *Synthesis, mesomorphism and luminescence properties of palladium(II) and platinum(II) complexes with dimeric Schiff base liquid crystals*, Inorg. Chim. Acta. 363 (2010), pp. 729–736.
[39] U. Caruso, R. Diana, B. Panunzi, A. Roviello, M. Tingoli, and A. Tuzi, *Facile synthesis of new Pd(II) and Cu(II) based metallomesogens from ligands containing thiophene rings*, Inorg. Chem. Commun. 12 (2009), pp. 1135–1138.
[40] S. Hayami, K. Danjobara, S. Miyazaki, K. Inoue, Y. Ogawa, and Y. Maeda, *Photo-induced spin transition iron(II) compounds with liquid-crystal properties*, Polyhedron 24 (2005), pp. 2821–2827.
[41] O.N. Kadkin, E.H. Kim, Y.J. Rha, S.Y. Kim, J. Tae, and M.-G. Choi, *Novel tetrahedratic smectic C and nematic mesophases in unsymmetrically 1,1'-Bis-substituted ferrocenomesogens*, Chem. Eur. J. 15 (2009), pp. 10343–10347.

[42] S. Hayami, N. Motokawa, A. Shuto, N. Masuhara, T. Someya, Y. Ogawa, K. Inoue, and Y. Maeda, *Spin transition at the mesophase transition temperature in a Cobalt(II) compound with branched alkyl chains*, Inorg. Chem. 46 (2007), pp. 1789–1794.
[43] F. Morale, R.L. Finn, S.R. Collinson, A.J. Blake, C. Wilson, D.W. Bruce, D. Guillon, B. Donnio, and M. Schroder, *Metal-directed columnar phase formation in tetrahedral zinc(II) and manganese(II) metallomesogens*, New J. Chem. 32 (2008), pp. 297–305.
[44] C.R. Bhattacharjee, G. Das, P. Mondal, S.K. Prasad, and D.S.S. Rao, *Plastic columnar mesomorphism in half-disc shaped oxovanadium(IV) Schiff-base complexes*, Liq. Cryst. 38 (2011), pp. 615–623.
[45] C.R. Bhattacharjee, G. Das, and P. Mondal, *Liquid-crystalline oxovanadium(IV) complexes accessed from bidentate [N, O] donor salicylaldimine Schiff base ligands*, J. Coord. Chem. 64 (2011), pp. 3273–3289.
[46] W. Pyzuk, A. Krowczynski, L. Chen, E. Gorecka, and I. Bickczantaev, *Binuclear liquid crystals incorporating dia- or para-magnetic transition metals*, Liq. Cryst. 19 (1995), pp. 675–677.
[47] M. Ghedini, S. Morrone, R. Bartolino, V. Formoso, O. Francescangeli, B. Yang, D. Gatteschi, and C. Znachini, *Transition metals complexed to ordered mesophases. Synthesis, mesomorphism, and X-ray and EPR characterization of a homologous series of N-(4-dodecyloxysalic ylidene)-4′-alkylanilines complexed to oxovanadium(IV)*, Chem. Mater. 5 (1993), pp. 876–882.
[48] H. Zheng, C.K. Lai, and T.M. Swager, *Complementary shapes in columnar liquid crystals: Structural control in homo- and heteronuclear bimetallic assemblies*, Chem. Mater. 6 (1994), pp. 2252–2268.
[49] H. Zheng, C.K. Lai, and T.M. Swager, *Controlling intermolecular interactions between metallomesogens: Side-chain effects in discotic copper, palladium, and vanadyl bis(P-diketonates)*, Chem. Mater. 7 (1995), pp. 2067–2077.
[50] Y. Abe, K. Nakabayashi, N. Matsukawa, M. Iida, T. Tanase, M. Sugibayashia, and K. Ohta, *Novel crystal structure and mesomorphism appeared in oxovanadium(IV) salen complexes with 4-substituted long alkoxy chains*, Inorg. Chem. Commun. 7 (2004), pp. 580–583.
[51] P.J. Alonso, M.L. Sanjuan, P. Romero, M. Marcos, and J.L. Serrano, *Vanadyl metal mesogen derivatives: an ESR study*, J. Phys. Condens. Mater 2 (1990), pp. 9173–9182.
[52] C.R. Bhattacharjee, G. Das, P. Mondal, S.K. Prasad, and D.S.S. Rao, *Lamellar columnar mesomorphism in a series of oxovanadium(IV) complexes derived from N,N′-di-(4-n-alkoxysalicylidene) diaminobenzene*, Inorg. Chem. Commun. 14 (2011), pp. 606–612.
[53] C.R. Bhattacharjee, G. Das, D.D. Purkayastha, and P. Mondal, *Synthesis, characterisation and mesomorphic properties of a homologous series of oxovanadium(IV) complexes containing a bidentate [N,O] donor Schiff base mesogen*, Liq. Cryst. 38 (2011), pp. 717–808.
[54] C.R. Bhattacharjee, G. Das, D.D. Purkayastha, P. Mondal, and P. Kanoo, *Vanadyl(IV) complexes of 4-alkoxy substituted [N,O] donor salicylaldimine Schiff base derived from chloro-/nitro-aniline: Synthesis, mesomorphism and DFT study*, J. Coord. Chem. 64 (2011), pp. 2746–2760.
[55] C. Lee, W. Yang, and R.G. Parr, *Development of the Colle-Salvetti correlation-energy formula into a functional of the electron density*, Phys. Rev. B 37 (1988), pp. 785–789.
[56] B. Delley, *An all-electron numerical method for solving the local density functional for polyatomic molecules*, J. Chem. Phys. 92 (1990), pp. 508–517.
[57] K. Suzuki, T. Nada, G. Sastre, N. Katada, and M. Niwa, *Periodic density functional calculation on the Brønsted acidity of modified Y-type zeolite*, J. Phys. Chem. C 113 (2009), pp. 5672–5680.

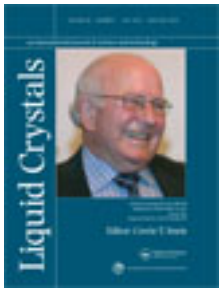

Liquid Crystals
Publication details, including instructions for authors and subscription information:
http://www.tandfonline.com/loi/tlct20

Photoluminescent columnar zinc(II) bimetallomesogen of tridentate [ONO]-donor Schiff base ligand

Chira R. Bhattacharjee [a], Chitraniva Datta [a], Gobinda Das [a], Dharitri Das [a], Paritosh Mondal [a], Subbarao Krishna Prasad [b] & D.S. Shankar Rao [b]

[a] Department of Chemistry, Assam University, Assam, India

[b] Centre for Soft Matter Research, Bangalore, India

Published online: 11 Apr 2013.

To cite this article: Chira R. Bhattacharjee, Chitraniva Datta, Gobinda Das, Dharitri Das, Paritosh Mondal, Subbarao Krishna Prasad & D.S. Shankar Rao (2013) Photoluminescent columnar zinc(II) bimetallomesogen of tridentate [ONO]-donor Schiff base ligand, Liquid Crystals, 40:7, 942-950, DOI: 10.1080/02678292.2013.788229

To link to this article: http://dx.doi.org/10.1080/02678292.2013.788229

Liquid Crystals, 2013
Vol. 40, No. 7, 942–950, http://dx.doi.org/10.1080/02678292.2013.788229

Taylor & Francis
Taylor & Francis Group

Photoluminescent columnar zinc(II) bimetallomesogen of tridentate [ONO]-donor Schiff base ligand

Chira R. Bhattacharjee[a]*, Chitraniva Datta[a], Gobinda Das[a], Dharitri Das[a], Paritosh Mondal[a], Subbarao Krishna Prasad[b] and D.S. Shankar Rao[b]

[a]*Department of Chemistry, Assam University, Assam, India;* [b]*Centre for Soft Matter Research, Bangalore, India*

(*Received 11 December 2012; final version received 18 March 2013*)

A new zinc(II) bimetallomesogenic complex, $[Zn_2L_2]$, of tridentate [ONO]-donor Schiff base ligand (L = N-(2-hydroxyethyl)-4-hexadecyloxysalicylaldimines) was synthesised and their mesomorphic and photoluminescence properties were investigated. The compounds were characterised by Fourier transform infrared spectroscopy (FTIR), ^{1}H and ^{13}C nuclear magnetic resonance (NMR), ultraviolet-visible spectroscopy (UV-Vis) spectroscopy, elemental analyses and fast atom bombardment (FAB) mass spectrometry. The mesomorphic behaviour of the complex was investigated by polarised optical microscopy, differential scanning calorimetry and X-ray diffraction (XRD) study. A rectangular or oblique columnar mesophase is conjectured on the basis of powder X-ray diffraction (PXRD) study. The complex is found to be blue light emitter in solution, in solid and in condensed states with broad emission maxima at ~427–464 nm. The density functional theory (DFT) calculations revealed a distorted square planar structure around each zinc(II) centre in the dinuclear framework. Time-dependent DFT spectral correlative study was undertaken to account for the electronic transition.

Keywords: Zinc; bimetallomesogen; columnar mesophase; photoluminescent; density functional theory

1. Introduction

Luminescent liquid crystalline materials have attracted increasing attention as functional materials owing to their versatile exploration of display devices, solar cells, information storage system and sensors.[1–3] Besides the well-known display applications of luminescent liquid crystals (LCs), their synthesis is still challenging. Most of the molecular emitters are highly emissive in solution and in solid states; however, luminescent properties in the mesomorphic states are quite rare.[4–6] Since the discovery and advancement of light-emitting devices, zinc complexes have received significant attention because of their interesting photoluminescent properties, high thermal, redox stability and great diversity of tunable electronic properties.[7–11] Design and planned synthesis of zinc(II) complexes with demanding requirements such as anisotropic fluidity, improved charge transport ability, changes in molecular organisation in response to external stimuli, light-emitting efficiency simultaneously open up new possibilities for their use in high-tech applications.[2,7–11] Discotic LCs are ideal materials for such multifunctional materials.[12–15] In columnar discotic phases, the high charge carrier mobility along the one-dimensional (1D) aromatic π–π stacked self-assembled columns in discotic LCs has been recognised as a desirable property for applications in photovoltaic cells, light-emitting diodes and field-effect transistors.[12–15] In this context, comprehensive research effort has been invested from our group recently in the design of metal-containing LCs with the aim of combining the unique properties of anisotropic fluids with the specific luminescent properties.[16–20] The molecular shape has a dominant control on the mesomorphic behaviour. A number of mononuclear salicylaldimine complexes have been documented;[21–23] however, very few examples of bi-metallomesogen are reported so far.[24–27] A binuclear zinc(II) tetradentate Schiff base showing smectic A phase was recorded.[24] Recently, we reported a new low-molecular-weight smectogenic one-ring tridentate [ONO]-donor Schiff base ligand.[28, 29] With lanthanides, the ligand occurring in zwitterionic form coordinated through phenolate-O donor site only,[28] while bi-metallic copper complexes were obtained from the tridentate binding of the same ligand.[29] The complexes exhibited smectic mesomorphism in both the cases. A non-mesogenic binuclear zinc complex with tetradentate 'salen'-type compartmental Schiff base ligand has been reported by us very recently.[30] In the present work, we intended to exploit a tridentate ligand for complexation with $Zn^{2+}(d^{10})$ to explore the possibility of generating luminescent bimetallomesogens. Interestingly, the complex showed rectangular (/oblique) columnar

*Corresponding author. Email: crbhattacharjee@rediffmail.com

mesomorphism alongside intense emissive property. Pertinent here is to mention that until now there appears to be no record of bimetallic zinc complex exhibiting columnar mesomorphism.

2. Experimental section

2.1 Physical measurements

C, H and N analyses were carried out using PE2400 elemental analyser. ^{1}H-NMR spectra were recorded on Bruker DPX-400 MHz spectrometer in $CDCl_3$ (chemical shift in δ) solution with tetramethylsilane (TMS) as internal standard. ^{13}C nuclear magnetic resonance (NMR) spectra were recorded on a JEOL AL300 FT NMR spectrometer. Ultraviolet-visible absorption spectra of the compounds in CH_2Cl_2 were recorded on a Shimadzu UV-1601PC spectrophotometer. Photoluminescence spectra were recorded on a Shimadzu RF-5301PC spectrophotometer. Fluorescence quantum yield in dichloromethane was determined by dilution method using 9,10-diphenyl anthracene as standard. Infrared spectra were recorded on a Perkin-Elmer L 120-000A spectrometer on KBr disc. Mass spectra were recorded on a Jeol SX-102 spectrometer with fast atom bombardment (FAB). Optical textures of the different phase of the compounds were studied using a polarising microscope (Nikon optiphot-2-pol) attached with Instec hot and cold stage HCS302, with STC200 temperature controller of 0.10C accuracy. Thermal behaviour of the compounds was studied using a Perkin-Elmer Pyris-1 differential scanning calorimeter (DSC) with a heating or cooling rate of 5°C/min. X-ray diffraction (XRD) studies were carried out using samples filled in Lindemann capillaries. The apparatus essentially involved a high-resolution X-ray powder diffractometer (PANalytical X'Pert PRO) equipped with a high-resolution fast detector PIXCEL. Quantum chemical calculation on Zn_2L_2 was carried out using density functional theory (DFT) as implemented in GAUSSIAN 09 package.

2.2 Materials

The materials were procured from Tokyo Kasei and Lancaster Chemicals. All solvents were purified and dried using standard procedures. Silica (60–120 mesh) obtained from Spectrochem was used for chromatographic Separation. Silica gel G (E-Merck, India) was used for TLC.

2.3 Synthesis of ligand

Synthesis of the ligand was given in our earlier report.[28]

2.4 Synthesis of zinc(II) complex

The ligand L (0.40 g, 1 mmol) was dissolved in minimum volume of dry dichloromethane. To this, an equimolar amount of zinc acetate $Zn(OAc)_2.2H_2O$ (0.22 g, 1 mmol) in methanol was then added slowly and stirred for 6 h at room temperature. A white solid formed immediately was filtered, washed with diethyl ether and recrystallised from chloroform-ethanol (1:1).

Yield: 0.45 g (75%) white-coloured solid. *Anal*. Calc. for $C_{50}H_{82}N_2O_6Zn_2$ (936.47): C, 64.02; H, 8.81; N 2.99. Found: C, 64.07; H, 8.82; N, 2.96%. ^{1}H NMR (400 MHz, $CDCl_3$): δ 0.89 (t, J = 6.4 Hz, $-CH_3$, 3H), 1.29–1.87 (m, $-CH_2$ of methylene proton in side chain), 3.70 (t, J = 4.1 Hz, $-CH_2N{=}C$, 2H), 4.01 (t, J = 8.1 Hz, $-OCH_2$, 2H), 7.13 (d, J = 8.4 Hz, $-C_6H_4$, 1H), 8.59 (s, $-N{=}CH$, ^{1}H). FAB Mass (m/e, fragment): m/z: calc. 936.47; found: 937.47[$M + H^+$]; IR (ν_{max}, cm^{-1}, KBr): 2922(ν_{as}(C–H), CH_3), 2824(ν_s(C–H), CH_3), 1612(νC=N), 1287(νC–O), 535(νM-N), 486(νM–O).

3. Results and discussion

The Schiff base ligand [L = (E)-5-(hexadecyloxy)-2-((2-hydroxyethylimino) methyl) phenol] has been synthesised following reported method.[28] The reaction of the ligand with an equimolar amount of zinc acetate in dichloromethane/methanol mixture under stirring condition leads to the formation of cream-coloured product of Zn_2L_2 in good yield (Scheme 1). Ligand-to-metal (1:1) stoichiometric ratio and purity of the compounds were confirmed by elemental analysis, IR, ^{1}H NMR and ^{13}C NMR spectroscopy. In particular, evidence for coordination of the Schiff base ligand to the Zn(II) ion was obtained from the IR spectrum by the disappearance of the OH signal and shift of the –CN stretching band to lower wave number (1612 cm^{-1}) relative to the free ligand. The absence of –OH signal in the ^{1}H NMR spectrum and the upfield shift of the iminic hydrogen signal lend further credence to the coordination of the Schiff base ligand.

The absorption spectra of Schiff base ligand and its zinc complex were recorded at room temperature (298 K) in dichloromethane solvent (the supplementary material for this article is available online at http://dx.doi.org/XXXX., Figure S1). The electronic spectrum of the ligand showed two strong bands one at ~280 nm owing to the π–π^* transition of the aromatic ring and another at ~308 nm due to the π–π^* transition of the C=N fragment. The complex showed four bands at ~289, ~292, ~297 and ~350 nm, respectively, which may arise from metal-perturbed ligand-centred transition.

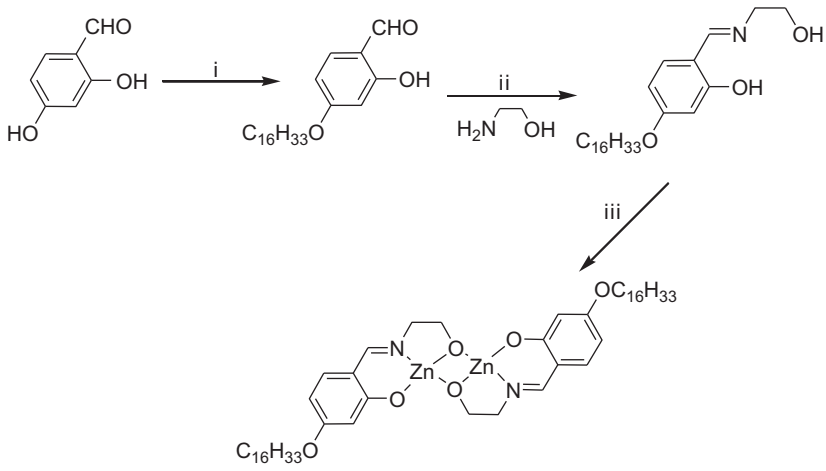

Scheme 1. (i) $C_{16}H_{33}Br$, $KHCO_3$, KI, dry acetone, Δ, 40 h, (ii) glacial AcOH, absolute EtOH, Δ, 4 h and (iii) $Zn(OAc)_2.H_2O$, MeOH, stir, 6 h.

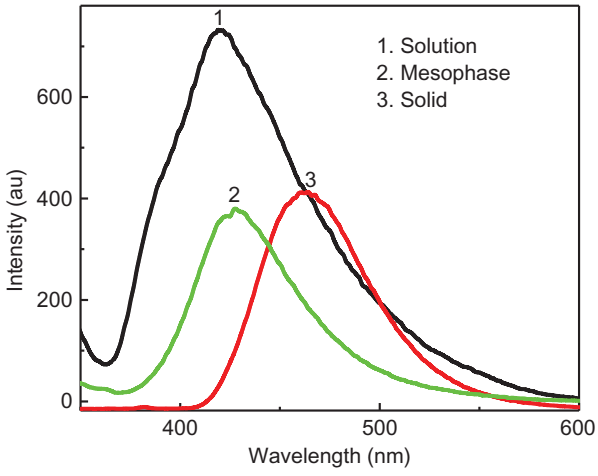

Figure 1. (colour online) Photoluminescence spectra of zinc complex.

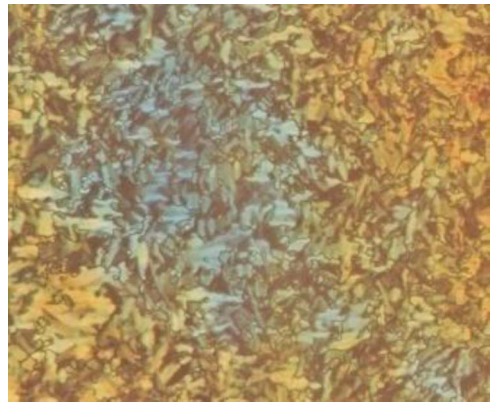

Figure 2. (colour online) POM texure of zinc complex.

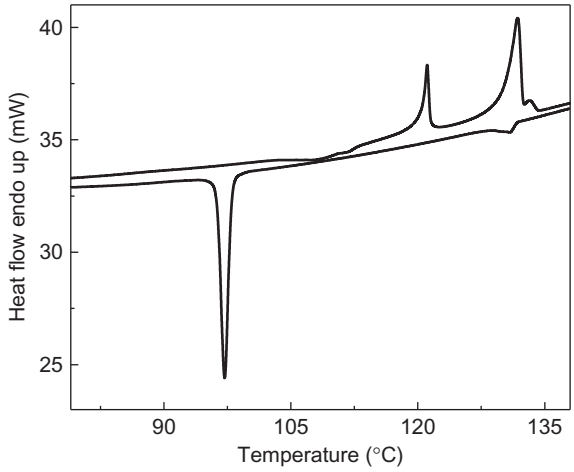

Figure 3. DSC thermogram of zinc complex.

The luminescent property of the ligand was described in our earlier report.[28] The complex is found to be emissive in solution, solid and mesomorphic states. The luminescence spectra (Figure 1) in the solid state were recorded by placing the compound in between two quartz plates. The emission maxima is red shifted from solution state (420 nm, $\Phi = 15\%$) to mesomorphic state (432 nm, $\Phi = 7\%$) and to the solid state (464 nm, $\Phi = 11\%$). The presence of stronger aggregation tendency in solid or mesomorphic state gives rise to a larger electronic delocalisation, resulting in an energy lowering of the electronic states.

The ligand showed a monotropic SmA phase. The detail mesomorphic behaviour of the ligand was reported in our earlier paper.[28] Quite interestingly, the complex showed enantiotropic columnar phase. During slow cooling of the zinc complex from clearing point, a spherulitic growth appeared from dark background of isotropic melt, which coalesce to a fan-like texture (Figure 2) at ~130.8°C revealing a typical columnar mesophase. DSC thermogram (Figure 3) for

Table 1. Thermal data of the Zn_2L_2 complex.

Compounds	T (°C)[a]	Transition[b]	ΔH (kJ mol^{-1})
Zn complex	121	Cr–Cr1 (heating)	13.3
	131.8	Cr1–Colr/o (heating)	34.2
	133.3	Colr/o–I (heating)	1.4
	131.7	I-Colr/o (cooling)	1.7
	97	Colr/o–Cr (cooling)	90.9

Notes: [a]Temperature at onset of peak. [b]Cr, crystal; Col_r/Col_o, columnar rectangular or oblique phase.

zinc complex exhibits three endothermic peaks and two exothermic peaks. A crystal to crystal transition was observed in DSC; thermal microscopy did not show any such type of transition. A very low enthalpy value (Table 1) for columnar to isotropisation and vice versa were noted for the complex. Analogous copper complex reported by us showed an enantiotropic SmA phase.[29] We do not have clear explanation for the formation of different mesophases upon changing the metal ion at this stage.

To get information on the structural aspects, XRD measurements were carried out in the mesophase. XRD pattern (Figure 4) shows intensity versus 2θ profile at $T = 125^{\circ}$C. The broad and diffuse peak in the high-angle region (inset in the figure) corresponding to a spacing of 4.44 Å reflects the liquid like ordering of the molecules within the columns. In the low-angle region, seven sharp peaks were seen. These peaks are indexed to a columnar phase with two-dimensional rectangular lattice, with lattice spacing being $a = 43.2$ Å and $b = 34.9$ Å. The data could as well be indexed to an oblique columnar phase (Col_{ob}) with a slightly better statistical error; in this case, the lattice parameters remain identical to that for the rectangular lattice with tilt of columns $\theta = 2.5°$

Table 2. XRD data of the Zn_2L_2 complex.

	Indexed to a rectangular lattice (Col_r)		Indexed to a oblique lattice (Col_{ob})	
d_{meas}	d_{calc}	(hk)	d_{calc}	(hk)
43.3	43.2	(10)	43.2	(10)
34.9	34.9	(01)	34.9	(01)
21.4	21.6	(20)	21.6	(20)
17.2	17.4	(02)	17.4	(02)
14.2	14.4	(30)	14.4	(30)
10.8	10.8	(40)	10.8	(40)
8.2	8.1	(24)	8.2	(24)
4.4				
Cumulative error	0.161		Cumulative error	0.145
	$a = 43.2$			$a = 43.2$
	$b = 34.9$			$b = 34.9$
				Tilt angle $\theta = 2.5$

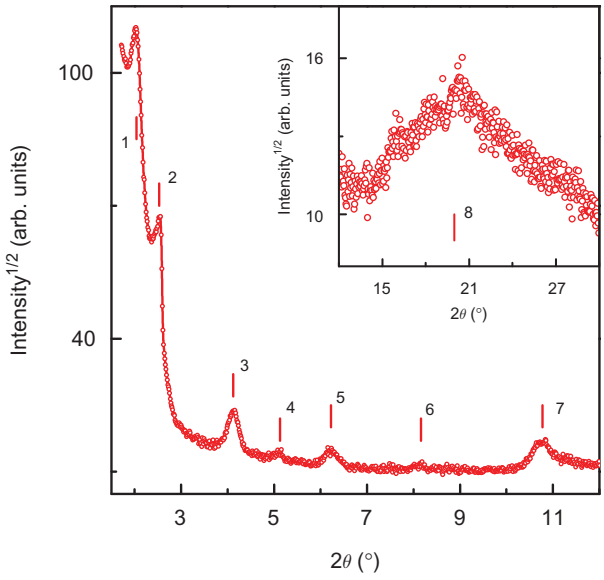

Figure 4. (colour online) X-ray diffraction pattern of Zn_2L_2 complex at 125° C.

(Table 2). Moreover, the radius of the non-discoid molecule (~27 Å) smaller than both the lattice constants ($a = 43.2$ Å and $b = 34.9$ Å). Therefore, a criss-cross arrangement of the molecules in perpendicular fashion, one on top of other (Figure 5), is contemplated to form the discoid shell.[4]

We have performed DFT calculations to determine the electronic structure of binuclear zinc complex. Time-dependent DFT (TD-DFT) calculations are carried out to study the electronic transitions observed in the experimental ultraviolet-visible spectroscopy (UV–Vis) spectra.[31]

DFT has become a very important tool as it allows considerable insight into the electronic structures of transition metal complexes. The GAUSSIAN 09 program package [32] was employed to carry out DFT

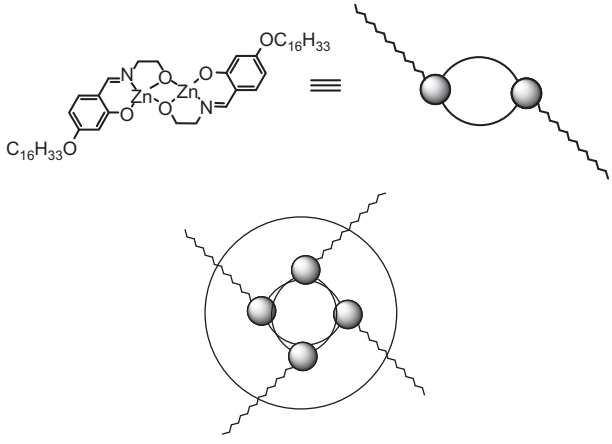

Figure 5. Molecular organisation in discoid shell.

calculations at the Becke's three-parameter functional and Lee–Yang–Parr functional (B3LYP) levels [33,34] of calculation. The 6-311G++ (d, p) basis set [35] for all atoms except for the zinc atoms, which has been described by the effective core potential of Wadt and Hay (Los Alamos ECP) included in the LanL2DZ basis set [36] was used for ground state geometry optimisation and frequency calculations. The gas-phase ground-state geometries of the binuclear zinc complex has been fully optimised using the restricted B3LYP methods without imposing any symmetry constrain with tight convergence criteria. Appropriate structure of the complex was confirmed as energy minima by calculating the vibrational frequency and confirming the absence of any imaginary frequencies. Based on the optimised geometry of the binuclear zinc complex, TD-DFT calculations were performed at the B3LYP level to study the spectroscopic and electronic properties of the title complex as an isolated molecule. As the spectroscopic experiment is performed in the dichloromethane as solvent, the solvent effects have been taken into account in the theoretical calculations. A solvation method of the polarisable continuum model (PCM) [37] using the integral equation formalism (IEF) variant [38] were considered in calculations. GAUSSSUM [39] program was used to calculate the fractional contributions of various groups to each molecular orbital.

Some of the important geometric parameters of the optimised binuclear zinc complex, evaluated by DFT calculation at B3LYP level, are reported in Table 3. From DFT data, it is noticed that the complex has an average Zn–O and Zn–N bond lengths in the range of 1.954–2.083 and 2.074–2.025 Å, respectively. The distance between the bridging oxygen atoms and zinc atoms are found slightly larger than the normal Zn–O bond lengths. The O1–Zn1–O3 and N1–Zn1–O2 bond angles are 147.8° and 136.6°, respectively,

Table 3. Selected bond lengths (Å) and angles (°) for the binuclear zinc complex evaluated at B3LYP level.

Structural parameter	Complex	Structural parameter	Complex
Zn1–O1	2.080	Zn2–O1	1.975
Zn1–O2	1.975	Zn2–O2	2.083
Zn1–O3	1.954	Zn2–O4	1.954
Zn1–N1	2.074	Zn2–N2	2.075
O1–Zn1–O3	147.8	O2–Zn2–O4	148.3
N1–Zn1–O2	136.6	N2–Zn2–O1	136.2
N1–Zn1–O1	80.6	N2–Zn2–O2	80.5
O2–Zn1–O3	121.1	O1–Zn2–O4	121.1
N1–Zn1–O3	92.3	N2–Zn2–O4	92.3
O1–Zn1–O2	82.6	O1–Zn2–O2	83.2
N1–O3–O2–O1	−39.3	N2–O4–O1–O2	39.2

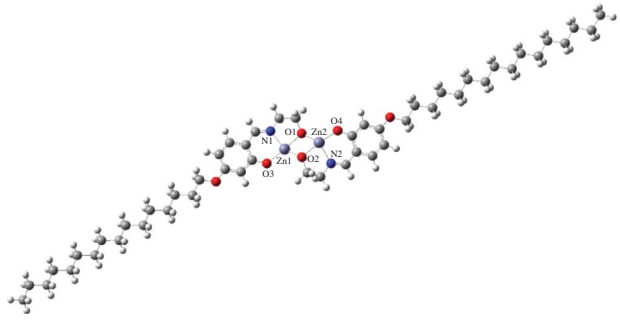

Figure 6. (colour online) Optimised structure of binuclear zinc complex.

while O2–Zn2–O4 and N2–Zn2–O1 bond angles are found to be 148.3° and 136.2°, respectively. The bond angels 80.6°, 121.1°, 92.3° and 82.6° are for N1–Zn1–O1, O3–Zn1–O3, N1–Zn1–O3 and O1–Zn1–O2, whereas the bond angles 80.5°, 121.1°, 92.3° and 83.2° are evaluated to be for N2–Zn2–O2, O1–Zn2–O4, N2–Zn2–O4 and O1–Zn2–O2, respectively, around the zinc atoms indicating distorted square planar geometry (Figure 6). The dihedral angles N1–O3–O2–O1 and N2–O4–O1–O2 as computed from DFT are found to be –39.3° and 39.2°, respectively (Table 3), reflecting a deviation from planarity.

Figures 7 and 8 demonstrate the energy and atomic orbital composition of the highest occupied molecular orbitals (HOMOs) and the lowest unoccupied molecular orbitals (LUMOs) for the zinc complex. It is noticed from Figure 7 that HOMO of the zinc complex is composed of a mixture of 2% Zn dπ orbital and 98% pπ orbitals of the ligand. The calculated LUMO and HOMO energies are –1.33 and –5.66 eV, respectively. The energy difference (δE) of the complex has been found to be 4.33 eV matches quite well with experimental value (~4.02 eV). High LUMO–HOMO energy gap implies the stability of the complex. HOMO–1, HOMO–2, HOMO–3 and HOMO–4 orbitals in the complex have a sizeable contribution from ligand pπ orbital, while HOMO–1 and HOMO–4 have also very little contribution from metal-bonding (dπ) orbitals. The electron densities LUMO, LUMO+1 and LUMO+3 orbitals in the title complex are localised across the ligand pπ^* orbitals as well as zinc p orbitals. In contrast, LUMO+2 and LUMO+4 is mainly located on the metal and the ligand pπ^* orbital. TD-DFT data suggested that the HOMO of the complexes comprises mainly ligand pi orbitals (98–100%). To explain the assignment of bands in the UV region, TD-DFT calculations have been carried out for ligand and its binuclear zinc complex. The calculated absorption bands in their ground state, their oscillator strength (f), energies and the

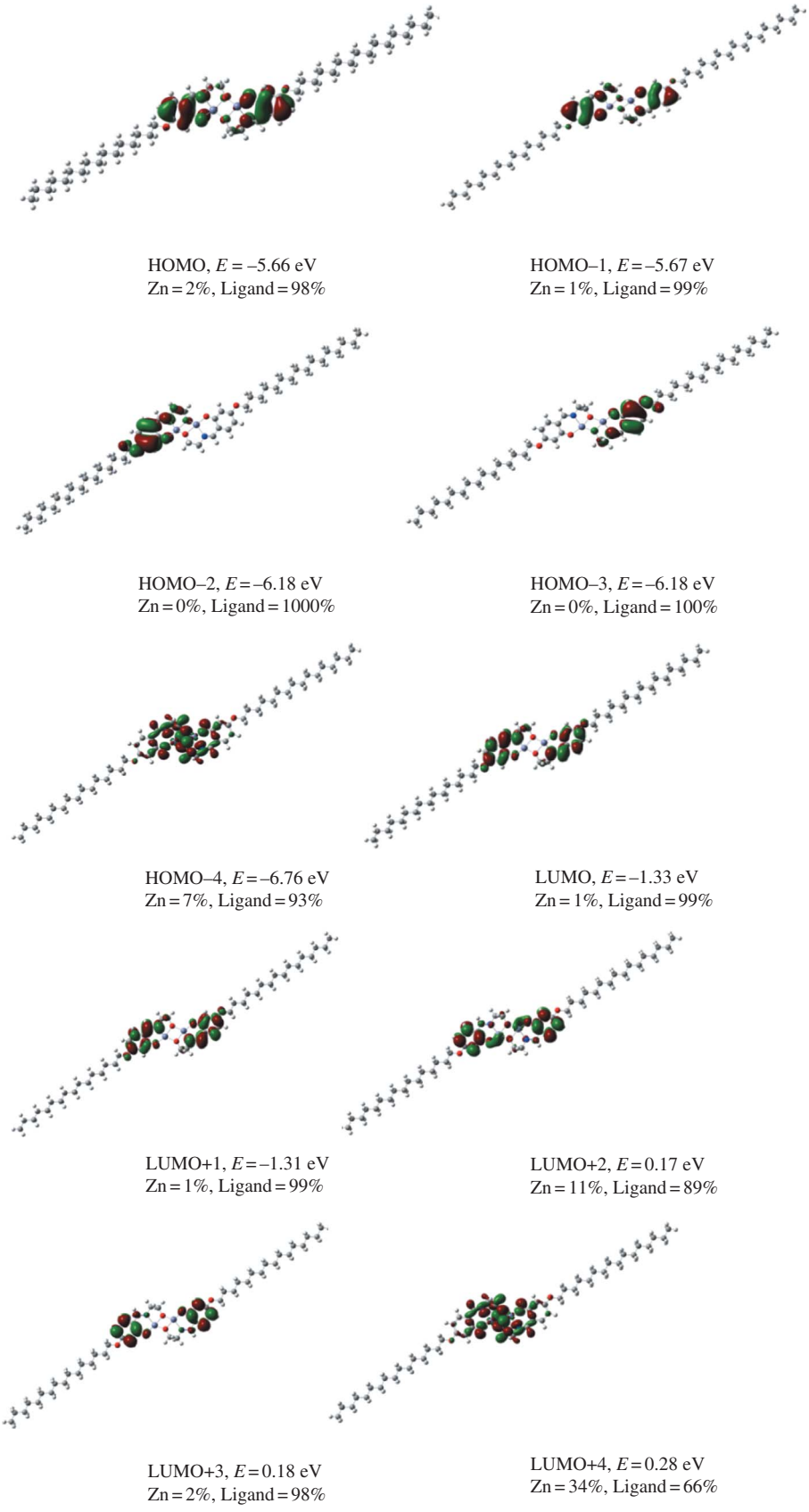

Figure 7. Contour plots of some selected molecular orbitals.

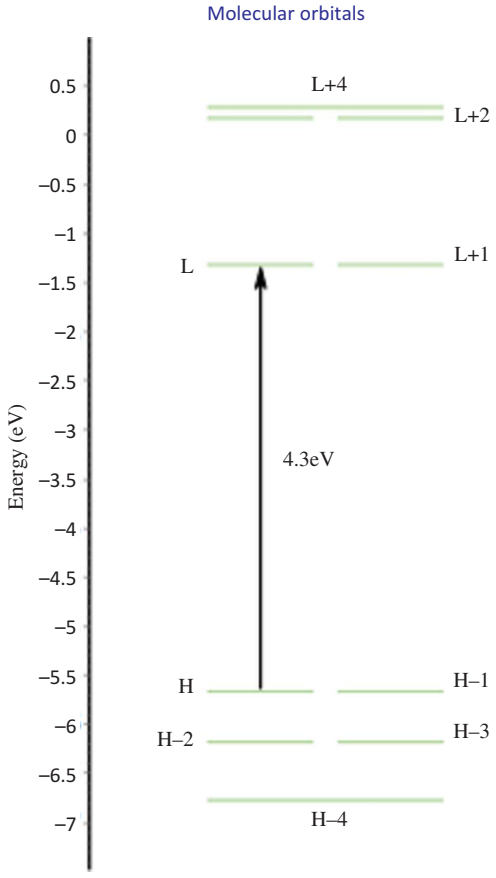

Figure 8. (colour online) Energy level diagram of MO.

band assignments are presented in Tables 4 and 5. The surface of each peak in the spectra is proportional to oscillator strength (f), which also reveals the probability of electronic transition. The electronic excitations with the highest oscillator strengths, the orbitals involved in these transitions with the percentage of contribution to each transition are presented in Tables 4 and 5.

The ligand shows two absorption band of electronic transitions at 294 and 269 nm. The band at 294 nm corresponds to HOMO→LUMO electronic transition owing to the L(π)→L(π^*), where HOMO corresponds to π bonding orbitals of C=N bond of the ligand while LUMO corresponds to π^* (anti-bonding) orbitals of the C=N (intra-ligand charge transfer). This transition is consistent with the experimental value of 308 nm. Another absorption band at 269 nm corresponds to HOMO→LMO+1 electronic transition due to the L(π) →L(π^*) transition of aromatic rings in the ligand.

The lower energy absorption band of zinc complex occurs at 329 nm, which could be assigned to either HOMO→LUMO+1 or HOMO–1→LUMO electronic transition predominantly due to an intra-ligand ($\pi\rightarrow\pi^*$) charge transfer. This transition resembles the experimental value of 350 nm, ε = 16,320 lmol^{-1} cm^{-1}. The absorption at 283 nm region is from HOMO–2→LUMO transition is of intra-ligand ($\pi\rightarrow\pi^*$) charge transfer type which is comparable with the experimental transition at 297 nm. The sharp peak at 277 nm (experimental value 293 nm) is caused by electron transfer from HOMO–4→LUMO+1 transition which is mainly due to M(dxy→L(π^*)/L($\pi\rightarrow\pi^*$). The relatively high energy absorption band occurring at 271 nm is assigned to HOMO–3 to LUMO+1 electronic transition comparable to the experimental result of 289 nm.

The results indicate that the UV-absorption spectra of the ligand and the bimetallic zinc complex calculated by the TD-DFT method are in good agreement with the experimental data. TD-DFT data indicate that the absorption maxima are at low energy in both ligand and complex which comprised mainly of ligand-based $\pi\rightarrow\pi^*$ transition with marginal contribution of metal-to-ligand charge transfer transition.

4. Conclusion

A novel bimetallic zinc complex has been prepared. Quite interestingly the complex is found to be mesogenic as well as luminescent. The complex exhibits blue emission in solution, in solid and in mesomorphic state. A rectangular (/oblique) columnar mesomorphism induced in the complex is evident from the POM, DSC and powder X-ray diffraction (PXRD) measurements. The complex reported here is believed to be the first example of edge-shared bimetallic zinc complex that showed columnar mesophase. A criss-cross arrangement of one molecule on top of the other with the flexible alkoxy arms spread out at 90° apart relative to each other has been proposed to explain

Table 4. The experimental absorption bands and the electronic transitions calculated with TD-DFT/B3LYP method for the ligand.

Key transition	Character	λ (nm)	E (eV)	f Osc. strength	Assignment	λ_{exp} (nm) ε (lmol^{-1} cm^{-1})
(72%) HOMO→LUMO	L(π) →L(π^*)	294	4.213	0.261	IL (C=N)	308/10794
(72%) HOMO→LUMO+1	L(π) →L(π^*)	269	5.392	0.124	IL (aromatic ring)	280/14137

Table 5. The experimental absorption bands and the electronic transitions calculated with TD-DFT/B3LYP method for binuclear zinc complex.

Key transition	Character	λ (nm)	*E* (eV)	*f* Osc. strength	Assignment	λ_{exp} (nm) ε ($lmol^{-1}$ cm^{-1})
(48%) HOMO–1→LUMO/ (44%) HOMO →LUMO+1	L(π)→L(π*)/ L(π)→L(π*)	329	3.768	0.320	IL	350 (16,320)
(28%) HOMO–2→LUMO/ (16%) HOMO–2→LUMO+1 / (15%) HOMO–3→LUMO+1	L(π)→L(π*)/ L(π)→L(π*)/ L(π)→L(π*)	283	4.381	0.816	IL	297 (32,739)
(26%) HOMO–4→LUMO+1/ (12%) HOMO–2→LUMO	$M(d_{xy})$→L(π*)/ L(π)→L(π*) L(π)→L(π*)	277	4.469	0.433	MLCT/IL	293 (33,604)
(50%) HOMO–3→LUMO+1/ (35%) HOMO–3→LUMO	L(π)→L(π*)/ L(π)→L(π*)	271	4.556	0.018	IL	289 (32,936)

their discotic character. A distorted square planar geometry is conjectured on the basis of DFT study. TD-DFT-computed electronic transition data matche well with the experimental results. The synthetic strategy may serve as paradigm to access multifunctional bimetallic complexes utilising tridentate donors.

Acknowledgements

The authors thank Sophisticated Analytical Instrument Facility (SAIF), North-Eastern Hill University (NEHU), Shillong for providing analytical and spectral data. The author Paritosh Mondal thanks the Department of Science and Technology, New Delhi for financial support (SR/FT/CS-86/2010) and CD and DD acknowledges financial support from University Grants Commission. The authors are also thankful to the Department of Biotechnology – e Library Consortium (DeLCON) of Bioinformatics Centre, Assam University, Silchar (India).

References

[1] Bushby RJ, Lozman OR. Discotic liquid crystals 25 years on. Curr Opin Coll Interf Sci. 2002;7:343–354.
[2] Neill OM, Kelly SM. Liquid crystals for charge transport, luminescence, and photonics. Adv Mater. 2003;15:1135–1146.
[3] Hanna J. Towards a new horizon of optoelectronic devices with liquid crystals. Opto Electron Rev. 2005;13:259–267.
[4] Ghedini M, Pucci D, Crispini A, Bellusci A, Deda ML, Aiello I, Pugliese T. A red emitting discotic liquid crystal containing the cyclopalladated nile red chromophore. Inorg Chem Commun. 2007;10:243–247.
[5] Cavero E, Uriel S, Romero P, Serrano JL, Giménez R. Tetrahedral zinc complexes with liquid crystalline and luminescent properties: interplay between nonconventional molecular shapes and supramolecular mesomorphic order. J Am Chem Soc. 2007;129:11608–11618.
[6] Dambal HK, Yelamaggad CV. Technologically promising, room temperature luminescent columnar liquid crystals derived from s-triazine core: molecular design, synthesis and characterization. Tet Lett. 2012;53:186–190.
[7] Cozzi PG, Dolci LS, Garelli A, Montalti M, Pordi L, Zaccheroni N. Photophysical poperties of Schiff-base metal complexes. New J Chem. 2003;27:692–697.
[8] Splan KE, Massari AM, Morris GA, Sun SS, Reina E, Nguyen SBT, Hupp JT. Photophysical and energy-transfer properties of (Salen) zinc complexes and supramolecular assemblies. Eur J Inorg Chem. 2003;2348–2351.
[9] Pucci D, Aiello I, Bellusci A, Crispini A, Ghedini M, Deda ML. Coordination induction of nonlinear molecular shape in mesomorphic and luminescent Zn^{II} complexes based on salen-like frameworks. Eur J Inorg Chem. 2009;4274–4281.
[10] Xing L, Zha MQ, Lu Y, Bing Y, Zhu CF, Synthesis YC. Characterization of zinc(II) complex with (1R, 2R)-(-)-diaminocyclohexane-N,N′-bis(3-tert-butyl-5-(4′-methylbenzoate)-salicylidene). Synth React Inorg Met Org Nano Met Chem. 2010;40:451454.
[11] Liuzzo V, Oberhauser W, Pucci A. Synthesis of new red photoluminescent Zn(II)-salicylaldiminato complex. Inorg Chem Commun. 2010;13:686–688.
[12] Kumar S. Self-organization of disc-like molecules: chemical aspects. Chem Soc Rev. 2006;35:83–109.
[13] Goodby JW, Gortz V, Cowling SJ, Mackenzie G, Martin P, Plusquellec D, Benvegnu T, Boullanger P, Lafont D, Queneau Y, Chambert S, Fitremann J. Thermotropic liquid crystalline glycolipids. J Chem Soc Rev. 2007;36:1971–2032.
[14] Sergeyev S, Pisula W, Geerts YH. Discotic liquid crystals: a new generation of organic semiconductors. Chem Soc Rev. 2007;36:1902–1929.
[15] Laschat S, Baro A, Steinke N, Giesselmann F, Hagele C, Scalia G, Judele R, Kapatsina E, Sauer S, Schreivogel A, Tosoni M. Discotic liquid crystals: from tailor-made synthesis to plastic electronics. Angew Chem Int Ed. 2007;46:4832–4887.
[16] Bhattacharjee CR, Das G, Mondal P, Rao NVS. Novel photoluminescent hemi-disc-like liquid crystalline Zn(II) complexes of $[N_2O_2]$ donor 4-alkoxy substituted salicyldimine Schiff base with aromatic spacer. Polyhedron. 2010;29:3089–3096.
[17] Bhattacharjee CR, Das G, Mondal P, Prasad SK, Rao DSS. Novel green light emitting nondiscoid liquid crystalline zinc(II) Schiff-base complexes. Eur J Inorg Chem. 2011;1418–1424.
[18] Bhattacharjee CR, Das G, Mondal MP. Photoluminescent hemi disc-shaped liquid crystalline

nickel(II) Schiff-base complexes. Eur J Inorg Chem. 2011;5390–5399.
[19] Bhattacharjee CR, Datta C, Das G, Chakrabarty R, Mondal P. Induction of photoluminescence and columnar mesomorphism in hemi-disc salphen type Schiff bases via nickel(II) coordination. Polyhedron. 2012;33:417–424.
[20] Bhattacharjee CR, Chakrabarty S, Das G, Mondal P. Emissive 'zinc(II)-salphen' core: building block for columnar liquid crystals. Liq Cryst. 2012;39: 1435–1442.
[21] G-Godquin AM, Maitlis PM, Metallomesogens: metal complexes in organized fluid phases. Angew Chem Int Ed. 1991;30:375–402.
[22] Espinet PM, Esteruelas A, Oro LA, Serrano JL, Sola E. Transition metal liquid crystals: advanced materials within the reach of the coordination chemist. Coord Chem Rev. 1992;117:215–274.
[23] Hoshino N. Liquid crystal properties of metal–salicylaldimine complexes: chemical modifications towards lower symmetry. Coord Chem Rev. 1998; 174:77–108.
[24] Lai CK, Leu YF. Smectic bimetallomesogens: synthesis, characterization and mesomorphic properties and the crystal structure of bis[N-(3-hydroxypropyl)-4-ctanoylsalicylaldiminato]copper(II) complex. Liq Cryst. 1998;25:689–698.
[25] Barbera J, Gimenez R, Marcos M, Serrano JL, Alonso PJ, Martinez JI. Paramagnetic bimetallomesogens. Chem Mater. 2003;15:958–964.
[26] Ames KA, Collinson SR, Blake AJ, Wilson C, Love JB, Bruce DW, Donnio B, Guillon D, Schroder M. Design of neutral metallomesogens from 5,5-dimethyldipyrromethane: metal ion mediated control of folding and hairpin structures. Eur J Inorg Chem. 2008;5056–5066.
[27] Chae HW, Kadkin ON, Choi MG. New heteropolynuclear metallomesogens: copper(II), palladium(II), nickel(II) and oxovanadium(IV) chelates with [3]ferrocenophane βcontaining Schiff's base and βaminovinylketone. Liq Cryst. 2009;36:53–60.
[28] Bhattacharjee CR, Das G, Goswami P, Mondal P, Prasad SK, Rao DSS. Novel photoluminescent lanthanidomesogens forming bilayer smectic phase derived from blue light emitting liquid crystalline, one ring O-donor Schiff-base ligands. Polyhedron. 2011;30:1040–1047.
[29] Bhattacharjee CR, Datta C, Das G, Mondal P. Liquid crystalline dinuclear copper(II) complexes accessed from photoluminescent tridentate [ONO]-donor Schiff base ligands. Liq Cryst. 2012;39:639–646.
[30] Bhattacharjee CR, Datta C, Das G, Mondal P. Novel photoluminescent mesogenic Schiff-base ligands bearing $[N_4O_4]$ donors and their bimetallic Zn(II) complexes. Mater Sci Eng C. 2012;32:735–741.
[31] Holland JP, Green JC. Evaluation of exchange-correlation functionals for time-dependent density functional theory calculations on metal complexes. J Comput Chem. 2010;31:1008–1014.
[32] Frisch MJ, Trucks GW, Schlegel HB, Scuseria GE, Robb MA, Cheeseman JR, Montgomery Jr. JA, Vreven T, Kudin KN, Burant JC, Millam JM, Iyengar SS, Tomasi J, Barone V, Mennucci B, Cossi M, Scalmani G, Rega N, Petersson GA, Nakatsuji H, Hada M, Ehara M, Toyota K, Fukuda R, Hasegawa J, Ishida M, Nakajima T, Honda Y, Kitao O, Nakai H, Klene M, Li X, Knox JE, Hratchian HP, Cross JB, Bakken V, Adamo C, Jaramillo J, Gomperts R, Stratmann RE, Yazyev O, Austin AJ, Cammi R, Pomelli C, Ochterski J, Ayala PY, Morokuma K, Voth GA, Salvador P, Dannenberg JJ, Zakrzewski VG, Dapprich SA, Daniels D, Strain MC, Farkas O, Malick DK, Rabuck AD, Raghavachari K, Foresman JB, Ortiz JV, Cui Q, Baboul AG, Clifford S, Cioslowski J, Stefanov BB, Liu G, Liashenko A, Piskorz P, Komaromi I, Martin RL, Fox DJ, Keith T, Al-Laham MA, Peng CY, Nanayakkara A, Challacombe M, Gill PMW, Johnson BG, Chen W, Wong MW, Gonzalez C, Pople JA. GAUSSIAN 03 (Revision C.02). Wallingford, CT: Gaussian, Inc; 2004.
[33] Ditchfield R, Hehre WJ, Pople JA. Self-consistent molecular-orbital methods: IX. An extended Gaussian-type basis for molecular-orbital studies of organic molecules. J Chem Phys. 1971;54:724–728.
[34] Lee C, Yang W, Parr RG. Development of the Colle-Salvetti correlation energy formula into a functional of the electron density. Phys Rev B. 1988;37: 785–789.
[35] Hariharan PC, Pople JA. Influence of polarization functions on MO hydrogenation energies. Theor Chim Acta. 1973;28:213–222.
[36] Hay PJ, Wadt WR. *Ab initio* effective core potentials for molecular calculations. Potentials for the transition metal atoms Sc to Hg. J Chem Phys. 1985;82: 270–283.
[37] Cance E, Mennucci B, Tomasi J. A new integral equation formalism for the polarizable continuum model: theoretical background and applications to isotropic and anisotropic dielectrics. J Chem Phys. 1997;107:3032–3041.
[38] Miertus S, Scrocco E, Tomasi J. Electrostatic interaction of a solute with a continuum. A direct utilization of *ab initio* molecular potentials for the prevision of solvent effects. J Chem Phys. 1981;55:117–129.
[39] O'Boyle NM, Tenderholt AL, Langner KM. cclib: a library for package-independent computational chemistry algorithms. J Comput Chem. 2008;29:839–845.

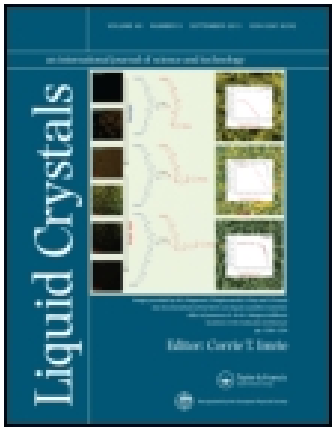

Liquid Crystals
Publication details, including instructions for authors and subscription information:
http://www.tandfonline.com/loi/tlct20

Influence of spacer group substituent on mesomorphism in copper complexes of 'salen' type Schiff bases bearing long alkoxy arm

Chitraniva Datta[a], Rupam Chakrabarty[a], Gobinda Das[a], Chira R. Bhattacharjee[a] & Paritosh Mondal[a]

[a] Department of Chemistry, Assam University, Silchar 788011, Assam, India

Published online: 09 Dec 2013.

Liquid Crystals, 2014
Vol. 41, No. 4, 541–551, http://dx.doi.org/10.1080/02678292.2013.862311

Influence of spacer group substituent on mesomorphism in copper complexes of 'salen' type Schiff bases bearing long alkoxy arm

Chitraniva Datta, Rupam Chakrabarty, Gobinda Das, Chira R. Bhattacharjee* and Paritosh Mondal

Department of Chemistry, Assam University, Silchar 788011, Assam, India

(*Received 21 November 2012; accepted 31 October 2013*)

Novel four-coordinate copper(II) complexes of the type [CuL], *L* = N, N′-di-(4-hexadecyloxysalicylidene)-4-substituted(X)l,2-diamino-benzene (*X* = H, CH_3, NO_2) were synthesised. The compounds were characterised by elemental analyses, Fourier transform infrared spectroscopy, ^1H, ^{13}C nuclear magnetic resonance, ultraviolet–visible spectroscopy and fast atom bombardment mass spectrometry. The liquid crystalline properties were ascertained using polarised optical microscopy, differential scanning calorimetry and powder X-ray diffraction technique. The ligands are non-mesomorphic, but the complexes with methyl (CH_3) or no substituent on the aromatic spacer showed rectangular columnar (Col_r) mesophase and rectangular plastic columnar (Col_{rp}) phase, respectively. An antiparallel dimeric association of half-disc shaped molecule forming a disc-like arrangement in the mesophase is proposed on the basis of X-ray diffraction study. The complex with nitro (NO_2) substituent in the spacer linkage decomposes before melting precluding any mesomorphic study. The density functional theory calculations carried out using Gaussian 09 program at B3LYP level revealed distorted square planar geometry around the metal centre. The natural charges and electronic configuration of the atoms of the complexes and free ligand were evaluated by natural bond orbital analysis.

Keywords: salen; copper; mesomorphism; DFT

1. Introduction

'Salen' type fragment as core unit in metal containing liquid crystals have drawn significant attention owing to the possibility of combining optical, electronic and magnetic characteristics with those of anisotropic fluidity.[1–6] Metal complexes of salicylidene-type Schiff base ligands are of immense interests owing to their facile synthesis, chemical stability, interesting broad range catalytic activity, and photophysical properties.[1–7] Complexes of paramagnetic metal ion, in particular, are quite significant in the context of novel ferroelectric/piezoelectric and non-linear optical (NLO) materials as they can be switched by weak external magnetic fields.[8–17] The liquid crystalline behaviour can be modulated by suitably chosen metal ions, long flexible alkoxy arms as well as spacers grafted on rigid aromatic core.[3–5] Coordination to metal ions can even induce mesomorphism from non-mesomorphic ligands.[5] Even minor alteration in the spacer linkage can lead to substantial changes in self-assembly pattern of molecules and in turn mesomorphic behaviour. A half-discoid ligand with a short range intermolecular correlation between peripheral aliphatic chains appended to an aromatic core upon coordination to metal ions often lead to discotic metallomesogens.[3–6, 18] The overlapping π-orbitals in a columnar stack of disc-like liquid crystals results in potential components for one-dimensional semiconductors, organic light emitting diodes, photovoltaic cells and field effect transistors.[19–29] A series of one-dimensional rod-like metallomesogenic salicylidene complexes based on 5-substituted long alkyl or alkoxy arms on aromatic rings exhibiting smectic mesomorphism are on record.[30–34] In contrast, there are only handful of documented examples involving 4-substituted 'salen' type metallomesogens.[3–6,35,36] Recently, a variety of structurally analogous 4-substituted zinc(II), oxovanadium(IV), nickel(II) using phenylene/cyclohexane diamine spacer exhibiting different types of columnar phases have been reported by us.[37–44] Quite surprisingly, liquid crystalline copper(II)-salen complexes bearing aromatic spacer, affording columnar mesophases have not yet been reported. Pertinent here is to mention that copper (II) complexes with cyclohexane diamine spacer have been reported to show rectangular columnar mesophase.[39] Set in this backdrop we embarked on the synthesis of copper(II) complexes of 'salen' type Schiff base ligand with different substituent on aromatic spacer group and explore their mesomorphic behaviour and collate with related reported [37–44] ligand systems with different divalent metal ions.

*Corresponding author. Email: crbhattacharjee@rediffmail.com

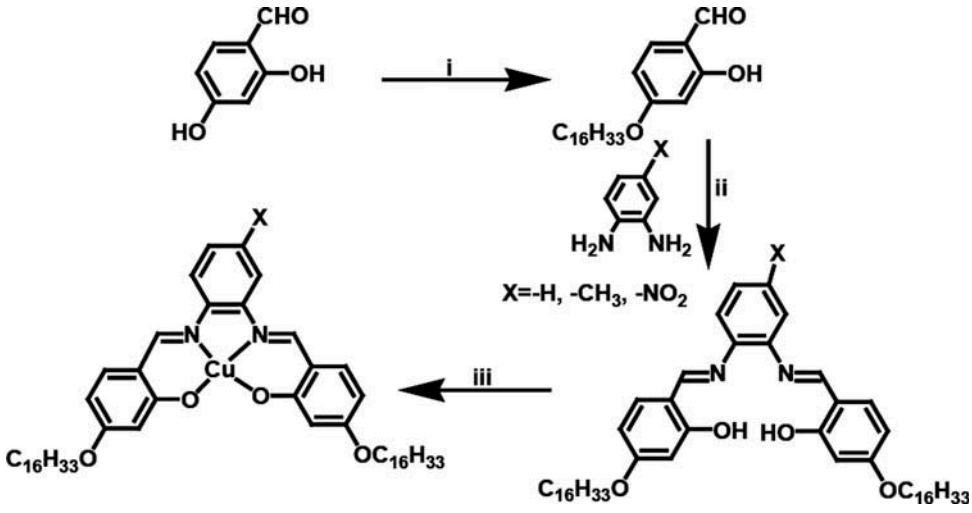

Scheme 1.

2. Results and discussion

The ligands [(L = N, N′-bis (4-(4′-n-hexadecyloxy)-salicylidene)1, 2-phenylenediamine/4-Me-1, 2-phenylenediamine/4-NO_2-1, 2-phenylenediamine), abbreviated as 16-opd/16-mpd/16-npd] could be accessed through a facile and straightforward procedure as reported in our earlier paper.[42] The complexes (Cu-16opd/Cu-16mpd/Cu-16npd), were prepared by the reaction of appropriate ligand with copper acetate (1:1 molar ratio) in methanol (Scheme 1). Isolated as brown coloured solids in good yields, the complexes were recrystallised from methanol/dicholoromethane. The compounds were characterised by elemental analyses, ^{1}H and ^{13}C nuclear magnetic resonance (NMR) (ligands only), Fourier transform infrared spectroscopy and ultraviolet–visible (UV–Vis) spectroscopy. From the infrared spectra, it was observed that the position of $\nu_{C=N}$ band of the free ligands appeared at 1610–1621 cm^{-1}, which shifted to lower frequencies at 1603–1606 cm^{-1}, respectively, upon complexation indicating azomethine nitrogen coordination with the metal. Moreover, absence of ν_{OH} mode of the ligands in the spectra of copper complexes further attests the coordination of phenolate oxygen atom to the metal ion. The fast atom bombardment (FAB)-mass spectra of the compounds matched well with their formula weights. Solution electrical conductivity of complexes recorded in dichloromethane (10^{-3}M) was found to be <10 Ω^{-1} cm^{-1} mol^{-1}, much lower than is expected for a 1:1 electrolyte, thus confirming the non-electrolytic nature of the complexes. The ^{1}H NMR spectra of ligands is described in our earlier reports.[42] The electronic spectra of compounds were recorded in dichloromethane solution (Table 1). The absorption spectra of Schiff base ligands are described in our earlier report.[42] In copper complexes the absorption bands appearing at ~265, ~319, ~350 and ~398 nm are attributed to the intraligand π→π* electronic transitions (Figure 1). In comparison to the free ligands, the absorption maxima undergoes a red shift in the complexes may be due to the metal-perturbed ligand-centred transition. In addition, a weak band appeared as shoulder at ~419–474 nm in the complexes, which may have arisen due to Jahn–Teller distortion in copper (d^9) system.[45] The spectrum for nitro-substituted

Table 1. UV-visible spectral data of ligands and copper complexes.

	λ_{max} (nm)	
Compound	π→π* (ε, l mol^{-1} cm^{-1})	LMCT (ε, l mol^{-1} cm^{-1})
16-opd	292 (22000) 329 (26800) 363 (18981)	–
Cu-16opd	265 (69944) 320 (76966) 345 (61235) 393 (94831)	422 (67865)
16-mpd	289 (19300) 330 (23100) 365 (18110)	–
Cu-16mpd	264 (54213) 320 (60842) 344 (50730) 392 (68202)	420 (55955)
16-npd	295 (13400) 335 (16851) 367 (21850)	–
Cu-16npd	264 (34269) 331 (43033) 358 (40561) 412 (46179)	474 (24101)

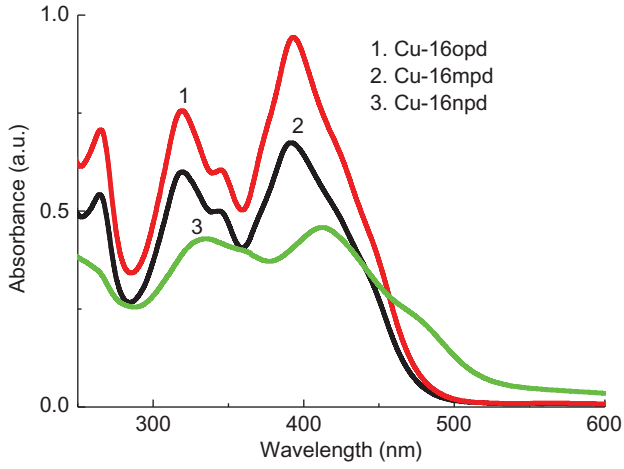

Figure 1. (colour online) Absorption spectra of complexes (dichloromethane; 10^{-5}M).

ligand and its copper complex slightly differs from the rest, which may be due to the strong electron withdrawing effect of the chromophoric nitro group in the aromatic spacer. The presence of nitro group in Cu-16npd complex increases the degree of conjugation reducing the energy gap thus shifting the absorption maxima to lower energy.[46]

The liquid crystalline properties of the complexes were investigated by polarised optical microscopy (POM), differential scanning calorimetry (DSC) and X-ray diffraction (XRD) technique. The thermal data are summarised in Table 2. The ligands are found to be non-mesomorphic. However, the complexes Cu-16opd and Cu-16mpd showed columnar mesomorphism but the mesomorphic behaviour of nitro-substituted complex, Cu-16npd could not be detected as it decomposes at ~225°C. While electronic effects associated with nitro (NO_2) and methyl (CH_3) substituent in the spacer group might be important, it is difficult to draw a structure–mesomorphism correlation. We surmise that a tetrahedral methyl substituent in the spacer force the neighbouring molecules above and below the plane sustaining weak intermolecular interactions. In POM study, upon cooling the sample from isotropic melt in particular, the complex Cu-16opd showed a typical mosaic texture (Figure 2) at ~100°C.The mesophase was later confirmed to be rectangular plastic columnar, Col_{rp} by XRD study. In DSC experiments, three transitions both in heating and cooling cycle were observed for the complex (Figure 3). The crystal to crystal transition observed at 53.7°C, could not be detected in POM study. Due to high viscous nature of the compound, a

Table 2. Transition temperature (°C), enthalpy (kJ mol^{-1}) and entropy values (ΔS, JK^{-1} mol^{-1}) of compounds according to the DSC measurements.

Compounds	Transition	Peak temperature (onset temperature)	Enthalpy (ΔH, kJ mol^{-1})	Entropy (ΔS, JK^{-1} mol^{-1})
Cu-16opd	Cr–Cr_1	57.8 (54.1)	3.2	0.055
	Cr_1–Col_{rp}	93.9 (92)	6.0	0.063
	Col_{rp}–I	132.9 (126)	22.4	0.168
	I–Colrp	100.2 (101)	23.8	0.237
	Col_{rp}–Cr	67.5 (69)	8.5	0.125
	Cr–Cr_1	53.7 (56)	2.6	0.048
Cu-16mpd	Cr–Col_r	90.4 (88.5)	13.9	0.038
	Col_r–I	165.7 (163.5)	12.7	0.028
	I–Col_r	152.6 (153.7)	11.6	0.027
	Col_r–Cr	69.4 (70.1)	2.5	0.007

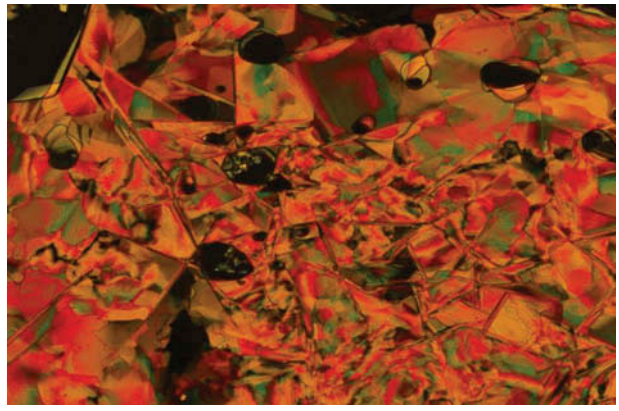

Figure 2. (colour online) POM texture of Cu-16opd complex at 100°C (20× magnification).

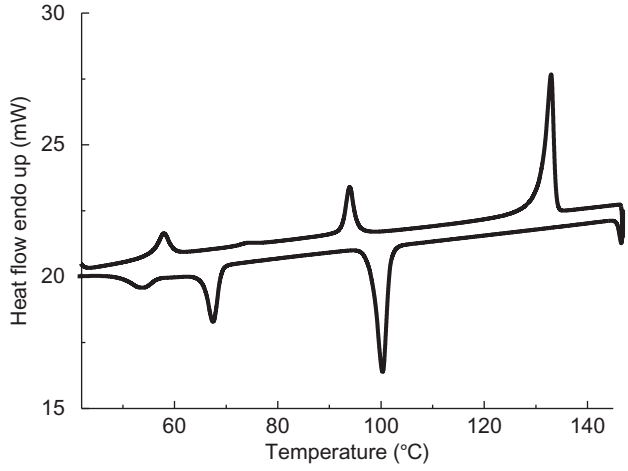

Figure 3. DSC thermogram of Cu-16opd complex at 10°C min^{-1} (N_2 atmosphere).

pronounced hysteresis in transition temperature is observed. High enthalpy values from isotropic to mesophase and vice versa clearly suggested that the mesophase is highly ordered. For Cu-16mpd, a typical broken fan-like texture (Figure 4) with some homeotropic region is formed on cooling from the isotropic liquid phase. In DSC (Figure 5), two peaks each for exothermic and endothermic transitions were found with low enthalpies, we have no suitable explanation for this behaviour at the moment. The nitro-substituted copper complex, Cu-16npd decomposed before melting precluding any POM study to ascertain the mesomorphic behaviour. Mesophase behaviour is thus appearing to be strongly dependent on the nature of metal ions as well as spacer linkage. A comparative assessment with previously reported

Figure 4. (colour online) POM texture of Cu-16mpd complex at 152°C (10× magnification).

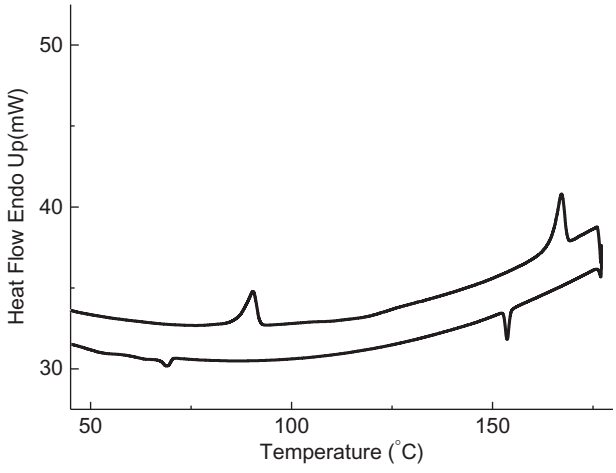

Figure 5. DSC thermogram of Cu-16mpd complex at 10°C min^{-1} (N_2 atmosphere).

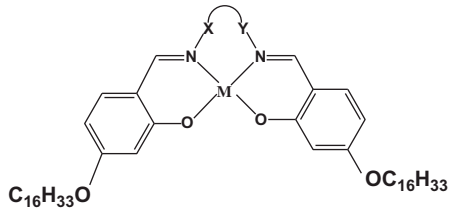

X-Y	M	Mesophase	Symmetry	Reference
	Cu	Col_{rp}	*c2mm*	Present work
	VO	Col_L	-	[43]
	Ni	Col_r	*c2mm*	[42]
	Zn	$Col_o \leftrightarrow Col_r$	P_{112}/P_{222}	[37]
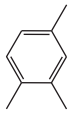	Cu	Col_r	-	Present work
	VO	$Col_{r1} \leftrightarrow Col_{r2}$	*c2mm*	[44]
	Ni	Col_r	*c2mm*	[42]
	Zn	Col_h	-	[38]
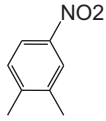	Cu	Nonmesogenic	-	Present work
	Ni	Col_r	*c2mm*	[42]

Chart 1.

related complexes is summarised in Chart 1. In our earlier work, we found VO-16opd complex showing lamello-columnar mesomorphism, Col_L [43] and VO-n-mpd (n = 14, 16, 18) exhibited rectangular columnar mesomorphism, Col_r.[44] The nickel complexes, Ni-16opd/Ni-16mpd/Ni-16npd all showed rectangular columnar mesomorphism.[42] As for zinc, the complexes, Zn-16opd and Zn-16mpd were earlier shown to exhibit rectangular and hexagonal columnar mesomorphism, respectively.[37, 38] Other than the oxovanadium complex which is square pyramidal, rest all complexes reported previously by us and the present copper complexes possess distorted square planar structure. While we obtained predominantly columnar phases (rectangular columnar Col_r, rectangular plastic columnar Col_{rp}, hexagonal columnar Col_h, oblique columnar Col_o, lamello columnar Col_L) in all structures, no specific trend was noticed regarding the nature of the phases. In addition to the local geometry around the metal ion the length of the flexible alkyl/alkoxy arm or nature of the spacer could as well be important to control the molecular assembly leading to a specific liquid crystalline phase. Temperature-dependent XRD studies were carried out for the Cu-16opd and Cu-16mpd complexes to confirm the mesophases. The powder X-ray diffraction (PXRD) pattern (Table 3) for Cu-16opd at 130°C in the low angle region consists of numbers of multiple peaks (Figure 6) In the wide angle region, a

Table 3. XRD data of copper complexes.

Compound	d_{obs} (Å)[a]	d_{calc} (Å)[b]	hk[c]	Parameters[d]
Cu-16opd	19.01	19.02	20	Col_{rp}
	13.91	13.92	11	a = 38.04Å
	12.41	12.43	31	b = 15.05Å
	10.33	10.32	40	S = 572.20Å^2
	9.11	9.12	01	V_m = 1573.44Å^3
	8.19	8.18	42	N = 4
	7.6	7.5		h = 10.33
	4.32	4.31	–	S_{col} = 286.10Å^2
Cu-16mpd	17.32	17.31	20	Col_r – $c2mm$
	12.72	12.73	11	a = 34.64 Å
	11.49	11.48	31	b = 13.68 Å
	8.41	8.42	40	S = 473.87 Å^2
	7.5	7.4		
	6.44	6.45	–	V_m = 1685.76 Å^3
	5.72	5.73		N = 4
	4.87	4.88		h = 11.49
				S_{col} = 236.93 Å^2

Notes: [a]d_{obs} and [b]d_{calc} are experimentally and theoretically measured diffraction spacings. [hk][c] are indexation of the reflections. Mesophase parameters[d] and molecular volume V_m is calculated using the formula: $V_m = M/\lambda\rho N_A$ where M is the molecular weight of the compound, N_A is the Avogadro number, ρ is the volume mass (≈1 g cm^{-3}) and $\lambda(T)$ is a temperature correction coefficient at the temperature of the experimerient (T). $\lambda = V_{CH2}(T^0)/V_{CH2}(T)$, T^0 = 25°C. $V_{CH2}(T) = 26.5616 + 0.02023.T$. For the Col_r phase, the lattice parameters a and b are deduced from the mathematical expression: $a = 2d_{20}$ and $1/d_{hk} = \sqrt{h^2/a^2 + k^2/b^2}$, where a and b are the parameters of the Col_r phase, S is the lattice area, S_{col} is the columnar cross-section (S = ab, $S_{col} = S/2$). The repeating columnar unit h is related to the molecular volume and the cross-section columnar area by the relationship $N \times V_{mol}/S$, where N is the number of molecular equivalent per repeat unit (in this case, to maintain the density along the column constant, N must be an integer or half-integer). Number of dimers constituting the rectangular disc, $N_D = N/2$.

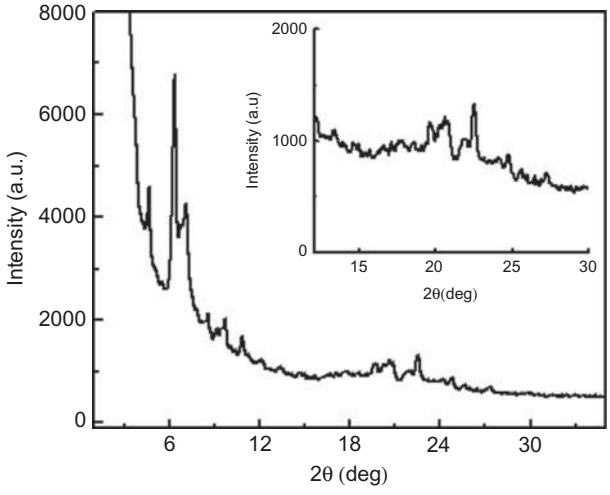

Figure 6. XRD pattern of Cu-16opd complex at 130°C.

diffuse peak is observed at 4.3 Å with a rather narrow width indicating partial melting of the aliphatic arms. The most important feature is the presence of twin peaks at 2θ ~ 20° and a sharp peak in the wide angle region generally observed in columnar plastic phase. [40,47] Occurrence of columnar plastic phase, denoted as Col_p, has been identified recently in discotic liquid crystals. The motional freedom of discs around the columnar axis in plastic phase is restricted.[48] The spacings of the first three reflections can be indexed to a rectangular lattice. For Cu-16mpd complex, in the small-angle region, a series of sharp Bragg peaks were present (Figure 7). The first two fundamental reflections can be indexed as the 11 and 20 reflections of a 2D rectangular lattice. Moreover, absence of any reflections with hk pairs ($h + k = 2n + 1$) in the diffractogram, suggest the mesophase symmetry to be $c2mm$ plane group. Furthermore, a diffuse reflection at 4.8 Å in the wide angle region confirms the liquid like nature of the molten alkyl chain.[18] If the arbitrarily considered periodicity (h) along the column and the average thickness of the molecular equivalents corresponding to the signal in the diffractogram is in the range of 10 to 13 Å, the dimeric interaction is expected to be preserved in the mesophase.[49,50] The reflection at 10.33 Å for Cu-16opd and at 11.49 Å for Cu-16mpd conveys the periodicity for the existence of dimeric interaction between the half-disc shaped molecules. This is also indicated from the less broad peak at ~7.6 Å in the wide angle region for both Cu-16opd and Cu-16mpd. For a corresponding average thickness along the column chosen arbitrarily for comparison sake and from measured molecular volume, the two complexes form a dimer per periodic stack of the columnar cross-section and four molecules (i.e. two dimers)

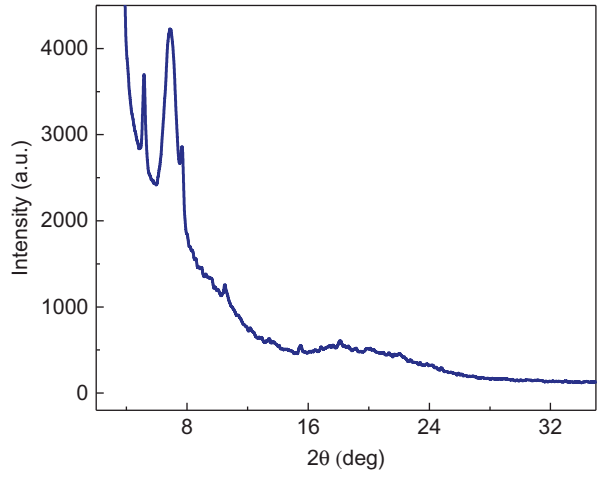

Figure 7. (colour online) XRD pattern of Cu-16mpd complex at 160°C.

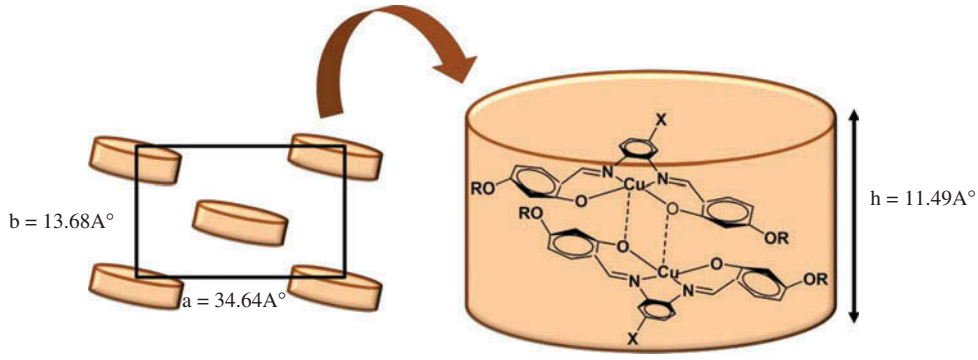

Figure 8. (colour online) Dimeric interactions of the half disc shaped molecules forming a disc-like shape.

pave the surface area of the rectangular lattice to make a repeating rectangular cell of ~10 Å thick (Figure 8). The radius of the semi-disc shaped molecule (~20.2 Å) as computed from density functional theory (DFT) study is almost half the lattice spacing (a = 38.04 Å) for Cu-16opd suggesting a face to face 'anti-parallel' assembly of the hemi-disc molecules in the columnar mesophase.[42]

DFT has become a readily available tool which allows considerable insight into the nature and electronic structures of transition metal complexes. The geometrical optimisations of all the copper complexes were performed using Becke's three-parameter non-local hybrid exchange potential and the nonlocal correlation functional of Lee, Yang, and Parr21 (B3LYP) with the 6-31G (d) basis set for all atoms except for copper, which has been described by the effective core potential of Wadt and Hay (Los Alamos ECP) included in the LanL2DZ basis set. The gas phase ground state geometries of the copper complexes were fully optimised using the unrestricted B3LYP methods without imposing any symmetry constrain with tight convergence criteria. Appropriate structures were confirmed as energy minima by calculating the vibrational frequencies using second derivative analytic methods, and confirming the absence of any imaginary frequencies.[51] For Cu^{2+} complexes, which are open-shell systems, the expectation value showed that the spin contamination of the unrestricted wave function was always very small.[52] All DFT calculations were carried out with the Gaussian 09 programs.[53] Natural charges were obtained from the natural bond orbital (NBO) population analysis.

Some of the significant geometric parameters of the optimised hydrogen-, methyl- and nitro-substituted copper complexes, evaluated by DFT calculation at B3LYP level are displayed in Table 4. The complexes have an average Cu–O and Cu–N bond lengths in the range of 1.911–1.916 and 1.986–1.993 Å, respectively. The average bond angles are

Table 4. Selected bond (Å) and angles (°) and other related parameters of Cu(II) complexes evaluated at B3LYP level.

Structure parameters	Cu-16opd	Cu-16mpd	Cu-16npd
Cu—O1	1.915	1.915	1.911
Cu—O2	1.914	1.914	1.916
Cu—N1	1.991	1.992	1.986
Cu—N2	1.991	1.990	1.993
C1—N1	1.313	1.313	1.316
C2—N2	1.313	1.313	1.319
C_{AR1}—O1	1.291	1.292	1.292
C_{AR2}—O2	1.291	1.292	1.289
O1—Cu—O2	89.8	89.8	89.9
N1—Cu—N2	83.2	83.2	83.1
O1—Cu—N1	93.6	93.5	93.6
O2—Cu—N2	93.6	93.5	93.4
O1—Cu—N2	176.6	176.6	176.5
O2—Cu—N1	176.6	176.6	176.4
O(1)O(2)N(2)N(1)	1.30	1.27	1.27
N(1)O(1)O(2)N(2)	−1.21	−1.18	−1.17
LUMO (eV)	−1.785	−1.847	−2.587
HOMO (eV)	−5.261	−5.161	−5.591
ΔE (eV)	3.476	3.314	3.004
Dipole moment (D)	3.224	3.844	4.174
Chemical hardness (eV)	1.738	1.657	1.502
Molecular length (Å)	42.76	42.76	42.75

in the range of 89.8–89.9° and 83.1–83.2° for O1–Cu–O2 and N1–Cu–N2, respectively, while, O1–Cu–N2 and O2–Cu–N2 bond angles are calculated to be 176.5–176.6° and 176.4–176.6°, respectively, around the copper atom indicating slight distortion of square planar geometry (Figure 9). The dihedral angles O(1)O(2)N(1)N(2) and N(1)O(1)O(2)N(2) as computed from DFT are found to lie in the range 1.18–1.30° (Table 4) reflecting slight deviation from planarity. A strained conformation of the $[N_2O_2]$-donor tetradentate ligand with long pendant alkyl side chains is believed to have caused little deviation from planar symmetry. The molecular length of the complexes based on the fully extended structure is found to be around 42.76 Å (measured from the two terminal end

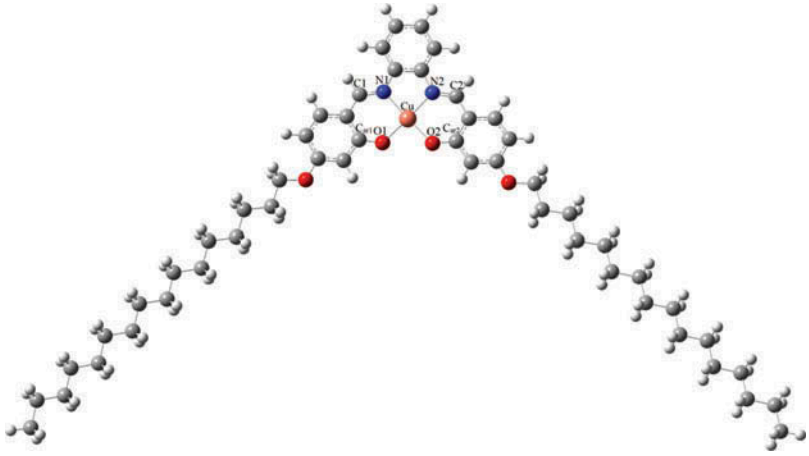

Figure 9. Optimised structure of Cu-16opd.

of the side alkyl chain), indicating no substituent effect on the molecular length. The optimised geometry also revealed that the oxygen and aromatic carbon ($O–C_{ar}$) distance increases from 1.271 in free ligand to 1.292 Å on complexation with copper. The $O–C_{ar}$ bond is weakened upon formation of complex, implying that oxygen atom acts as a donor atom.

DFT has emerged as a practical and effective computational tool with which electronic structure of transition metal complexes can be studied easily. DFT with NBO analysis allows considerable insight into the nature of metal–ligand bonding. The natural charges and electronic configuration of the atoms of the complexes and free ligand evaluated by NBO analysis are summarised in Table 5. The calculated natural charges on the copper ions are considerably lower than the formal charge, +2. The electronic population on p_x, p_y and p_z orbitals of copper atom in its hydrogen-, methyl- and nitro-substituted ligands are found to be (0.1186, 0.1164 and 0.0937), (0.1186, 0.1145 and 0.0910) and (0.1183, 0.1162 and 0.0934), respectively. However, occupancy at the d_{xy}, d_{xz}, d_{yz}, $d_{x^2-y^2}$ and d_{z^2} orbitals of copper atoms in their complexes with hydrogen, methyl and nitro containing ligands are (1.4205, 1.9964, 1.9846, 1.9960 and 1.9686), (1.4328, 1.9948, 1.9838, 1.9957 and 1.9712) and (1.4190, 1.9961, 1.9847, 1.9969, 1.9689), respectively. All the d-orbitals are occupied by more than 1.96 e^- except the d_{xy} (~1.42 e^-) orbitals. Comparing the atomic charges in the free ligands and their complexes with copper, it can be seen that the atomic charge redistribution occur on all the atoms in the complexes. The calculated natural atomic charges on copper atoms in its complexes with hydrogen-, methyl- and nitro-substituted ligands are found to be +0.964, +0.963 and +0.968, respectively, attesting ligand-to-metal charge transfer in all the complexes. According to the NBO analysis, the electronic configuration of Cu in Cu-16opd complex is: [core] $4S^{0.34}3d^{9.37}4p^{0.33}$, which corresponds to 18 core electrons, 9.71 valence electrons (on 4S and 3d atomic orbitals) and 0.33 Rydberg electrons (mainly on 4p

Table 5. Natural atomic charges and natural electron configuration of the ligands and their complexes with Cu^{2+} evaluated at B3LYP level.

		16-opd		16-mpd		16-npd	
	Atoms	Charge	Configuration	Charge	Configuration	Charge	Configuration
Ligand	O1	−0.675	[core]$2S^{1.70}2p^{4.96}3d^{0.01}$	−0.670	[core]$2S^{1.70}2p^{4.96}3d^{0.01}$	−0.667	[core]$2S^{1.70}2p^{4.95}3d^{0.01}$
	O2	−0.675	[core]$2S^{1.70}2p^{4.96}3d^{0.01}$	−0.669	[core]$2S^{1.70}2p^{4.96}3d^{0.01}$	−0.656	[core]$2S^{1.70}2p^{4.94}3d^{0.01}$
	N1	−0.436	[core]$2S^{1.34}2p^{4.07}3p^{0.01}3d^{0.01}$	−0.436	[core]$2S^{1.34}2p^{4.08}3p^{0.01}3d^{0.01}$	−0.446	[core]$2S^{1.34}2p^{4.09}3p^{0.01}3d^{0.01}$
	N2	−0.436	[core]$2S^{1.34}2p^{4.07}3p^{0.01}3d^{0.01}$	−0.434	[core]$2S^{1.32}2p^{4.09}3p^{0.01}3d^{0.01}$	−0.422	[core]$2S^{1.32}2p^{4.08}3p^{0.01}3d^{0.01}$
Complex	O1	−0.669	[core]$2S^{1.66}2p^{5.00}3p^{0.01}$	−0.671	[core]$2S^{1.67}2p^{4.99}3p^{0.01}$	−0.663	[core]$2S^{1.66}2p^{4.99}3p^{0.01}$
	O2	−0.669	[core]$2S^{1.66}2p^{5.00}3p^{0.01}$	−0.671	[core]$2S^{1.67}2p^{4.99}3p^{0.01}$	−0.666	[core]$2S^{1.66}2p^{4.99}3p^{0.01}$
	N1	−0.571	[core]$2S^{1.30}2p^{4.26}3p^{0.01}$	−0.573	[core]$2S^{1.31}2p^{4.25}3p^{0.01}$	−0.578	[core]$2S^{1.30}2p^{4.27}3p^{0.01}$
	N2	−0.571	[core]$2S^{1.30}2p^{4.26}3p^{0.01}$	−0.573	[core]$2S^{1.31}2p^{4.25}3p^{0.01}$	−0.578	[core]$2S^{1.30}2p^{4.26}3p^{0.01}$
	Cu	0.964	[core]$4S^{0.34}3d^{9.37}4p^{0.33}$	0.963	[core]$4S^{0.33}3d^{9.38}4p^{0.32}$	0.968	[core]$4S^{0.34}3d^{9.36}4p^{0.33}$

orbital) give the 28.04 electrons. This is consistent with the calculated natural atomic charge on copper atom (+0.968e) in Cu-16opd complex. The natural atomic charge on oxygen atoms of the ligands hardly changes on complexation with copper ion. However, while, the atomic charges on nitrogen atom of the ligands changes significantly on complexation from –0.436 and –0.436 to –0.571 and –0.571, –0.436 and 0.434 to –0.573 and –0.573 and from –0.446 and –0.422 to –0.578 and –0.578, respectively, on complexation of hydrogen-, methyl- and nitro-containing ligands with copper ions (Table 5).

Frontier molecular orbital plays an important role in determining the electronic properties of molecules.[54] Lowest unoccupied molecular orbital (LUMO) and highest occupied molecular orbital (HOMO) energies of the complexes with 16-opd, 16-mpd and 16-npd ligands are calculated to be –1.785 eV and –5.261eV, –1.847 eV and –5.161 eV and –2.587 eV and –5.591 eV, respectively. The corresponding energy differences (ΔE) of the complexes are found to be 3.476 eV, 3.314 eV and 3.004 eV, respectively. The LUMO and HOMO energy as well as their energy differences of the complexes depend on the electronic nature of the substituents. The energy differences decrease in the order of 16-opd > 16-mpd > 16-npd. The HOMO–LUMO energy differences evaluated from the lowest energy UV–Vis band for Cu-16opd, Cu-16mpd and Cu-16npd is 2.93 eV, 2.96 eV and 2.62 eV, respectively, are somewhat lower than that obtained from DFT studies. This can be accounted by considering extensive intermolecular interactions in the solution phase (UV–Vis study) in comparison to free gaseous molecule in DFT study. A low HOMO–LUMO energy gap implies a low kinetic stability and high chemical reactivity, because it is energetically favourable to add electrons to LUMO or to extract electrons from a HOMO. We further calculated the chemical hardness values of hydrogen-, methyl- and nitro-substituted copper complexes from their LUMO and HOMO energy difference. The chemical hardness values of hydrogen-, methyl- and nitro-substituted complexes are found to be 1.738, 1.657 and 1.502 eV, respectively. According to maximum hardness principle [55] higher hardness value indicates higher stability. Hence, lower chemical hardness value obtained for nitro-substituted complex indicated lower stability of the complex compared to the unsubstituted and methyl substituted complex.

3. Conclusion

A series of copper-salen complexes with different substituent on the spacer group have been successfully synthesised and their mesomorphic behaviour were investigated. The phase transition behaviour of the compounds as a function of the spacer group substituent and divalent metal ions has been quite rewarding to explore. The ligands are found to be non-mesomorphic, but their complexes were found to exhibit columnar mesomorphism. The mesophase formation has been shown to be strongly dependant on the substituent of the spacer linkage in salphen group. The copper complex with methyl substituted salen group showed rectangular columnar mesophase (Col_r) and without methyl group showed rectangular columnar plastic mesophase (Col_{rp}). Quite surprisingly the $–NO_2$ substituted salen complex lacks any mesomorphism. A distorted square planar four coordinate geometry for the newly synthesised complex is proposed on the basis of DFT study.

4. Experimental section

4.1 Physical measurements

The C, H and N analyses were carried out using Carlo Erba 1108 elemental analyser (Waltham, MA, USA). Molar conductance of the compounds was determined in dichloromethane (ca 10^{-3} mol L^{-1}) at room temperature using MAC-554 conductometer (Macroscientific Works, New Delhi, India). The ^1H and ^{13}C NMR spectra were recorded on Bruker Advance 400 MHz (Bruker, Kolkata, India) spectrometer in $CDCl_3$ (chemical shift in δ) solution with Tetramethylsilane (TMS) as internal standard. UV–Vis absorption spectra of the compounds in dichloromethane were recorded on a Shimadzu UV-1601 PC spectrophotometer (Shimadzu, Asia pacific, Pte. Ltd., Singapore). Mass spectra were recorded on a JEOL SX-102 (JEOL, Tokyo, Japan) spectrometer with FAB. The optical textures of the different phase of the compounds were studied using a polarising microscope (Nikon optiphot-2-pol, Nikon Corporation, Tokyo, Japan) attached with Instec (Boulder, CO, USA) hot and cold stage HCS302, with STC200 temperature controller of 0.1°C accuracy. The thermal behaviour of the compounds were studied using a Perkin-Elmer DSC (Perkin Elmer International, Schwerzenbach, Switzerland) Pyris-1 spectrometer with a heating or cooling rate of 10°C/min. Variable temperature PXRD of the samples were recorded on a Bruker D8 Discover instrument using Cu–Kα radiation. Quantum chemical calculations on Cu-16opd/Cu-16mpd/Cu-16npd were carried out using DFT as implemented using Gaussian 09 program at B3LYP level.

4.2 Materials

The materials were procured from Tokyo Kasei, Japan, and Lancaster Chemicals, USA. All solvents

were purified and dried using standard procedures. Silica (60–120 mesh) from Spectrochem was used for chromatographic separation. Silica gel G (E-Merck, India) was used for thin layer chromatography.

4.3 Synthesis and analysis

The synthesis of the ligands are described in our earlier report.[40]

4.3.1 Synthesis of copper (II) complexes

General procedure: The ligand 16-opd (0.079 g, 0.1 mmol) or 16-mpd (0.081 g, 0.1 mmol) or 16-npd (0.084 g, 0.1 mmol) was dissolved in minimum volume of absolute methanol. To this, an equimolar amount of copper acetate Cu $(OAc)_2.2H_2O$ (0.019 g, 0.1 mmol) in methanol was then added slowly and stirred for 2 h at room temperature. A brown solid formed immediately was filtered, washed with diethyl ether and recrystallised from dichloromethane–methanol (1:1).

4.3.2 Cu-16opd

Yield = 0.073 g, 75%. FAB Mass (m/e, fragment): m/z: calc. 857.5; found: 858.5[$M + H^+$]; Anal. Calc. for $C_{52}H_{78}N_2O_4Cu$: C, 72.7; H, 9.2; N 3.26. Found: C, 72.72; H, 9.1; N, 3.2%. IR (ν_{max}, cm^{-1}, KBr): 2921 (ν_{as}(C–H), CH_3), 2860 (ν_s(C–H), CH_3), 2848 (ν_{as}(C–H), CH_2), 1611 (νC=N).

4.3.3 Cu-16mpd

Yield = 0.065g, 65%. FAB Mass (m/e, fragment): m/z: calc. 871.5; found: 872.5 [$M + H^+$]; Anal. Calc. for $C_{53}H_{80}N_2O_4Cu$: C, 72.9; H, 9.2; N 3.2. Found: C, 73; H, 9.3; N, 3.1%. IR (ν_{max}, cm^{-1}, KBr): 2921 (ν_{as}(C–H), CH_3), 2860 (ν_s(C–H),CH_3), 2848 (ν_{as}(C–H), CH_2), 1613 (νC=N).

4.3.4 Cu-16npd

Yield = 0.072 g, 70%. FAB Mass (m/e, fragment): m/z: calc. 902.5; found: 903.5 [$M + H^+$]; Anal. Calc. for $C_{52}H_{77}N_3O_6Cu$: C, 69.1; H, 8.6; N 4.6. Found: C, 69.2; H, 8.5; N, 4.5%. IR (ν_{max}, cm^{-1}, KBr): 2921 (ν_{as}(C–H),CH_3), 2860 (ν_s(C–H), CH_3), 2848 (ν_{as}(C–H), CH_2), 1615 (νC=N).

Acknowledgements

The authors thank Sophisticated Analytical Instrument Facility (SAIF), North Eastern Hill University (NEHU), Shillong, and Central Drug Research Institute (CDRI), Lucknow, for analytical and spectral data. We are also thankful to Department of Biotechnology -e Library Consortium (DeLCON) of Bioinformatics Centre, Assam University, Silchar (India).

Funding

CD and RC acknowledge financial support from University Grants Commission (UGC), Government of India. One of the authors, Paritosh Mondal, thanks Department of Science and Technology, New Delhi, for financial support (SR/FT/CS-86/2010).

References

[1] Rezvani Z, Ghanea MA, Nejati KS, Baghaei A. Syntheses and mesomorphic properties of new oxygen-bridged dicopper complex homologous derived from azo-containing salicylaldimine Schiff base ligands. Polyhedron. 2009;28:2913–2918.

[2] Pucci D, Aiello I, Bellusci A, Callipari G, Crispini A, Ghedini M. Copper(II) and Nickel(II) complexes of a tetradentate ligand containing an n,n′-bis(salicylidene) dodecane-1, 10-diamine core. Mol Cryst Liq Cryst. 2009;500:144–154.

[3] Abe Y, Nakabayashi K, Matsukawa N, Iida M, Tanase T, Sugibayashia M, Ohta K. Novel crystal structure and mesomorphism appeared in oxovanadium(IV) salen complexes with 4-substituted long alkoxy chains. Inorg Chem Commun. 2004;7:580–583.

[4] Abe Y, Nakabayashi K, Matsukawa N, Takashima H, Iida M, Tanase T, Sugibayashi M, Mukai H, Ohta K. Syntheses, structures, and mesomorphic properties of two series of oxovanadium(IV) salen and salpn complexes with 4-substituted long alkoxy chains. Inorg Chim Acta. 2006;359:3934–3946.

[5] Abe Y, Nakazima N, Tanase T, Katano S, Mukai H, Ohta K. Syntheses, structures, and mesomorphism of a series of Cu(II) salen complexes with 4-substituted long alkoxy chains. Mol Cryst Liq Cryst. 2007;466:129–147.

[6] Pucci D, Aiello I, Bellusci A, Crispini A, Ghedini M, La Deda M. Coordination induction of nonlinear molecular shape in mesomorphic and luminescent Zn^{II} complexes based on salen-like frameworks. Eur J Inorg Chem. 2009;4274–4281.

[7] Chico R, Dominguez C, Donnio B, Coco S, Espinet P. Liquid crystalline salen manganese(III) complexes: mesomorphic and catalytic behaviour. Dalton Trans. 2011;40:5977–5983.

[8] Lai CK, Leu Y-F. Smectic bimetallomesogens: synthesis, characterization and mesomorphic properties and the crystal structure of bis[N-(3-hydroxypropyl)-4-octanoylsalicylaldiminato] copper(II) complex. Liq Cryst. 1998;25:689–698.

[9] Guillevic M-A, Light ME, Coles SJ, Gelbrich T, Hursthouse MB, Bruce DW. Synthesis of dinuclear complexes of rhenium(I) as potential metallomesogens. J Chem Soc Dalton Trans. 2000;1437–1445.

[10] Espinet P, Hernandez C, Martin-Alvarez JM, Miguel JA. Formation of trinuclear palladium orthometalated complexes with unprecedented asymmetrical (μ_3-S) (μ_3-X) bridges (X = OH, SR, O_2CR) from μ_2-hydroxo

dimeric complexes and CS_2. Inorg Chem. 2004;43:843–845.
[11] Lai CK, Lin R, Lu MY, Kao KC. Smectic bimetallomesogens in β-enaminoketonate copper complexes: the steric effect of a methyl substituent on the core group and the crystal structure. J Chem Soc. Dalton Trans. 1998;1857–1862.
[12] Ku SM, Wu C-Y, Lai CK. Bimetallomesogens: formation of calamitic or columnar mesophases by μ-exogenous-bridged groups in N,N′-(propan-2-ol)-bis(4 alkoxysalicylaldimine) copper(II) complexes. J Chem Soc. Dalton Trans. 2000;3491–3492.
[13] Li SY, Chen CJ, Lo PY, Sheu HS, Lee GH, Lai CK. H-Bonded metallomesogens derived from salicyladiminates. Tetrahedron. 2010;66:6101–6112.
[14] Barbera J, Gimenez R, Marcos M, Serrano JL, Alonso PJ, Martinez JI. Paramagnetic bimetallomesogens. Chem Mater. 2003;15:958–964.
[15] Chae HW, Kadkin ON, Choi M-G. New heteropolynuclear metallomesogens: copper(II), palladium(II), nickel(II) and oxovanadium(IV) chelates with [3]ferrocenophane-containing Schiff's base and β-aminovinylketone. Liq Cryst. 2009;36:53–60.
[16] Marcos M, Omenat A, Barbera J, Duran F, Serrano JL. Structural study of metallomesogens. J Mater Chem. 2004;14:3321–3327.
[17] Lai CK, Serrette AG, Swager TM. Discotic bimetallomesogens: building blocks for the formation of new columnar arrangements of transition metals. J Am Chem Soc. 1992;114:7948–7949.
[18] Morale F, Date RW, Guillon D, Bruce DW, Finn RL, Wilson C, Blake AJ, Schroder M, Donnio B. Columnar mesomorphism from hemi-disk like metallomesogens derived from 2,6-bis[3′,4′,5′-tri(alkoxy)phenyliminomethyl]pyridines (L): Crystal and molecular structures of $[M(L)Cl_2]$ (M=Mn, Ni, Zn. Chem Eur J. 2003;9:2484–2501.
[19] Kumar S. Self-organization of disc-like molecules: chemical aspects. Chem Soc Rev. 2006;35:83–109.
[20] Goodby JW, Gortz V, Cowling SJ, Mackenzie G, Martin P, Plusquellec D, Benvegnu T, Boullanger P, Lafont D, Queneau Y, Chambert S, Fitremann J. Thermotropic liquid crystalline glycolipids. J Chem Soc Rev. 2007;36:1971–2032.
[21] O'Neill M, Kelly SM. Liquid crystals for charge transport, luminescence and photonics. Adv Mater. 2003;15:1135–1146.
[22] Cristiano R, Gallardo H, Bortoluzzi AJ, Bechtold IH, Campos CEM, Longo RL. Tristriazolotriazines: a core for luminescent discotic liquid crystals. Chem Commun. 2008;5134–5136.
[23] Sergeyev S, Pisula W, Geerts YH. Discotic liquid crystals: a new generation of organic semiconductors. Chem Soc Rev. 2007;36:1902–1929.
[24] Shirota Y, Kageyama H. Charge carrier transporting molecular materials and their applications in devices. Chem Rev. 2007;107:953–1010.
[25] Sawamura M, Kawai K, Matusuo Y, Kanie K, Kato T. Stacking of conical molecules with a fullerene apex into polar columns in crystals and liquid crystals. Nature. 2002;419:702–705.
[26] Seguy I, Jolinat P, Destruel P, Mamy R. Red organic light emitting device made from triphenylene hexaester and perylene tetraester. J Appl Phys. 2001;89:5442–5448.
[27] Van de Craats AM, Stutzmann N, Bunko O, Nielsen MM, Watson M, Müllen K, Chanzy HD, Sirringhaus H, Friend RH. Meso-epitaxial solution-growth of self-organizing discotic liquid-crystalline semiconductors. Adv Mater. 2003;15:495–499.
[28] Laschat S, Baro A, Steinke N, Giesselmann F, Hägele C, Scalia G, Judele R, Kapatsina E, Sauer S, Schreivogel A, Tosoni M. Discotic liquid crystals: from tailor-made synthesis to plastic electronics. Angew Chem Int Ed. 2007;46:4832–4887.
[29] Cavero E, Uriel S, Romero P, Serrano JL, Giménez R. Tetrahedral zinc complexes with liquid crystalline and luminescent properties: interplay between non-conventional molecular shapes and supramolecular mesomorphic order. J Am Chem Soc. 2007;129:11608–11618.
[30] Rezvani Z, Abbasi AR, Nejati K, Seyedahmadian M. Syntheses, characterization and glass-forming properties of new bis[5-((4-^{n}dodecyloxyphenyl)azo)-N-(4-^{n}alkoxyphenyl)-salicylaldiminato] nickel (II) complex homologues. Polyhedron. 2005;24:1461–1470.
[31] Nejati K, Rezvani Z. Syntheses, characterization and mesomorphic properties of new bis(alkoxyphenylazo)-substituted N,N' salicylidene diiminato Ni(II), Cu(II) and VO(IV) complexes. New J Chem. 2003;27:1665–1669.
[32] Rezvani Z, Ghanea MA, Nejati K, Baghaei SA. Syntheses and mesomorphic properties of new oxygen-bridged dicopper complex homologous derived from azo-containing salicylaldimine Schiff base ligands. Polyhedron. 2009;28:2913–2918.
[33] Bhattacharjee CR, Datta C, Das G, Mondal P. Liquid crystalline dinuclear copper(II) complexes accessed from photoluminescent tridentate [ONO]-donor Schiff base ligands. Liq Cryst. 2012;39:639–646.
[34] Bhattacharjee CR, Datta C, Das G, Mondal P. Green emissive salicylaldimine-based polar Schiff bases with short alkoxy tails and their copper(II)/oxovanadium (IV) complexes: synthesis and mesomorphism. Liq Cryst. 2012;39:373–385.
[35] Abe Y, Iyoda A, Seto K, Moriguchi A, Tanase T, Yokoyama H. Synthesis, structures and ion-association properties of a series of Schiff base oxidovanadium(V) complexes with 4-substituted long alkoxy chains. Eur J Inorg Chem. 2008;2148–2157.
[36] Abe Y, Akao H, Yoshida Y, Takashima H, Tanase T, Mukai H, Ohta K. Syntheses, structures, and mesomorphism of a series of Ni(II) salen complexes with 4-substituted long alkoxy chains. Inorg Chim Acta. 2006;359:3147–3155.
[37] Bhattacharjee CR, Das G, Mondal P, Prasad SK, Rao DSS. Novel green light emitting nondiscoid liquid crystalline zinc(II) Schiff-base complexes. Eur J Inorg Chem. 2011;1418–1424.
[38] Bhattacharjee CR, Das G, Mondal P, Rao NVS. Novel photoluminescent hemi-disclike liquid crystalline Zn(II) complexes of $[N_2O_2]$ donor 4-alkoxy substituted salicyldimine Schiff base with aromatic spacer. Polyhedron. 2010;29:3089–3096.
[39] Bhattacharjee CR, Das G, Mondal P. Novel non-discoid chiral copper(II)-salen type $[N_2O_2]$ donor Schiff base complexes with a cyclohexane diamine spacer: synthesis, electrochemistry, columnar mesomorphism and DFT study. Liq Cryst. 2011;38:441–449.

[40] Bhattacharjee CR, Das G, Mondal P, Prasad SK, Rao DSS. Plastic columnar mesomorphism in half-disc-shaped oxovanadium(IV) Schiff base complexes. Liq Cryst. 2011;38:615–623.
[41] Bhattacharjee CR, Das G, Mondal P. Photoluminescent hemi disc-shaped liquid crystalline nickel(II) Schiff-base complexes. Eur J Inorg Chem. 2011;5390–5399.
[42] Bhattacharjee CR, Datta C, Das G, Chakrabarty R, Mondal P. Induction of photoluminescence and columnar mesomorphism in hemi-disc salphen type Schiff bases via nickel(II) coordination. Polyhedron. 2012;33:417–424.
[43] Bhattacharjee CR, Das G, Mondal P, Prasad SK, Rao DSS. Lamellar columnar mesomorphism in a series of oxovanadium(IV) complexes derived from N,N/-di-(4-n-alkoxysalicylidene) diaminobenzene. Inorg Chem Commun. 2011;14:606–612.
[44] Bhattacharjee CR, Datta C, Das G, Mondal P. Induced columnar mesomorphism in non-discoid VO^{2+} salphen complexes: transition between two rectangular columnar phases. Liq Cryst. 2012;39:819–826.
[45] Chakravorty A, Basu S. Visible absorption spectra of copper-ethylene-diamine *bis*(acetylacetone) in the crystalline state. Nature. 1959;184:50–51.
[46] Silverstein RM, Bassler GC, Morrill TC. Spectrometric identification of organic compounds. 5th ed. Canada: Wiley; 1974.
[47] Yelamaggad CV, Achalkumar AS, Rao DSS, Nobusawa M, Akutsu H, Yamada J, Nakatsuji S. The first examples of discotic radicals: columnar mesomorphism in spin-carrying triphenylenes. J Mater Chem. 2008;18:3433–3437.
[48] Glusen B, Heitz W, Kettner A, Wendroff JH. A plastic columnar discotic phase D_p. Liq Cryst. 1996; 20:627–633.
[49] Binnemans K, Lodewyckx K, Cardinaels T, Parac-Vogt TN, Bourgogne C, Guillon D, Donnio B. Dinuclear lanthanide schiff-base complexes forming a rectangular columnar mesophase. Eur J Inorg Chem. 2006;150–157.
[50] Chico R, Domínguez C, Donnio B, Coco S, Espinet P. Liquid crystalline salen manganese(III) complexes: mesomorphic and catalytic behaviour. Dalton Trans. 2011;40:5977–5983.
[51] Huang H, Hughes RP, Rheingold AL. Synthesis and structural characterization of group 6 transition metal complexes with terminal fluoromethylidyne (CF) ligands; a DFT/NBO/NRT comparison of bonding characteristics of terminal NO, CF and CH ligands. Dalton Trans. 2011;40:47–55.
[52] Rincón E, Yáñez M, Toro-Labbé A, Mó O. Effect of Ni(II), Cu(II) and Zn(II) association on the keto-enol tautomerism of thymine in the gas phase. Phys Chem Chem Phys. 2007;9:2531–2537.
[53] Frisch MJ, Trucks GW, Schlegel HB, Scuseria GE, Robb MA, Cheeseman JR, Scalmani G, Barone V, Mennucci B, Petersson GA, Nakatsuji H, Caricato M, Li X, Hratchian HP, Izmaylov AF, Bloino J, Zheng G, Sonnenberg JL, Hada M, Ehara M, Toyota K, Fukuda R, Hasegawa J, Ishida M, Nakajima T, Honda Y, Kitao O, Nakai H, Vreven T, Montgomery JA, Peralta JE Jr, Ogliaro F, Bearpark M, Heyd JJ, Brothers E, Kudin KN, Staroverov VN, Kobayashi R, Normand J, Raghavachari K, Rendell A, Burant JC, Iyengar SS, Tomasi J, Cossi M, Rega N, Millam JM, Klene M, Knox JE, Cross JB, Bakken V, Adamo C, Jaramillo J, Gomperts R, Stratmann RE, Yazyev O, Austin AJ, Cammi R, Pomelli C, Ochterski JW, Martin RL, Morokuma K, Zakrzewski VG, Voth GA, Salvador P, Dannenberg JJ, Dapprich S, Daniels AD, Farkas Ö, Foresman JB, Ortiz JV, Cioslowski J, Fox DJ. Gaussian 09. Wallingford CT: Gaussian; 2009.
[54] Fleming I. Frontier orbitals and organic chemical reactions. London: Wiley; 1976.
[55] Parr RG, Chattaraj PK. Principle of maximum hardness. J Am Chem Soc. 1991;113:1854–1855.